[redacted]

(NASA-CR-79767) GENERATION-1 SIMULATION OF THE HEATED BLEED ENGINE (Aerojet-General Corp., Azusa, Calif.) 228 p

N75-75636

Unclas
00/98 25263

NERVA PROGRAM

[redacted]

X66-85782

(ACCESSION NUMBER) (THRU) (PAGES) (CODE) (NASA CR OR TMX OR AD NUMBER) (CATEGORY)

FACILITY FORM 602

Aerojet-General® CORPORATION

A SUBSIDIARY OF THE GENERAL TIRE & RUBBER COMPANY

AZUSA, CALIFORNIA • SACRAMENTO, CALIFORNIA • DOWNEY, CALIFORNIA • FREDERICK, MARYLAND

THE GENERAL TIRE

NASA Offices and Research Centers Only

[redacted]

LIBRARY

Con Doc 62-503

4/17/64

C66-7977

~~CONFIDENTIAL RESTRICTED DATA~~

~~GROUP 1~~

~~EXCLUDED FROM AUTOMATIC REGRADING~~
~~DOD DIR 5200.10 DOES NOT APPLY~~

AGC OFFICIAL CERTIFYING CLASS ☒ AND/OR GROUP ☒
INDICATE NAME (TYPED OR PRINTED) SIGNATURE AND DEPT. NO

CLASSIFICATION CHANGE

To UNCLASSIFIED
By authority of NASA Hqs TD 75-370
Changed by [illegible] Date 6/30/75
Classified Document Master Control Station, NASA
Scientific and Technical Information Facility

REPORT 2223
GENERATION -I SIMULATION OF THE HEATED BLEED ENGINE (U)

AGC 6133.25

~~Notice: This material contains information affecting the national defense of the United States within the meaning of the Espionage Laws, Title 18, U. S. C., Sections 793 and 794, the transmission or revelation of which in any manner to an unauthorized person is prohibited by law~~

SNP-1

Aerojet-General® CORPORATION
A SUBSIDIARY OF THE GENERAL TIRE & RUBBER COMPANY
AZUSA CALIFORNIA • SACRAMENTO CALIFORNIA

NERVA OPERATIONS

~~EXCLUDED FROM THE GDS~~

~~RESTRICTED DATA~~

NASA Offices and Research Centers Only

~~ATOMIC ENERGY ACT OF 1954~~

~~CONFIDENTIAL RESTRICTED DATA~~

D/C 62-503

Page intentionally left blank

Page intentionally left blank

ABSTRACT

A description of the Generation-I Engine Simulator, and the analog-computer circuit for reactor simulation, is presented. The results of the analyses of the computer-control system for achieving simulated nuclear engine characteristics are also incorporated. The test runs and test results are extensively described including an analysis of the data.

Page intentionally left blank

Page intentionally left blank

TABLE OF CONTENTS

		Table	Figure	Page
I.	INTRODUCTION			I-1
	A. Background			I-A-1
	B. Test Purposes and Objectives			I-B-1
	C. Description of Test System Apparatus			I-C-1
	Instrumentation for Engine Simulator	I-C,1		I-C-3
	Schematic Diagram, Engine Simulator		I-C,1	
	Instrumentation Diagram, Engine Simulator		I-C,2	
	D. Test System			I-D-1
	1. Heat-Capacity Start Tests			I-D-1
	2. Computer-Controlled Test			I-D-1
	3. Reactor-Simulator Control			I-D-2
II.	SYSTEM DESIGN			II-A-1
	A. Selection and Design of Physical Components			II-A-1
	Thermal Properties at 520°R of Materials	II-A,1		II-A-6
	Beryllium and Aluminum Compared			
	Energy Extracted per Unit Volume		II-A,1	
	Internal Temperatures		II-A,2	
	Inverse Thermal Diffusivity		II-A,3	
	Thermal Conductivity		II-A,4	
	B. Reactor Simulator			II-B-1,1
	1. Design Considerations			II-B-1,1
	2. Nonlinear Reactor Equations			II-B-2,1
	Schematic Diagram, Cold-Bleed Nuclear Engine		II-B-2,1	

TABLE OF CONTENTS (cont.)

	Table	Figure	Page
3. Specific Reactor Equations			II-B-3,1
System Constants, Reactor Simulator Equations	II-B-3,1		II-B-3,1
4. Linearization of Equations			II-B-4,1
Reactor Simulator Equations	II-B-4,1		
5. Reactor Control Loop			II-B-5,1
Block Diagram, Reactor Control Loop		II-B-5,1	
Block Diagram, Temperature Control Loop		II-B-5,2	
Root-Locus Plot, Reactor Control Loop		II-B-5,3	
6. Reactor Simulator Circuit			II-B-6,1
Analog-Computer Circuit Representation		II-B-6,1	
7. Simulator Responses			II-B-7,1
Transient Responses			
of Inner Reactor Loop to Step Input		II-B-7,1	
of Reactor Simulator to Ramp Input, T_c', T_{ro}, W_c		II-B-7,2	
of Reactor Simulator to Ramp Input, P_{fD}, T_c'		II-B-7,3	
III. COMPUTER-CONTROL SYSTEM ANALYSIS			III-A-1
A. Performance Criteria			III-A-1
1. Basis of Design			III-A-1
2. Criteria for Load Valve			III-A-1

TABLE OF CONTENTS (cont.)

		Table	Figure	Page
	3. Criteria for Gas-Farm Control Loop			III-A-2
	4. Criteria for Bleed-Line Flow Control Valve			III-A-2
	5. Performance Specifications			III-A-2
B.	Analytical Procedures			III-B-1
	1. Nonlinear Analysis			III-B-1
	2. Linear Analysis			III-B-1
C.	Nonlinear System Analysis			III-C-1
	1. General Equations - Test System Hardware			III-C-1
	2. Analog-Computer Setup			III-C-2
	3. Computer Results			III-C-2
	Nonlinear System Equations C-BEST System	III-C,1		III-C-4
	Coefficients for Equations, C-BEST System	III-C,2		III-C-9
	Steady-State Solution to Nonlinear (C-BEST) Equations	III-C,3		
	Performance-Time Characteristics, C-BEST System		III-C,1	
D.	Linear System Analysis			III-D-1
	1. Load Valve Control Loop			III-D-1
	2. Bleed-Line Control Loop			III-D-3
	3. Gas-Farm Valve Control Loop			III-D-3
	4. Turbine-Power Control Loop			III-D-4
	Block Diagram, Load Valve Control Loop		III-D,1	

TABLE OF CONTENTS (cont.)

	Table	Figure	Page
Flow Area as Function of Blade Angle, Load Valve		III-D,2	
Root-Locus Plot, Load Valve Control System		III-D,3	
Block Diagram, Bleed-Line Control Loop		III-D,4	
Flow Coefficient as Function of Valve Position, Bleed-Line Valve		III-D,5	
Root-Locus Plot, Bleed-Line Control System		III-D,6	
Block Diagram, Gas-Farm Valve Control Loop		III-D,7	
Effective Flow Area, Gas-Farm Valve		III-D,8	
Root-Locus Plot, Gas-Farm Control System		III-D,9	
Block Diagram, Turbine Power Control Loop		III-D,10	
Flow Area as Function of Blade Angle, TPCV		III-D,11	
Root-Locus Plot, Turbine Power Control System		III-D,12	
IV. TEST PROCEDURES			IV-A-1
A. Computer-Control System Checkout			IV-A-1
B. Test Procedures			IV-B-1

TABLE OF CONTENTS (cont.)

		Table	Figure	Page
V.	TEST RUNS			V-A-1
A.	Test No. 1.1-01-NXS-001			V-A-1
	LH_2 Pump Performance Characteristics		V-A,1	
	LH_2 Pump Heat Exchanger Performance		V-A,2	
	LH_2 Pump Heat Exchanger Performance		V-A,3	
	LH_2 Pump Heat Exchanger Performance		V-A,4	
	Mixing Section Performance		V-A,5	
	Turbine Performance		V-A,6	
B.	Test No. 1.1-01-NXS-002			V-B-1
	LH_2 Pump Performance Characteristics		V-B,1	
	LH_2 Pump Heat Exchanger Performance		V-B,2	
	LH_2 Pump Heat Exchanger Performance		V-B,3	
	LH_2 Pump Heat Exchanger Performance		V-B,4	
	LH_2 Pump Mix Section Performance		V-B,5	
	LH_2 Pump Turbine Performance		V-B,6	
C.	Test No. 1.1-01-NXS-003			V-C-1
	Hydra TPA Performance Characteristics		V-C,1	
	LH_2 Pump Heat Exchanger Performance		V-C,2	
	LH_2 Pump Heat Exchanger Performance		V-C,3	
	LH_2 Pump Heat Exchanger Performance		V-C,4	
	LH_2 Pump Mix Section Performance		V-C,5	
	LH_2 Pump Turbine Performance		V-C,6	
D.	Test No. 1.1-01-NXS-004			V-D-1
E.	Test No. 1.1-01-NXS-005			V-E-1
	LH_2 Pump Heat Exchanger Performance		V-E,1	
	LH_2 Pump Heat Exchanger Performance		V-E,2	
	LH_2 Pump Heat Exchanger Performance		V-E,3	

TABLE OF CONTENTS (cont.)

		Table	Figure	Page
	LH_2 Pump Heat Exchanger Performance		V-E,4	
	LH_2 Pump Mix Section Performance		V-E,5	
	LH_2 Pump Performance Characteristics		V-E,6	
	Reactor Simulator Outputs		V-E,7	
	Valve Positions		V-E,8	
	Valve Error Signals		V-E,9	
F.	Test No. 1.1-01-NXS-006B			V-F-1
	LH_2 Pump Performance Characteristics		V-F,1	
	LH_2 Pump Heat Exchanger Performance		V-F,2	
	LH_2 Pump Heat Exchanger Performance		V-F,3	
	LH_2 Pump Heat Exchanger Performance		V-F,4	
	LH_2 Pump Mix Section Performance		V-F,5	
	LH_2 Pump Turbine Performance		V-F,6	
	Valve Positions		V-F,7	
	Reactor Simulator Outputs		V-F,8	
	Valve Error Signals		V-F,9	
G.	Test No. 1.1-01-NXS-007			V-G-1
H.	Test No. 1.1-01-NXS-008			V-H-1
	LH_2 Pump Suction Conditions		V-H,1	
	LH_2 Pump Discharge Conditions		V-H,2	
	LH_2 Pump Performance		V-H,3	
	Line Load Valve Performance		V-H,4	
	Heat Exchanger Inlet and Outlet Pressures		V-H,5	
	Heat Exchanger Inlet and Outlet Temperatures		V-H,6	

TABLE OF CONTENTS (cont.)

	Table	Figure	Page
Heat Exchanger Flow Rate		V-H,7	
Heat Exchanger Fluid Bulk Temperature		V-H,8	
Heat Exchanger Wall Temperatures		V-H,9	
Mixing Section Outlet Conditions		V-H,10	
Turbine Inlet and Exhaust Conditions		V-H,11	
Turbine Performance		V-H,12	
Reactor Simulator Outputs		V-H,13	
Valve Positions		V-H,14	
Valve Error Signals		V-H,15	
VI. ANALYSIS OF TEST RESULTS			VI-A-1
A. Correlation of Test Results			VI-A-1
Flow-metering Equations	VI-A,1		VI-A-3
Correlation of Flow Rates	VI-A,2		
B. Turbopump Performance			VI-B-1
Turbopump Performance, Test 1.1-01-NXS-008	VI-B,1		VI-B-1
Turbine Efficiency as Function of Velocity Ratio		VI-B,1	
C. Heat Capacity Heat Exchanger Performance			VI-C-1
Heat Transfer Rate and Heat Flux		VI-C,1	
Heat Transfer Coefficients		VI-C,2	
Fluid Conditions at Heat Exchanger Inlet		VI-C,3	

TABLE OF CONTENTS (cont.)

	Table	Figure	Page
VII. CONCLUSIONS AND RECOMMENDATIONS			VII-A-1
A. Heat-Capacity Startup			VII-A-1
B. Propellant Feed System Operation			VII-B-1
C. Computer Control System Operation			VII-C-1
VIII. NOMENCLATURE			VIII-1

APPENDIX A - LINEARIZATION OF NEUTRON KINETICS EQUATIONS

APPENDIX B - ANALYTICAL AND EXPERIMENTAL DETERMINATION OF CONTROLLER-TRANSFER FUNCTIONS

SECTION I

INTRODUCTION

I. INTRODUCTION

A. BACKGROUND

During the NERVA Engine proposal effort of Aerojet in early 1961, Aerojet-General Corporation undertook a test program to gain operating experience and experimental data pertaining to the operation of a liquid-hydrogen propellant-feed-system in a nuclear rocket engine.

The principal parts of the experimental feed system used in this program consisted of a centrifugal-type, liquid-hydrogen pump driven by a two-stage, impulse turbine, both components possessed the performance characteristics required for a NERVA Engine employing the cold-bleed cycle. To demonstrate the feasibility of heat-capacity startup, turbine fluid was bled from the pump discharge line and passed through an aluminum mockup of a reflector segment. A highly pressurized source of gaseous hydrogen was available to supply power to the turbine when the thermal capacity of the aluminum heat exchanger was exhausted.

In order to regulate both the power input to the turbine and the pump load in accordance with the startup conditions in a nuclear rocket engine, a small portable analog computer was set up to simulate factors of reactor kinetics and heat-transfer and fluid dynamics in both reflector and reactor. It was anticipated that pump discharge pressure would be fed into the computer, and computer outputs transferred to the physical system by means of four servo-actuated, flow-control valves.

The resulting system, called the Cold-Bleed Engine Simulation Test System (C-BEST), was tested in March 1961 with several pump tests and two heat-capacity start tests. Failure of two power supplies in the portable analog computer ruled out the use of that equipment in that test series because of the lack of spares, and because the test schedule allowed insufficient time for repairs. Some results of C-BEST tests are included in this report since they are pertinent to the analysis of the Generation I Engine Simulator.

After award to Aerojet of Contract SNP-1 for design of the NERVA Engine, the C-BEST system was revised to form the Generation-I Engine Simulator System which was tested in September and October of 1961, to fulfill the contractual obligation of Task Item 10, Contract SNP-1.

Major changes from the C-BEST configuration included insertion of a second-generation turbopump, placement of the heat exchanger in a vertical

position, addition of thermocouples in intermediate locations in the heat exchanger, provision for longer flow-straightening sections ahead of flow-measuring orifices, and improvements of the overspeed safety system. Based upon additional data pertaining to the dynamic performance of the reactor control loop, which had become available from analyses conducted for the NERVA Proposal effort, the original analog-computer circuit was revised. An additional power supply was added to eliminate the previously incurred overload condition, the two power supplies that had previously failed were repaired, and the portable computer was entirely reworked to reduce the possibility of ground loops. Furthermore, experimental frequency responses were run on the flow-control valve servo-actuators after the conclusion of the C-BEST tests.

In consideration of the design revisions and the new information available from both C-BEST and actuator tests, it was necessary to treat the Generation-I Engine Simulator as a completely new system so far as the analysis of system performance and control system design was concerned.

B. TEST PURPOSES AND OBJECTIVES

One major purpose of the Generation I Engine Simulator was to demonstrate the feasibility of initiating turbopump "bootstrapping" by utilizing the thermal energy available in the propellant-feed system and, especially, in the reflector of the engine prior to the time radiation heating becomes significant (in the NERVA engine, all the propellant flows through the reflector). Lack of time and funding factors did not permit the construction of a full-scale simulated reflector. However, a properly designed reflector segment could be used to heat turbine-drive fluid because the thermal capacity of the segment would have the same proportionality to the total heat capacity of the reflector as turbine flow would have to the total flow through the reflector.

The second major purpose of the test system was to gain data and operating experience with a full-scale, liquid-hydrogen propellant-feed system during a start transient; information that was directly related both to the design of the propellant feed system, and to the analysis and design of the NERVA engine control system. It was necessary to obtain knowledge concerning the effect of various pump inlet pressures on the start transient, and on the bootstrap capability of the pump; in addition, experimental data concerning the dynamic response of the propellant feed system to variations of pump load and turbine energy was required for the NERVA engine dynamic analysis. During engine startup, and after the engine reactor reaches a power level sufficient to vaporize the propellant in the reflector, the propellant feed system is subjected to an increasing pump load simultaneously with an increasing energy input to the turbine. In order to produce these two related events, and to investigate the effects on turbopump bootstrapping of a continuous rise in reactor power, a small portable analog computer was provided to simulate, in real-time, the effects of reactor heat transfer and fluid dynamics. Although the inadequacy of such a small computer was recognized, still, it was considered useful as an adjunct in achievement of the test objectives. Furthermore, since the NERVA program called for the design of a much more sophisticated engine simulator involving an analog computer, and since Aerojet had never before attempted partial system testing of an engine, use of this smaller computer was felt to be justified in acquiring practical knowledge and experience attending the problems of integrating physical components with an analog computer to achieve simulated system performance.

Another purpose of the test system was to investigate the transient heat-transfer characteristics of the simulated reflector segment, as a supplement to a theoretical analysis of heat transfer to boiling liquid hydrogen at pressures below the critical point. The analysis was aimed at determining the mechanism of two-phase flow instability, if it existed, and to derive a set of equations describing the boiling process that would be applicable to the analog computer study of the startup control problem.

C. DESCRIPTION OF TEST SYSTEM APPARATUS

The general configuration and relative locations of components of the Generation-I Engine Simulator is shown in Figure I-C, 1. Propellant flow was initiated by pressurizing the LH_2 tank with gaseous hydrogen. A regulating system on the tank was provided to hold the tank pressure, as preselected for a given test, to within a specified tolerance of ±0.5 psi.

Fluid left the pump and passed through a vaned, flow-straightening section, and through a square-edged flow-metering orifice, 3.807 inches in diameter. Part of the flow entered the bleed line, and the rest went through a parallel section, one branch of which contained a 2.35-in.-dia., square-edged orifice (ΔP_{fYo}), and the other a 5-in. butterfly valve (the load valve) which could be positioned by a servo-controlled hydraulic actuator. The bypass orifice was provided to avoid any possibility of unloading the pump in the event of load-valve closure. Following the bypass section, the hydrogen entered a duct, 140-ft long, and was burned off at the end.

The bleed-line flow passed first through a square-edged orifice, 1.25-in.-dia, (ΔP_{BPO}), and then through the bleed-line valve. Downstream from the bleed-line valve, the fluid entered at the bottom of the heat-capacity heat exchanger placed vertically in the test stand.

A check valve was initially installed at the heat-exchanger exit to prevent gaseous hydrogen (which entered the mixing section from the gas farm) from blowing back through the bleed line to the discharge line where it could, by vaporizing the liquid propellant, unload the pump.

A mixing section was provided to allow thermal mixing of liquid and gaseous hydrogen, which enters, respectively, from the bleed line and from the line to the gas-farm. Since in the gas-farm, hydrogen gas was stored at 2600 psig, gas pressure was reduced to, and maintained at, 800 psig, by three pressure regulators upstream of the ΔP_{GH2S} flow-metering orifice (2.15-in. diameter, square-edged). The gas-farm valve controlled the flow of gaseous hydrogen.

The turbine supply line contained the turbine power control valve, a square-edged orifice, 2.25-in.-dia, and a turbine safety shutoff valve, in that order, and terminated at the turbine nozzle.

The portable analog computer, which was used for reactor simulation, consisted of two consoles containing 18 dc chopper-stabilized operational amplifiers. Of the 18 amplifiers, four were used as error detectors, as indicated in

Figure I-C, 1, in the servo loops, and the remainder were used for reactor simulation. The Universal Sequence unit, part of the facility at Test Stand C-6, was used to transfer control signals between the computer and the test stand. The patchboard in the sequence unit allowed a flexible setup whereby individual servo loops could be easily checked out prior to test, and facilitated test operations by permitting control functions to be changed at the control console.

Figure I-C, 2 shows an instrumentation diagram of the system, while instrument ranges are given in Table I-C, 1. Based upon studies made by the Instrumentation Dept. of the Test Division, Liquid Rocket Plant, AGC, it was concluded that the maximum expected error in pressure transducers is $\pm 0.48\%$ of the point, and includes errors due to transducer inaccuracies, as well as those in the data acquisition system. These same studies show that a maximum error of $\pm 0.44^{\circ}F$ in temperatures was obtained with platinum-element resistance probes, however, the data from Generation-I tests indicates discrepancies of 1 to 4° in temperatures below $-400^{\circ}F$. The platinum resistance probes were used to measure LH_2 temperatures, whereas copper-constantin thermocouples were used for higher temperature ranges, as indicated in Table I-C, 1. The accuracy expected of the c-c thermocouples was $\pm 1^{\circ}F$ for temperatures down to approx. $-300^{\circ}F$.

The above mentioned studies indicate that turbine-type flow meters for service have maximum errors of $\pm 0.85\%$. However, the flow meter used in Generation-I engine simulator tests was volumetrically calibrated with water, therefore, as indicated above, the measured temperatures of LH_2 may have been in error by a few degrees. Thus, mass flow rates calculated according to flow meter readings would be 10 to 15% in error because of the error involved in picking LH_2 density from a T-S diagram.

TABLE I-C, 1

INSTRUMENTATION FOR GENERATION-I ENGINE SIMULATOR*

Function	Range				
	psig	°F	lb/sec	rpm	Pot
P_{fT}	0 - 100				
P_{fs}	0 - 100				
P_{fD}	0 - 1000				
ΔP_{fDo}	0 - 200				
P_{fYo}	0 - 1000				
ΔP_{fYo}	0 - 200				
P_{LLVi}	0 - 1000				
P_{LLVo}	0 - 1000				
P_{BPo}	0 - 1000				
ΔP_{BPo}	0 - 500				
P_{BFCVi}	0 - 1000				
P_{Hei}	0 - 1000				
P_{Heo}	0 - 1000				
P_{GH_2S}	0 - 1000				
ΔP_{GH_2S}	0 - 500				
P_{GH_2CVi}	0 - 1000				
P_{GH_2CVo}	0 - 1000				

TABLE I-C,1 (cont.)

Function	Range				
	psig	°F	lb/sec	rpm	Pot
P_{msi}	0 - 1000				
P_{mso}	0 - 1000				
P_{TS}	0 - 1000				
ΔP_{TS}	0 - 500				
P_{Ti}	0 - 1000				
P_{Te}	0 - 100				
T_{fT}		-430 to -300			
T_{fFM}		-430 to -300			
T_{fS}		-430 to -300			
T_{fD}		-430 to -300			
T_{fYo}		-430 to -300			
T_{BPO}		-430 to -300			
T_{Hei}		-430 to -300			
T_{Heo}		-300 to +100			
T_{GH_2S}		0 to +100			
$T_{GH_2VO(O)}$		0 to +100			
T_{msi}		-300 to +100			
T_{mso}		-300 to zero			

TABLE I-C, 1 (cont.)

Function	Range				
	psig	°F	lb/sec	rpm	Pot
T_{Ts}		-300 to zero			
T_{Ti}		-300 to zero			
T_{Te}		-300 to zero			
F_{MF}			0 - 100		
L_{LLV}					Pot
L_{TPCV}					Pot
L_{BFCV}					Pot
L_{GH_2CV}					Pot
L_{FSV}					Pot
$T_{g\ 1-6}$		Amb to -400			
$T_{w\ 1-6}$		Amb to -400			
T_{LLVo}		-300 to -430			
P_{fDe}	0 - 100				
T_{fDe}		-300 to -430			
N_T				0 - 30,000	

TABLE I-C, 1 (cont.)

For analog computer operation

Function	Range psig	Range °F	Remarks
P_{fD}	0 - 1000		Set gain to 0.010 volts/psi
ΔP_{fDo}	0 - 100		Set gain to 0.100 volts/psi
P_{mso}	0 - 1000		Set gain to 0.010 volts/psi
T_{mso}		+100 to -320	Amplify with Kintel Model 110 or 111. Gain setting of 70.

*For instrument locations, see Figure I-C, 2.

LEGEND

1. SAFETY VALVE
2. TURBINE FLOW METER
3. FUEL SUCTION VALVE
4. PUMP
5. TURBINE
6. LOAD VALVE
7. BLEED-LINE VALVE
8. HEAT-CAPACITY HEAT EXCHANGER
9. CHECK VALVE
10. MIXING SECTION
11. TURBINE CONTROL VALVE
12. GAS-FARM CONTROL VALVE
13. SERVO AMPLIFIER
14. TURBINE SHUT-OFF VALVE

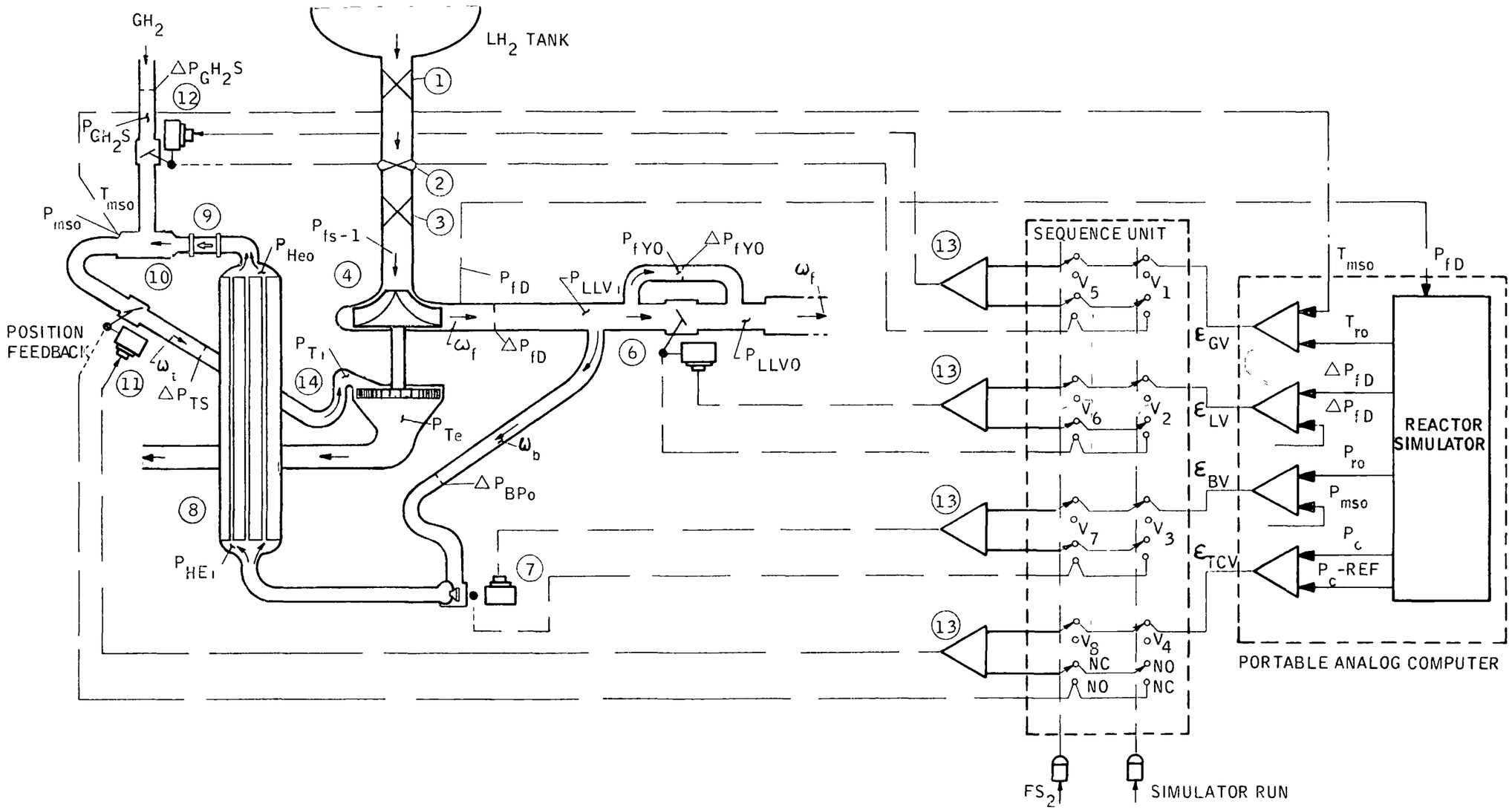

GEN. I ENGINE SIMULATOR SCHEMATIC DIAGRAM

Figure I-C,1

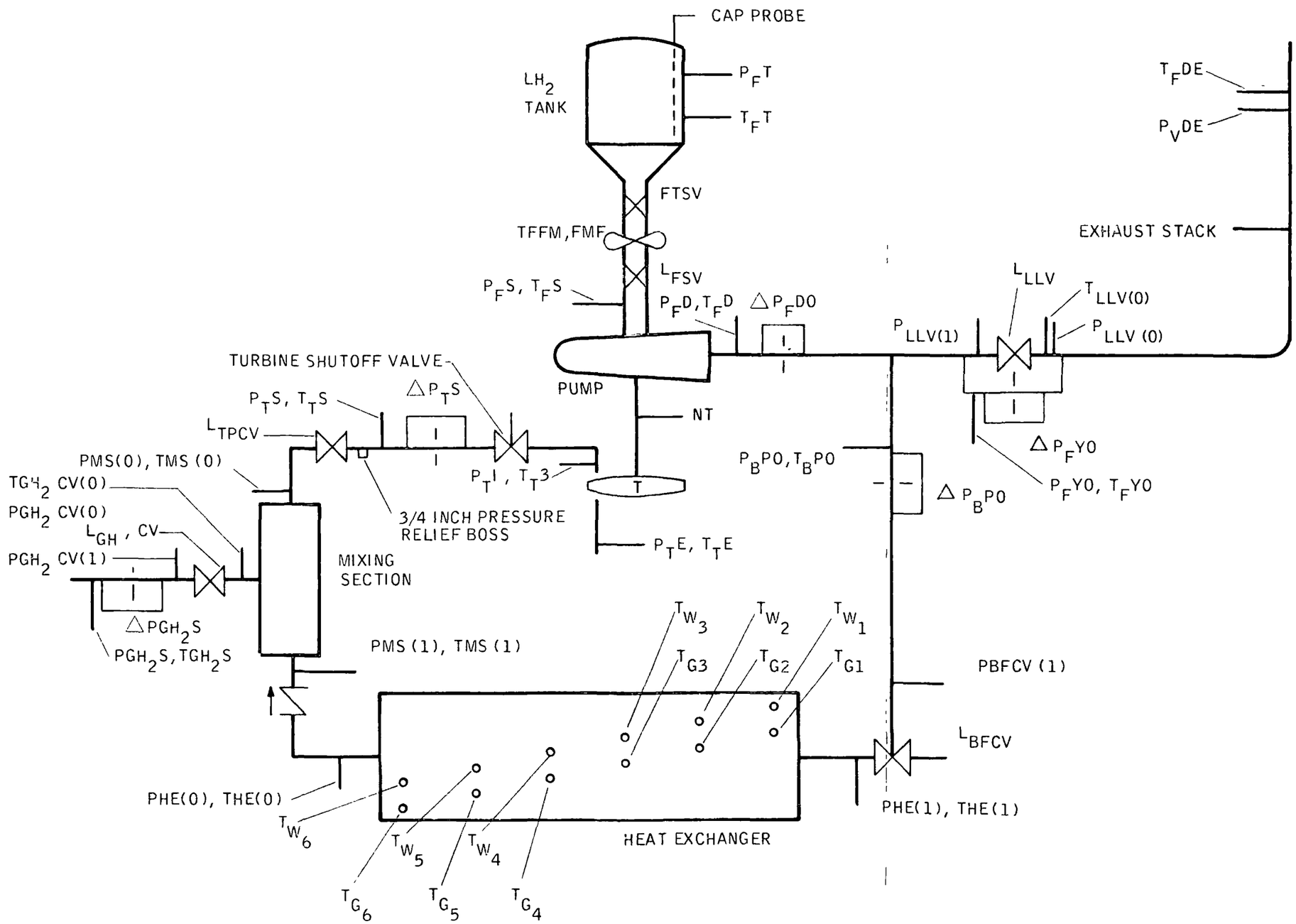

GEN. I ENGINE SIMULATOR SYSTEM INSTRUMENTATION DIAGRAM

Figure I-C,2

D. TEST SYSTEM OPERATION

1. Heat-Capacity Start Tests

In the first series of heat-capacity start tests, the analog computer was inoperative. The gas-farm valve remained closed at all times during these tests, while the bleed-line valve remained open. The turbine-power control valve (TPCV) remained either completely open or at a predetermined position. Similarly, the load valve remained fixed at a predetermined position, such that the resistance to flow of the parallel pipe section corresponded, approximately, to the resistance of the nuclear engine. The flow control valve positions were maintained by the hydraulic servo-actuators which received position commands from the sequencing unit. As Figure I-C, 1 illustrates, the set of relays operated by the "simulator run" switch were not energized for heat-capacity start tests; consequently, they were in the normally closed position so that the fixed voltages V_1 to V_4 were applied to the servo-actuators, which were made positional since the position feedback loops were also closed.

Prior to the start of a test, which was initiated by opening the fuel suction valve, the safety valve was opened to allow the suction line to be cooled by liquid hydrogen. Tank pressure could be maintained at any desired level to provide a net positive suction pressure (NPSP). A portion of the hydrogen flowing through the pump entered the bleed-line where it acquired additional heat in the heat-capacity heat exchanger on its way to the turbine. Sufficient thermal energy was imparted to the fluid by the pump, lines, and reflector segment (heat exchanger) to drive the turbine. However, as the suction line and pump were cooled to the temperature of LH_2, the load on the pump increased, while the energy available at the turbine decreased; consequently, turbopump speed rose to a peak, then decayed.

The level of propellant in the tank was monitored by means of a capacitance probe and when the level in the tank dropped to 15%, shutdown (FS-2) was initiated. On FS-2, the second set of relays in the sequence unit were energized, a new set of input voltages, V_5 - V_8, were applied to the servo amplifiers to position the valves for the shut down operation.

2. Computer-Controlled Test

The start of a computer controlled test was identical to the start of a heat-capacity start test. From the start at FS-1, the computer processed the signals from the pressure and temperature transducers, but the flow control valves were held to pre-set positions by the sequencing unit, that is, the

simulator-run switch was not closed. Not until stable LH_2 appeared at the pump exit, assuring a load on the pump, was control of the test system transferred to the analog computer. Control was transferred at the control room console by closing the simulator-run switch which operated the relays in the sequencing unit. When these relays were energized, the signals from the error detecting amplifiers in the computer were applied directly to the servo-valve amplifiers. Simultaneously, the positional servos were converted to velocity controllers by removal of the valve position feedback signals. The reason for delaying computer takeover was to avoid the possibility of applying auxiliary power from the gas farm to the turbine while the pump was unloaded.

The primary input to the computer was pump discharge pressure (P_{fD}), as a voltage. The computer circuit was set up to solve, in real time, the equations describing fluid dynamics, heat transfer, and neutron kinetics in the nozzle, reflector, and reactor. As the result of applying pump discharge pressure to the computer, computer voltages were generated which could be considered to represent real engine variables such as chamber pressure and temperature, total flow rate, and pressure and temperature at the inlet to the TPCV.

3. Reactor-Simulator Control

The Reactor Simulator included the entire control loop, one of the two primary engine control systems. The Engine Programmer (which, in the real engine, programs the reference inputs of chamber pressure and temperature for the engine control systems) was also simulated. On transferring control of the test system to the Reactor Simulator, the simulated Engine Programmer started a programmed rise in P_c and T_c references, and the variables in the Reactor Simulator followed this program. The other primary control loop, which took thrust-chamber pressure (P_c) as a reference, regulated P_c through the TPCV, which controlled pump discharge pressure. Part of the latter loop was real, since it included the prototype TPCV and the turbopump, while part of it was simulated, since P_c and $P_{c\text{ - ref.}}$ were generated in the computer, though the computed value of P_c was a direct function of pump discharge pressure.

Pressures and temperatures generated as voltages in the computer were references against which the actual values, appropriately transduced and scaled, were compared. Any errors that existed were reduced to zero by the four flow-control valve servo-actuators. One output of the computer was the analog solution for total weight flow rate (w_r), which reflected the resistance to flow caused by a rise in reactor power. The flow rate was compared to actual pump delivery (w_f), as measured by the differential pressure drop across the orifice at the pump exit (Figure I-C, 1), and any error was reduced to zero by the servo actuated load valve, with the result that actual pump delivery closely followed computed flow rate.

The bleed-line and gas-farm valves acted together to control pressure and temperature at the inlet to the TPCV. Control of temperature was accomplished by comparing actual fluid temperature (T_{mso}) with the analog solution for reflector outlet temperature resulting from heat transferred to the propellant in the reflector. Admission of warm gas to the test system, by the gas-farm valve, compensated for the lack of radiation heating in the test apparatus. Pressure control was obtained in a similar way by using the error between actual pressure (P_{mso}) and computed pressure (P_{ro}) to position the bleed-line valve.

These three valves (TPCV, and gas-farm and bleed-line valves) were necessary to transfer computer outputs to the test system, that is, to load the pump and to condition the turbine drive fluid in accordance with conditions in the real engine. However, the TPCV was a component of the real engine and, as such, controlled turbopump speed.

Chamber pressure (P_c) was computed as a function of actual pump discharge pressure and compared with P_{c-ref}, which was also generated in the computer, and the error, if any existed, actuated the TPCV servo system. Since the computed chamber pressure was a direct function of actual pump discharge pressure which was controlled, indirectly, by the TPCV, the turbine power control loop was a direct representation of the corresponding loop in the real engine. The Load, Bleed-Line, and Gas-Farm flow-control valves served only to transfer computer outputs to the propellant feed system.

The function of the computer was to relate the load imposed on the pump by reactor heating to the energy input at the turbine, which was also a function of reactor power output.

SECTION II

SYSTEM DESIGN

II. SYSTEM DESIGN

A. SELECTION AND DESIGN OF PHYSICAL COMPONENTS

As indicated in paragraph I, A, the C-BEST system was revised to form the Generation-I Engine Simulator system in order to carry out the contractual obligation of Task Item 10 of Contract SNP-1. At the time that the C-BEST system was designed, the heat-capacity heat exchanger was designed as a reflector segment for heating the turbine drive fluid, with the object of minimizing the cost of the system.

When the C-BEST system was reviewed for adaptation to the Generation I Simulator, it was realized that a full-scale reflector would provide more realistic engine conditions. However, the cost involved ($120,000) and the time to fabricate a full-sized aluminum reflector were overriding considerations. In addition, the more sophisticated Generation-II system was planned for Phase II of the NERVA program, and was being fabricated. Consequently, it was decided to continue with the C-BEST system, but to improve its instrumentation system and to increase the safety provisions. Some of these modifications have been previously listed, and other design considerations are included in the following component descriptions·

1. Pump Suction Line

In the C-BEST system, the existing suction line at the test facility was approximately 20 feet long and designed for high pressure, therefore, it contained a considerable mass of material. In addition, the tank shutoff valve was located about 10 feet from the pump inlet. These factors caused an unrealistically large heat input to the liquid hydrogen during startup, since the mass of material between the shutoff valve and the pump inlet could not be pre-chilled prior to startup without also pre-chilling the pump.

So that this unrealistic heat input problem could be eliminated for the contractual tests, a new line and valve combination was designed, but costly facility modifications would have been required if a true mock-up of the NERVA line and tank shut-off combination were installed. As a compromise, a 5-in. butterfly valve was installed approximately 20 in. above the pump inlet - this short section of pipe representing the NERVA suction line - and another safety shutoff valve was installed at the tank outlet. The use of two valves in the suction supply line allowed the line to be cooled prior to a test, and also provided a margin of safety in the event one valve failed during an emergency shutdown.

A 10-in. Potter mass flowmeter was located between the two valves. Although equipped to measure mass flow rate, the flowmeter was used to measure volumetric flow only.

2. Turbopump

The pump and turbine were mounted on a common shaft, using oil lubricated bearings, which were heated electrically to prevent lubricant freezing.

An 11.9-in.-dia aluminum impeller, designated as a "second-generation" part, was used in this centrifugal pump. It was radial bladed, had inducer vanes at the suction end, and a suction diameter of 7-in.

A three-stage, pressure compounded, full admission turbine was used in the Generation-I system. The total throat area of the first-stage nozzle was 1.87 in.^{2}, and the mean blade diameter was 10.98 in.

3. Heat Capacity Heat Exchanger

Design of a heat capacity heat exchanger, to simulate the engine neutron reflector for the Generation-I Engine Simulator, required establishing temperatures and pressures of the fluid at the exit of the heat exchanger identical, at any time, with similar properties of the fluid at the exit of the engine reflector. that is, the instantaneous heat-exchanger pressure drop and rate of fluid heating should always be the same as for the reflector.

a. Heating the Simulated Reflectors

Since there was no nuclear heat generation in the simulated reflector, methods of heating the simulated reflector had to be considered, all were discarded because of cost and complexity. In addition, a heat-capacity type of heat exchanger provided good startup simulation of the effects of the engine reflector. The total heat capacity of the beryllium and graphite reflector, between ambient air temperature (520°R) and LH_2 temperature (50°R), was calculated to be 217,640 Btu. Based upon a typical startup schedule (see Ref. 1), it was found that the power generated in the reflector was 4.6 Mw (see Ref. 2) 15 seconds after the beginning of a 30-sec turbopump startup, or approximately 34,000 Btu generated by nuclear heating during this period. Since this was only 16% of the energy stored as heat capacity, it was postulated that, for the first 15 sec of the startup, no simulation of the nuclear heating effect was necessary.

b. Cost Factors of Simulation

The cost of beryllium created another problem of simulation. Sufficient funds were not available to construct a heat exchanger of beryllium in the exact shape of the engine reflector. The first decision, therefore, was to build the heat exchanger as a segment of the engine reflector. Because only a percentage of the available fluid was used to drive the turbine, it was decided to build a heat exchanger to match only that segment of the reflector through which the turbine drive fluid passed. At the time the system was originally designed, the cold-bleed engine cycle was the basis for scaling the heat-exchanger. In that cycle, turbine weight flow was 13 lb/sec out of a total of 83 lb/sec. Thus, a heat exchanger in the ratio of 13/83, or approximately 1/6 scale, was designed. Since the cost of even this 1/6 scale heat exchanger would still have been prohibitive if it were constructed of beryllium, it was decided to construct the heat exchanger of aluminum. Although originally chosen largely because of availability, subsequent investigation has shown that aluminum provides the best available simulation of the thermal properties of beryllium.

c. Comparison of Possible Heat-Exchanger Materials

Table II-A, 1 shows a comparison of the thermal properties of aluminum, beryllium, and some other materials. The heat capacity of the aluminum heat-exchanger is 34,260 Btu between 50°R and 520°R, while the heat capacity of 13/83 of the reflector is 34,083 Btu, so the available heat capacities are nearly the same.

Additional work to analyze the effect of substituting aluminum for beryllium has been accomplished for the Generation-II Engine Simulator. These results are also applicable to the Generation I system. From Figure II-A, 1, which shows heat capacity as a function of temperature relative to 50°R for both aluminum and beryllium, it can be seen that equal amounts of cooling will produce almost equal material temperatures, down to approximately 250°R. Since the heat exchanger is not cooled to this temperature until about 16 seconds after flow initiation, the substitution of aluminum for beryllium is valid for this interval.

The problem remains of insuring that the rate of heat removal, or the heat-transfer rate, is equivalent for both the aluminum heat exchanger and the beryllium reflector. In Figure II-A, 2, which compares the computed temperatures of equal sections of beryllium and aluminum cooled at the rates indicated by the C-BEST test data, temperatures as a function of time are seen to be very nearly the same for both materials. This is partially because the

thermal properties, as represented by the inverse thermal diffusivity shown in Figure II-A,3, and the thermal conductivity shown in Figure II-A,4, are very close above 300°R, but more importantly, because the major thermal resistance is the fluid heat transfer coefficient which, for equal geometries and wall temperatures, is the same for both materials. Thus, equal heat extraction will give equal material temperatures and, for these equal wall temperatures, equal flow geometries will result in equal cooling rates.

d. Flow Geometry of Heat Exchanger

The heat-exchanger pressure drop also depends on flow geometry and wall temperature, and, to obtain equal pressure drop as well as equal heat transfer, the flow geometry of the heat exchanger should be equal to that of the reflector. Since full information concerning the reflector geometry was not available when the heat exchanger was designed, calculations were performed to determine a hole size which would give a pressure drop equal to the computed reflector pressure drop. Based upon these calculations, 200 3/16-in.-dia. holes, as shown in Figure II-A,5, were calculated to be proper for the heat capacity heat exchanger.

Thermal capacitance was provided by 52 1-in.-thick by 11.5-in.-dia. aluminum discs, housed in a 5/8-in. thick stainless steel case with flanged and bolted heads. The holes were aligned by two rods piercing all plates, and were oriented in eight concentric circles, numbered outward from the center.

Six CC thermocouples, evenly spaced for the length of the heat exchanger, extended into six of the 41 holes in the seventh circle of fuel passage holes to record hydrogen temperatures. In addition, six similarly located CC thermocouples extending toward the same holes were positioned 0.05 to 0.07-in. short of the coolant holes to record the wall temperature.

4. Mixing Section

The mixing section was 5-in-dia. by 27-in. pipe, of Schedule 40 stainless steel. Flow from the heat-capacity heat exchanger was directed axially through the mixing section, and the gas-farm supply was introduced into the mixing section at right angles near the upstream end.

5. Turbine-Power-Control and Shutoff Valves

The TPCV, designed specifically for the NERVA engine, was a 3-in. butterfly valve, and was hydraulically operated. The detailed specifications

of the electro-hydraulic servo-actuator are given in Appendix B. The actuator had been used in the C-BEST system, but the TPCV replaced the 4-in. valve previously used, which had been designed for the second stage of the Titan missile.

A turbine-supply shut-off valve, located downstream from the TPCV, consisted of a plug which could be driven shut by an electrically detonated explosive charge, and was included as precautionary measure to prevent destruction of the turbopump in the event of an overspeed. It could close in 0.006 sec. after receipt of an electrical signal, either from the overspeed trip system or from the control console.

6. Flow-Control Valves and Servo-Actuators

All three of the flow-control valves and their electrohydraulic servo-actuators had also been used in the C-BEST system. Detailed specifications of the servo-actuators are given in Appendix B.

The load valve (LV) was a 5-in. XLR-87 (Titan) butterfly valve, modified for hydrogen service.

The bleed-line valve (BLV) was a modified XLR-87, gas-generator, double-poppet-type valve. Flow was allowed through both the oxidizer and fuel ports of the valve.

The gas-farm valve (GFV) was a modified XLR-91 3-in. butterfly valve.

The details of the actuator-valve driving linkages are given in Appendix B. Since the actuators had been designed for proof pressures of 1000 psi, it was necessary to operate the cylinders with hydraulic supply pressure of 800 psig, although the servo-valves were rated for 3000 psi.

TABLE II-A,1

THERMAL PROPERTIES AT 520°R OF MATERIALS

Material	Specific Heat C_p Btu/lb°R	Density ρ lb/in.^{3}	$C_p \rho$ Btu/in.^{3}°R	Thermal Conductivity K Btu/in.-sec°R	Inverse Thermal Diffusivity $1/\alpha$ sec/in.^{2}
Aluminum	0.215	0.0978	0.0210	0.00205	10.2
Beryllium	.43	.0658	.0283	.00223	12.7
Copper	.092	.324	.0298	.00517	5.75
Paraffin	.69	.032	.0221	.0000034	6580
LiH	.98	.0284	.0278	.000099	280
Stainless Steel	.108	.287	.0310	.000178	174
Mild Steel	.100	.283	.0283	.000857	33
Titanium	.125	.16	.0200	.000141	142
White Pine	.42	.0144	.0060	.0000167	360
Maple	.42	.0246	.0103	.0000202	394

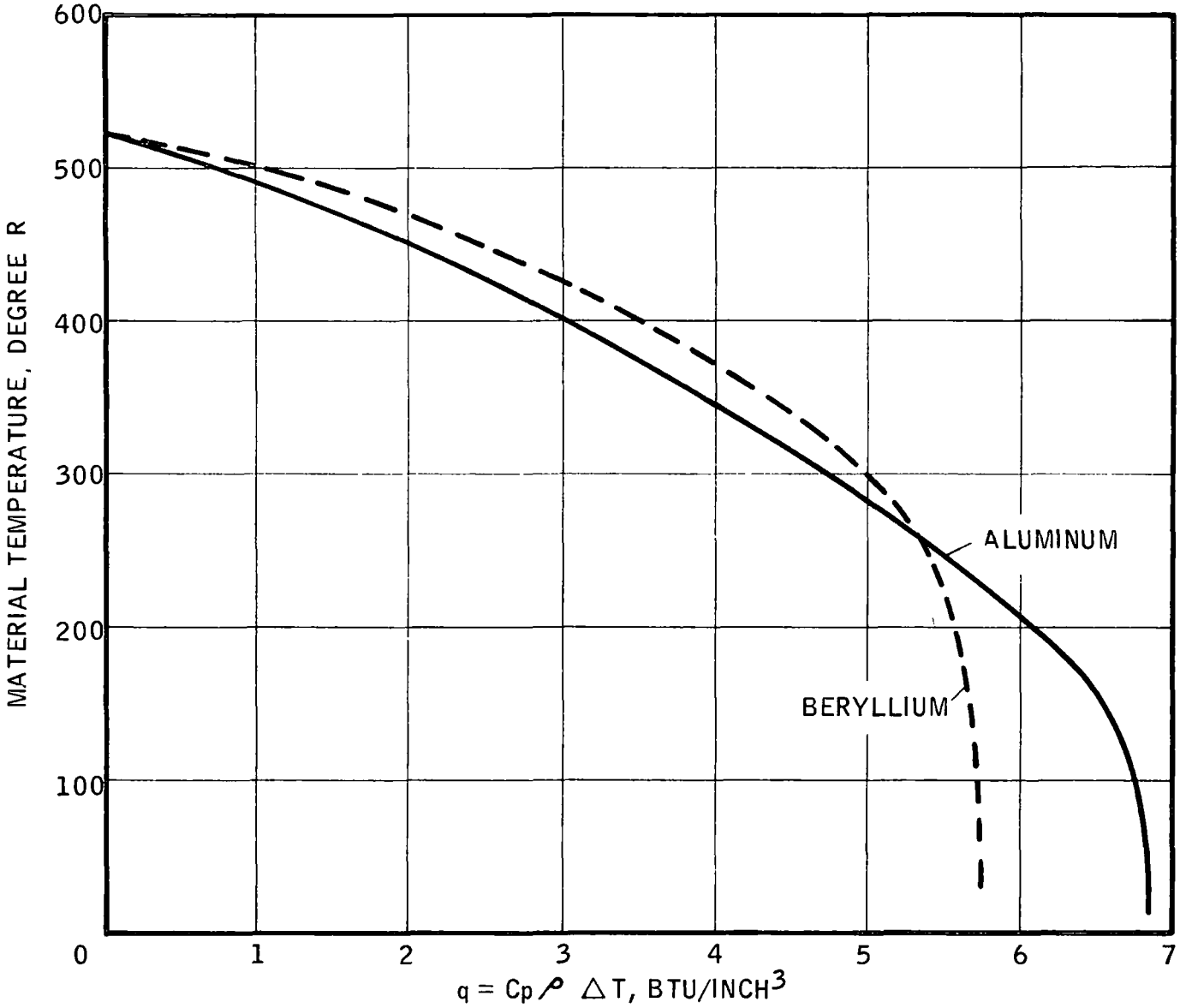

ENERGY EXTRACTED PER UNIT VOLUME, q ,
AS A FUNCTION OF TEMPERATURE

Figure II-A,1

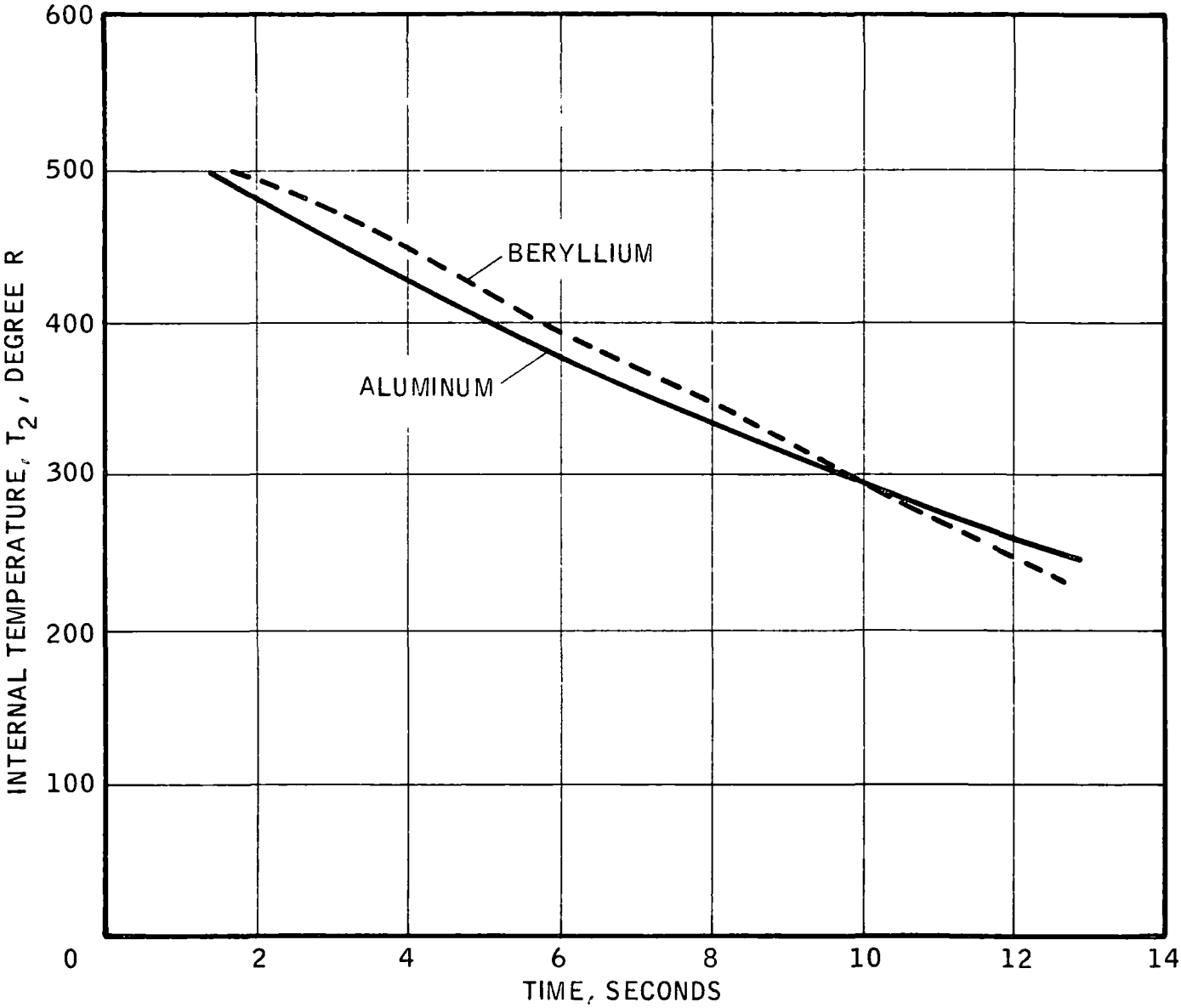

COMPARISON OF INTERNAL TEMPERATURE, T_2,

AS A FUNCTION OF TIME FOR BERYLLIUM AND ALUMINUM

Figure II-A.2

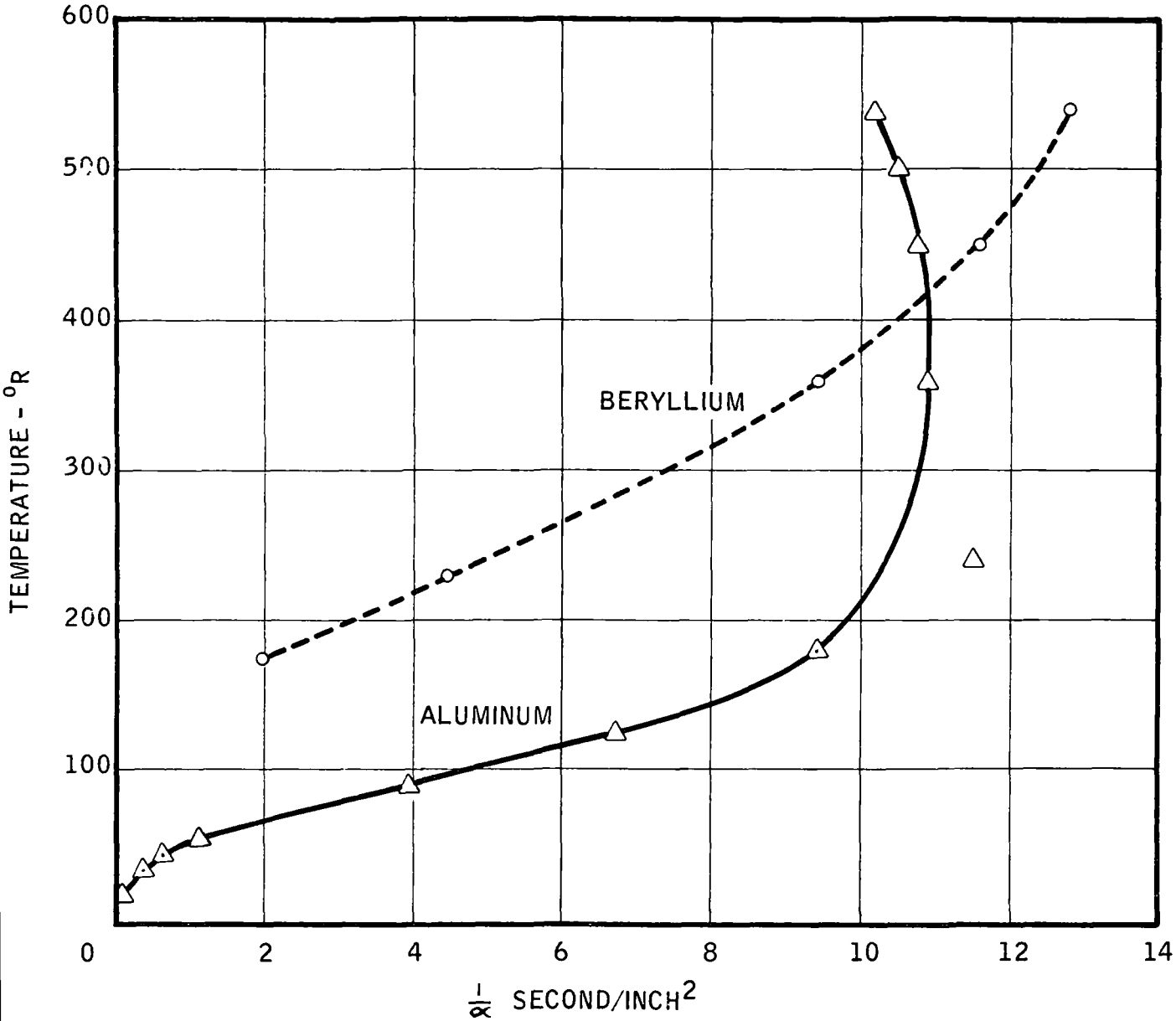

INVERSE THERMAL DIFFUSIVITY $\frac{1}{\alpha}$, AS A FUNCTION OF TEMPERATURE

Figure II-A,3

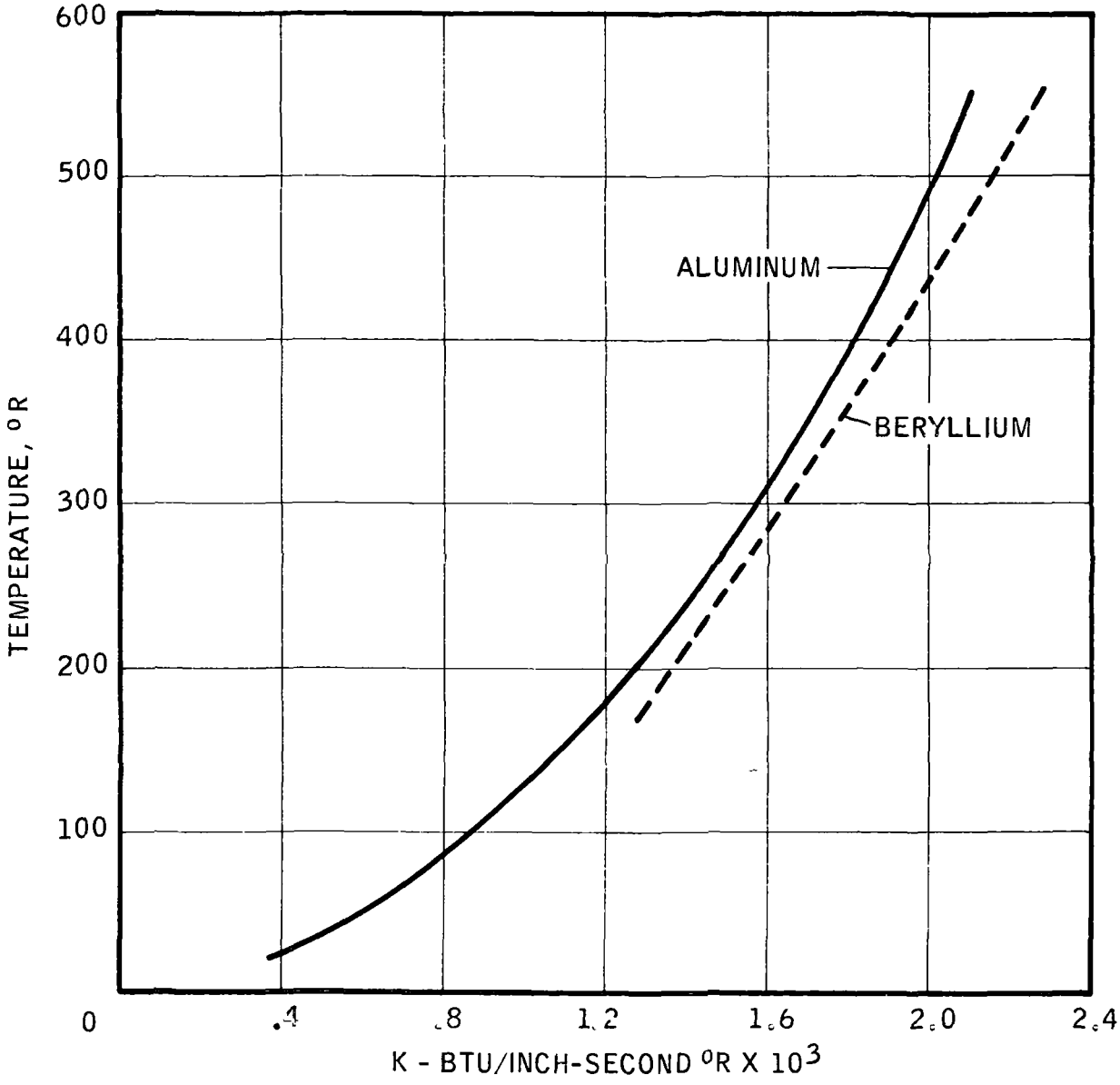

THERMAL CONDUCTIVITY AS A FUNCTION OF TEMPERATURE

Figure II-A,4

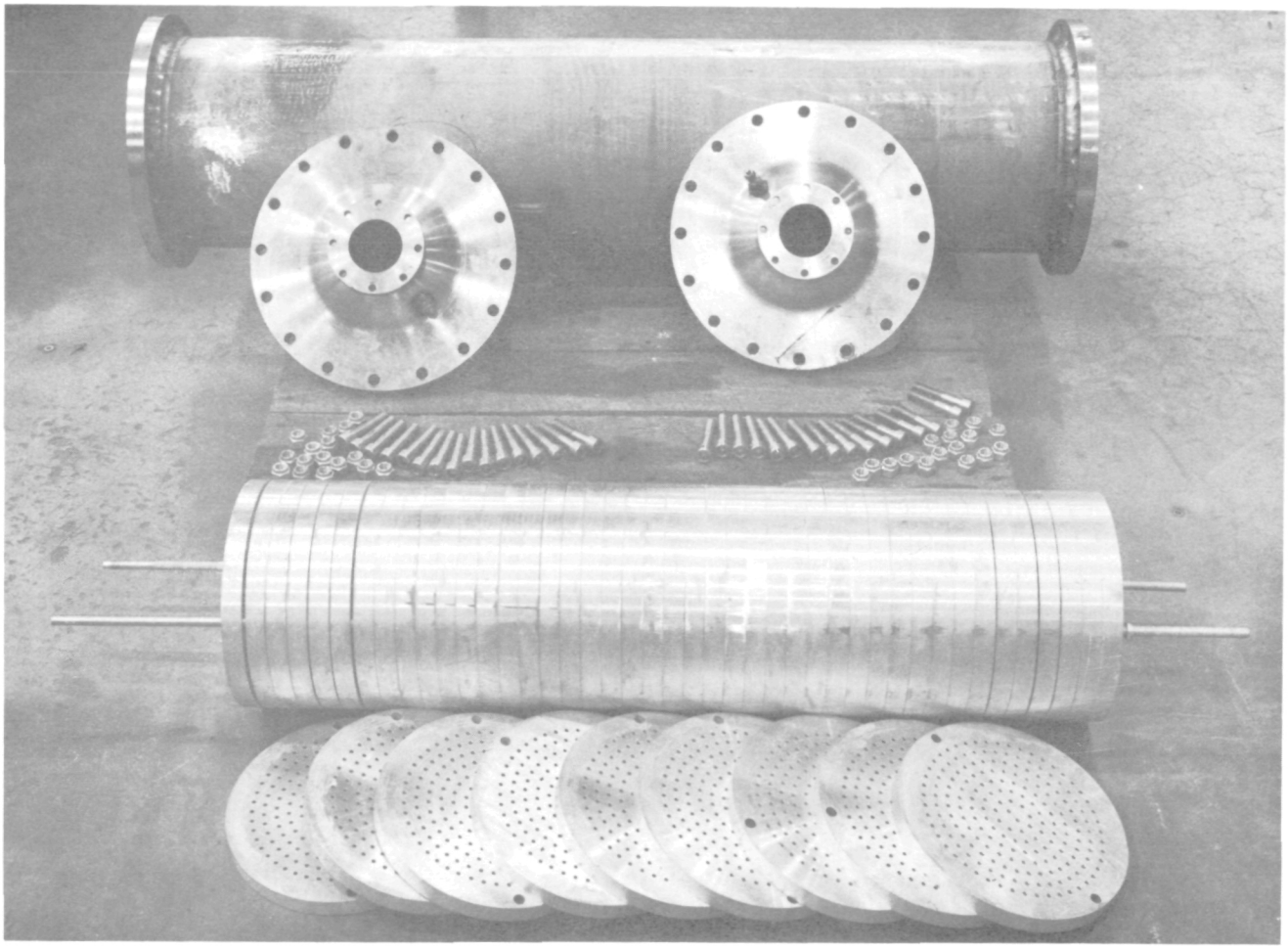

HEAT-CAPACITY, HEAT EXCHANGER

Figure II-A,5

B. REACTOR SIMULATOR

1. Design Considerations

At the beginning of the C-BEST Program, the portable computer available for use as a reactor simulator was equipped with 12 operational amplifiers, and with the limited funds available, it was possible to build 6 more amplifiers. But of the 18 amplifiers thus available, 4 would have to serve as error detectors to provide the signals necessary to actuate the flow-control valve servos. Thus, the problem of designing a reactor simulator for this particular series of tests resolved itself to the problem of reducing the reactor equations in such a way as to permit a solution with but 14 operational amplifiers, while still retaining the essential dynamic characteristics of the simulated engine components. Under ordinary circumstances, an analog computer of sufficient size would be set up to solve the complete set of nonlinear equations describing the components to be electronically simulated. Reduction of these nonlinear equations included their linearizing about the design operating point, taking the Laplace Transform, and developing transfer functions by algebraic reduction of the operational equations. By using RC networks for the input and feedback impedances of the operational amplifiers to simulate transfer functions, maximum utilization of the available amplifiers was achieved.

Reactor simulation must, of course, include the reactor and turbine power control loops as well as pertinent functions of the Engine Programmer. In the real engine, the rise in reference chamber temperature (or core outlet temperature) is programmed over a period of about 30 seconds to limit the approximate rate of change of temperature in the core fuel elements to less than 200° per second. Considering the fact that the facility tank held only enough propellant for a total run time of about 30 seconds, it was necessary to program the rise of simulated reactor core outlet temperature to a period less than 20 seconds, so that a reserve could be maintained for shutdown. Thus, the dynamic response characteristics of the prototype reactor control system had to be modified to allow the Reactor Simulator to respond adequately to steeper ramp inputs. Other simplifications, resulting from the necessity of using linearized system equations, were made in the prototype reactor controls.

2. Nonlinear Reactor Equations

The equations describing reactor and reflector characteristics are based on the schematic diagram of the cold-bleed cycle nuclear engine, Figure II-B-2, 1. The parameter schedule accompanying the figure reflects the design point performance data available at the beginning of the C-BEST Program. Since there was little change in this parameter schedule at the inception of Phase I of the NERVA program, these values were retained for the Generation I system.

A comparison of Figures I-C-1 and II-B-2, 1 shows that, of the components comprising the test system, only the turbopump and the TPCV were parts of the corresponding nuclear engine. Thus, the Reactor Simulator represented the remainder of the nuclear engine, including the pressure drop from the pump to the thrust chamber, heat transfer to the fluid in the reflector and reactor core, neutron kinetics, and reactor and turbine-power control system characteristics.

The general equations which formed the basis for Reactor Simulator design, excluding those for the reactor control loop and Engine Programmer functions, are listed in the first column of Table II-B-4, 1. The assumptions and simplifications in these equations, which were derived for design point conditions, are given below.

a. Pressure Drop

The pressure drop in a constant area duct is derived from the momentum equation for a compressible fluid, which states that the net force acting on a mass of fluid in the line equals mass rate of flow times velocity change plus the frictional resistance to flow. Substitution for velocity from the equation of continuity yields pressure drop in terms of flow rate squared and inlet and outlet densities. The density in the term for frictional head loss is a mean value.

b. Heat Transfer

According to the design-point data given in Figure II-B-2, 1, the propellant enters the reflector in a gaseous state. Hence, the heat-transfer equations for both reflector and reactor core were written for gas only.

The heat generated by radiation in the reflector wall, as well as in the reactor core, is proportional to neutron flux level, and the difference

between quantity of heat generated and quantity of heat transferred to the fluid by convection, represents that quantity stored in the wall. Equations C-1 and G-1 of Table II-B-4, 1 were based on the assumption that the temperature gradient in the wall is negligible. The heat transferred to the fluid across the boundary results in an increase in the enthalpy of the gas. Film coefficients of heat transfer are functions of flow rate.

c. Plenum Capacitance

In Equations D-1 and H-1 of Table II-B-4, 1, the time rate of change of mass, equal to the net flow, was replaced by substituting, for the derivative of gas density, an expression in terms of dP/dt obtained by differentiating the adiabatic equation, P/ρ^k = constant.

d. Turbine Flow Rate

Because of the lack of computing equipment, it was necessary to simplify the equation for turbine flow rate by treating the variable area of the TPCV as a fixed resistance to flow, which was sufficient for reactor simulation.

By equating the equations for flow through the TPCV and the turbine nozzle, and assuming ideal throttling occurred, an expression relating pressure ratio and area ratio was obtained,

$$\frac{P_{T1}}{P_{ro}} = \frac{A_{TCV} \quad \psi_{TCV}}{A_t \quad \psi_t} \tag{1}$$

where

ψ = functions of pressure ratios across the valve and nozzle

Throughout most of a start transient, sonic flow will exist in the turbine nozzle, hence, ψt is constant. In the range of valve operation of interest here, the pressure ratio across the valve was greater than critical pressure ratio, and a plot of area ratio as a function of P_{T1}/P_{ro} showed that, in this region, the pressure ratio changed very little even for large changes of valve area. Thus, P_{T1}/P_{ro} may be treated as a constant.

e. Neutron Kinetics

The equations for neutron kinetics are well known (References 3 and 4). Total reactivity was taken as the difference between control drum effectiveness and negative temperature reactivity. The positive contribution to reactivity by the propellant was not taken into account because it would have value only if actual hydrogen density, measured at the heat exchanger exit, could be applied to the reactor control loop. Again, the lack of computing equipment forced the assumption that, throughout the startup transient, hydrogen density at the core entrance was low enough to have negligible effect on reactivity.

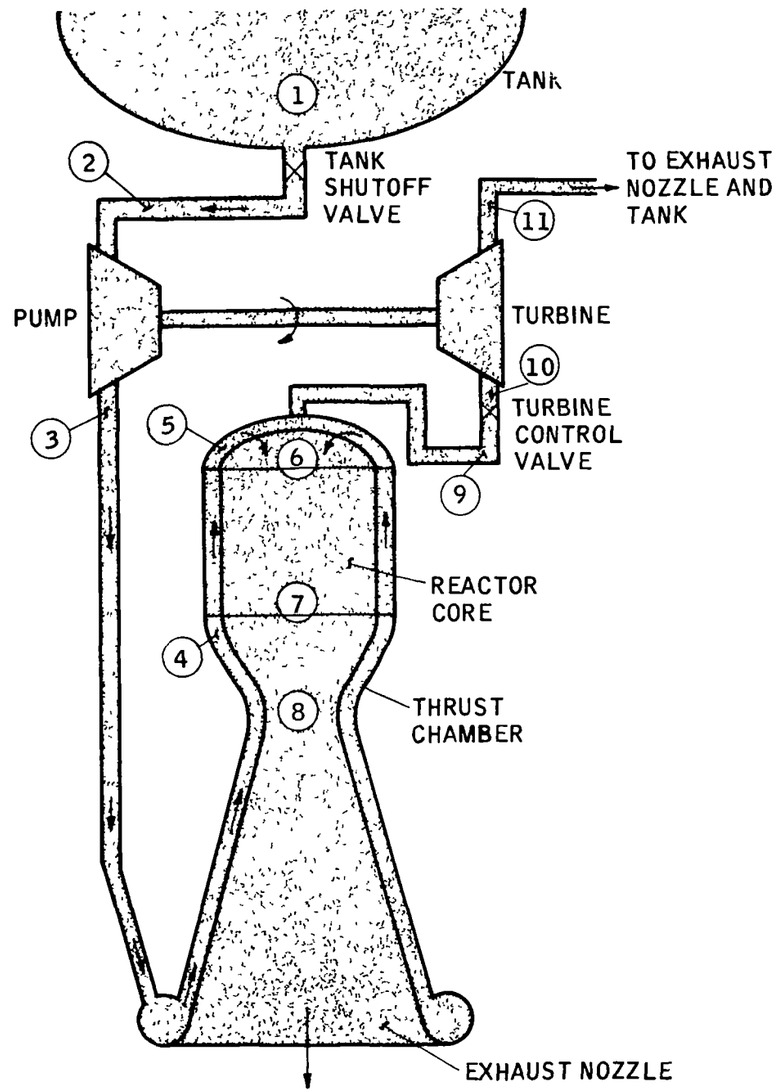

FULL POWER CONDITIONS:

OVERALL ENGINE THRUST, LB ———— 56,430
MAIN THRUST CHAMBER, THRUST, LB ——— 55,000
TURBINE EXHAUST NOZZLE THRUST, LB ——— 1,430
OVERALL ENGINE SPECIFIC IMPULSE, SEC ——— 670
CHAMBER SPECIFIC IMPULSE, SEC ———— 774
TURBINE NOZZLE SPECIFIC IMPULSE, SEC ——— 110

PARAMETER SCHEDULE AT FULL POWER

STATION	W LB/SEC	p (psia)	T (^{o}R)	HEAT, BTU/SEC E INPUT
1	83	35	40	0
2	83	35	40	+ 40
3	83	800	50	+ 35,230
4	83	700	120	+ 22,400
5	83	650	200	0
6	70	650	200	$+1.04 \times 10^{6}$
7	70	550	4090	0
8	70	550	4090	---
9	13	650	200	0
10	13	500	200	-1,950
11	13	50	140	

COLD-BLEED CYCLE NUCLEAR ENGINE SCHEMATIC DIAGRAM

Fig. II-B-2,1

3. Specific Reactor Equations

Values for the system constants appearing in the non-linear equations of Table II-B-4, 1 are given in Table II-B-3, 1. The constants and their values are divided into two groups one group representing either values taken from model specifications for the system shown in Figure II-B-2, 1, or known material properties, the second group being quantities derived by substituting the values of both known parameters and design point variables into the general equations and solving for the unknown constants. Consequently, the substitution of the system constants into the general equations yields a set of specific equations which will satisfy design point conditions stated in Figure II-B-2, 1. These specific equations are shown in the second column of Table II-B-4, 1 and are the equations to be linearized.

The proportionality constants, K_1 and K_2 (Table III-B-3, 1), were derived from a heat balance for design-point conditions, using a value of 1.22×10^{15} neutrons/sec for total neutron flux, as based on known core dimensions and heat flux. To derive the heat transfer coefficient for the core (h_c), an arbitrary value of $4500^{\circ}R$ was assigned for the core-wall temperature at design point conditions. This temperature was reasonable in itself, but also yielded a realistic value for h_c.

The heat-transfer coefficient for the reflector (h_r) was calculated by Nusselt's equation at design-point conditions, yielding a value of $208^{\circ}R$ for reflector-wall temperature. In order to obtain a heat balance for the fluid in the reflector at the given design point conditions, it was necessary to assign a value of 3.37 to the specific heat (c_{pr}) and a value of 3.82 to c_{pc}.

In the specific heat-transfer equations, the factor hA_s was replaced by $Cw^{0.8}$, where C was found by equating the two factors and substituting known design point values.

TABLE II-B-3, 1

SYSTEM CONSTANTS FOR REACTOR SIMULATOR EQUATIONS

A. Given Values of Constants

Symbol	Value	Units	Symbol	Value	Units
A_c	204	in.^{2}	A_n	60.2	in.^{2}
A_d	19.6	in.^{2}	A_r	25.2	in.^{2}

TABLE II-B-3, 1 (cont.)

Symbol	Value	Units	Symbol	Value	Units
A_t	2.64	in.^{2}	V_p	9	ft.^{3}
A_{sc}	90,300	in.^{2}	W_{cw}	2385	lb
A_{sr}	28,050	in.^{2}	W_{rw}	2100	lb
c_{cw}	0.54	Btu/lb$^\circ$R	ψ_n	0.467	
c_{rw}	0.12	Btu/lb$^\circ$R	ψ_t	0.484	
D_c	0.468	in.	β_1	0.00026	
D_d	5.0	in.	β_2	0.00156	
D_r	0.187	in.	β_3	0.00191	
g	32.2	ft/sec^2	β_4	0.001995	
k	1.4		β_5	0.000607	
K_T	1.525×10^{-6}	$\delta k/^\circ R$	β_6	0.000173	
ℓ^*	2.5×10^{-5}	sec	λ_1	0.0128	sec^{-1}
L_c	52	in.	λ_2	0.0315	sec^{-1}
L_d	5.66	ft	λ_3	0.125	sec^{-1}
L_r	52	in.	λ_4	0.325	sec^{-1}
R	767	ft./$^\circ$R	λ_5	1.55	sec^{-1}
V_c	4.65	ft.^{3}	λ_6	4.50	sec^{-1}

TABLE II-B-3, 1 (cont.)

B. Derived Values of Constants

Symbol	Value	Units
c_{pc}	3.82	Btu/lb ^{o}R
c_{pr}	3.37	Btu/lb ^{o}R
f_c	0.1325	
f_d	0.1204	
f_r	0.00187	
h_c	4.88×10^{-3}	Btu/sec in.^{2} ^{o}R
h_r	0.0166	Btu/sec in.^{2} ^{o}R
K_1	1.836×10^{-11}	Btu/sec/neutron
K_2	8.53×10^{-10}	Btu/sec/neutron
r_{TCV}	0.77	

4. Linearization of Equations

The total differential of a function of several variables, f (x, y, z), is defined as

$$\Delta f = \frac{\partial f}{\partial x} \Delta x + \frac{\partial f}{\partial y} \Delta y + \frac{\partial f}{\partial z} \Delta z \qquad (2)$$

which states that the differential of a function is equal to the sum of the partial differentials obtained by letting the variables change one at a time. Hence, each partial derivative is equal to the slope at a point on each curve relating the function with one dependent variable. The point in question is the point about which the incremental changes in the variables occur. In this case, the design point has been chosen as the point for which the linearization is to be done, and design point variables can be used to evaluate the partial derivatives analytically.

Application of Equation (2) to the specific equations shown in Table II-B-4, 1 yields the linear differential equations (in operational form) as listed in the third column, Table II-B-4, 1.

These equations are valid for use only in an operating region close to the design point. However, the analog computer will solve these equations continuously from zero to design point. Although a steady-state solution is possible, the deviation of the solution from design point will be very large because of the nature of the linearizations.

Some simplification and alteration of these linear equations (A-3 through J-3) of Table II-B-4, 1 is possible without loss of essential design-point time constants. In performing this operation, the object was to obtain a set of equations which would have a steady-state solution at the given design point.

To provide some reasonable basis for simplifying the linear equations, steady-state solutions were obtained with the original set of nonlinear equations at low power levels. It was found that a change of density with flow rate, during a rise in power, had the effect of making pressure drop proportional to flow. Hence, the terms expressing incremental changes of density were discarded, and the proportionality constants in the pressure-flow relations reduced by a half. Small terms were discarded. Where the linearization of a product of two variables doubled the effectiveness of the incremental variables, the gain factors were cut in half.

To achieve a heat balance when using design-point values for the incremental variables, the coefficients of the heat transfer equations were slightly reduced. Fluid temperature at the reflector entrance was assumed to be constant since, in the real engine, this temperature can be expected to initially drop at a rapid rate to a level not far below its design-point value.

The resulting set of linear equations were combined to eliminate certain variables that are not needed for engine simulation, and were written in transfer function form to facilitate construction of a computer circuit utilizing a minimum number of amplifiers. (For convenience, the Δ-notation was dropped.) These equations are listed in the fourth column of Table II-B-4, 1, Equations L-1 through L-8.

These equations retain the principal dynamic characteristics created by flow and heat transfer in the reflector and reactor core, though attention is restricted to the region of the design point. Even so, it can be shown that the time constants in the nonlinear case do not vary greatly from this one. These equations are also satisfied by design-point values of the variables, a condition required for steady-state operation of the simulated engine. Most importantly, the effect of an increase of core exit gas temperature, produced by an increase in power level, results in an increase in the pressure drop across the core.

The linearization of the neutron kinetics equations is carried out in Appendix A, where it is shown that reactor kinetics can be represented, over the range of interest here, by a simple transfer function in the form of Equation L-7, of Table II-B-4, 1. The net change of reactivity is shown in EquationL-8 of that table.

TABLE II-B-4.1

REACTOR SIMULATION EQUATIONS

Equations derived and used for Reactor Simulator design, exclusive of those for the Reactor Control Loop and the Engine Programmer

	NON-LINEAR EQUATIONS	SPECIFIC EQUATIONS Based on System Constants listed in Table II-B-3.1	LINEAR EQUATIONS	COMBINED LINEAR EQUATIONS IN TRANSFER FUNCTION FORM (For convenience, the Δ-notation has been dropped)
A	Pressure Drop-Pump to Reflector Entrance			
	$P_{fd} - P_{ri} = \frac{144\, w_r^2}{g A_d^2}\left(\frac{1}{\rho_{ri}} - \frac{1}{\rho_{fD}}\right) + f\left(\frac{L}{D}\right)\left(\frac{144}{2g\rho A_d^2}\right) w_r^2$ (A-1)	$P_{fD} - P_{ri} = 0.01165\left(\frac{1}{\rho_{ri}} - \frac{1}{\rho_{fD}}\right) w_r^2 + 0.00952\,\frac{w_r^2}{1/2(\rho_{ri} + \rho_{fD})}$ (A-2)	$\Delta P_{fD} - \Delta P_{ri} = 2.41\,\Delta w_r - 82.3\,\Delta\rho_{ri}$ (A-3)	$P_{fD} - P_{ro} = 1.809\, w_r$ (L-1)
B	Reflector Pressure Drop			
	$P_{ri} - P_{ro} = \frac{144 w_r^2}{g A_d^2}\left(\frac{1}{\rho_{ro}} - \frac{1}{\rho_{ri}}\right) + f\left(\frac{L}{D}\right)\left(\frac{144}{2g\rho A_r^2}\right) w_r^2$ (B-1)	$P_{ri} - P_{ro} = 0.00705\left(\frac{1}{\rho_{ro}} - \frac{1}{\rho_{ri}}\right) w_r^2 + 0.001832\,\frac{w_r^2}{1/2(\rho_{ro} + \rho_{ri})}$ (B-2)	$\Delta P_{ri} - \Delta P_{ro} = 1.21\,\Delta w_r - 139.3\,\Delta\rho_{ro} + 31.8\,\Delta\rho_{ri}$ (B-3)	$T_{ro} = \frac{(7.44 \times 10^{-14})}{(1.05\,S + 1)}\, n + \frac{(0.0209\,S + 1)}{(1.05\,S + 1)}(123.2) - 0.1744\,\frac{(0.542\,S + 1)}{(1.05\,S + 1)}\, w_r$ (L-2)
C	Reflector Heat Transfer			
	$c_{rw} w_{rw} \frac{dT_{rw}}{dt} = k_1 n - h_r A_{cr}(T_{rw} - T_r)$ (C-1)	$252\,\frac{dt_{wr}}{dt} = (1.836 \times 10^{-11})\, n - 13.7\, w_r^{0.8}(T_{rw} - T_r)$ (C-2)	$252\,S\,\Delta T_{rw} = (1.836 \times 10^{-11})\,\Delta n - 465(\Delta T_{rw} - 0.5\,\Delta T_{ro} - 0.5\,\Delta T_{ri}) - 217\,\Delta w_r$ (C-3)	$(0.01653\,S + 1)\, P_{ro} = 1.353\, w_r + 0.947\, P_c + 0.0858\, T_{ro}$ (L-3)
	where	where		
	$h_r A_{cr}(T_{rw} - T_r) = c_{pr} w_r (T_{ro} - T_{ri})$	$13.7\, w_r^{0.8}(T_{rw} - T_r) = 3.37\, w_r (T_{ro} - T_{ri})$		
	$h_r = f(w_r)^{0.8}$	$T_r = \frac{1}{2}(T_{ri} + T_{ro})$		
	$T_r = \frac{1}{2}(T_{ri} + T_{ro})$			
D	Plenum Capacitance			
	$\frac{dP_{ro}}{dt} = \frac{k R T_{ro}}{144 V_p}(w_r - w_c - w_t)$ (D-1)	$\frac{dP_{ro}}{dt} = 0.83\, T_{ro}(w_r - w_c - w_t)$ (D-2)	$512.2\,\Delta T_{ro} - 47.2\,\Delta T_{ri} + 52.5\,\Delta w_r = 465\,\Delta T_{rw}$ (D-3)	$(2.93\,S + 1)\, T_{cw} = (1.94 \times 10^{-12})\, n + 0.5\, T_{ro} + 0.5\, T_c$ (L-4)
E	Turbine Flow Rate			
	$w_t = A_t\sqrt{\frac{2g}{R}}\,\frac{r_{TCV} P_{ro}^{\dagger}\, t}{\sqrt{T_{Ti}}}$ (E-1)	$w_t = 0.286\,\frac{P_{ro}}{\sqrt{T_{ro}}}$ (E-2)	$S\,\Delta P_{ro} = 166(\Delta w_r - \Delta w_c) + 6.5\,\Delta T_{ro} - 4.05\,\Delta P_{ro}$ (E-3)	$(0.00032\,S + 1)\, P_c = 0.733\, P_{ro} + 0.01796\, T_c$ (L-5)
	where			
	$r_{TCV} = \frac{P_{Ti}}{P_{ro}} = \text{constant}$			
F	Reactor Pressure Drop			
	$P_{ro} - P_c = \frac{144 w_c^2}{g A_c^2}\left(\frac{1}{\rho_c} - \frac{1}{\rho_{ro}}\right) + f\left(\frac{L}{D}\right)\left(\frac{144}{2g\rho A_c^2}\right) w_c^2$ (F-1)	$P_{ro} - P_c = (1.075 \times 10^{-4})\left(\frac{1}{\rho_c} - \frac{1}{\rho_{ro}}\right) w_c^2 + (7.92 \times 10^{-4})\,\frac{w_c^2}{1/2(\rho_c + \rho_{ro})}$ (F-2)	$\Delta P_{ro} - \Delta P_c = 2.86\,\Delta w_c - 1167\,\Delta\rho_c + 1.99\,\Delta\rho_{ro}$ (F-3)	$T_{cw} = 0.986\, T_c + 4.72\, P_{ro} - 4.72\, P_c$ (L-6)
G	Reactor Heat Transfer			
	$c_{cw} w_{cw} \frac{dT_{cw}}{dt} = k_2 n - h_c A_{sc}(T_{cw} - T_{ca})$ (G-1)	$1290\,\frac{d\,T_{cw}}{dt} = (8.53 \times 10^{-10})\, n - 14.65\, w_c^{0.8}(T_{cw} - T_{ca})$ (G-2)	$1290\,S\,\Delta T_{cw} = (8.53 \times 10^{-10})\,\Delta n - 440(\Delta T_{cw} - 0.5\,\Delta T_{ro} - 0.5\,\Delta T_c) - 11{,}830\,\Delta w_c$ (G-3)	
	where	where		
	$h_c A_{sc}(T_{cw} - T_{ca}) = c_{pc} w_c (T_c - T_{ro})$	$14.65\, w_c^{0.8}(T_{cw} - T_{ca}) = 3.82\, w_c (T_c - T_{ro})$		
	$h_c = f(w_c)^{0.8}$	$T_{ca} = \frac{1}{2}(T_{ro} + T_c)$		
	$T_{ca} = \frac{1}{2}(T_{ro} + T_c)$			
H	Thrust Chamber Capacitance			
	$\frac{dP_c}{dt} = \frac{k R T_c}{144 V_c}(w_c - w_n)$ (H-1)	$\frac{dP_c}{dt} = 1.6\, T_c (w_c - w_n)$ (H-2)	$487.4\,\Delta T_c - 47.4\,\Delta T_{ro} - 2970\,\Delta w_c = 440\,\Delta T_{cw}$ (H-3)	
J	Nozzle Flow Rate			
	$w_n = A_n\sqrt{\frac{2g}{R}}\,\frac{P_c^{\dagger}\, n}{\sqrt{T_c}}$ (J-1)	$w_n = 8.14\,\frac{P_c}{\sqrt{T_c}}$ (J-2)	$0.625\,S\,\Delta P_c = 4090\,\Delta w_c - 35\,\Delta T_c - 520\,\Delta P_c$ (J-3)	
K	Neutron Kinetics			
	$\frac{dn}{dt} = \frac{\delta k}{\ell^*} n - \frac{\beta}{\ell^*} n + \sum_{i=1}^{6} \lambda_i C_i$ (K-1)	$\frac{dn}{dt} = \frac{\delta k}{2.5 \times 10^{-5}}\, n - \frac{0.0065}{2.5 \times 10^{-5}} + \sum_{i=1}^{6} \lambda_i C_i$ (K-2)	See Appendix A	Reactor Kinetics (from Appendix A)
	where	where		$\frac{n}{\delta k} = (4.21 \times 10^{-4})\,\frac{n_o}{\ell^*}\,\frac{(10\,S + 1)}{S(0.00382\,S + 1)}$ (L-7)
	$\frac{dC_i}{dt} = \frac{\beta_i}{\ell^*} n - \lambda_i C_i$	$\frac{dC_i}{dt} = \frac{\beta_i}{2.5 \times 10^{-5}}\, n - \lambda_i C_i$		Net change of Reactivity (from Appendix A)
	$i = 1, \quad 6$	$i = 1, \quad 6$		$\delta k = \delta k_c - (1.525 \times 10^{-6})\, T_{cw}$ (L-8)
	$\delta k = \delta k_c - k_T T_{cw}$	$\delta k = \delta k - (1.525 \times 10^{-6})\, T_{cw}$		

Table II-B-4,1

5. Reactor Control Loop

The linear equations of Table II-B-4, 1 represent the reflector-reactor characteristics required for engine simulation. However, the equations for the reactor control loop and the Engine Programmer must be added to complete the set of equations whose solution is to be instrumented on the analog computer (Reactor Simulator).

The NERVA Engine Programmer is a complicated device; it is required to act as a sequencing unit, signal generator, and error detector; and it is required to perform all of these functions not only for engine control during startup, operation and shutdown, but also for safety and malfunction control.

For purposes of the Generation I Engine Simulator, a single integrator was used as a signal generator to provide the reference inputs of chamber temperature and pressure to the simulated engine control systems. The chief reason for this decision was simply that no more than one operational amplifier could be spared for the Engine Programmer. However, since a live reactor was not used, the single malfunction and safety system required applied only to the turbopump, and control of this system under malfunction conditions was vested in a facility automatic overspeed trip circuit. Furthermore, the simplification of the simulation and the few tests (four, in all) scheduled to be run with the computer permitted only the simplest of startup programs - ramp inputs. In addition, since the Reactor Simulator was to start operating at the same time propellant flow was initiated, the sequenced startup of the NERVA reactor to the initial low power level did not have to be considered

The ramp inputs of desired temperature and pressure can be expressed by

$$T_{c\ reference} = \begin{cases} Rt, \text{ for } t < t_1 \\ 4090^{\circ}R \text{ for } t \geq t_1 \end{cases} \tag{3}$$

$$P_{c\ reference} = \begin{cases} K_3\, Rt, \text{ for } t < t_1 \\ 550 \text{ psia, for } t \geq t_1 \end{cases} \tag{4}$$

The velocity constant (R) is determined by dividing the desired reference value by t_1, the time required for the ramp to reach the desired value. The constant K_3 merely relates the T_c reference input to P_c reference, and allows the use of a single integrator for both functions.

In the NERVA engine, the reactor-control loop is designed to control the rate of change of core exit gas temperature during startup and shutdown, and to regulate this temperature at design point. Control of reactor power level will be exercised within the temperature control loop. The actual NERVA control system will contain shim and regulating control drums, their electro-pneumatic actuators, ion-chambers, and thermocouples for sensing and feeding back neutron flux level and gas temperature, respectively.

Since the representation of such a complex system was not warranted for the Reactor Simulator, the simulated control system was designed to provide adequate response to a ramp input of T_c-reference. In consideration of the requirements that flexibility be provided for selection of the ramp input, and that a ramp of 5 seconds might be necessary to make maximum use of the limited propellant storage available, a velocity error constant (K_v) of 8.18 sec^{-1} was taken as the criterion for designing the simulated reactor controller. This velocity constant would allow an error of 100^oR between T_c and T_c-reference during a 5-sec ramp. Another specification was the requirement for a well-damped response, that is, for a damping ratio of about 0.6.

A block diagram of the reactor control loop is shown in Figure II-B-5,1, where the transfer functions were obtained algebraically through elimination of P_c and P_{ro} in Equations L-4, 5, and 6 of Table II-B-4,1 by using the relation

$$P_{ro} - P_c = 1.43\, w_c \tag{5}$$

and then solving the resulting equations for T_c and T_{cw} in terms of n, w_c, and T_{ro}. The controller transfer function (G_{cr}) is the desired equation for completing the Reactor Simulator network.

Assuming for the time being, that the disturbance functions, U_1 and U_2, are zero, and letting $n_o = 1.22 \times 10^{15}$, the inner loop of the block diagram in Figure II-B-5,1 can be reduced to

$$\frac{T_{cw}}{\delta k_{cr}} = \frac{(3.56 \times 10^7)(S + 0.1)}{(S + 0.0674)(S + 0.308)(S + 262)} \tag{6}$$

A Bode plot of this transfer function shows that it can be approximated very closely by a much simpler expression over the frequency range of interest,

$$\frac{T_{cw}}{\delta k_{cr}} \approx \frac{6.55 \times 10^5}{(5.8\,S + 1)} \tag{7}$$

A proportional-plus-integral controller will provide the desired response characteristics. The final control loop configuration is shown in Figure II-B-5.2.

The controller gain constant (K_{cr}) can be determined from the velocity error constant (K_v)

$$K_v = 8.18^{-1} = K_{cr}\,(6.65 \times 10^5) \tag{8}$$

Therefore,

$$K_{cr} = 1.23 \times 10^{-5},\ \delta k/\text{degree error} \tag{9}$$

Using this value of K_{cr}, the open-loop response becomes

$$\frac{T_c}{E_{T_c}} = 1.41\ \tau_{cr}\ \frac{\left(S + \frac{1}{\tau_{cr}}\right)}{S\,(S + 0.1725)} \tag{10}$$

The closed-loop response becomes

$$\frac{T_c}{T_c'} = \frac{2.82\,(S + 0.5)}{(S + 2.41)\,(S + 0.587)} \tag{11}$$

where

the prime notation indicates the reference T_c.

If a root locus plot is prepared of Equation 11 (see Figure II-B-5,3), the controller time constant (τ_{cr}) is determined to be 2 seconds.

The reactor controller equations can now be written.

$$\frac{\delta k_{cr}}{E_{T_c}} = (1.23 \times 10^{-5})\ \frac{(2\,S + 1)}{S} \tag{12}$$

and

$$E_{T_c} = T_c' - T_c \tag{13}$$

This controller proved to be stable and provided adequate response characteristics when the simulated reactor control loop was subjected to disturbances in flow rate (w_c). See Section II-B-7.

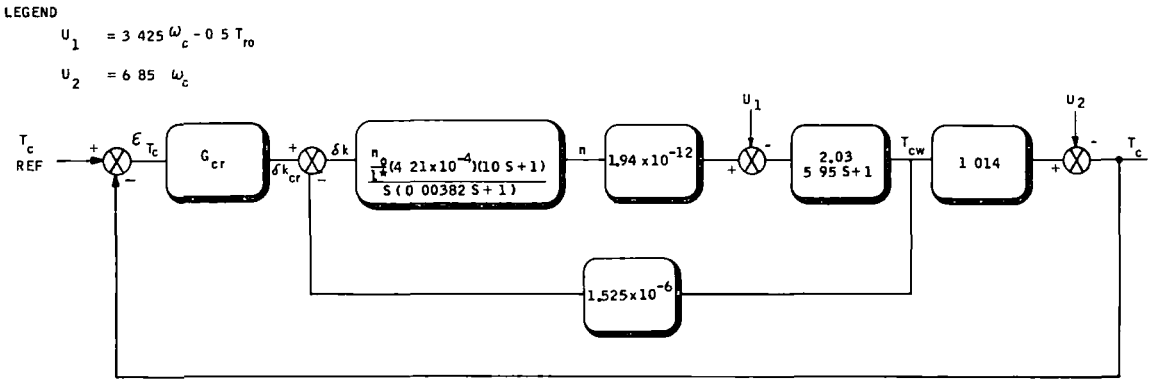

BLOCK DIAGRAM OF REACTOR CONTROL LOOP FOR REACTOR SIMULATOR

Figure II-B-5,1

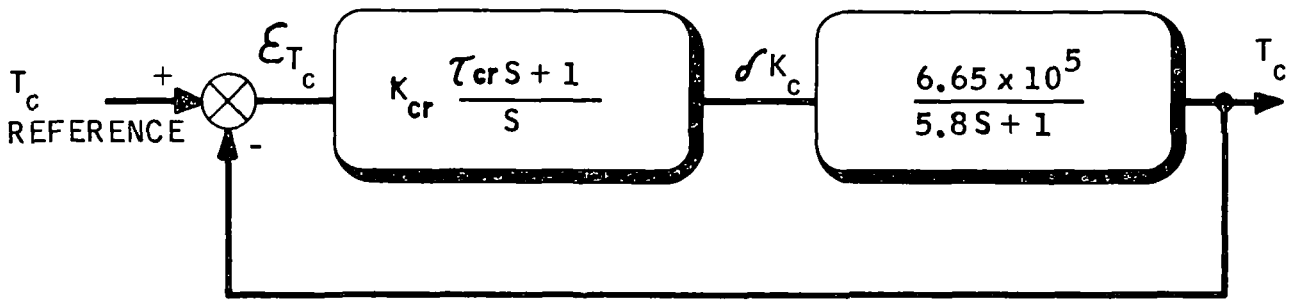

BLOCK DIAGRAM OF TEMPERATURE CONTROL LOOP IN REACTOR SIMULATOR

Figure II-B-5,2

NOTE.

OPEN-LOOP RESPONSE = $1\ 41\,\tau_{cr}\ \dfrac{(S + 1/\tau_{cr})}{S\,(S + 0\ 1725)}$

LEGEND

X = OPEN-LOOP POLES
o = OPEN-LOOP ZEROS
□ = CLOSED-LOOP POLES
● = CLOSED-LOOP ZEROS

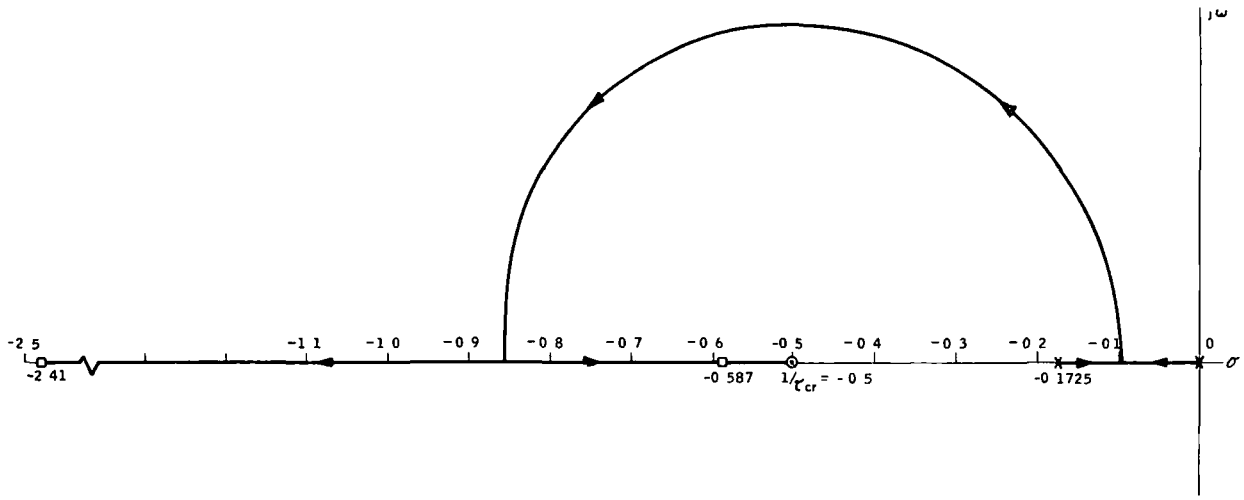

SIMULATED REACTOR CONTROL LOOP ROOT-LOCUS PLOT

Figure II-B-5,3

6. Reactor Simulator Circuit

The transfer functions of Equations L-1 through L-6 of Table II-B-4, 1, and of Equations 3, 4, 12, and 13, are simulated by the computer circuit in Figure II-B-6, 1. Scale factors, as indicated in the Figure, were chosen so that signals from the pressure and temperature transducers could be fed directly into the computer. The maximum output of all pressure transducers at Test Stand C-6 is 30 millivolts. With a gain of 700 on the Kintel-114 transducer amplifiers, a full-range signal of 21 volts was available. However, for convenience a scale factor of 0.01 v/psi was chosen, Scale factors of 0.01 volts per psi for T_{ro}, T_c, and T_{cw} were also chosen for convenience. The gain of the signal from the T_{mso} temperature transducer and associated amplifier was 0.0305 v/^{o}. This was taken into account by Potentiometers #5 and #6 to match the value of 0.025 v/^{o} assigned to T_{ro}.

Amplifier 5S represents the $T_{c\ reference}$ programmer with the limit set at 4090°R. In the initial setup for simulated engine tests, Amplifier 5S began integrating on "Simulator Run". The remainder of the computer circuit began operation at FS-1.

Potentiometer 6S at Amplifier 12 represents the coefficient K_3 in Equation 4. Thus, one input to Amplifier 12 is $P_{c\ reference}$.

The four amplifiers, No. 4, 6, 8, and 12, are the error detectors for the feedback control loops in the Engine Simulator, and also include the compensation required for stability and performance. The analysis of the computer-control system and the determination of compensation is given in Section III.

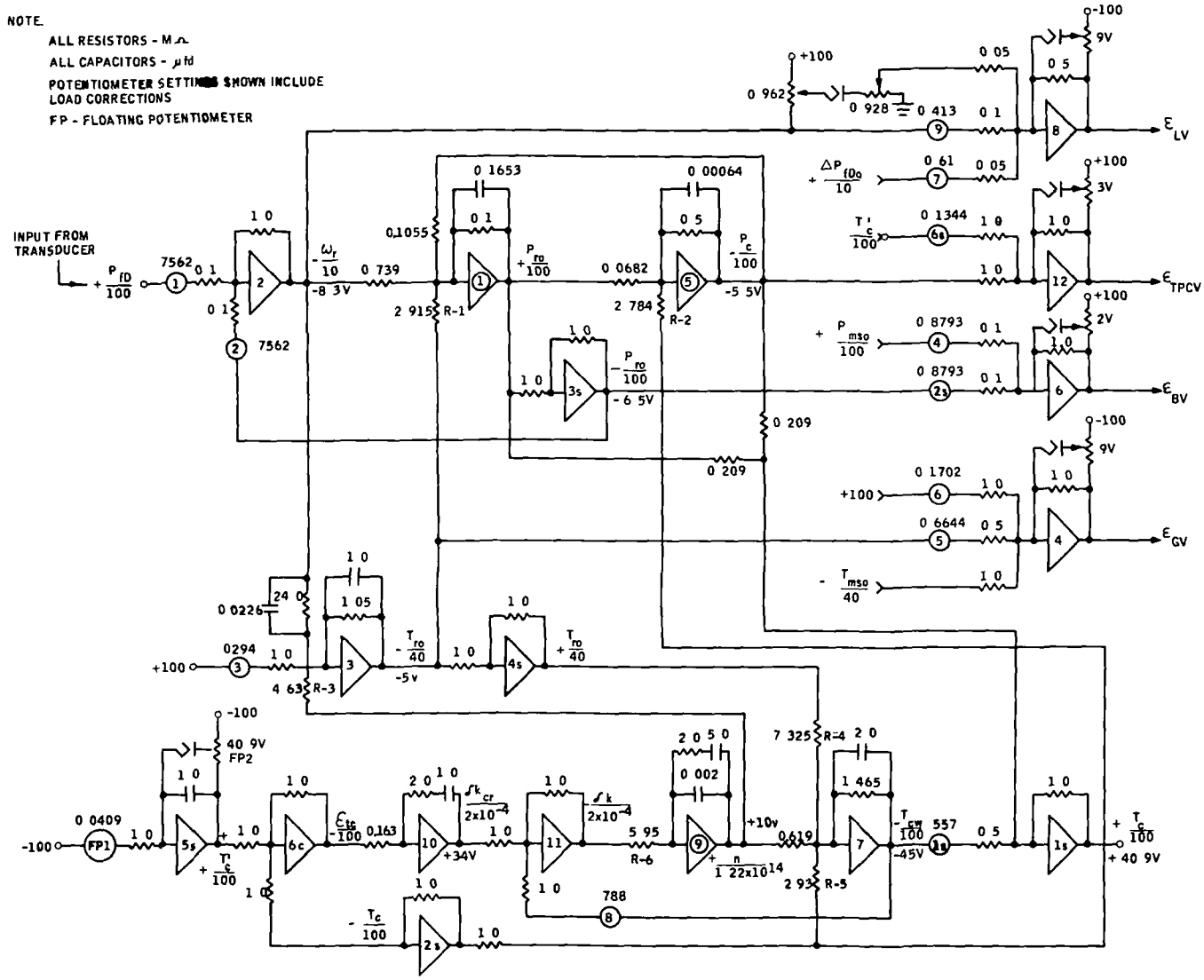

REACTOR SIMULATOR ANALOG COMPUTER CIRCUIT REPRESENTATION

Figure II-B-6,1

7. Simulator Responses

After fabrication, the analog-computer circuit for reactor simulation was checked both statically and dynamically. First, the dynamic characteristics of the inner loop of Figure II-B-5, 1 were determined by applying a step change of reactivity (δk_{cr}) to Amplifier 11 in Figure II-B-6, 1. The voltages, $P_c/100$, $P_{ro}/100$, and $T_{ro}/40$, were fixed at the design-point values shown on the circuit diagram. The response of T_{cw} to this step input is shown in Figure II-B-7, 1. The time constant of this response agrees very well with that of Equation 7, and the measured steady-state gain is 6.53×10^5 $^oR/\delta k$.

Figure II-B-7, 2 shows the transient response of the simulated reactor loop of Figure II-B-5, 2 to a ramp input of T_c'. As before, $P_{ro}/100$, $P_c/100$, and $T_{ro}/40$ were fixed. The steady-state velocity lag error between T_c and T_c' (Figure II-B-7, 2) is 100^oR, as specified for the velocity error constant, K_v, which is 8.18 sec.$^{-1}$.

To determine the stability and performance of the Reactor Simulator when P_c and P_{ro} are functions of time, i.e., when the disturbance functions U_1 and U_2 are not zero, the simulator was subjected to a ramp input of P_{fD} with T_c equal to 0. The resulting transients are shown in Figure II-B-7, 3.

Application of P_{fD} generated downstream pressures P_{ro} and P_c, and the flow rate w_r. Since $T_c' = 0$, the temperature control loop constrained T_c to be zero, which means that neutron flux level (n) remained at its initially low level (1.8 volts). Consequently, very little change can be detected in T_{ro}.

About five and one-half seconds after $t = 0$, a ramp input of T_c' was applied while P_{fD} was still increasing. The generation of power now produced an increase in reflector-gas exit temperature (T_{ro}). As core-exit gas temperature (T_c) and (to a minor extent) T_{ro} increased, chamber pressure (P_c) and reflector outlet pressure (P_{ro}) increased at a more rapid rate so that total reflector flow rate (w_r) increased less rapidly than before. Although these effects are not quantitatively accurate (because of the linear approximations), nevertheless they are at least qualitatively, the very characteristics required of the Reactor Simulator.

The transient responses shown in Figures II-B-7, 2 and 3 were very useful during the test program as a means of checking the static and dynamic accuracy of the simulator. After the analog computer was shipped to the LRP test area at Sacramento, and the circuit reconnected, these transient responses were duplicated exactly within the limits of accuracy with which oscillographs could be read. Throughout the test program only one amplifier had to be replaced (not however, during a a test) and usage of Figures II-B-7, 2 and 3 facilitated the detection of the malfunction and subsequent computer checks.

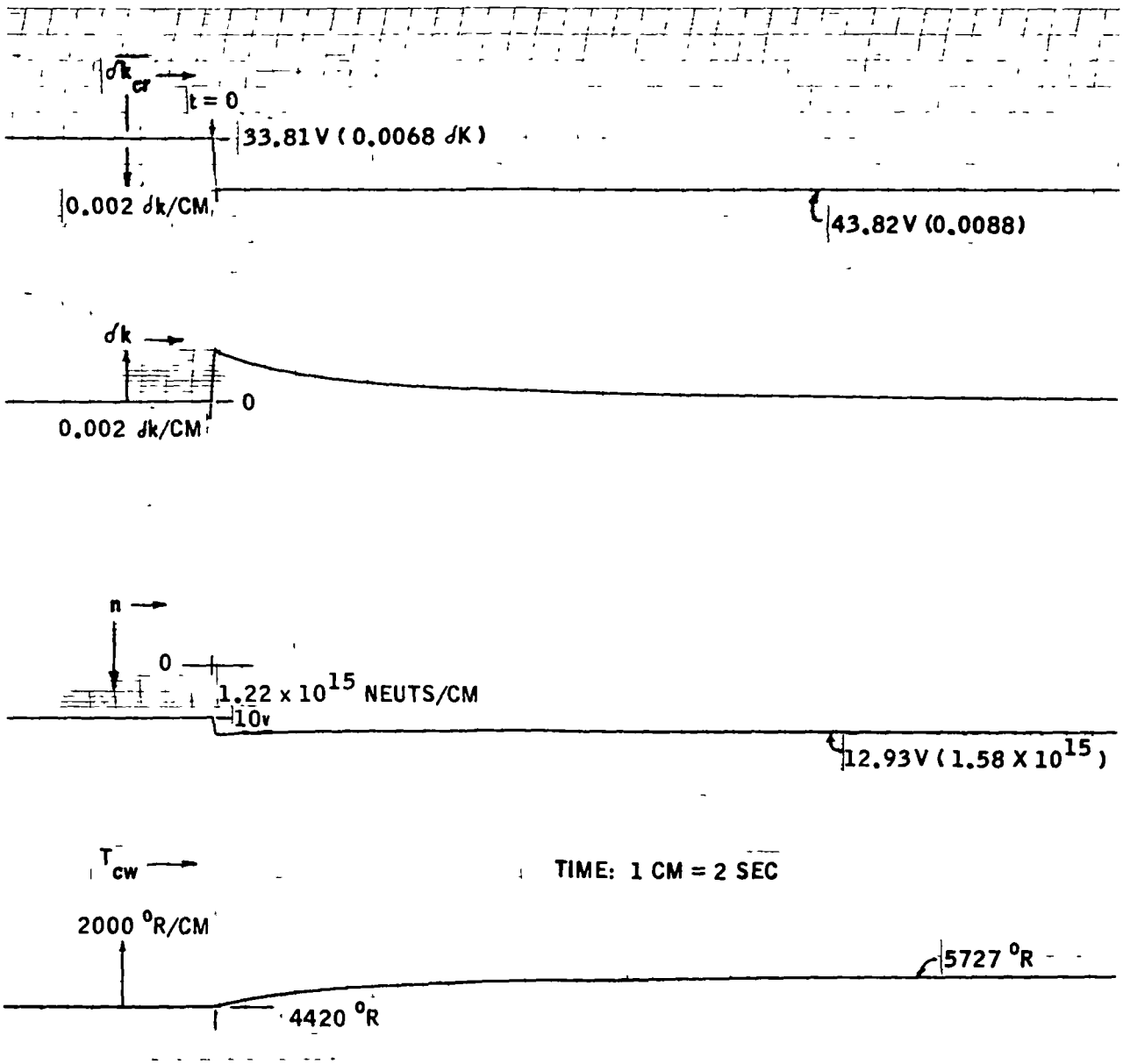

TRANSIENT RESPONSE OF INNER REACTOR LOOP TO STEP INPUT OF $\delta k_{cr} = 0.002$ T_{ro}, w_c FIXED, STEP INCREASE INTRODUCED AT DESIGN POINT

Fig. II-B-7,1

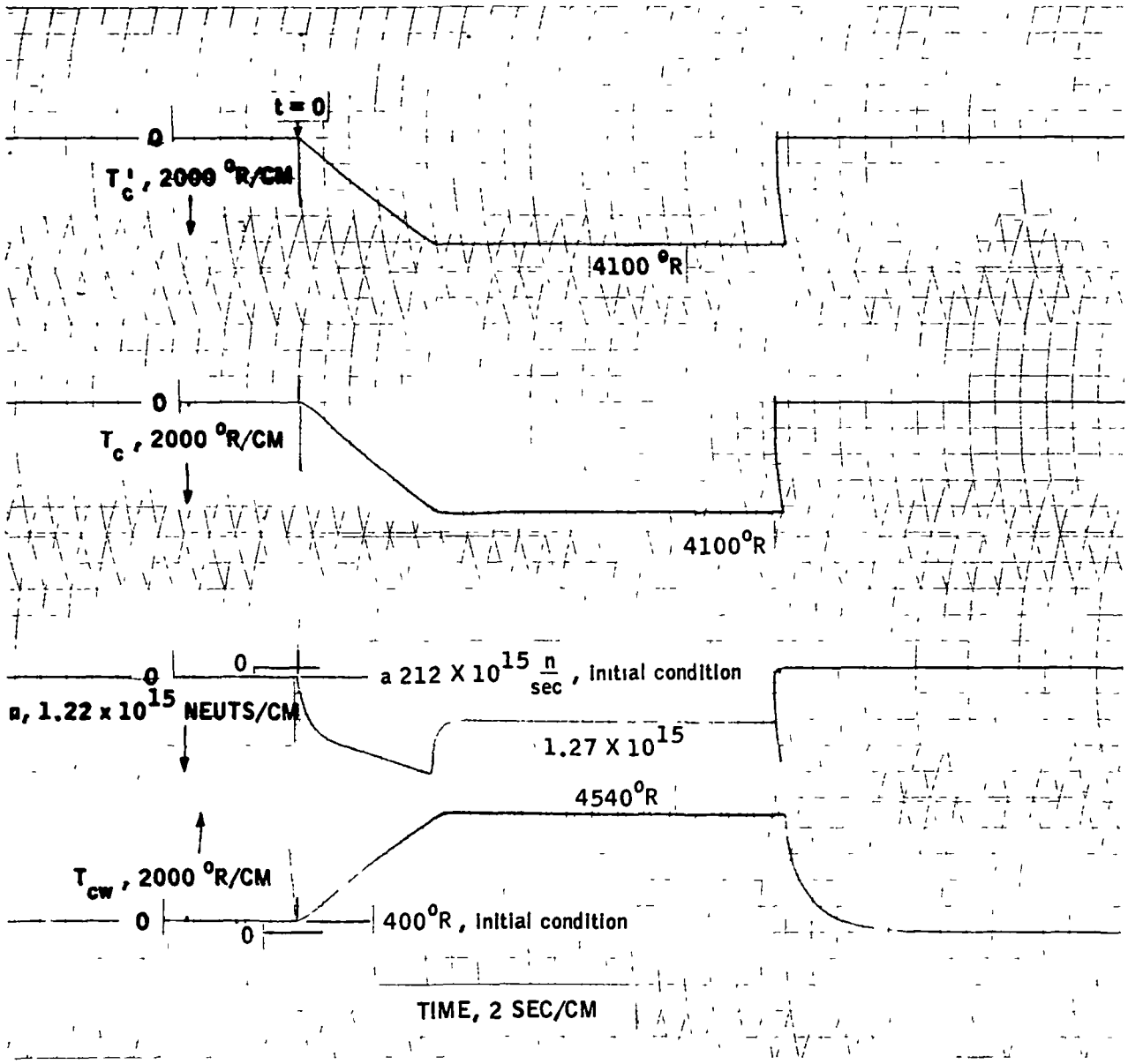

TRANSIENT RESPONSE OF REACTOR SIMULATOR TO RAMP INPUT OF T_c'. T_{ro} AND w_c FIXED

Fig. II-B-7,2

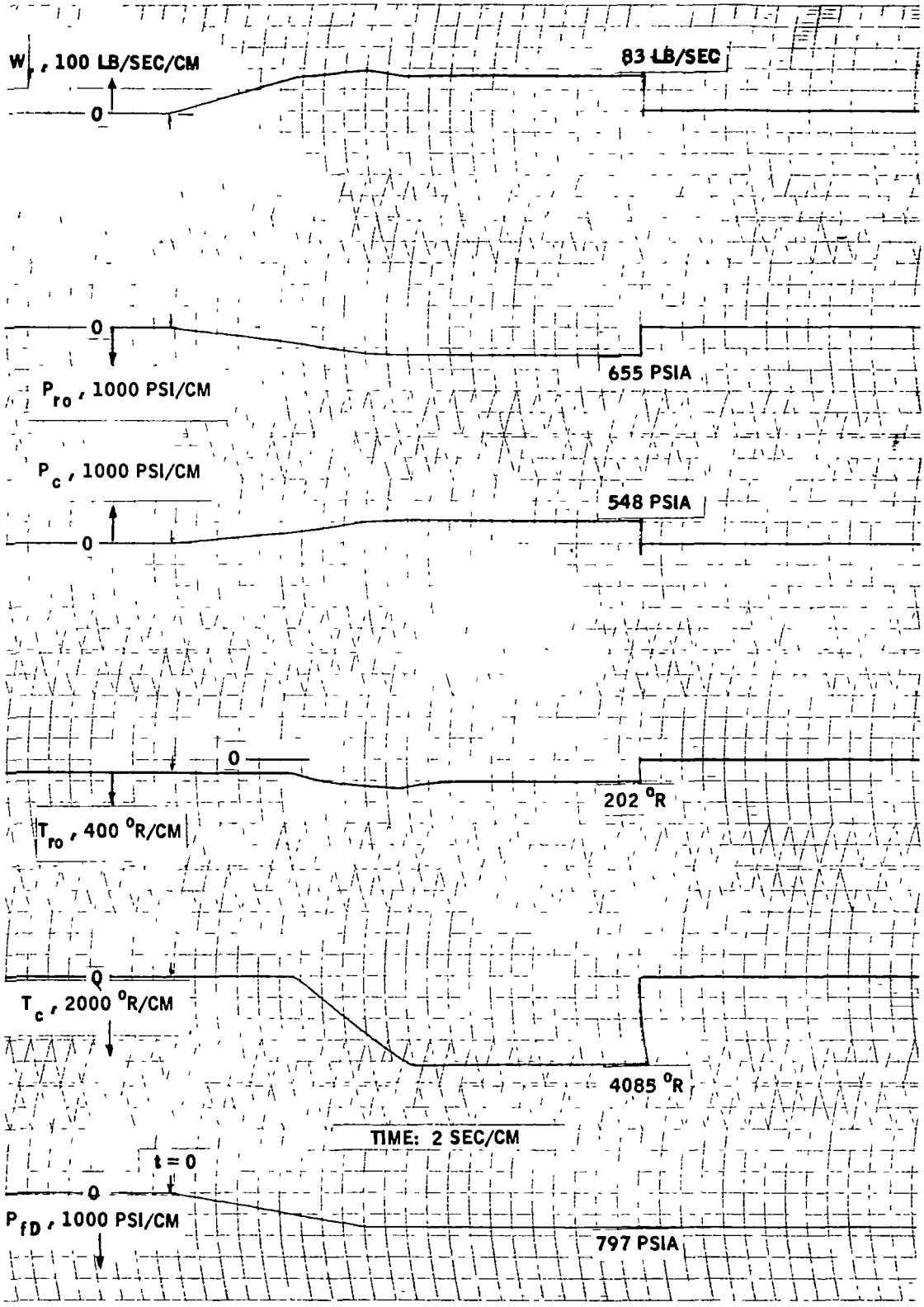

TRANSIENT RESPONSE OF REACTOR SIMULATOR TO RAMP INPUTS OF P_{fD} AND T_c'

Fig. II-B-7,3

SECTION III

COMPUTER-CONTROL SYSTEM ANALYSIS

III. COMPUTER-CONTROL SYSTEM ANALYSIS

A. PERFORMANCE CRITERIA

1. Basis of Design

A logical and considered approach to the design of a simulated engine would be the synthesis of the transfer-controller (load, bleed-line, and gas-farm valve servo systems) characteristics that are necessary for integrating the physical components and analog computer, but without interposing dynamic effects extraneous to the real engine. From these characteristics, dynamic response requirements would be established for the design of the transfer control systems.

Considering the fact that the components in the Generation-I Simulator, outside of the turbopump, represented a simplified approximation to a cold-bleed nuclear rocket engine, that the servo-actuators were already a part of the system, and that the analog computer consisted of only 18 operational amplifiers, such a synthesis was not applicable. Therefore, the performance criteria for the computer-control system, including the reactor simulator circuit (design of which is detailed in the preceding section), were based solely on the assumptions that both the hardware and computer were representative of a nuclear engine and that, if no steady-state error existed between computer-demanded variables and system variables, the dynamic characteristics of this nuclear engine would be preserved. The latter assumption implies the use of velocity-type controllers in the load, bleed-line, and gas-farm valve control loops. It may also be inferred from the foregoing assumptions that the turbine-power control system should be designed for this representative engine in the same sense that the reactor control loop was designed (see II, B, 5).

Before establishing dynamic response requirements, it is well to consider in detail the operation of the transfer controllers.

2. Criteria for Load Valve

The function of the load valve is to simulate the resistance to flow of the reactor core. This is accomplished by comparing computed reflector-flow-rate with actual pump delivery, any error actuates the Load-Valve controller to move the valve in a direction to reduce the error to zero. This method of transferring the computer output to the test hardware was chosen to avoid the necessity of computing the flow impedance of the Load Valve and the exhaust duct. Actual flow rate is proportional to the ΔP measured across an orifice near the

pump exit. Computed flow rate is a function of pump discharge pressure and was converted to a ΔP-demand for direct comparison with the measured ΔP. Since computed flow rate follows the pump pressure, the output of this control system must be capable of following a rate of change of P_{fD}, another reason for making this a velocity-type controller.

3. Criteria for Gas-Farm Control Loop

There were two reasons for the selection of turbine supply temperature (T_{mso}) as the controlled output of the gas-farm control loop, the input being computed reflector outlet temperature (T_{ro}). A primary objective of the Generation I Engine Simulator test program was the demonstration of the feasibility of heat-capacity bootstrapping, therefore the gas-farm valve was required to remain closed until sometime after the heat capacity of the heat exchanger had diminished. Energy was to be added from the gaseous hydrogen source only after the temperature of turbine bleed fluid had dropped below a predetermined value. This condition was met by designing the Generation-I system to simulate the cold-bleed engine cycle in which the turbine inlet temperature (equal to reflector outlet temperature) is 200°R at design operating conditions. Since the temperature of the fluid emerging from the heat-capacity heat-exchanger could be expected to decay slowly, a considerable time would elapse before T_{mso} would become less than T_{ro}, which follows a uniform rate-of-change of reactor power. Note that, from Figure II-B-7, 3, T_{ro} starts at 120°R and increases to 200°R at design point. By permitting the gas-farm controller to be activated only when T_{mso} decreased below T_{ro}, the completion of the heat-capacity portion of the starting transient was assured. This provision in itself was also a safety feature, because it also assured the existence of a load on the pump before the admission of external power.

4. Criteria for Bleed-Line Flow-Control Valve

In order to relate the turbine energy input to reactor power, it was necessary to make both the pressure and the temperature (P_{mso} and T_{mso}) at the TPCV equal to simulated reflector outlet pressure and temperature. Assuming the fluid to be static in the plenum above the reactor, temperature and pressure would be a direct measure of energy and, in the cold-bleed engine, plenum conditions would be the same as those at the TPCV (Figure II-B-2, 1). Hence, the bleed-line flow-control valve operated to make P_{mso} equal to the computed reflector outlet temperature, P_{ro}.

5. Performance Specifications

Performance specifications for the transfer control systems could only be defined in general terms, because the dynamic characteristics of

the given servo-actuators were fixed. Previous sections have pointed out the necessity of designing the load, gas-farm, and bleed-line control systems as velocity controllers capable of following the velocity outputs of the Reactor Simulator. Based upon the test results of C-BEST in March 1961, it was possible to predict the most probable rate of increase of pump discharge pressure that might occur in the Generation-I Simulator. Given such velocities, and considering that the computed command signals would have the same rates, it was also possible to establish velocity error coefficients as a guide to the design of each of the controllers, provided that permissible velocity-lag errors were first selected. The choice of the allowable errors and the selection of velocity error coefficients is discussed in the pertinent sections dealing with the analysis of individual control loops. In general, servo equalization was designed to provide well-damped responses.

The criteria for designing the TPCV control loop were based on the assumption that the computer-hardware-control system was representative of a nuclear engine. The transient performance specifications established for this engine required that it be capable of following a ramp input of P_c reference of 110 psi/sec with a velocity-lag error of 25 psi, that P_c be held to the set-point value of 550 psia with zero error, and that the maximum permissible turbine speed overshoot be 10% or less.

The ramp input was based upon the desire to bring the engine to a steady-state operating point in 5 seconds, obtaining the longest possible run time at steady-state.

The limitation on overshoot arose from considerations for safe operation of the turbopump. It was planned to set the overspeed trip sensor at a level not far above the maximum speed expected in a test.

A limitation on peak speed was required to avoid a premature shutdown during a start transient.

B. ANALYTICAL PROCEDURES

1. Nonlinear Analysis

Both a nonlinear and a linear analysis were undertaken to determine the transient response characteristics of the computer-control system. The former involved the application of an analog computer to the solution of the nonlinear equations describing the characteristics of the physical components. To this analog model of the test system, it was planned to connect the portable computer representing the reactor, and to analyze and synthesize required controller characteristics as well as to predict Generation-I system performance.

As an aid to the formulation of nonlinear system equations, an analysis was performed of data obtained in the last of the March 1961 tests on theCold-Bleed Engine Simulator, data which was representative of expected results from the Generation I Engine Simulator tests. More importantly, the two systems were so much alike that the mathematical model of the latter could be verified by comparing analog computer results to test data from the former system. This was done and the results of that particular study are reported in Section III, C, below.

2. Linear Analysis

The linear analysis was originally intended as a supplement to the nonlinear analysis. As a supplement, a linear system analysis could provide great insight into nonlinear system characteristics, and could guide nonlinear control-system synthesis by expressing gains and time constants in terms of system parameters.

Toward this end, the linear analysis was undertaken, but unforeseen circumstances forced the abandonment of the analog computer approach, and a return to complete reliance on a transfer-function analysis of the system. This decision was based on a number of factors. However, the most important consideration was that repeated malfunctions of the differential analyzer, coupled with a dearth of maintenance personnel, left too vague a period of time in which to complete the analysis before the start of an inflexible test schedule.

The shortcomings of a linear analysis, however, were mitigated by the fact that control of the test system would not be turned over to the computer until stable LH_2 appeared in the pump. It was evident, from C-BEST heat-capacity starts, that, when stable liquid appeared, turbopump speed was over 10,000 rpm and that pump discharge pressure increased rapidly. Similar results could be expected in the Generation-I system.

Allowing time for visual observation of temperature and pressure and manual operation of the "Simulator Run" switch, it was reasonable to expect discharge pressure as well as speed to be at a high level when the computer assumed control. Also anticipated was a necessity for limiting maximum turbopump speed to somewhere below 20,000 rpm because of uncertainties regarding pump operation at higher speeds.

Thus, the Generation I Simulator could be expected to operate in a restricted range in which the nonlinearities of the system would not be severe. The validity of this line of reasoning was demonstrated by the test results.

C. NONLINEAR SYSTEM ANALYSIS

This analysis is based on an analog-computer simulation of the Cold-Bleed Engine Simulation Test System, with which heat-capacity start tests were run in March 1961. Those tests were run without utilizing either the portable analog computer for reactor simulation or any of the flow-control valves, the system was operated in an open-loop condition. As shown in Figure I-C,1, the hardware consisted of the LH_2 turbopump, piping, flow-measuring orifices, heat-capacity heat-exchanger, and mixing section. The load valve was closed, the bleed-line valve was fully open, the TPCV was fully open, and the gas-farm valve was closed. The equations described below were also necessary for the linear system analysis.

1. General Equations - Test System Hardware

The component equations given in Table III-C,1 were derived partly on theoretical grounds and partly by extrapolating empirical coefficients from test data. The data chosen for analysis as the most representative was obtained in Test No. 1.1-01-ZXF-005, March 1961, and some pertinent results are shown in Figure III-C,1. All of the variables shown in Figure I-C,2 were measured in that test. In addition to yielding empirical coefficients, the data analysis also provided a basis for setting up the theoretical equations.

a. Flow Equations

The flow equations were based on the premise that the computer would start closed-loop control of the test system only after LH_2 appeared at the pump exit. For this condition, the test data indicated that LH_2 very quickly filled the piping down to the load valve and the heat-exchanger, while gaseous conditions prevailed downstream of these sections. Very good correlation between flow rates, in various parts of the test system, was obtained by applying the hydraulic equations for the flow-metering orifices to the test data with flow coefficients from the ASME Fluid Meters Report, Reference 5. The test data indicated that, for liquid hydrogen, pipe friction losses were negligible in comparison to pressure drops across orifices and other large discontinuities. Empirical flow coefficients, given in Table III-C,2, were determined by applying the theoretical equations to the test data. The bleed-line valve and TPCV were treated as orifices, and flow coefficients were extrapolated from the Fluid Meters report.

b. Heat-Capacity Heat-Exchanger

The constant in the equation for the convective heat-transfer coefficient was extrapolated from a heat balance of the transient data

based on numerical integration methods. Equation 11 of Table III-C,1, which was used for determining the temperature of the fluid leaving the heat-exchanger, was correlated with experimental data. The best fit with the data was obtained by using the average values for L and c_v given in Table III-C,2.

c. Turbopump

The pump torque and head rise equations were obtained from predicted characteristics given in a Technical Memorandum prepared by Dept. 8130 of LRP, in February 1961. The turbine torque equation was expressed in terms of inlet pressure, temperature, and speed, by combining the equations for ideal torque, turbine-nozzle spouting velocity, and efficiency. Turbine parameters were obtained from a Technical Memorandum from Dept. 8130, December 1960. Because no actual pump performance characteristics were available, Equations (2), (3), and (4) of Table III-C,1 were checked against the test data. Only fair correlation was obtained.

2. Analog-Computer Setup

Interest had been centered on that part of the start transient occurring after LH_2 filled the piping downstream of the pump, therefore no attempt had been made to write the two-phase flow equations for the beginning of the transient. However, for the analog computer to produce a more realistic start transient, the variation of pump discharge density with time was determined from test data and programmed on the computer by means of an integrator and function generator.

The function-generator output is shown in Figure III-C,1, which indicates that, at first, density increased slowly from a very low value, then rose rapidly to density of LH_2. In the pump equations, the density was allowed to vary only in the N^2 terms. To be consistent, the inlet temperature to the heat-exchanger was also programmed with time according to the test results.

In the turbine equation, the pressure ratio (P_{Te}/P_{T1}) was taken to be constant and equal to 0.09. Sonic flow through the turbine nozzle was assumed for all conditions, so the compressible flow coefficient (ψ_t) was set equal to the sonic value.

3. Computer Results

With P_{fs} constant and equal to 40 psig, corresponding to the real test condition, the starting transient shown in Figure III-C,2, was obtained

with the analog-computer simulation. The experimentally-determined speed and pump discharge pressure are superposed for comparison.

Table III-C,3 lists the steady-state values of the variables obtained at the peak speed corresponding to liquid density in the pump. These steady-state values were later used in the linear analysis for evaluating partial derivatives, because they not only are a solution to the nonlinear equations, but also agree closely with experimental data.

From the correlation between computer and experimentsl start transients, several conclusions can be drawn that will have an important bearing on the linear system analysis.

a. The startup transient was dominated by the dynamic characteristics of the turbopump and by the heat transfer to the fluid. The latter can be considered in two distinct stages. First, vaporization of the propellant in the suction line and pump produced negligible load on the pump, but sufficient flow was generated by tank pressure to accelerate the turbine. The higher initial acceleration obtained on the analog model resulted from the assumption that sonic conditions at the turbine nozzle prevailed at all times. During this first stage, very little heat transfer occurred in the heat-capacity heat-exchanger. However, as soon as stable LH_2 appeared in the pump, the heat-exchanger dominated energy transfer to the fluid.

b. Given the proper pump discharge pressure, it was not surprising that the steady-state values for flow rates and pressures in the system, obtained at peak speed, should agree closely with the corresponding test data, since empirical coefficients had been derived from that data. The important factor here is that the predicted pump-head-rise characteristic yielded nearly correct values of discharge pressure.

c. In addition, the predicted pump-torque characteristic was verified, by the correlation between the start transients, particularly after density in the pump became comparable to a liquid state. This conclusion follows from the fact that turbopump response is a function of both M_t and M_p, but the turbine torque equation was considered valid, at least for the higher nozzle pressure ratios.

d. The computer results as well as the data analysis indicated that steady-state equations could be used for the pressure-flow equations, and calculations showed that the transport lag in the bleed line was much smaller than the time constant of either the heat-exchanger or turbopump. Note that a transport lag was actually included, as represented by the bleed-line pressure-drop equations coupled with the integration of P_{mso} in Equation (15) of Table III-C,1.

TABLE III-C,1

NONLINEAR SYSTEM EQUATIONS
COLD-BLEED ENGINE SIMULATION TEST SYSTEM
(See Figure III-D,1 for Linearized Equations)

A. TURBOPUMP DYNAMICS

$$I \frac{dN}{dt} = M_t - M_p \tag{1}$$

B. TURBINE TORQUE

$$M_t = \left\{ C_D A_t C_1 r \sqrt{\frac{k}{k-1}\left[1 - \left(\frac{P_{te}}{P_{t1}}\right)^{(k-1)/k}\right]} \right\} \psi_t P_{t1} - \left\{ \frac{C_2 r^2 C_D A_t}{\sqrt{2gR}} \right\} \frac{\psi_t P_{t1} N}{\sqrt{T_{mso}}} \tag{2}$$

C. PUMP TORQUE

$$M_p = C_{p1}\, \rho_{fD}\, N^2 + C_{p2}\, w_f\, N - C_{p3} \frac{w_f}{\rho_{fD}} \tag{3}$$

D. PUMP DISCHARGE PRESSURE

$$P_{fD} = P_{fs} + C_{p4}\, \rho_{fD}\, N^2 + C_{p5}\, w_f\, N - C_{p6} \frac{w_f}{\rho_{fD}} \tag{4}$$

where

P_{fs} = constant

E. PUMP DISCHARGE ORIFICE

$$w_f = K_{fd}\, A_{fDo} \sqrt{2g\, \rho_{fD}\, (P_{fd} - P_{LLV})/144} \tag{5}$$

TABLE III-C,1 (cont.)

F. BLEED-LINE ORIFICE

$$w_b = K_{BPO} A_{BPO} \sqrt{2g \rho_{BPO} (P_{BPO} - P_{He1})/144} \tag{6}$$

where

$$\rho_{BPO} \approx \rho_{fD}$$

G. LOAD-VALVE AND BYPASS ORIFICE

$$w_\ell = (K_{fyo} A_{fyo} + K_{LV} A_{LV}) \sqrt{2g \rho_{fyo} (P_{LLV} - P_{fDI})/144} \tag{7}$$

where

$$\rho_{fyo} \approx \rho_{fd}$$

H. EXHAUST LINE PRESSURE LOSS

$$P_{fDI} - 14.7 = K_{fDI} w_\ell^{\,2} \tag{8}$$

J. MASS CONSERVATION

$$w_f = w_b + w_\ell \tag{9}$$

K. BLEED-LINE VALVE

$$w_b = (KA_{bv}) \sqrt{2g \rho_{fD} (P_{LLV} - P_{BPO})/144} \tag{10}$$

TABLE III-C,1 (cont.)

L. HEAT-CAPACITY HEAT EXCHANGER WALL TEMPERATURE

$$c_a W_a \frac{dT_a}{dt} = - h A_s (T_a - T_{he}) \tag{11}$$

where

$T_a = 520^{\circ}R$ at $t = 0$

$h = f (w_b)^{0.8}$

$T_{he} = \frac{1}{2} (T_{He1} + T_{Heo})$

$T_{He1} = 210u(t) - 20\ tu(t) + 20\ tu(t-8)$

M. HEAT EXCHANGER, CONSERVATION OF ENERGY

$$144 \left(\frac{P_{He1}}{\rho_{He1}} - \frac{P_{Heo}}{\rho_{Heo}} \right) = 778 (L + c_v T_{Heo} - c_v T_{Hei}) - 778 \frac{q}{w_b} \tag{12}$$

where

$$q = \begin{cases} hA_s (T_a - T_{he}) & , \text{ when } T_{he} < T_a \\ 0 & , \text{ when } T_{he} \geqq T_a \end{cases}$$

$\rho_{He1} = 4.2$

$$\rho_{Heo} = \frac{144\ P_{Heo}}{R\ T_{Heo}}$$

TABLE III-C,1 (cont.)

N. HEAT EXCHANGER PRESSURE LOSS

$$P_{Hei} - P_{Heo} = \frac{144\ K_1}{g\ A^2} \left(\frac{1}{\rho_{Heo}} - \frac{1}{\rho_{Hei}} \right) w_b^{\ 2} \tag{13}$$

P. PRESSURE LOSS, HEAT-EXCHANGER EXIT

$$P_{Heo} - P_{mso} = K_2 \frac{w_b^{\ 2}}{\rho_{Heo}} \tag{14}$$

Q. MIXING SECTION, CONSERVATION OF MASS

$$\frac{dP_{mso}}{dt} = \frac{k\ R}{144\ V_m} T_{mso} \left(w_b + w_g - w_t \right) \tag{15}$$

R. MIXING SECTION, CONSERVATION OF ENERGY

$$\frac{dT_{mso}}{dt} = \frac{1}{V_m\ \rho_{mso}} \left[w_b\ T_{Heo} + w_g\ T_g - w_t\ T_{mso} \right] \tag{16}$$

where

$$T_g = \text{constant}$$

$$\rho_{mso} = \frac{144\ P_{mso}}{R\ T_{mso}}$$

S. TURBINE SUPPLY ORIFICE

$$P_{Ti} = 0.922\ P_{Ts} \tag{17}$$

TABLE III-C,1 (cont.)

T. TURBINE POWER CONTROL VALVE, PRESSURE LOSS

$$P_{Ts} = P_{mso} \left[f(A_{TCV}) \right] \tag{18}$$

U. TURBINE NOZZLE FLOW

$$w_t = \frac{C}{\sqrt{1 - \beta^4}} \sqrt{\frac{2g}{RT_{mso}}} \left[\frac{r^{2/k} \left(\frac{k}{k-1}\right) \left(1 - r^{(k-1)/k}\right) (1 - \beta^4)}{1 - \beta^4 r^{2/k}} \right]^{1/2} P_{T1} \tag{19}$$

where

$$r \triangleq \frac{P_{te}}{P_{t1}}$$

V. GAS-FARM VALVE FLOW

$$w_g = C_D A_{gv} \sqrt{\frac{2g}{RT_g}} P_h \psi_t \tag{20}$$

where

P_h = regulated pressure at GFV

TABLE III-C.2

COEFFICIENTS FOR EQUATIONS OF COLD-BLEED ENGINE SIMULATOR TEST SYSTEM

Symbol	Value	Units	Description	Source
A_{BPO}	1.23	in.^{2}	Orifice area	
A_{fDo}	11.38	in.^{2}	Orifice area	
A_{fYo}	5.11	in.^{2}	Orifice area	
A_s	6200	in.^{2}	Heat transfer surface area	
A_t	2.64	in.^{2}	Throat area, turbine nozzle	*
c_a	0.20	Btu/lb^{o}R	Specific heat, aluminum	
c_v	1.86	Btu/lb^{o}R	Specific heat, hydrogen	
C_d	0.89		Discharge coefficient, empirical	
C_1	4.52		Coefficient of U/C in turbine efficiency equation	*
C_2	7.54		Coefficient of $(U/C_o)^2$ in turbine efficiency equation	*
Cp_1	2.526×10^{-5}		Constant in pump torque equation	**
Cp_2	7.19×10^{-3}		Same	**
Cp_3	0.115		Same	**
Cp_4	3.16×10^{-5}		Constant in pump head-rise equation	**

TABLE III-C.2 (cont.)

Symbol	Value	Units	Description	Source
Cp_5	1.769×10^{-3}		Same	**
Cp_6	0.0327		Same	**
D_b	3.068	in.	Inside diameter, turbine fluid bleed line	
D_{ℓ_1}	3.068	in.	Inside diameter, bypass pipe	
D_f	5.047	in.	Inside diameter, pump discharge line	
g	32.2	ft/sec^2	Gravitational constant	
I	0.0733	$ft\text{-}lb\text{-}sec^2$	Moment-of-inertia, turbopump rotor	*
k	1.4		Specific heat ratio	
KA_{bv}			Effective area of Bleed-Line valve, see Figure III-D.5	
K_{BPO}	0.604		Flow coefficient	***
K_{fD}	0.734		Flow coefficient	***
K_{fD_1}	0.12		Empirical coefficient	
K_{fYo}	0.517		Empirical flow coefficient for ΔP_{fYo} orifice and pipe	
$K_{LV}A_{LV}$			Effective area of Load valve, see Figure III-D.2	

TABLE III-C,2 (cont.)

Symbol	Value	Units	Description	Source
K_1	2.24		Empirical coefficient	
K_2	0.138	$sec^2(in.^2)(ft^3)$	Empirical coefficient	
K_3	0.922		Empirical coefficient	
L	120	Btu/lb	Latent heat of vaporization	
r_t	0.388	ft	Turbine mean blade radius	*
R	767	$ft/^oR$	Gas constant	
v_m	0.5	ft^3	Mixing section volume	
W_a	500	lb	Weight of aluminum, heat-capacity heat exchanger	

*Technical Memorandum, Dept. 8130, LRP, 30 December 1960.

**Technical Memorandum, Dept. 8130, LRP, 22 February 1961.

***Fluid Meters, Their Theory and Application, ASME, 1959.

TABLE III-C.3

STEADY-STATE SOLUTION TO NONLINEAR (C-BEST) SYSTEM EQUATIONS

N_T	= 14,950 rpm	P_{T1}	= 257 psia
P_{fs}	= 54 psia	P_{TS}	= 291 psia
P_{fD}	= 407 psia	T_{Heo}	= 358°R
P_{LLV}	= 386 psia	T_{TS}	= T_{T1} = 368°R
P_{BPO}	= 366 psia	T_{mso}	= 365°R
P_{He1}	= 348 psia	T_{He1}	= 60°R
P_{Heo}	= 303 psia	ρ_{mso}	= 0.156 lb/ft^3
P_{mso}	= 303 psia	w_b	= 4.21 lb/sec
w_f	= 48.63 lb/sec	w_ℓ	= 44.2 lb/sec

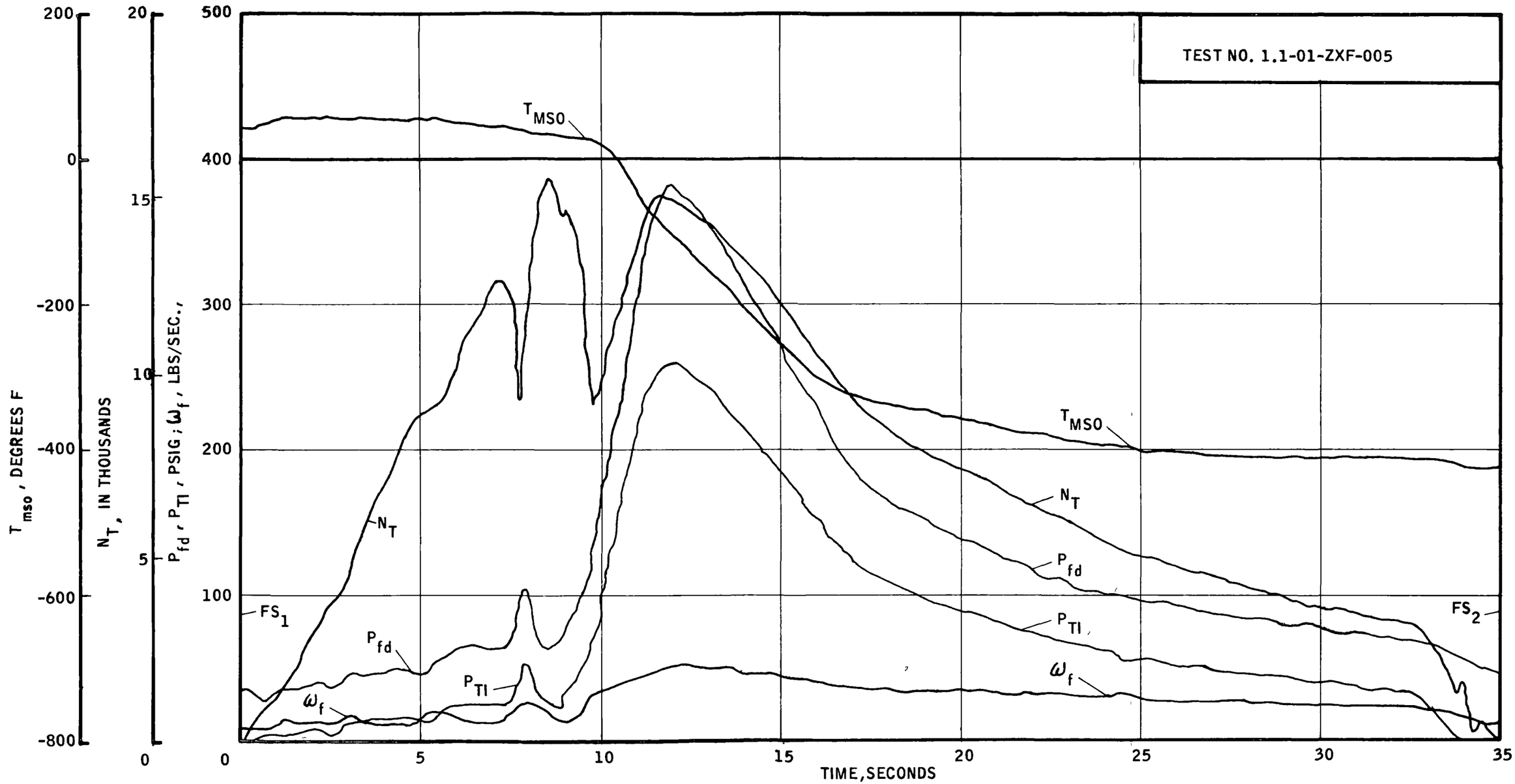

COLD-BLEED ENGINE SIMULATION TEST PERFORMANCE-TIME CHARACTERISTICS 3-16-61

Figure III-C,1

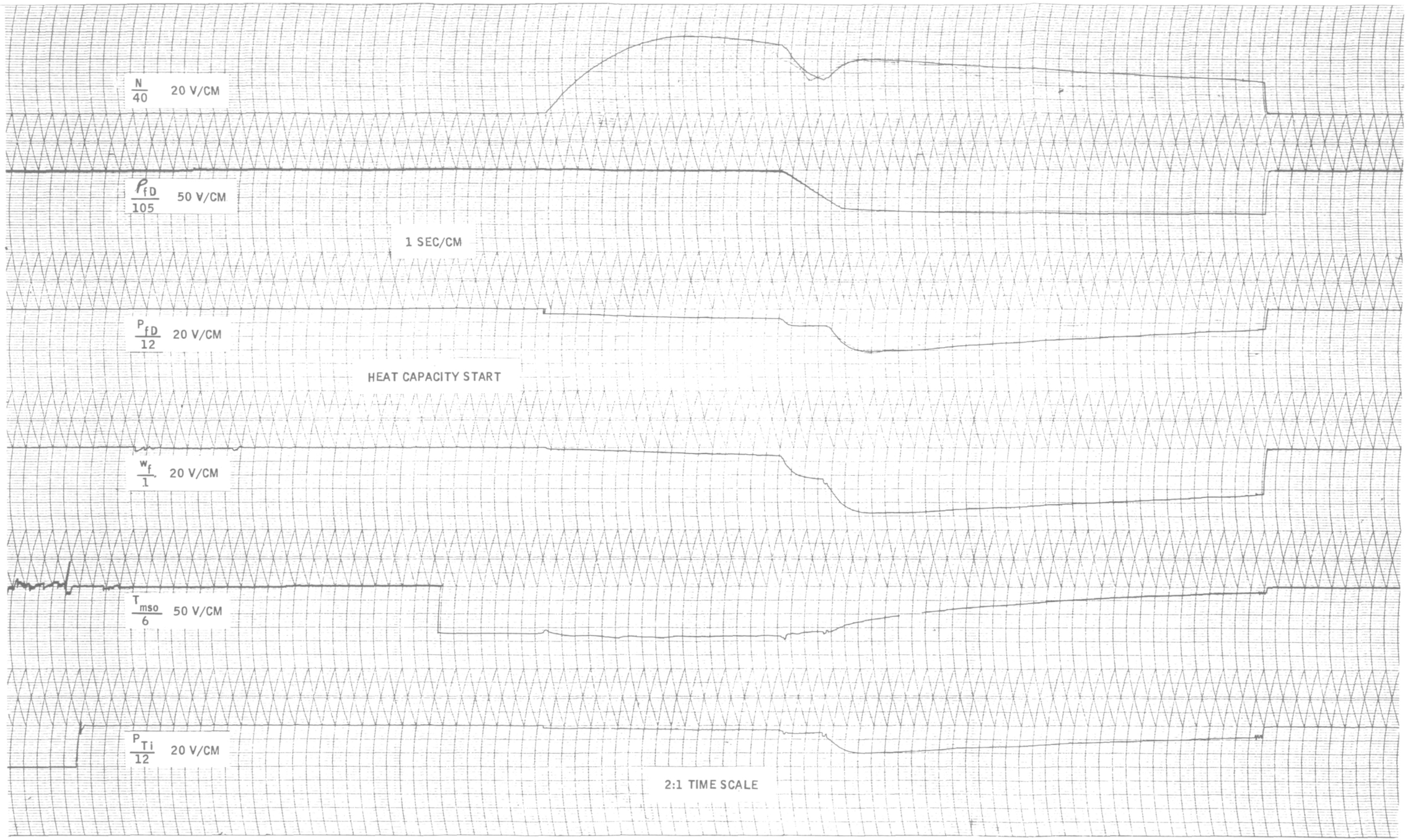

COLD-BLEED ENGINE SIMULATOR TEST PERFORMANCE CHARACTERISTICS

Figure III-C,2

D. LINEAR SYSTEM ANALYSIS

In preceding sections, the dynamic characteristics of the Reactor Simulator and of test system components were defined. The characteristics of the hydraulic flow-control subsystems are analyzed in Appendix B.

The objective of this section is to determine the kind and degree of compensation required in each of the flow-control loops to achieve desired performance. Neither on the test stand nor on an analog computer is it practical to close these loops by trial-and-error methods. The procedure followed here is to apply the techniques of linear feedback control system synthesis to determine control functions necessary for the achievement of desired performance.

Of the four feedback control loops comprising the Generation-I Engine Simulator, three are necessary for transferring computer outputs to the test hardware to simulate nuclear engine performance, and the fourth, the turbine-power control loop, represents one of the two real engine control systems. The other real engine control loop is incorporated into the reactor simulator (portable analog computer). The three subsidiary loops, which control the flow of hydrogen through the Load, Bleed-Line, and Gas-Farm valves, were analyzed, and the results then incorporated into the analysis of the turbine-power control loop; this analysis involves the entire system, including the test hardware and the reactor simulator.

1. Load Valve Control Loop

The reference input to this control loop is $\Delta P'_{fDo}$, generated in the reactor simulator as a function of the computed reflector flow rate (w_r). The components in the loop include: the error detecting amplifier (No. 8 in Figure II-B-6,1); the Kintel servo amplifier; the hydraulic servo-actuator (without position feedback); the load valve; the pump discharge line; the ΔP_{fDo} orifice; the ΔP_{fDo} pressure transducer and amplifier; and the signal transmission line back to the error detector.

In linearizing the equations of Table III-C,1, ρ_{fD} was taken to be constant and equal to 4.2 lb/ft^3, and w_b and P_{fD} were considered to be input disturbances to this control loop. To account for a possible time lag in the exhaust duct, the effect of fluid inertia was added to Equation (8), Table III-C,1. The linearized equations, in transfer function form, are shown in the block diagram of Figure III-D,1, where the variables are really incrementals. The servo-actuator transfer function is described in Appendix B; the gain of the Load

valve (K_{LV}) is the appropriate slope on the curve of Figure III-D,2; the dynamic characteristics of the pipe are defined by K_e and τ_e; and the output ΔP_{fDo} (in volts) is taken as the output of the transducer amplifier. According to Appendix B, K_a, the gain of servo-valve amplifier and torque motor, = 25 milliamps/volt. However, in Figure III-D,1, the torque-motor gain is shown to be 2.5 milliamps/volt and the amplifier gain as K_a. Splitting the gain in this manner was done for expediency, since all the servo amplifiers had been modified (subsequently to the experimental frequency responses) to have gains variable from 1 to 5.

In order to determine K_aG_c, the input disturbances of P_{fD} and w_b are, in the first instance, considered to be zero. To define K_e and τ_e, several operating points were considered, and it was found that, for the operating range of interest, K_e and τ_e varied very little from the values given in Figure III-D,1, in which the values were based on design operating conditions.

From Figure III-B-7,3, the maximum rate of change of w_r is 13.2 lb/sec^2 for a ramp input of $\dot{P}_{fD}$ = 90 psi/sec. In the computer, $\dot{w}_r$ would be 1.32 volts/sec. The C-BEST test data, Figure III-C,1, indicates that higher rates of change of P_{fD} (in the order of 140 psi/sec) may be expected. Then

$$\text{Maximum } \dot{w}_r = (140/90)(1.32) = 2.06 \text{ volts/sec} \tag{14}$$

By the linearized relation,

$$\Delta P'_{fDo} = 1.372\ w_r \tag{15}$$

it is shown that

$$d/dt\ (\Delta P'_{fDo}) = 2.82 \text{ volts/sec} \tag{16}$$

If a velocity error coefficient (K_v) is chosen as equal to 2 sec^{-1}, then the velocity-lag error is 1.41 volts, or in terms of flow rate, about 10 lb/sec. A smaller velocity error can be expected in the actual system because, according to Figure III-B-7,3, the ramp input of $T_{c\ reference}$ reduces $\dot{w}_r$ to 5 from 13.2 lb/sec. Hence, the loop gain will be based on a K_v of 2 sec^{-1}. The open-loop gain of the block diagram, Figure III-D,1, is 0.332 K_aG_c; therefore, K_aG_c = 6.1 for the selected K_v.

The closed-loop roots of the load-valve control system were obtained by the root-locus plot shown in Figure III-D,3. Only gain compensation was required in this case. The value of $K_a = 1$ was assigned to the servo-valve amplifier, and $G_c = 6.1$ was assigned to Amplifier 8 in the reactor-simulator circuit.

2. Bleed-Line Control Loop

The reference input to this loop is P_{ro} (in volts), and the output is P_{mso} (in psi), or 0.01 P_{mso} (in volts). Included in the loop are the bleed-line valve and actuator, the heat-exchanger, the mixing section, the pressure transducer and amplifier, and the error detector.

To simplify the reduction of linearized equations, P_{LLV} and w_g were treated as disturbances, and the temperatures in the heat exchanger were assumed to be constant; an assumption which was based on the observation that heat-exchanger temperatures decayed slowly. In addition, the chief effect of the temperature change was an increase in pressure drop, and the assumption of constant temperature did not introduce too large an error.

After combining and reducing the system equations, the block diagram of Figure III-D,4 was constructed. The servo-actuator transfer function is described in Appendix B. K_{bv} is the slope of the curve in Figure III-D,5. The gain $K_{b\ell}$ and time constants τ_1, τ_2, and τ_3, define the dynamic characteristics of the bleed line and mixing section.

The open-loop gain is $0.84\ K_{ab}G_{cb}$. The value of $K_{ab}G_{cb}$ was determined from the root locus plot, Figure III-D,6, for a velocity error coefficient of 30 sec^{-1}. As shown in Figure III-B-7,3, the maximum rate of change of P_{ro} was 64 psi/sec, or 6.4 volts/sec; therefore, the velocity lag error would be only 2.13 psi. The worst error expected was in the range of 5 psi. To attain an overall K_v of 30 sec^{-1}, corresponding to a $K_{ab}G_{cb}$ of 35.7; K_{ab} was assigned a value of 5, and G_{cb} (Amplifier 6) a value of 7.15. Corresponding to the open loop gain of 30, the closed-loop roots of the characteristic equation were determined as shown on the root-locus plot.

3. Gas-Farm Valve Control Loop

The reference input for this control loop is T_{ro} (in volts), and the controlled output is T_{mso}. The block diagram is shown in Figure III-D,7. The characteristics of the servo-actuator are the same as for the Load Valve (see App. B). The gain K_{gv} of the Gas-Farm valve (GFV) is the lesser slope of

the curve in Figure III-D,8. The gain K_4 is the change in mixing section temperature per unit change of valve area, and was obtained by combining the equations for the GFV, mixing section, and turbine supply line. When combining these equations, the input from the heat exchanger was considered a disturbance, and the resistance to flow offered by the TPCV was assumed constant. The gain K_{th} is the gain of the temperature probe and amplifier. The time constant of the temperature probe was estimated as 0.1 sec.

The dominant closed-loop roots considered were complex conjugate roots for values of open-loop gain sufficiently high enough to yield desired velocity lag errors. For that reason, the open-loop gain that would provide a closed-loop damping ratio of 0.6 was determined first. The closed-loop roots are shown on the root-locus plot of Figure III-D,9, and the corresponding value of root-locus gain is 153,500. Since the system gain is 0.99 $K_{ag}G_{cg}$, the required value of $K_{ag}G_{cg}$ is found by

$$K_{ag}G_{cg} = \frac{(.0455)(0.1)(153,500)}{(0.028)(5750)(.99)} = 4.4 \qquad (16)$$

Thus, the velocity-error coefficient is 4.35 for the system of Figure III-D,7. The expected velocity of T_{ro} was 1.5 volts/sec; therefore, the velocity-lag error (E_{gv}) would be 0.345 volts. Given an instrumentation calibration of 0.0305 volts/degree, the velocity-lag error would be 11.3°R. The error detector was assigned a gain of one, and the value 4.4 was assigned to the servo-amplifier gain, K_a.

4. Turbine-Power Control Loop

The reference input to this control loop is P_c' (in volts). In Figure III-B-6,1, $P_c' = 0.1344\ T_c'$ at Amplifier 12, where it is compared to the controlled variable P_c (in volts). P_c is generated directly as a result of actual pump discharge pressure (P_{fD}) fed into the computer as a voltage from the transducer amplifier. The error signal (E_{TPCV}) actuates the servo-actuator which operates the TPCV. Control of turbine power effectively controls pump discharge pressure. Thus, P_c is brought into correspondence with P_c'.

In previous sections, the subsidiary control loops were designed as though they were non-interacting. That approach allowed the selection of error detector and servo-amplifier gains, so that the dynamic characteristics of each of the subsidiary control loops are now defined. Each of the subsidiary loops can be considered a dynamic element in the turbine power control loop. However, the previously neglected disturbance functions, which are really

cross-coupling terms, were taken into account in the reduction of the complete system block diagram. The reduction was carried through by both algebraic and block diagram reduction techniques, and numerical coefficients were retained throughout the process. In the reduction of the multiple-loop diagram many of the transfer function poles were cancelled by zeros which appeared in the forward path because poles existed in the feedback paths of subsidiary loops.

The resulting block diagram is shown in Figure III-D,10. The transfer function (θ_o/i) is that of the TPCV actuator, and is developed in Appendix B. The gain of the TPCV is the maximum slope of the effective flow area curve in Figure III-D,11. The dynamics of the turbopump and flow loop are characterized by a single first-order lag. Since the damping coefficient for the turbopump is a function of pump delivery, the effect of the load flow control system is to increase the damping on the turbopump. Thus, the turbopump time constant of 0.0775 seconds is the result of combining the turbopump and load-valve system in the block diagram reduction. Under steady-flow conditions at design point, the turbopump time constant was calculated to be 0.100 seconds.

The roots of the characteristic equation are determined in Figure III-D,12 for a damping ratio $\zeta = 0.62$, corresponding to an overshoot of 10%. The corresponding open-loop gain is $K_{at}G_{ct} = 3$, and the velocity error coefficient is 10.2 sec^{-1}. For a ramp input of 110 psi/sec, the velocity-lag error between P_c' and P_c is about 11 psi. In the computer, Amplifier 12 was assigned unity gain, and $K_a = 3$ was assigned to the servo amplifier.

LEGEND:

G_c	= NETWORK COMPENSATION	K_{rsv}	$= \dfrac{\overline{\omega}_{ev}}{(KA_{LV})}$, LB/SEC/IN.^{2}
K_a	= SERVO AMPLIFIER GAIN, v/v	R_1	$= 2\,(\overline{P_{fD} - P_{LLV}})/\overline{\omega}_f$, SEC/IN.^{2}
K_1	= 1.62, IN.^{3}/SEC/MA	R_2	$= 2\,(\overline{P_{LLV} - P_{fDl}})/\overline{\omega}_l$, SEC/IN.^{2}
A_p	= 10 , IN.^{2}	R_3	$= 2\,(\overline{P_{fDl}}/\overline{\omega}_l)$, SEC/IN.^{2}
τ_h	= 0.0455, SECOND	L_3	$= L_e / g A_e$, SEC^2/IN.^{2}
K_o	= 0.75 RAD/IN.	R_o	$= 2\,(\Delta\overline{P}_{fDo})/\overline{\omega}_f$, SEC/IN.^{2}
K_{LV}	= 0.12 IN.^{2}/ DEGREE	K_e	$= K_{rsv} R_2/(R_1+R_2+R_3)$, LB/SEC/IN.^{2}
τ_e	= 0.0074, SECOND	τ_e	$= L_3/(R_1+R_2+R_3)$, SECOND
R_o	= 1.372	K_e	= 1.16, LB/SEC/IN^2

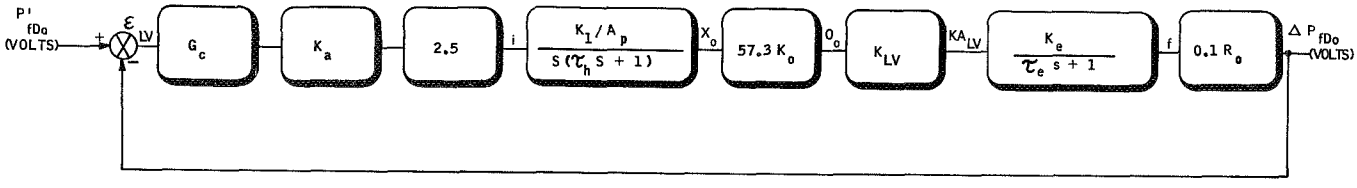

BLOCK DIAGRAM OF LOAD VALVE CONTROL LOOP

Figure III-D,1

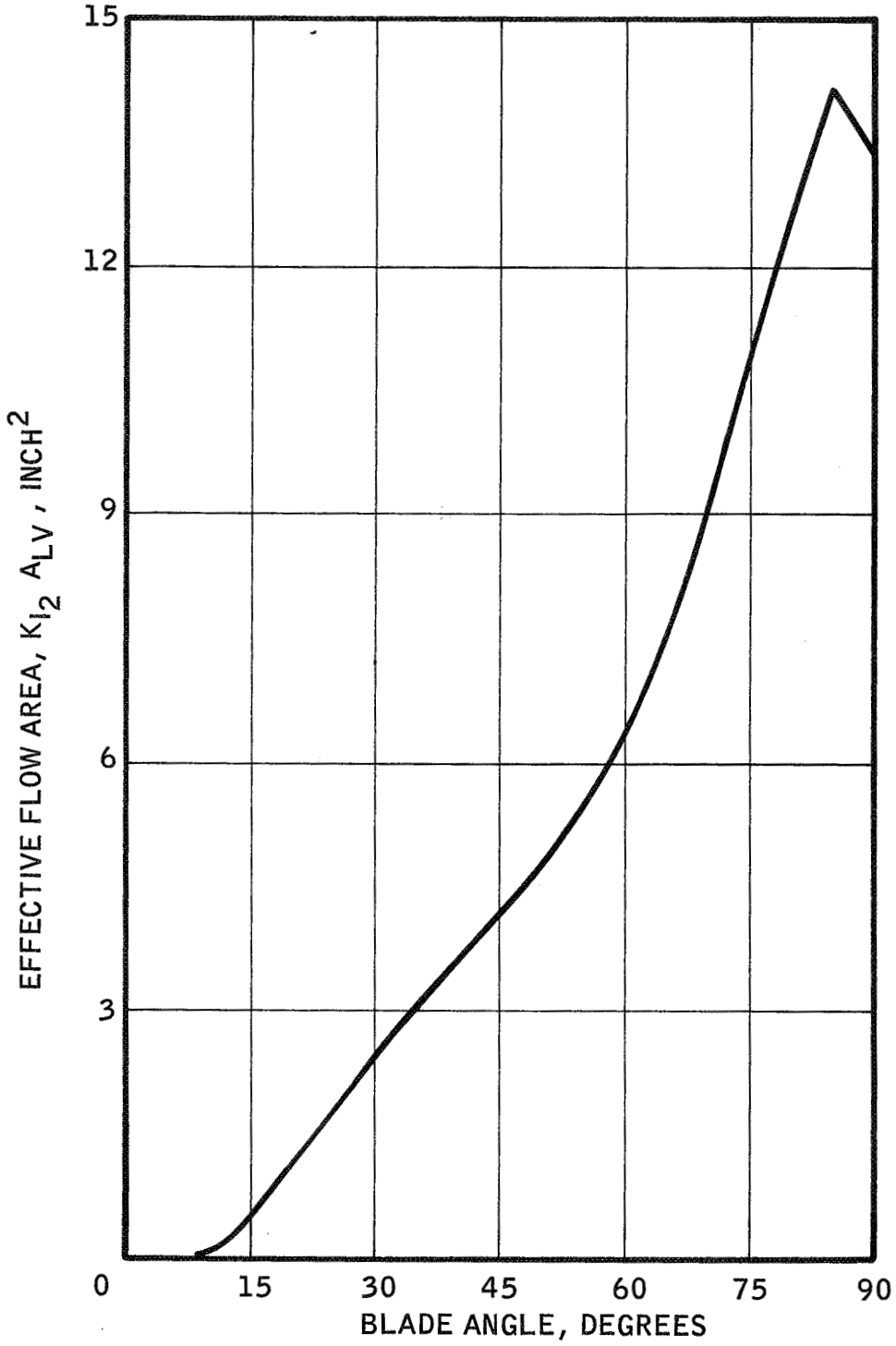

EFFECTIVE FLOW AREA AS A FUNCTION OF BLADE ANGLE

LOAD VALVE

Figure III-D,2

NOTE:

$$\text{OPEN-LOOP RESPONSE} = \frac{0.332\, K_a\, G_c}{(0.0455)(0.0074)} \cdot \frac{1}{S(S+22)(S+135.2)}$$

$K_a G_c = 6.1$ FOR $K_v = 2\ \text{SEC}^{-1}$

LEGEND:

X = OPEN-LOOP POLES

□ = CLOSED-LOOP POLES

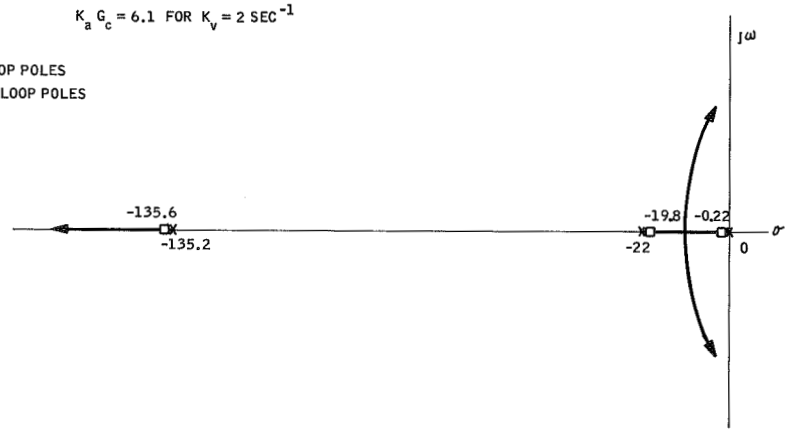

LOAD-VALVE CONTROL SYSTEM ROOT-LOCUS PLOT

Figure III-D,3

LEGEND:

K_1 = 2.6 IN.^{3}/SEC/MA

τ_h = 0.004 SECOND

A_p = 2.95 IN.^{2}

K_{bv} = 1.26 IN.^{2}/IN.

K_b = 30.2 PSI/IN.^{2}

τ_1 = 0.0176 SECOND

τ_2 = 0.005 SECOND

τ_3 = 0.0162 SECOND

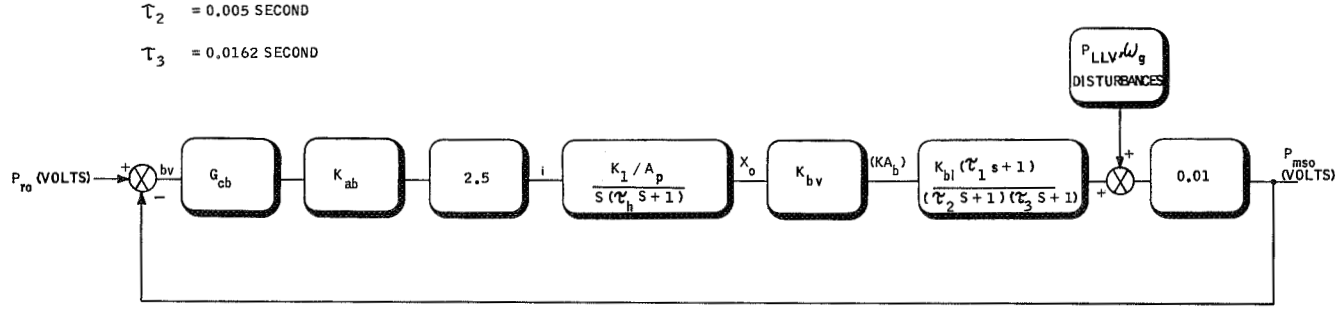

BLOCK DIAGRAM OF BLEED-LINE CONTROL LOOP

Figure III-D,4

NOTE: $KA_b = 0.1892\ K_\omega$

$$K_\omega = \frac{\text{FLOW (lb.sec)}}{\sqrt{\triangle P\ (\text{psi}) \times \text{Sp.Gr.}}}$$

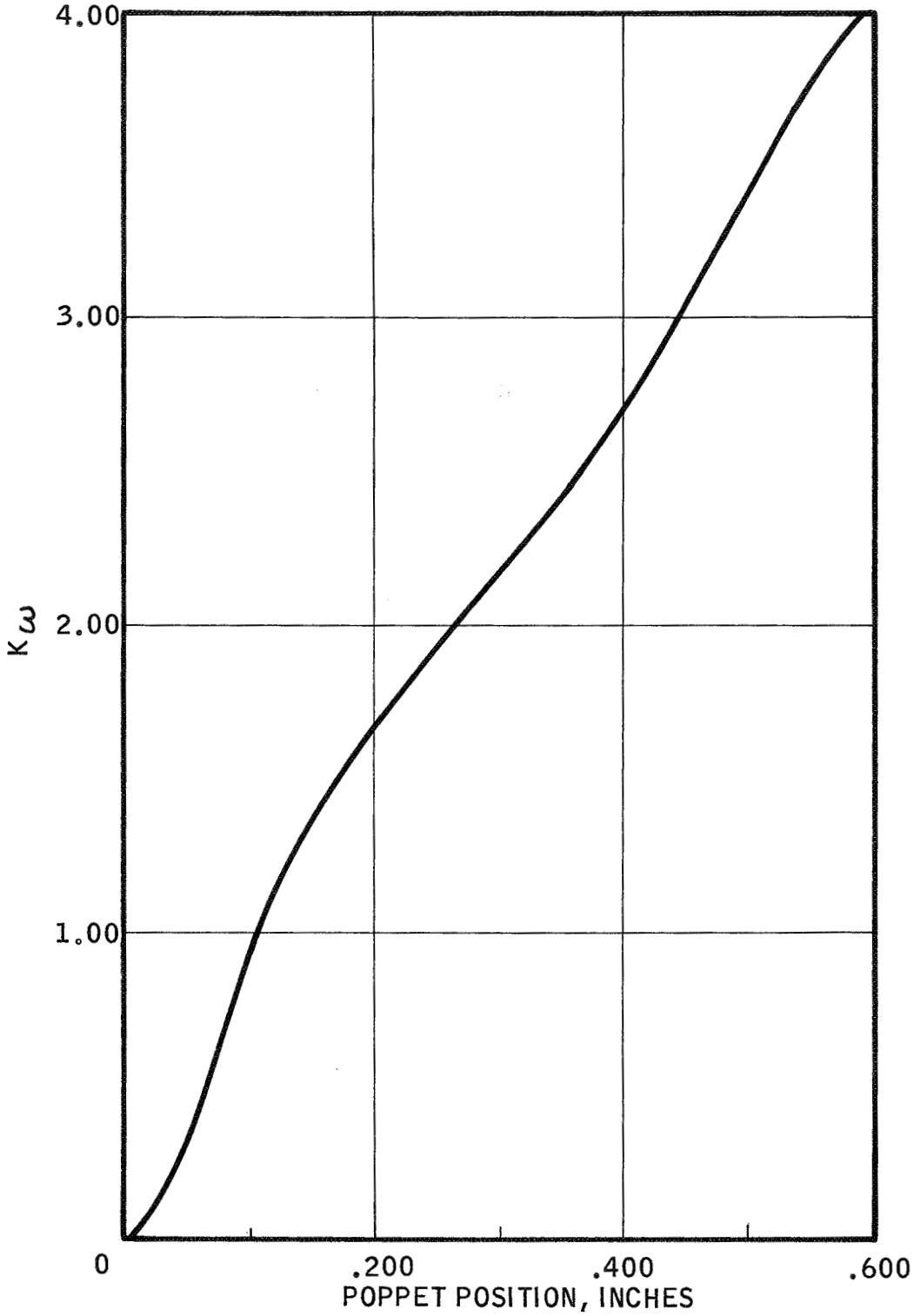

FLOW COEFFICIENT (K_ω)

AS A FUNCTION OF VALVE POSITION BLEED-LINE VALVE

Figure III-D,5

NOTE: OPEN-LOOP RESPONSE = $\dfrac{0.84\, K_{ab}\, G_{cb}\,(50{,}000)}{S\,(S+200)\,(S+250)}$

$K_{ab}\, G_{cb} = (5)(7.15)$ FOR $K_v = 30\ \mathrm{SEC}^{-1}$

LEGEND:

X = OPEN-LOOP POLES

□ = CLOSED POLES

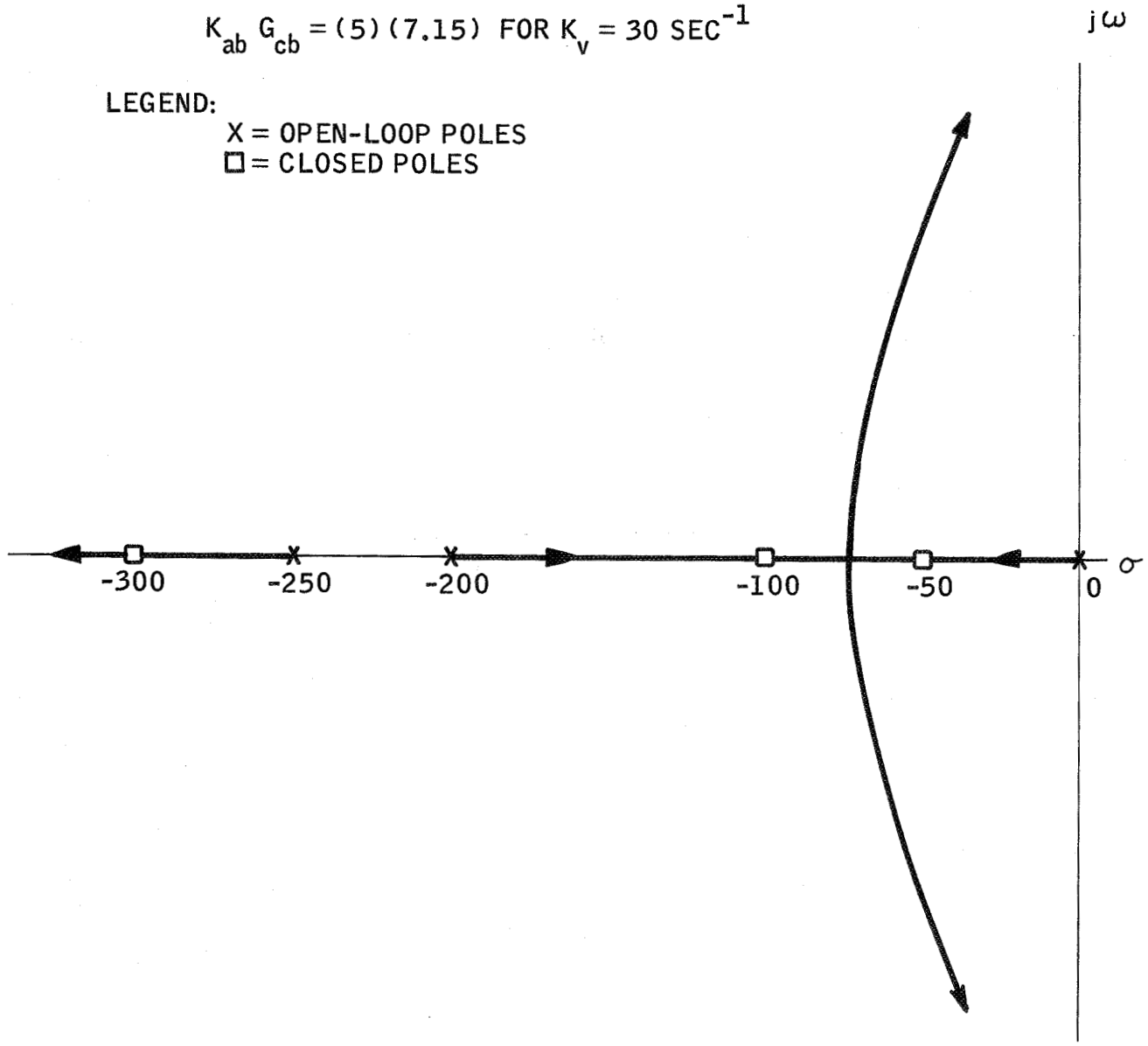

ROOT LOCUS PLOT FOR BLEED-LINE CONTROL SYSTEM

Figure III-D,6

LEGEND:

K_1	= 1.62	ω_n	= 7518
A_p	= 10 IN.^{2}	ζ	= 0.82
K_o	= .75 RAD/IN.	K_{th}	= .0305
K_{gv}	= .0577	τ_{th}	= 0.1 SECOND
K_y	= 32.2 DEGREES/IN.^{2}		
τ_4	= .028 SECOND		

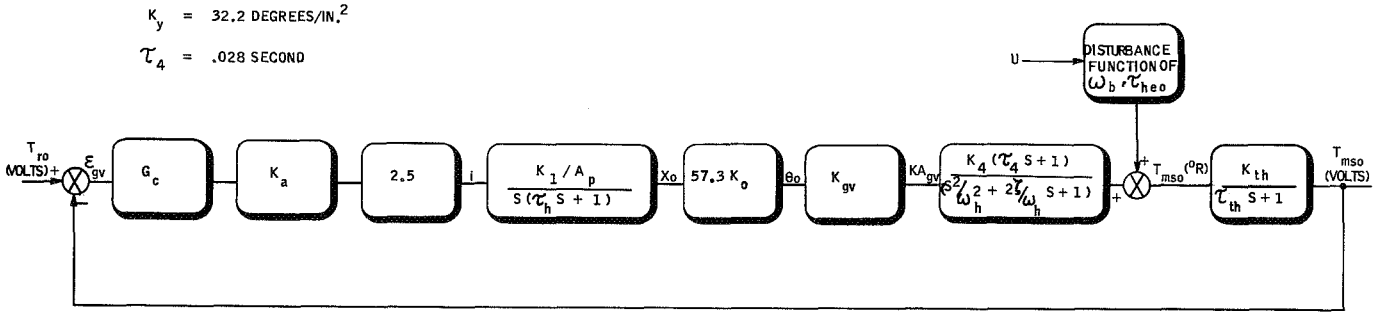

BLOCK DIAGRAM OF GAS-FARM VALVE CONTROL LOOP

Figure III-D,7

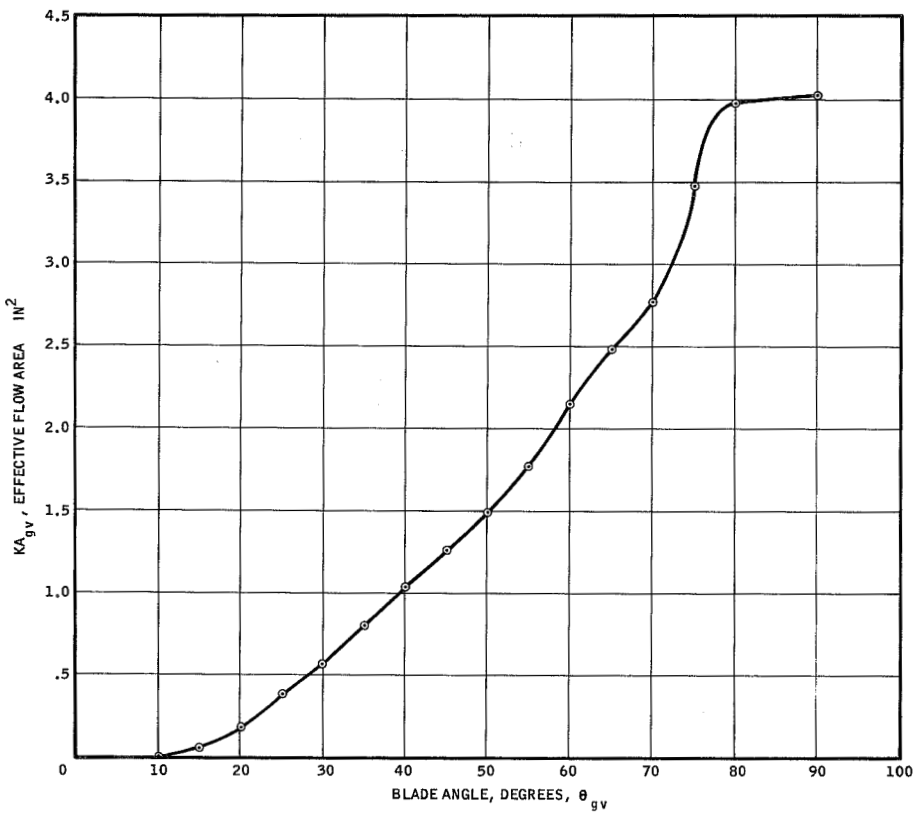

GAS-FARM VALVE EFFECTIVE FLOW AREA

Figure III-D,8

NOTE:

$$\text{OPEN-LOOP RESPONSE} = \frac{35{,}400\, K_{ag}\, G_{cg}\,(S + 35.7)}{S\,(S+10)\,(S+22)\,(S^2 + 124\,S + 5750)}$$

$K_{ag}\, G_{cg} = (1)(4.4)$ FOR $K_v = 4.35\ \text{SEC}^{-1}$

LEGEND:

X - OPEN-LOOP POLES

□ -CLOSED-LOOP POLES

o - OPEN-LOOP ZEROS

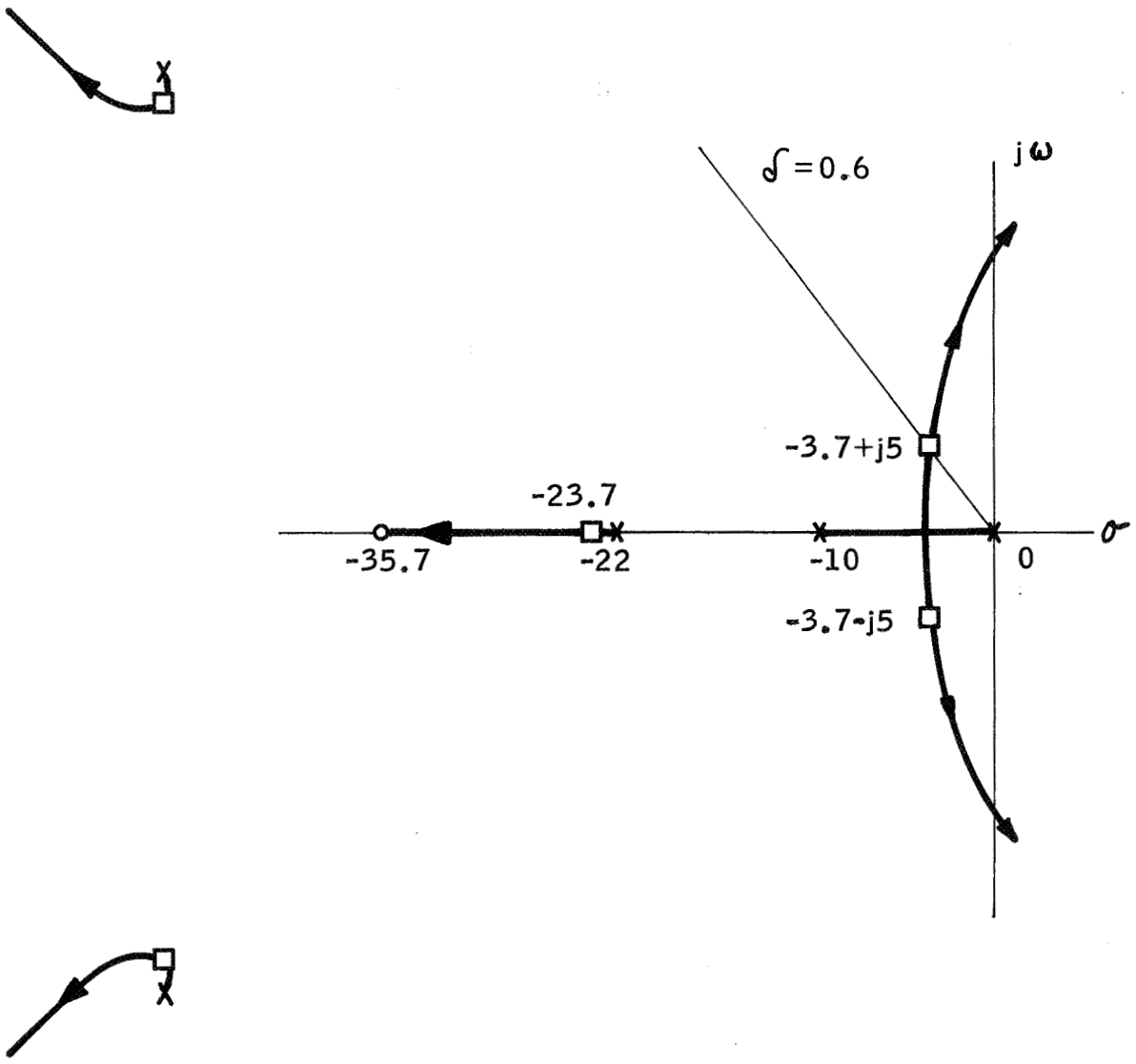

ROOT LOCUS PLOT FOR GAS-FARM CONTROL SYSTEM

Figure III-D,9

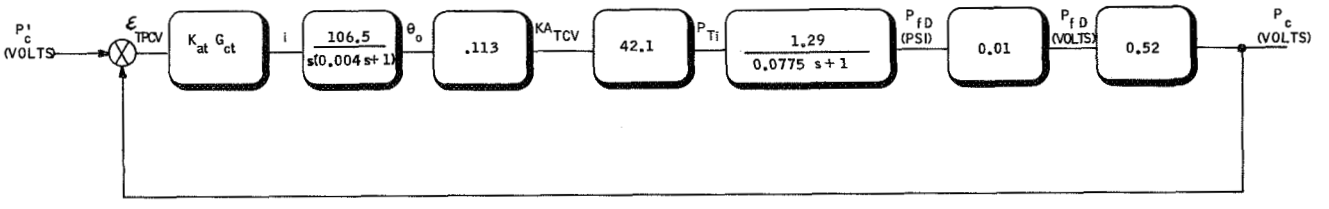

BLOCK DIAGRAM FOR TURBINE POWER CONTROL LOOP

Figure III-D,10

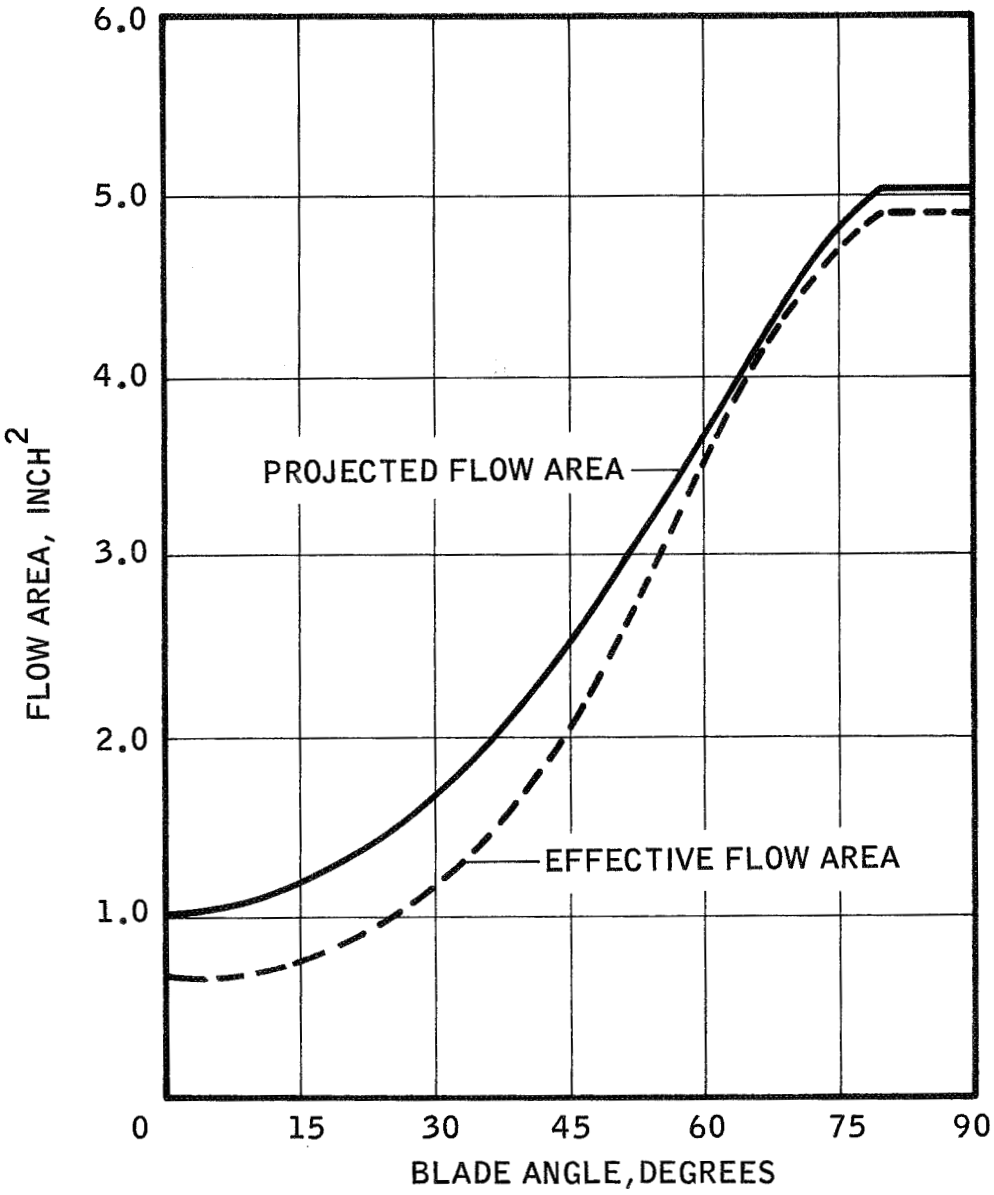

FLOW AREA AS A FUNCTION OF BLADE ANGLE PROTOTYPE TPCV

Figure III-D,11

NOTE: OPEN-LOOP RESPONSE $= \dfrac{11{,}000\ K_{at}\ G_{ct}}{S\,(S+12.9)\,(S+250)}$

$K_{at}\ G_{ct} = (1)\,(3)$ FOR $K_v = 10.2\ \mathrm{SEC}^{-1}$

LEGEND:

X = OPEN-LOOP POLES
□ = CLOSED-LOOP POLES

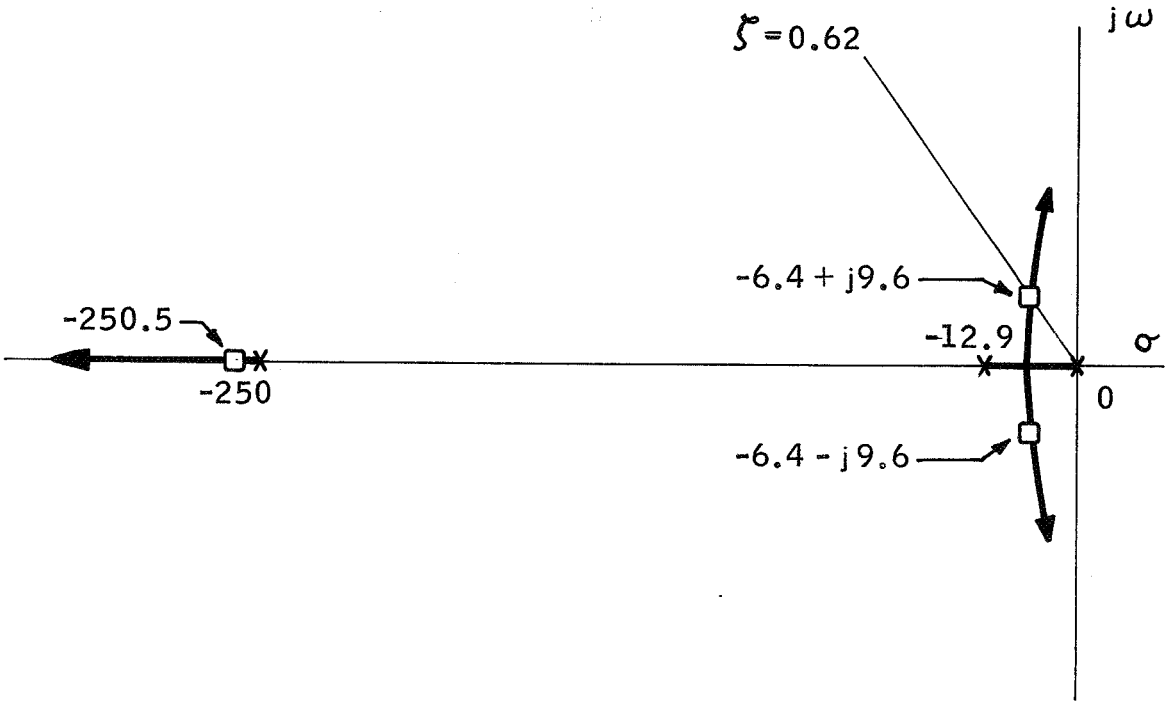

ROOT LOCUS PLOT FOR TURBINE POWER CONTROL SYSTEM

Figure III-D,12

IV. TEST PROCEDURES

A. COMPUTER-CONTROL SYSTEM CHECKOUT

After the analog computer (Reactor Simulator) was installed in the Control Room at Test Stand C-6, the control loops were individually checked for continuity, polarity of transducer signals, and polarity of servo-actuator error signals. Since the velocity-control loops could not be closed without hydrogen flowing in the system, the servo-actuators were checked as positional controllers, using the sequencing arrangement shown in Figure I-C,1. Taking the P_{mso} loop as a typical example, the pressure transducer was removed from the test system and a pressure of 650 psi applied by means of a portable hand-loader. The resulting signal was brought down to Amplifier 6, Figure II-B-6,1, where the reference voltage, P_{ro}, was applied by an initial-condition Pot. on the output of Amplifier 1. By raising and lowering P_{ro}, the bleed-line valve was opened and closed, indicating continuity and correct signal polarity.

In the case of the T_{mso} loop, the temperature resistance bulb was removed from the mixing section and dipped into a Dewar of liquid nitrogen, providing a fixed reference temperature of -320°F. By increasing or decreasing the output of Amplifier 3 above or below a voltage corresponging to -320°F, the gas-farm valve was opened or closed.

No noise problem was encountered with any of the transducer signals despite the necessarily high amplification. However, an error in the pressure signals in the order of -3.5% was noted during the checkout procedure. This loss was attributed to attenuation in the signal transmission lines.

The static and dynamic performance of the computer alone was checked prior to a test run by applying a 5-sec ramp input of $T_{c\ reference}$, with P_{fD} = 8 volts, and comparing the transient response of the circuit to that of Figure II-B-7,2.

B. TEST PROCEDURES

The procedure followed in all tests was essentially the same: the safety valve (Figure I-C, 1) was opened and the pump supply line allowed to fill with LH_2 down to the suction valve near the pump; the tank pressure regulator was set for tank pressure, as specified for each test, just before countdown; countdown began when the supply line had cooled until liquid phase hydrogen (as indicated by pressure and temperature probes) existed throughout; on fire-switch closure (FS-1), the suction valve opened and LH_2 began flowing into the pump (initially at ambient temperature). With the exception of the load valve, initial valve positions were as follows: Bleed-line valve open; TPCV open; Gas-Farm valve closed. In the first four tests the load valve was closed, but in the last four, various starting positions were used.

In computer-controlled tests, the same procedure was followed, but control of the flow-control valves was transferred from the sequence unit to the analog computer only when stable LH_2 appeared at the pump exit. This point was indicated by a steady pump discharge temperature, T_{fD}, of -418°F and a smoothly rising pressure, P_{fD}.

Shutdown was initiated either when propellant tank level had dropped to 15% of capacity, or when a malfunction occurred. On FS-2, the second set of relays in the sequence unit was energized. If the computer was in operation, the sequencing unit also removed the actuating error signals, leaving only the position command signals shown as V_5 to V_8 in Figure I-C, 1. These signals commanded the BLV, TPCV, and GFV to close, thus stopping flow to the turbine. Simultaneously, the load valve was opened to increase the load on the pump. In the event any of the valves failed to close, a manual switch was to be closed immediately to fire the turbine shut-off valve.

V. TEST RUNS

The first four test runs were strictly heat-capacity start tests; that is, the computer was not used for engine simulation. However, operation of the computer was checked out during two of these runs by feeding the pump discharge pressure signal to it. The last four runs were computer-controlled tests. Individual changes made in the system from run to run are noted below.

During all the tests, the overspeed trip switch was set for 18,000 rpm. This was an arbitrary limit set by the pump group because of a lack of pump data by which impeller thrust loads could be predicted. Hence, it was necessary to lower the steady-state operating point of the system by reducing the reference set-points in the computer.

A. TEST NO. 1.1-01-NXS-001 (Figures V-A, 1, 2, 3, 4, 5, 6)

Tank pressure was set at 22.5 psig prior to FS-1. The turbine started to accelerate at 1800 rpm/sec about 1.0 sec after the fuel suction valve opened, and reached a peak speed of 5750 rpm at FS-1 + 39.2 sec. P_{fD} reached a peak of about 32 psig. Oscillations in P_{fD} appeared at 16 sec after FS-1 and continued through the peak, with a maximum amplitude of about ± 5 psi. P_{fS} increased slightly to 25 psig and also exhibited oscillations of ± 1.5 psi. The frequency of oscillation was about 4 cps on the discharge side and about 1.5 cps on the suction side of the pump.

The low discharge pressure was attributed to both the low speed and the low fluid density. The low speed occurred as a result of excessive pressure loss, 16 psi at the peak point, in the 2 in. ball-check valve downstream of the heat exchanger.

UNCLASSIFIED

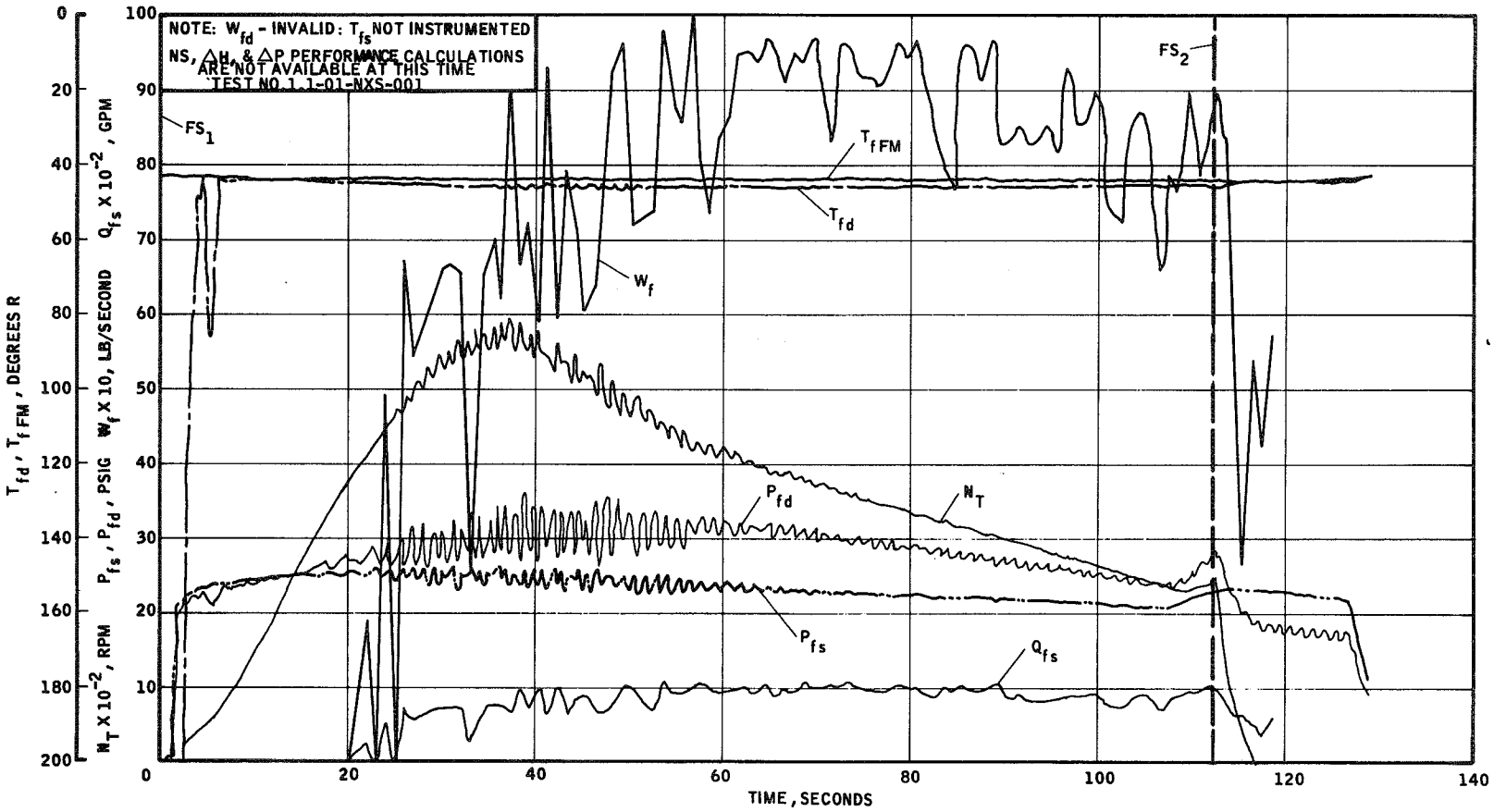

LH_2 PUMP PERFORMANCE CHARACTERISTICS
9-18-61

Figure V-A,1

UNCLASSIFIED

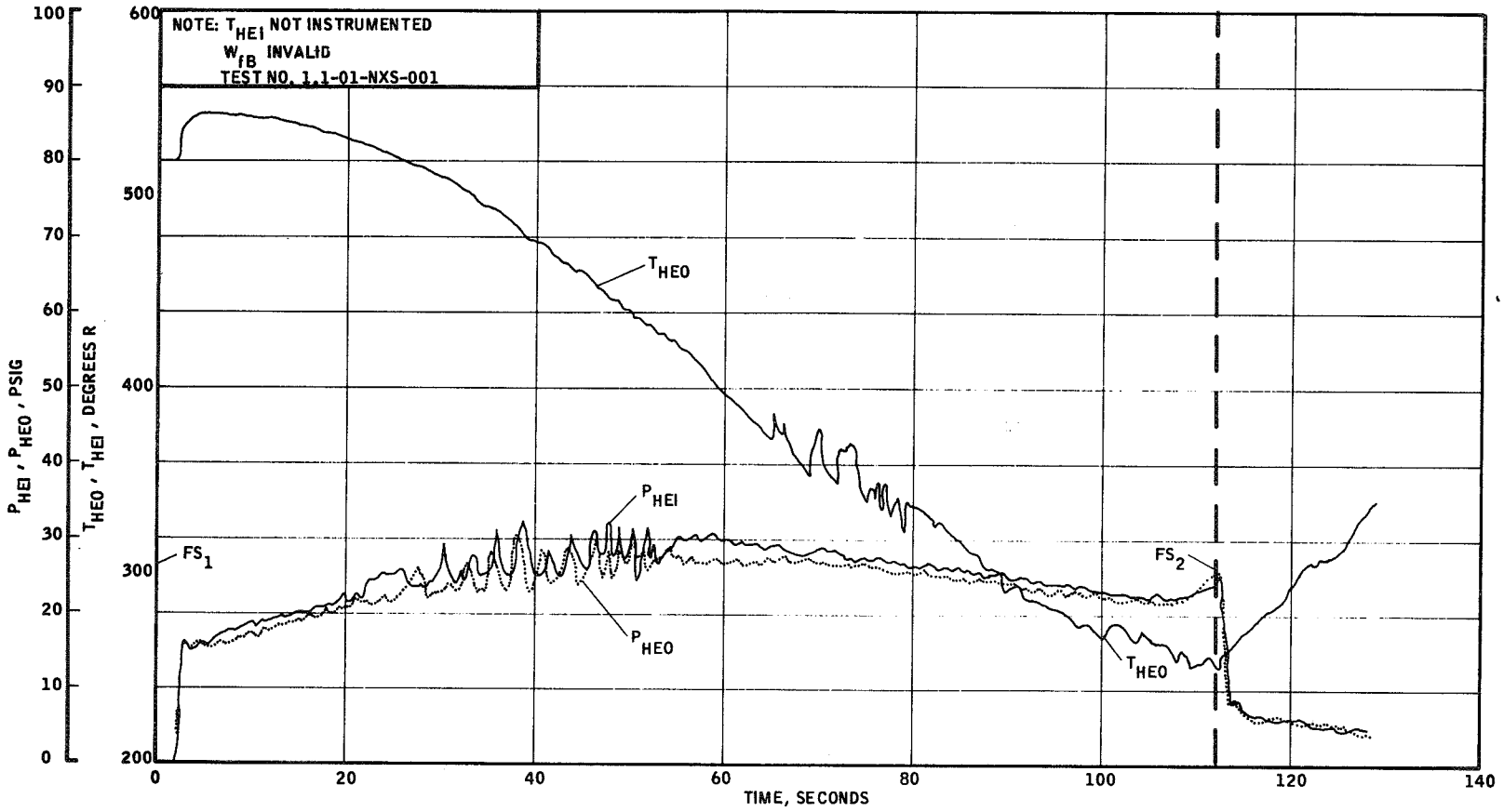

LH_2 PUMP HEAT EXCHANGER PERFORMANCE
9-18-61

Figure V-A,2

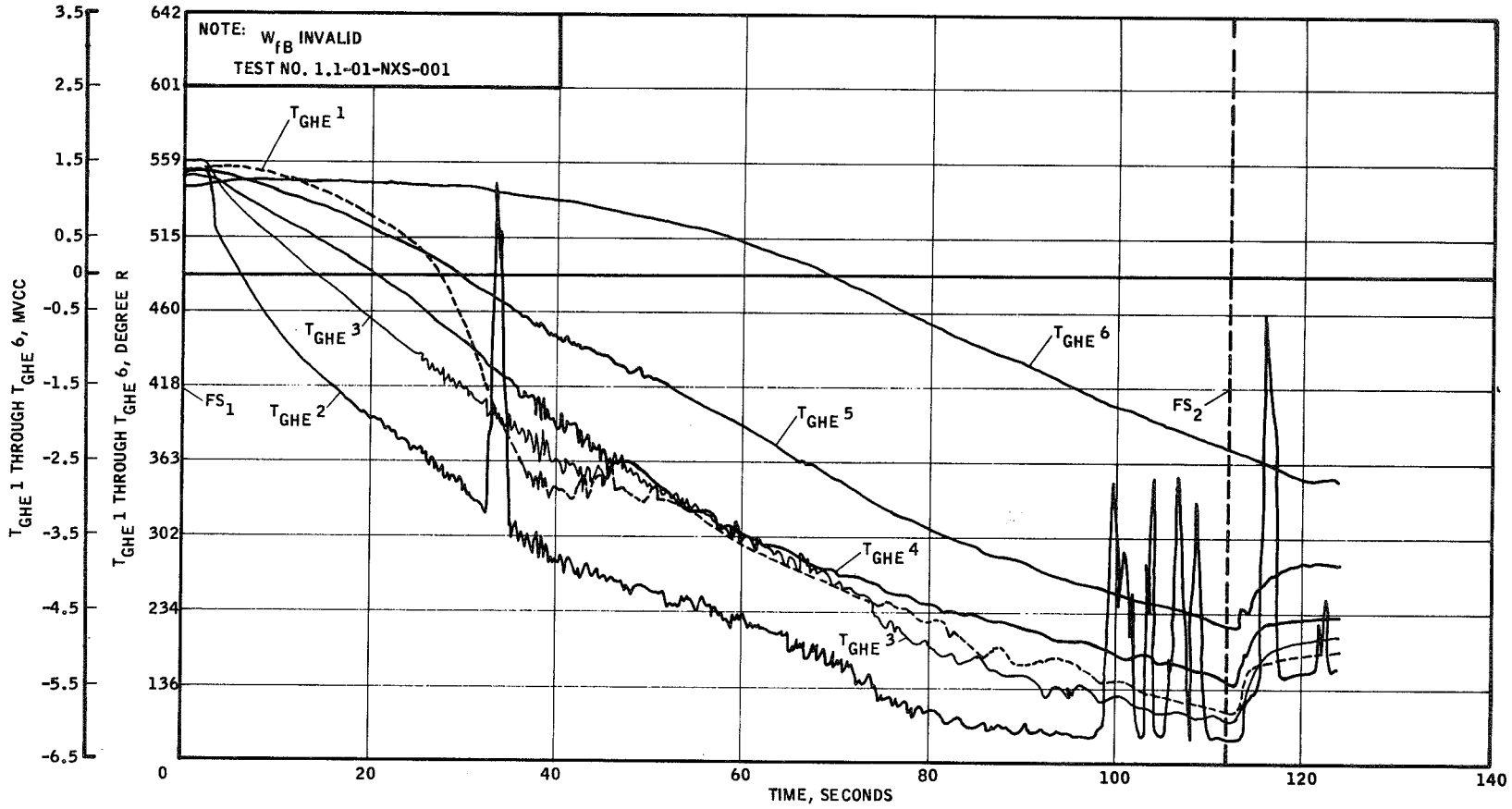

LH_2 PUMP HEAT EXCHANGER PERFORMANCE
9-18-61

Figure V-A,3

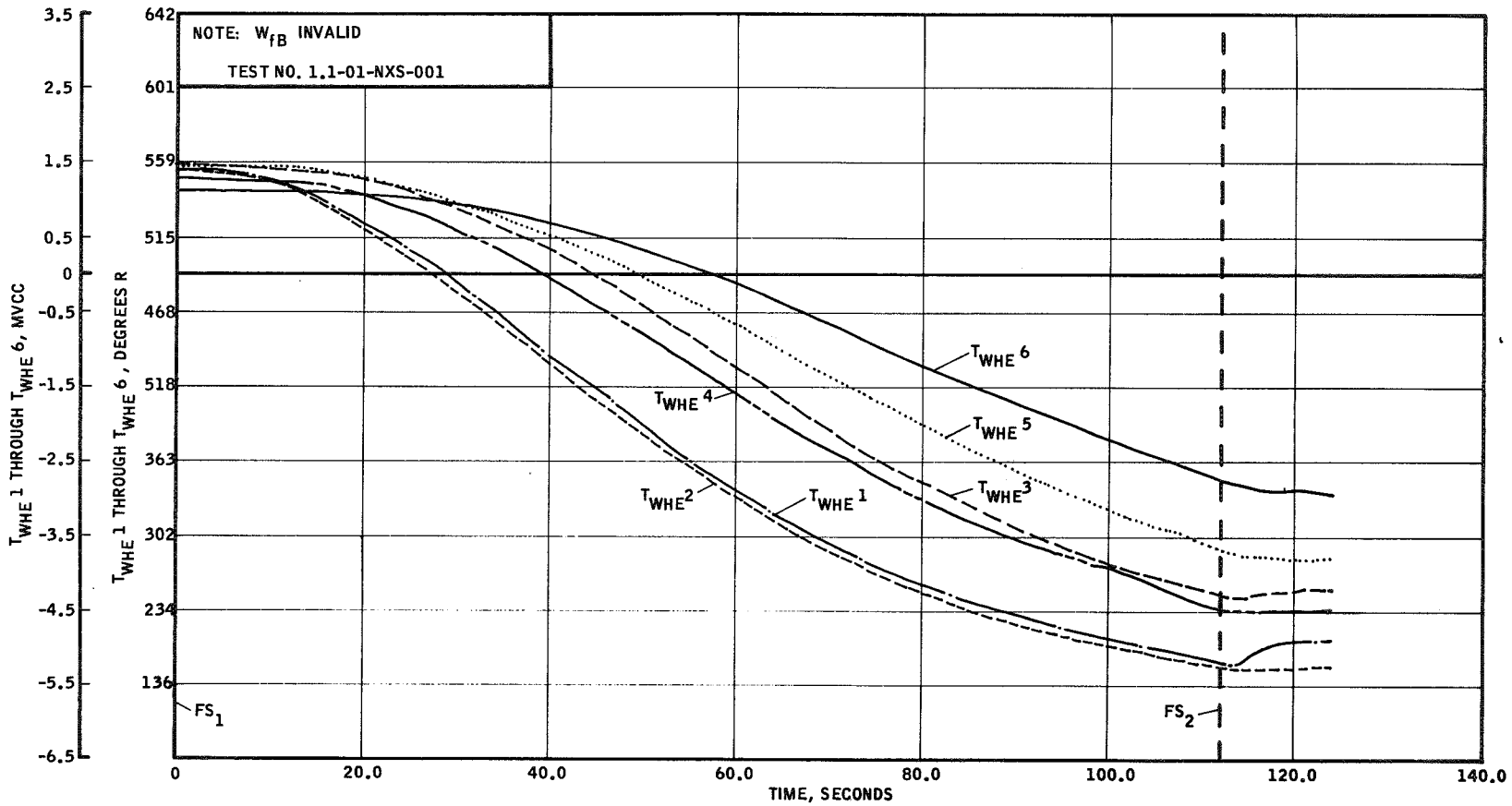

Figure V-A,4

LH_2 PUMP HEAT EXCHANGER PERFORMANCE

9-18-61

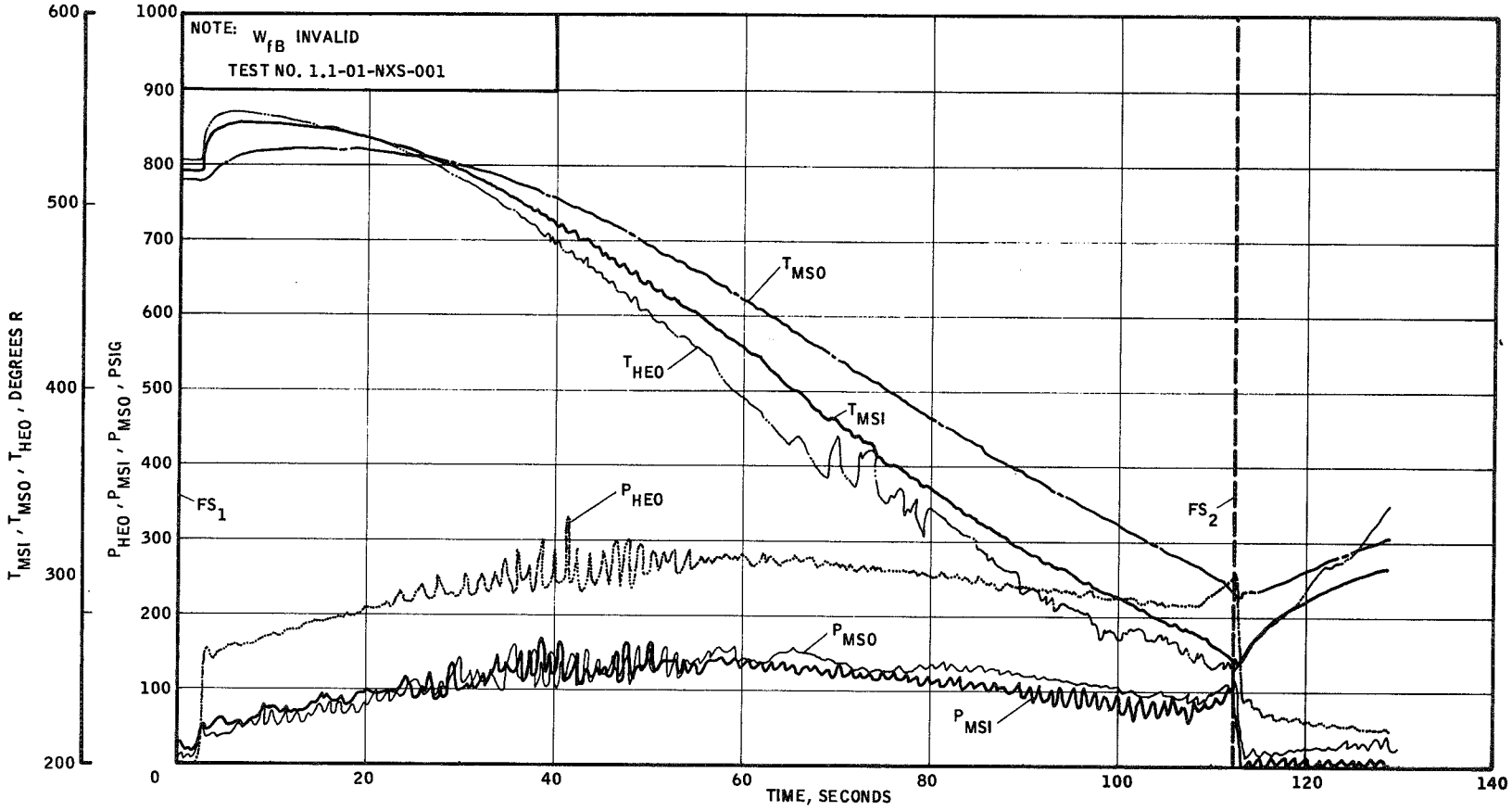

MIXING SECTION PERFORMANCE
9-18-61

Figure V-A,5

UNCLASSIFIED

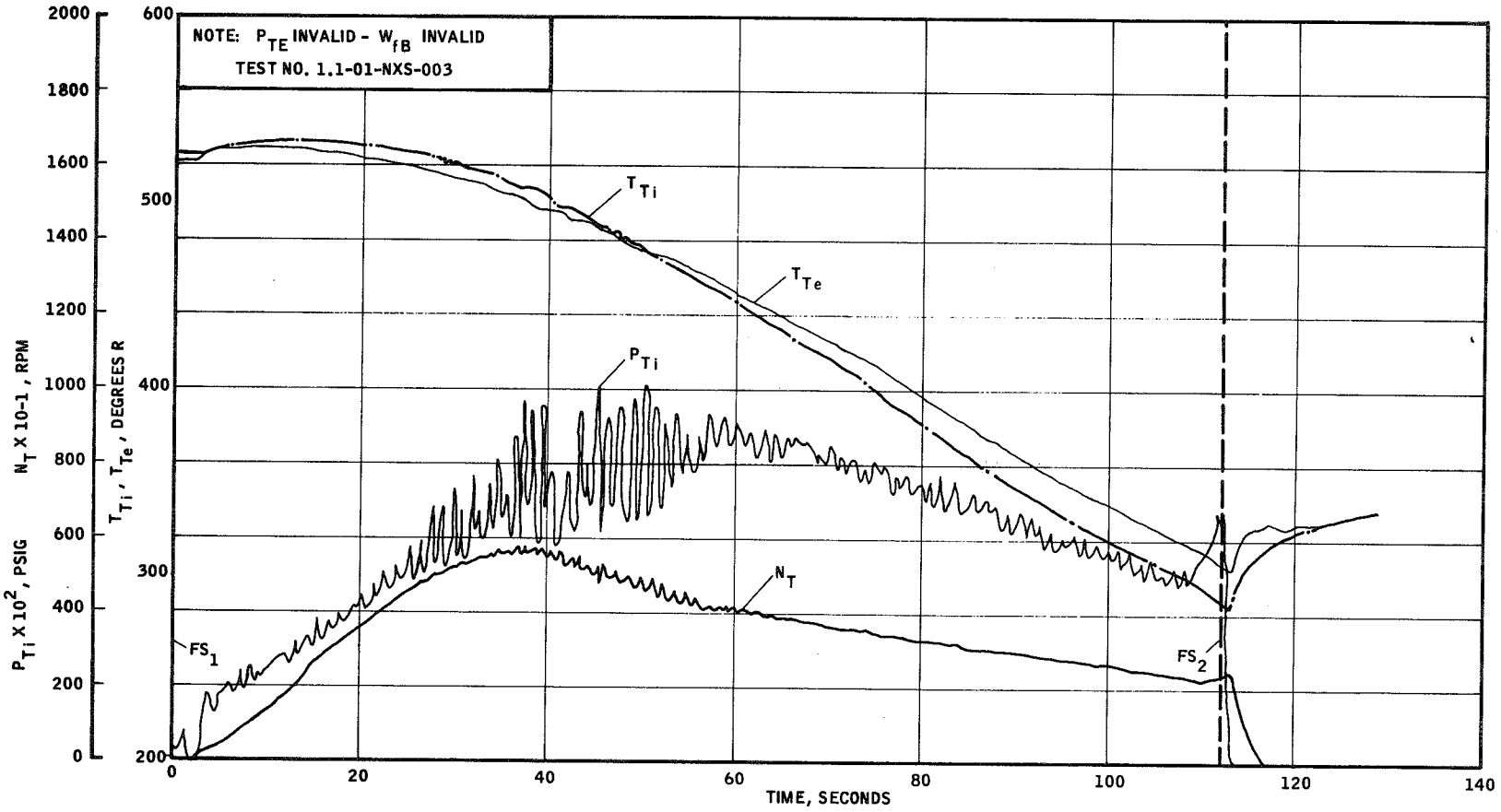

TURBINE PERFORMANCE
9-18-61

Figure V-A,6

UNCLASSIFIED

B. TEST NO. 1.1- 1-NXS-002 (Figures V-B, 1, 2, 3, 4, 5, 6)

Prior to this test, the ball-check valve was replaced by a section of two-inch tube. Tank pressure was again set at 22.5 psig. Because of freezing, the fuel suction valve failed to open for a period of 17.4 sec after FS-1. When it did open, the turbopump accelerated at an average rate of 1000 rpm/sec, reaching a maximum speed of 10,800 rpm, with a corresponding P_{fD} equal to 160 psig. At the same peak, 36 sec after the valve opened, P_{fS} was 18 psig. The flow rate at the peak was 31 lb/sec, but the maximum rate was 36.6 lb/sec about 6 seconds later.

Oscillations appeared in P_{fD} 13 seconds after the suction valve opened, increasing from zero to a maximum of ± 25 psi. On the suction side, the maximum amplitude was ± 6 psi. This time, the frequency on both sides of the pump was the same: about 1.5 cps.

On the last surge, turbopump speed peaked at 13,300 rpm with P_{fD} being 35 psig. As P_{fD} rose, speed dropped, but recovered to reach the second peak at 10,800 rpm because of the higher flow rate. The drop across the 2-in. tube was 8.7 psi at the peak P_{fD}.

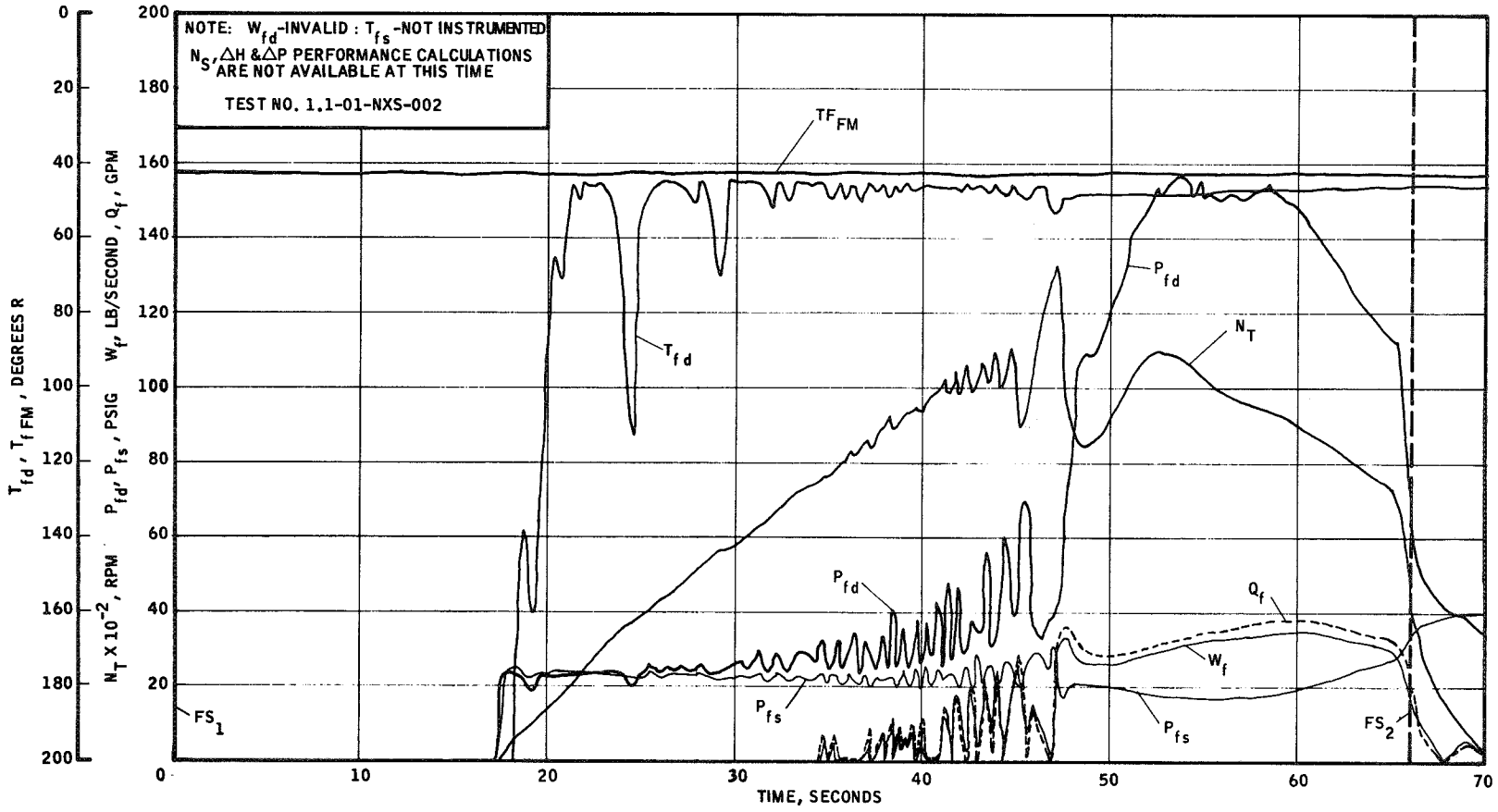

LH_2 PUMP PERFORMANCE CHARACTERISTICS
9-19-61

Figure V-B,1

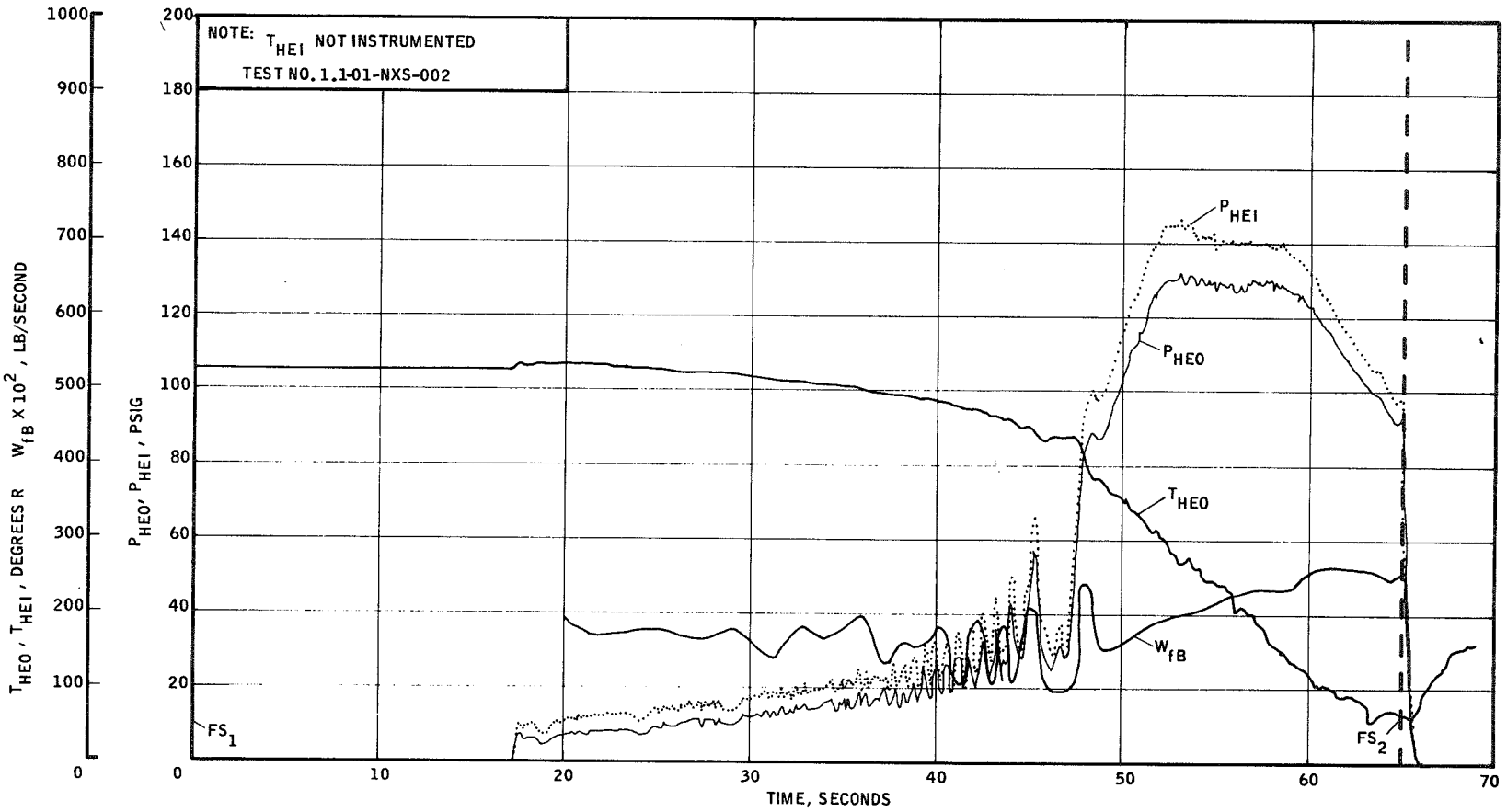

LH_2 PUMP HEAT EXCHANGER PERFORMANCE

9-19-61

Figure V-B,2

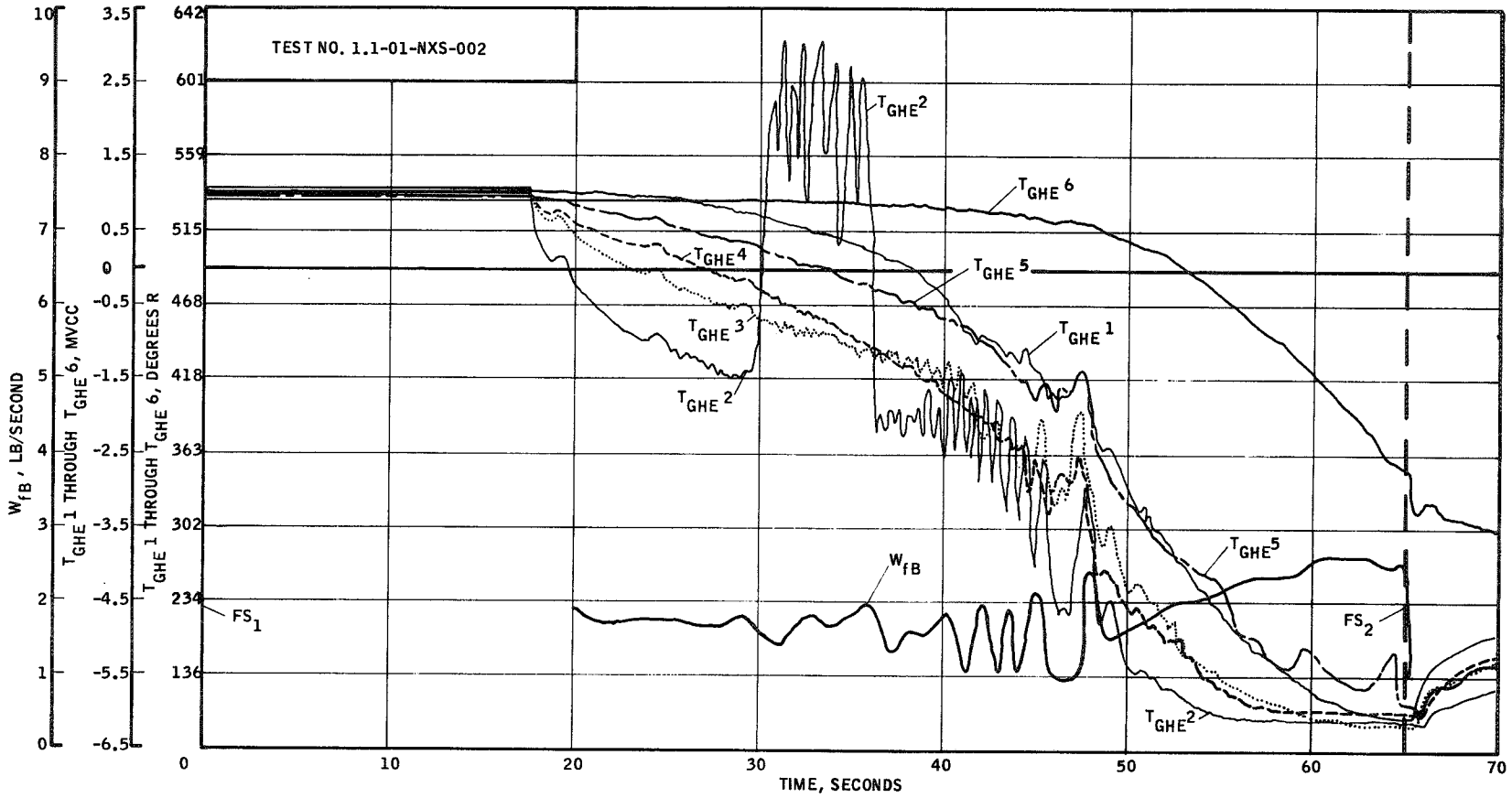

LH_2 PUMP HEAT EXCHANGER PERFORMANCE
9-19-61

Figure V-B,3

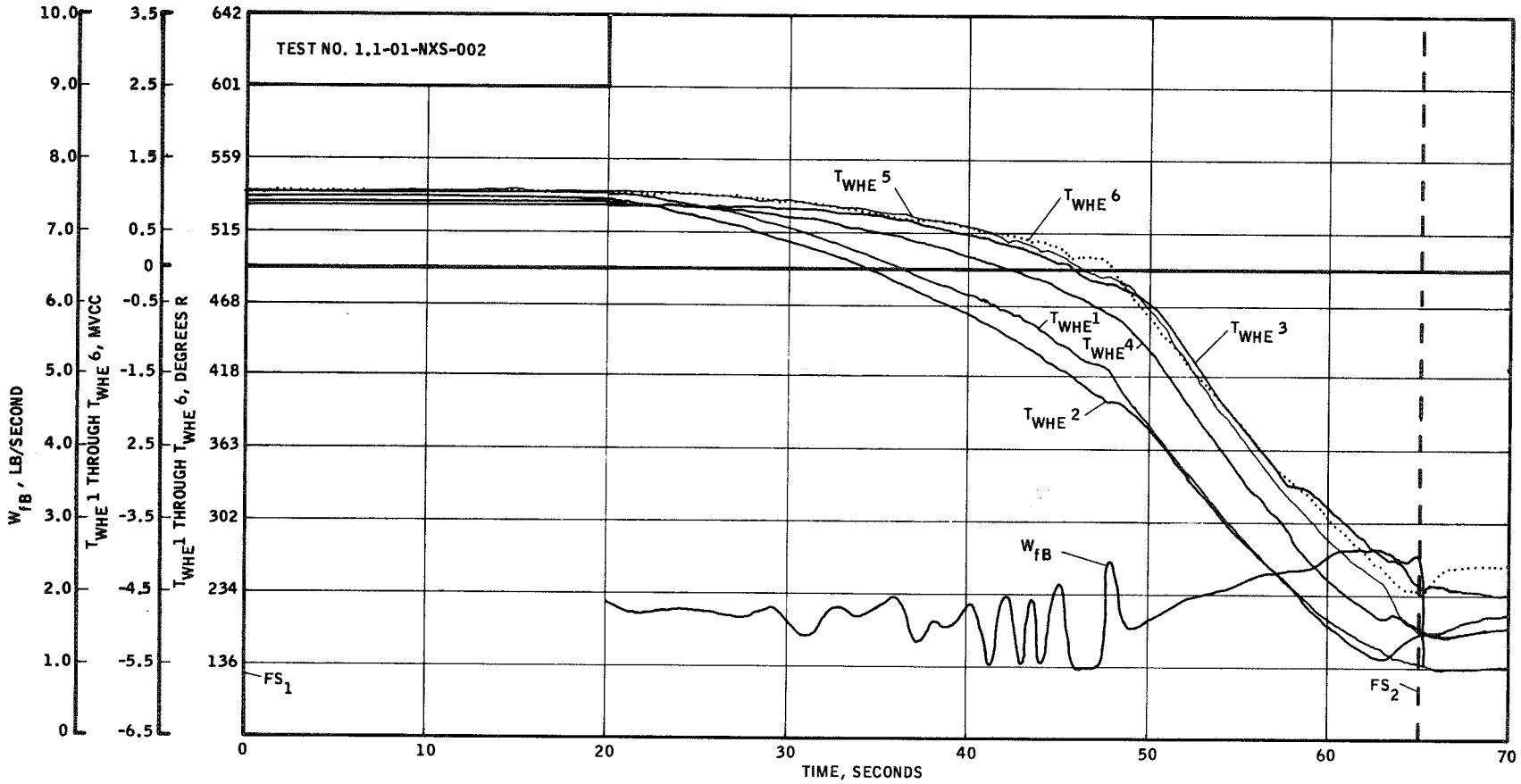

LH_2 PUMP HEAT EXCHANGER PERFORMANCE

9-19-61

Figure V-B,4

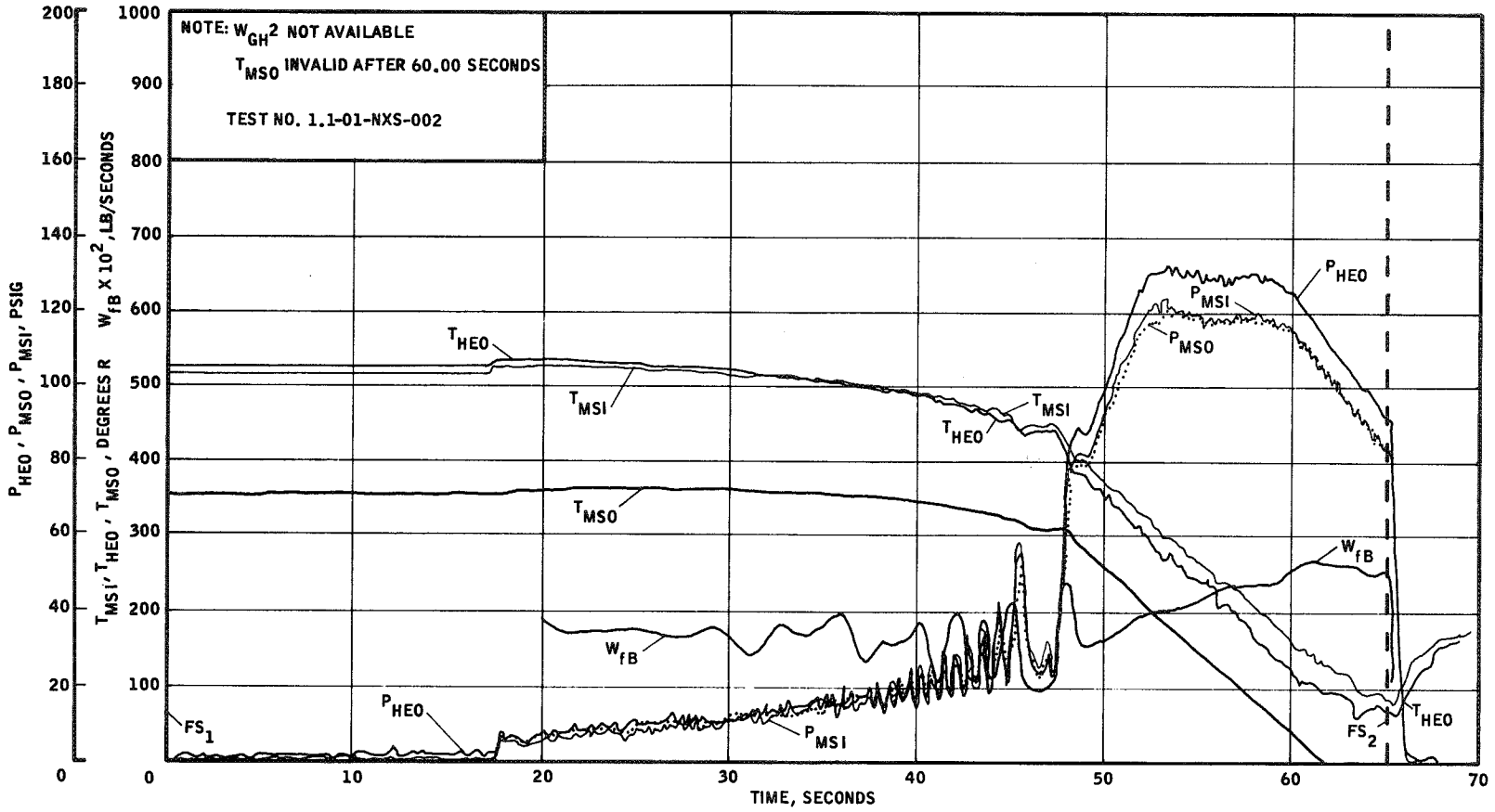

LH_2 PUMP MIX SECTION PERFORMANCE
9-19-61

Figure V-B,5

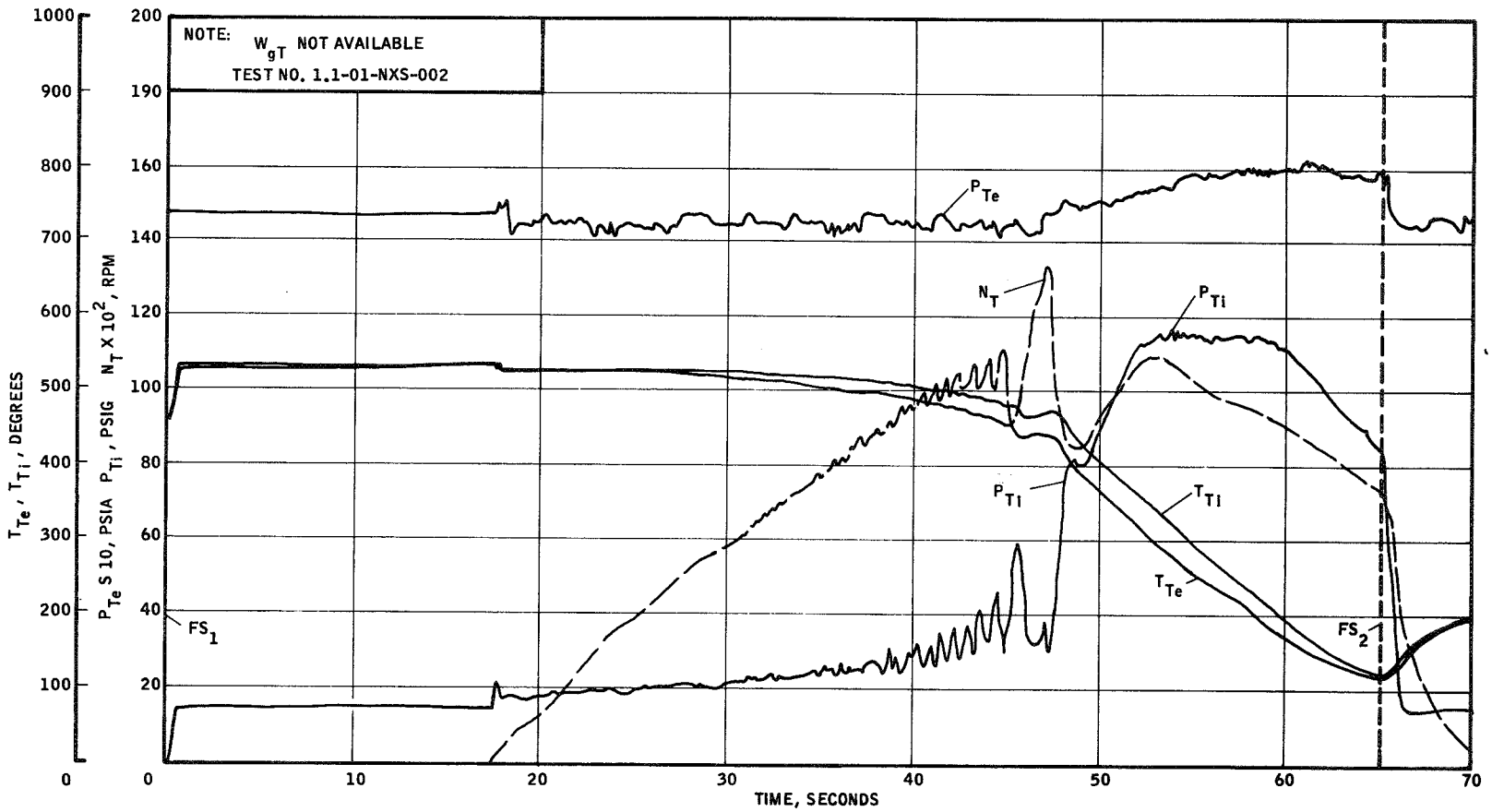

LH_2 PUMP TURBINE PERFORMANCE
9-19-61

Figure V-B,6

C. TEST NO. 1.1-01-NXS-003 (Figures V-C, 1, 2, 3, 4, 5, 6)

For this test, the 2-in. tube was replaced by a 3-in. pipe, and a 2-in. flapper-type check valve was installed ahead of the heat exchanger. A heating coil was wrapped around the hydraulic actuator of the fuel suction valve to prevent it from refreezing.

Tank pressure was set at 62 psig. The turbopump accelerated at 3200 rpm/sec, reaching a peak speed of 17,000 rpm at 7.7 sec after valve opening, and following the first dip. At that peak, P_{fD} was 470 psig, and P_{fS} was 39.5 psig. The first peak speed of about 15,200 rpm occurred 5.5 sec after valve opening when P_{fD} was 75 psig, at the bottom of an oscillation. Speed decreased steadily from the second peak to 5500 rpm when FS-2 initiated shutdown. Duration was 28.2 sec. Oscillations occurred again at a frequency of 3 cps, and built up to a peak amplitude of $\pm$40 psi.

The flapper-type check valve was retained for the remaining tests as its operation appeared to absorb only about 7% of the total pressure drop across the bleed line.

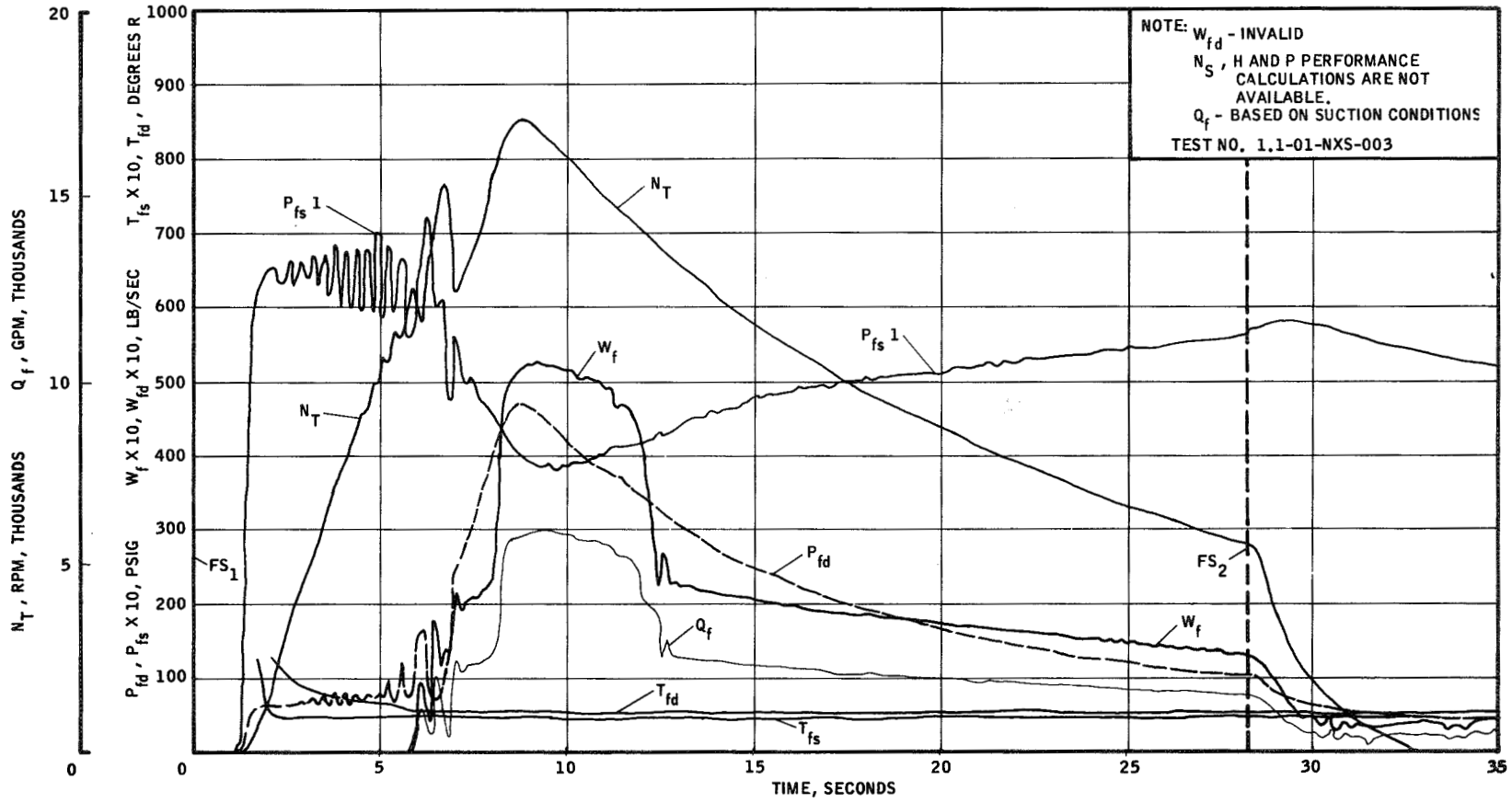

LH_2 TPA PERFORMANCE CHARACTERISTICS
9-28-61

Figure V-C,1

UNCLASSIFIED

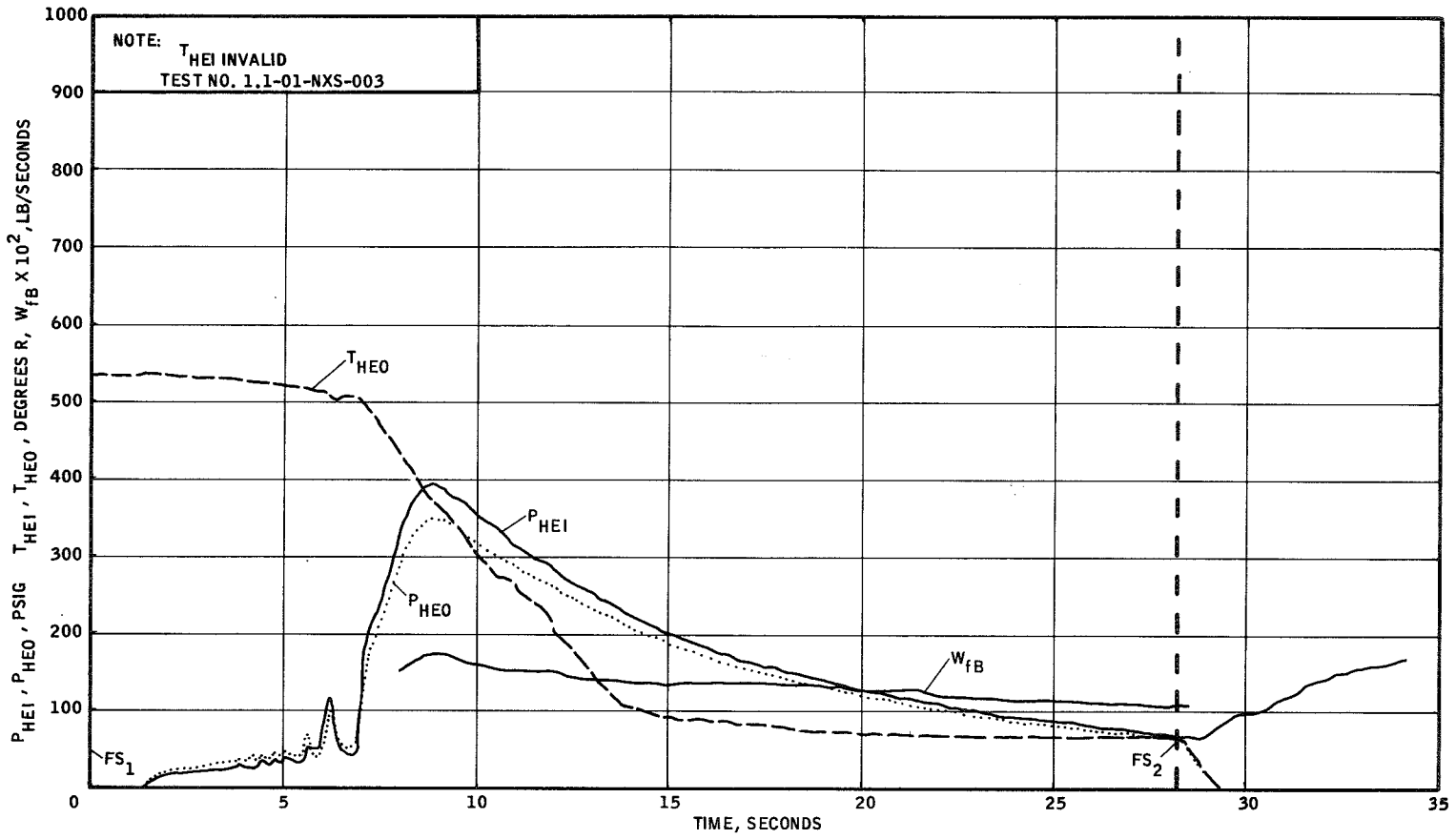

LH_2 PUMP HEAT EXCHANGER PERFORMANCE
9-28-61

Figure V-C,2

UNCLASSIFIED

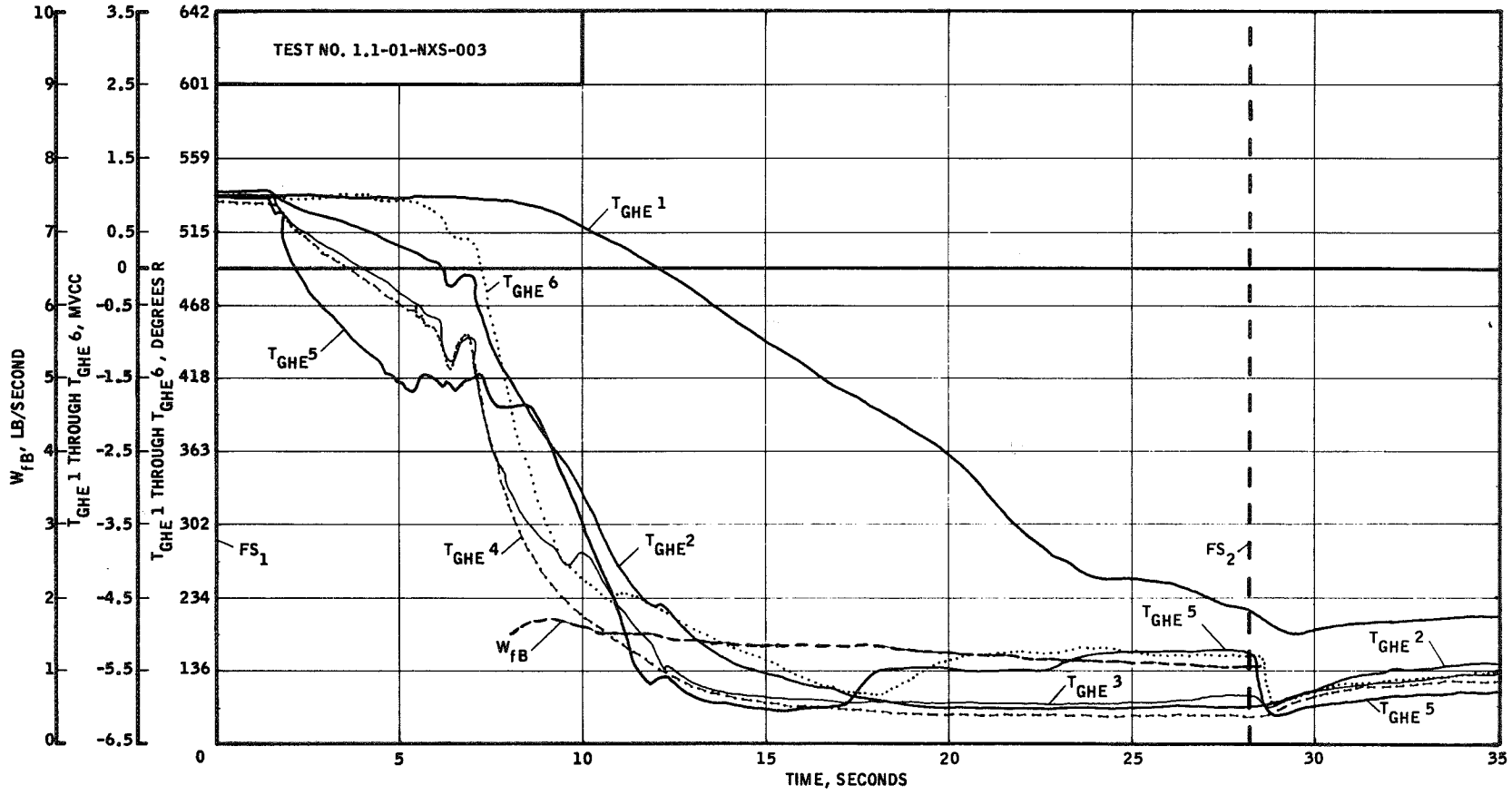

LH_2 PUMP HEAT EXCHANGER PERFORMANCE
9-28-61

Figure V-C,3

UNCLASSIFIED

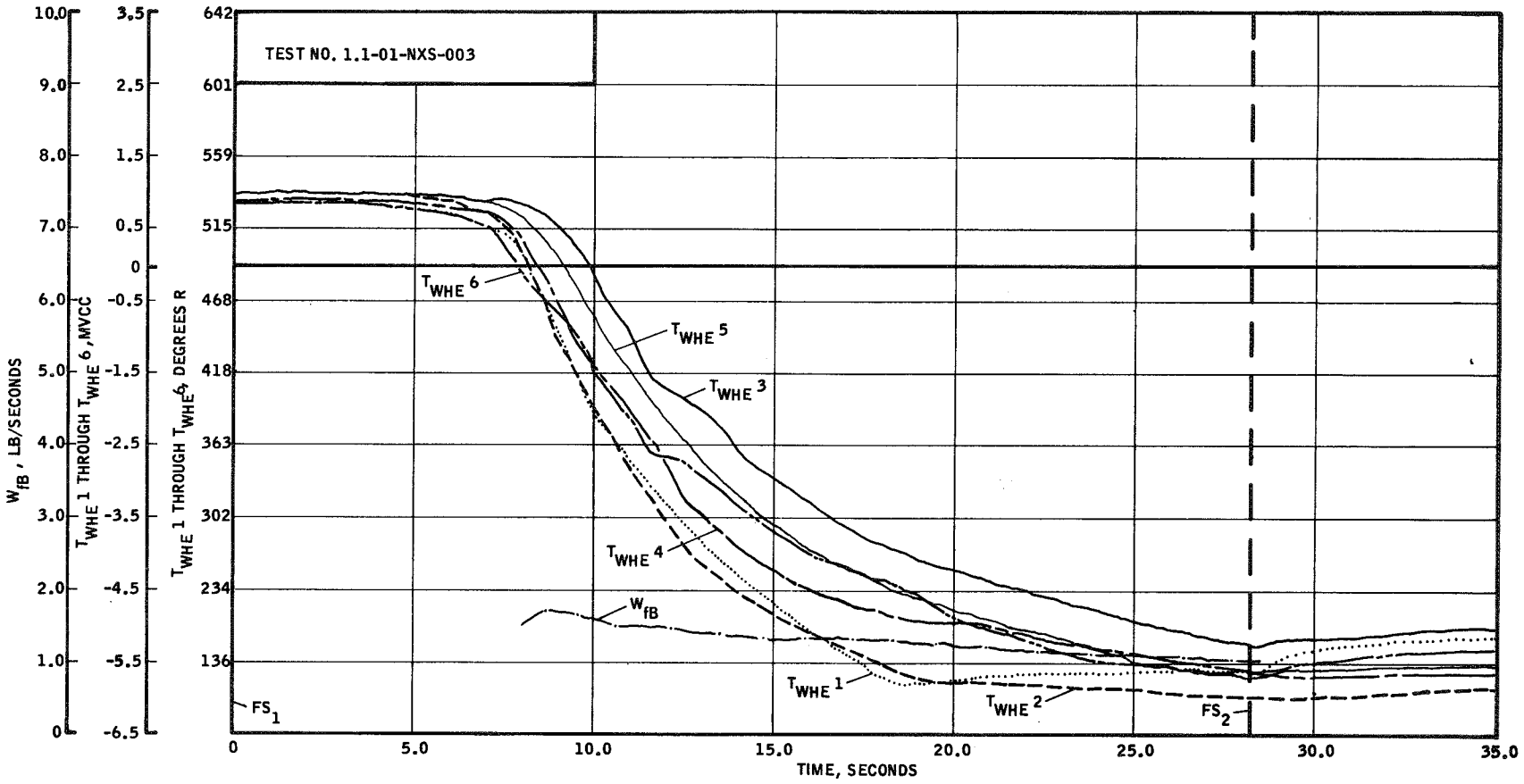

LH_2 PUMP HEAT EXCHANGER PERFORMANCE
9-28-61

Figure V-C,4

UNCLASSIFIED

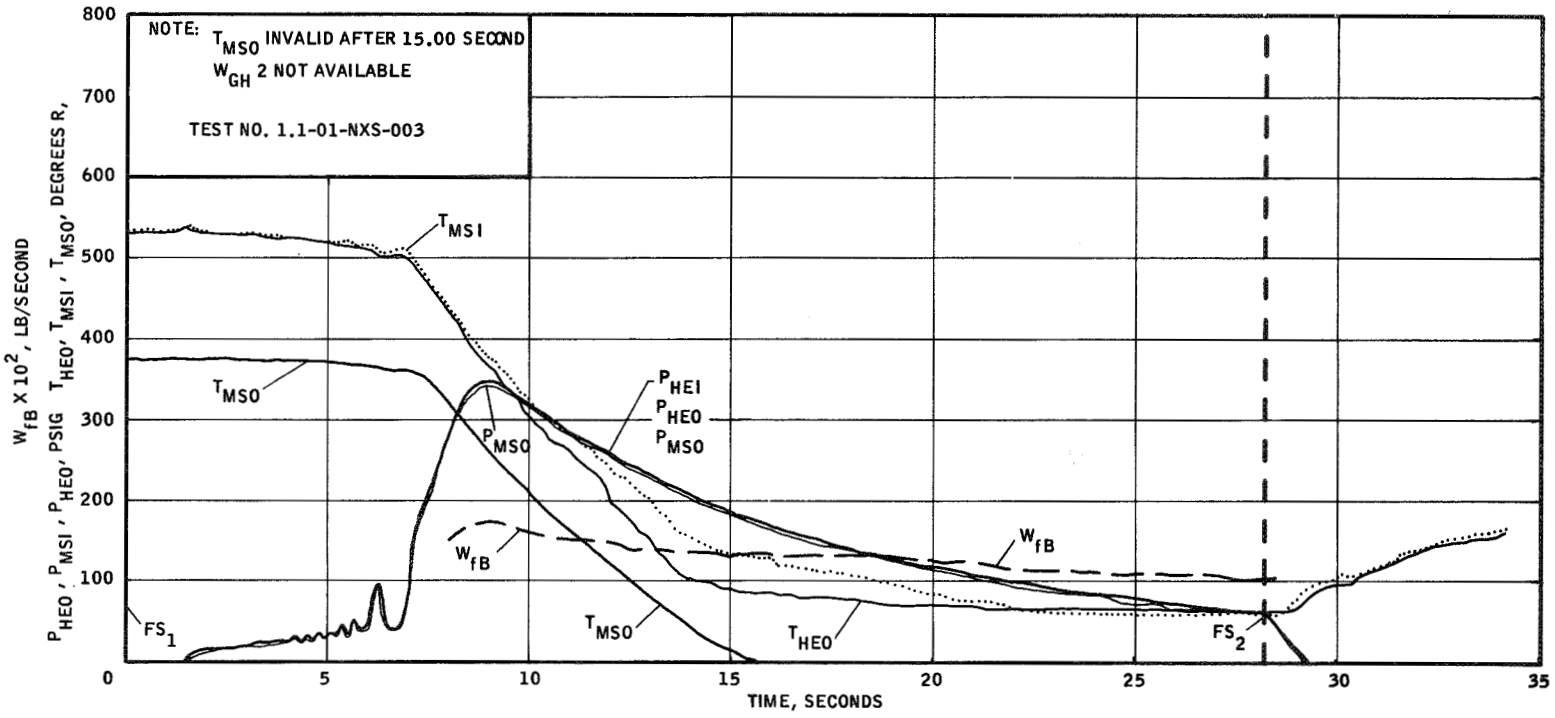

LH$_2$ PUMP MIX SECTION PERFORMANCE
9-28-61

Figure V-C,5

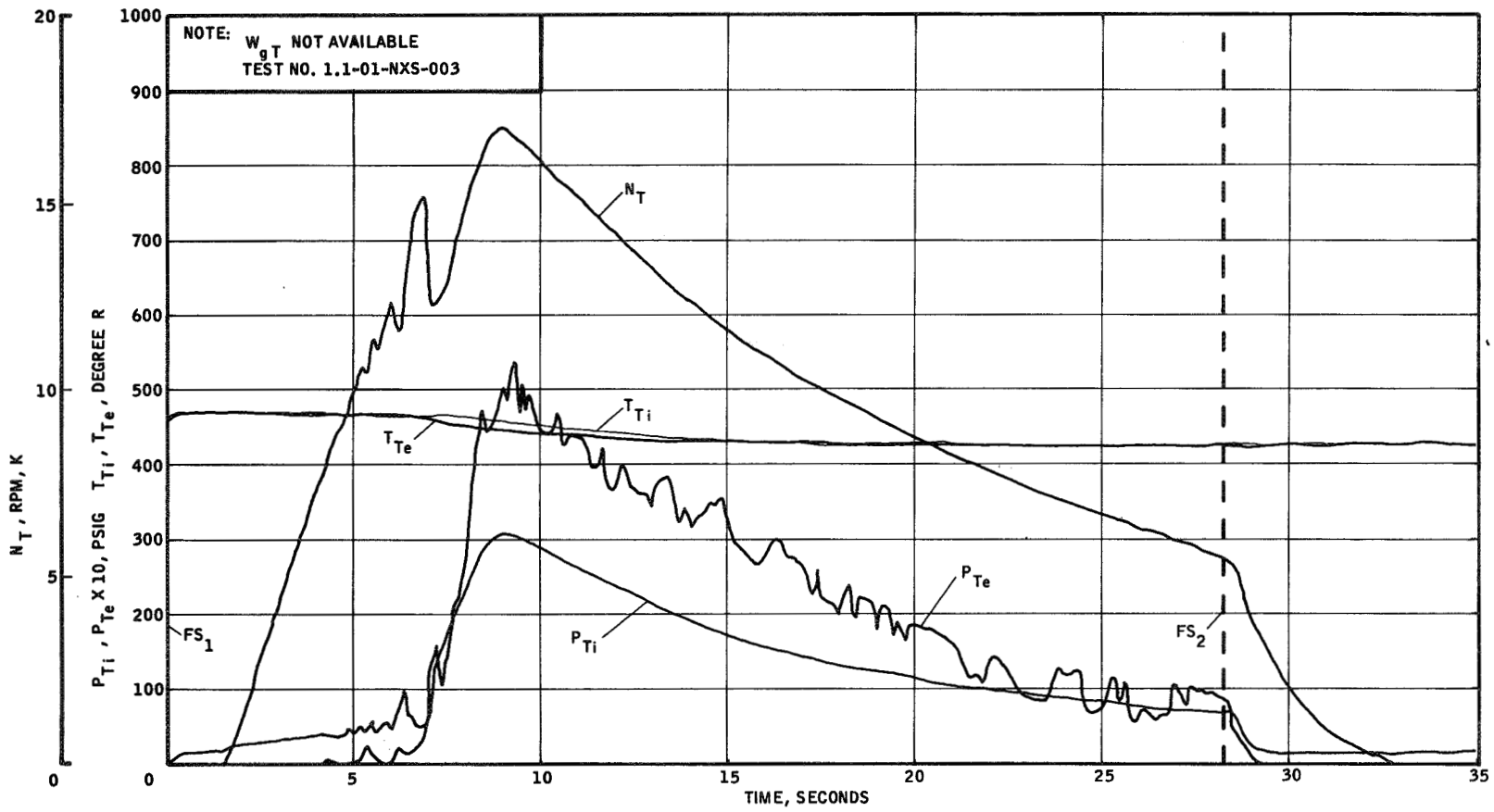

LH_2 PUMP TURBINE PERFORMANCE
9-28-61

Figure V-C,6

D. TEST NO. 1.1-01-NXS-004

This test was a checkout of the turbine overspeed shutdown system. The overspeed sensing circuit was set to close the FS-2 at a speed of 10,800 rpm. Turbine speed was very slowly increased until, at a recorded speed of 10,780 rpm, the overspeed trip closed FS-2 and fired the turbine shut-off valve. The time lapse between FS-2 and the drop in turbine nozzle pressure was determined to be 0.030 sec.

The computer-controlled tests were to be run with the overspeed trip set at 18,000 rpm. Assuming the turbine accelerated from this level at a rate of 160,000 rpm/sec, it would reach a speed of 22,800 rpm by the time the turbine shutoff valve closed. Since the maximum safe pump speed is 36,000 rpm, there was ample margin for pump protection.

E. TEST NO. 1.1-01-NXS-005 (Figures V-E, 1 through 9)

This was the first test in which the computer controlled the system.

Because of the limitation on maximum pump speed, it was necessary to lower the P_c reference set-point in the computer from the design-point value of 550 to 495 psia (4.95 volts). The value of P_{fD} which would yield a steady-state value of P_c equal to 495 in the computer was 680 psia (6.8 volts). From the pump-torque characteristics, the corresponding speed was estimated at 16,500 rpm. The T_c reference set-point was left at the design value of 4090°R (40.9 volts). Both T_c reference and P_c reference inputs started as ramp inputs at the instant control was given to the computer, rising from zero to their set-point values in 5 seconds. The 5-second ramp was chosen to bring the system to a steady-state point as quickly as possible.

Tank pressure was set at 40 psig. The heat-capacity portion of the start was similar to occurrences in previous tests. The computer began operating on FS-1, accepting P_{fD}, and generating w_r, P_{ro}, T_{ro}, and P_c. Figure V-E,7 shows three of the computer outputs and the T_c reference ramp input. At 13.4 seconds after FS-1, stable LH_2 appeared in the pump, and engine control was transferred to the computer by the "Simulator Run" switch. At the same instant, both T_c and $P_{c\,reference}$ ramp inputs were started, at which point speed was 10,800 rpm and P_{fD} was 210 psig. Almost immediately thereafter speed and discharge pressure began to decrease because of the combined effect of two factors. As shown in Figure V-E,8, the load valve opened because w_f was apparently less than w_r and the TPCV closed because P_c was greater than $P_{c\,reference}$. As a result of TPCV closure, P_{mso} exceeded the computed value of P_{ro}, so the Bleed-Line Valve closed. The combined effect of closing the TPCV, thus cutting turbine power, and of opening the LV, which increased pump load, was to cause a sharp decrease in speed. As the ramp input of $P_{c\,reference}$ overtook P_c, the TPCV started to reopen, and turbopump speed started increasing. The bleed-line valve had opened earlier because the rapid decay of P_{mso} had allowed P_{ro} to exceed P_{mso}. The load valve remained open until almost the end of the run. In Figure V-E,8, note that w_r reverses polarity at about FS-1+ 16.4 sec.

About 18 seconds after FS-1, a loud explosion was heard, so shutdown was immediately initiated. However, it turned out that the spark plug on the turbine exhaust stack had failed to ignite the hydrogen gas at FS-1; it was merely a delayed ignition. It made little difference in run time as tank capacity was already low. No damage to the stand resulted from the explosion.

A study of the valve error signals, Figure V-E, 8, and valve position traces indicated that the control loops were operating properly, although the Gas-Farm valve did not open, since the lowest temperature reached in the mixing section was about 285°R. In order for the GFV to open, T_{mso} had to go below 200°R, the steady-state value for T_{ro}. Although the load-valve actuator responded properly to its error signal, a post-test investigation revealed that the P_{fDo} pickup had been inadvertently placed downstream of the orifice where, because of pressure recovery, its output signal underwent a sign reversal. Therefore, the feedback signal was added to the command signal from w_r, and the LV opened.

In the computer, the sign reversal of w_r arose because the ramp input of $T_{c\ reference}$ forced P_{ro} to become greater than the input P_{fD}.

The noise that appeared on the output of Amplifier 2, did so only during a test. No trouble could be found in the amplifier or computer circuit, and no noise existed in the instrumentation circuit during pre-run calibrations taken at the computer. Therefore, the noise was attributed to vibration at the P_{fD} pickup. A 0.005-μ fd-capacitor was inserted in the amplifier feedback to suppress the noise level in further tests.

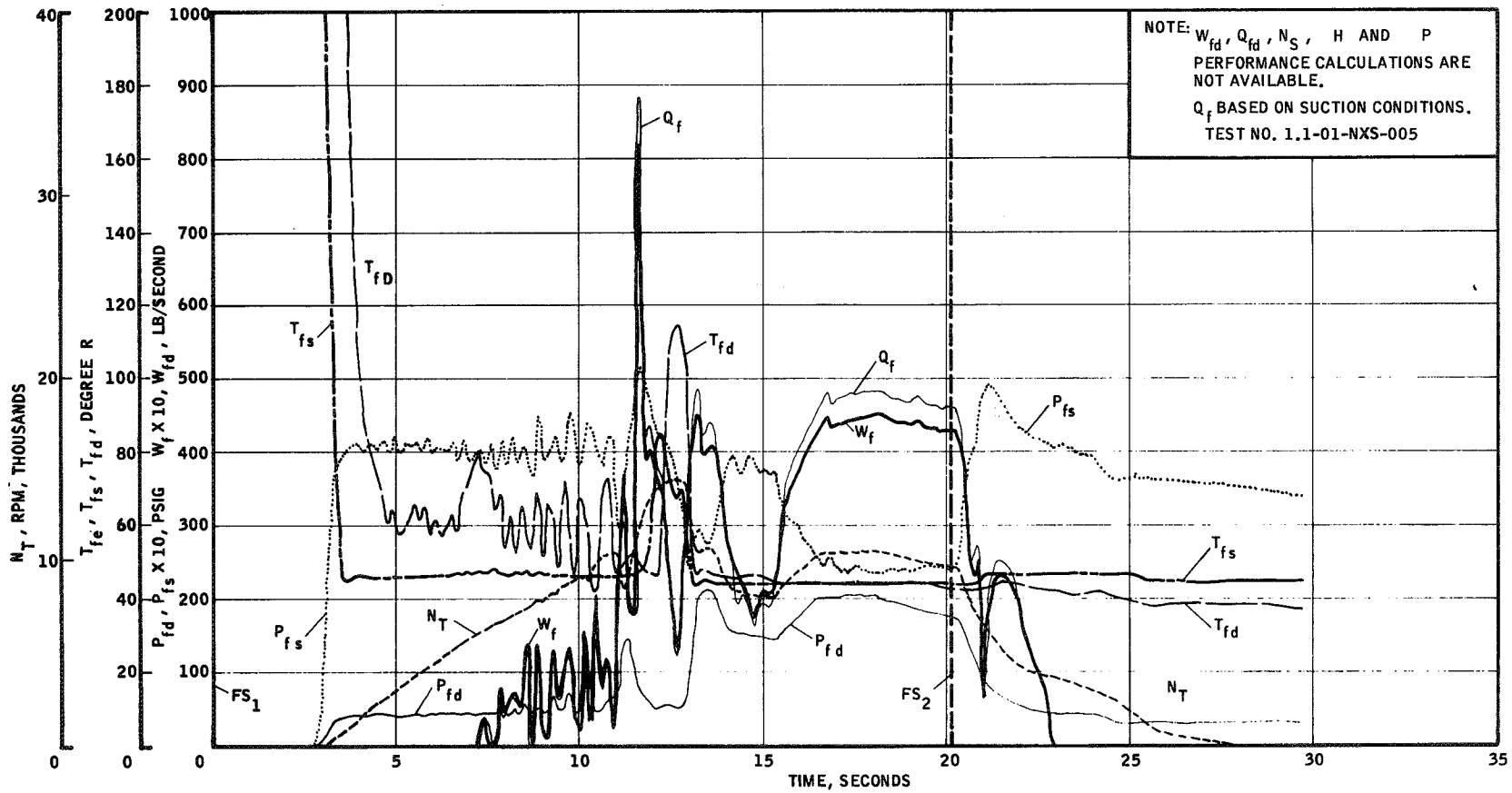

LH_2 PUMP HEAT EXCHANGER PERFORMANCE
10-05-61

Figure V-E,1

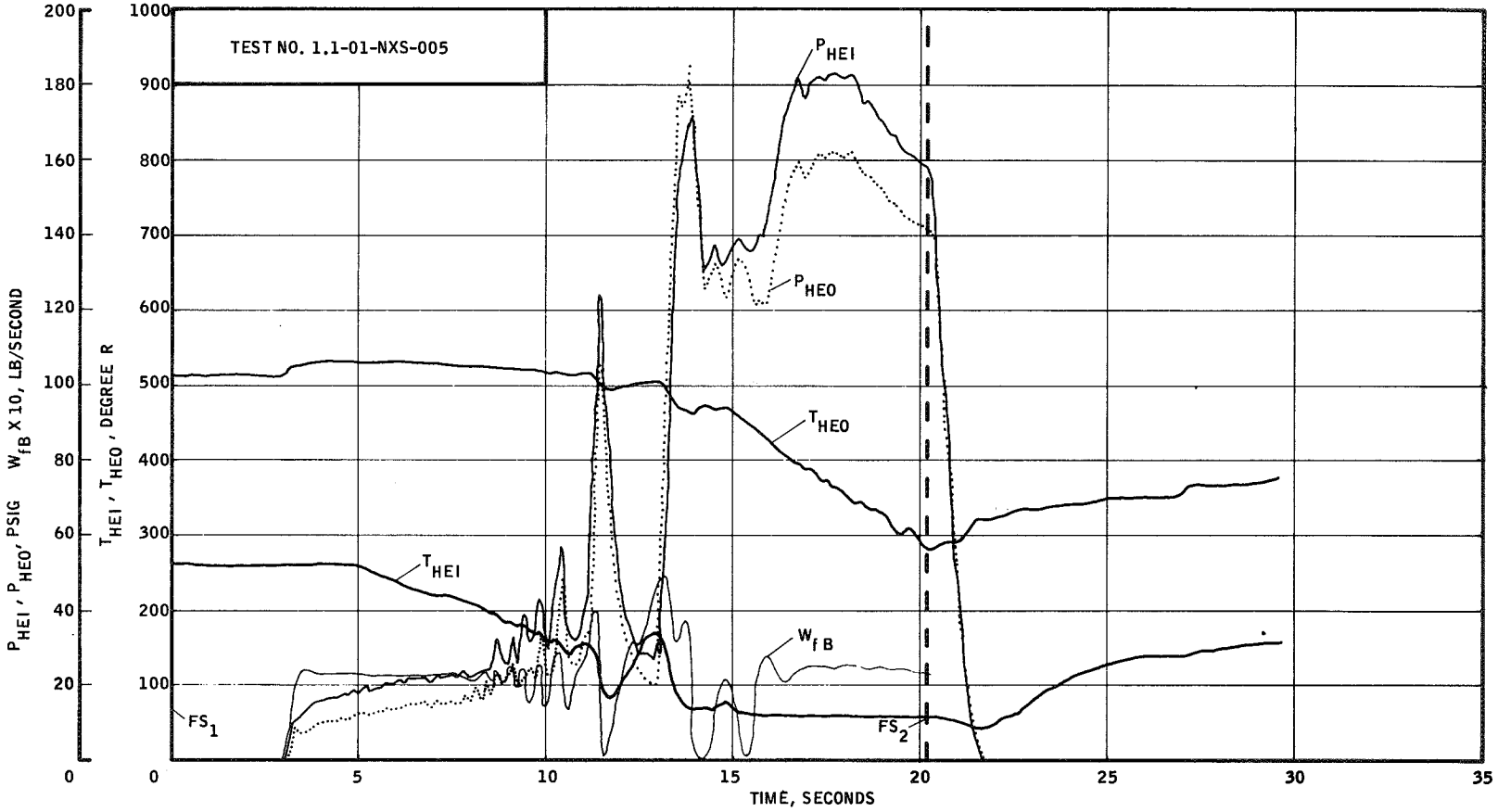

LH_2 PUMP HEAT EXCHANGER PERFORMANCE
10-05-61

Figure V-E,2

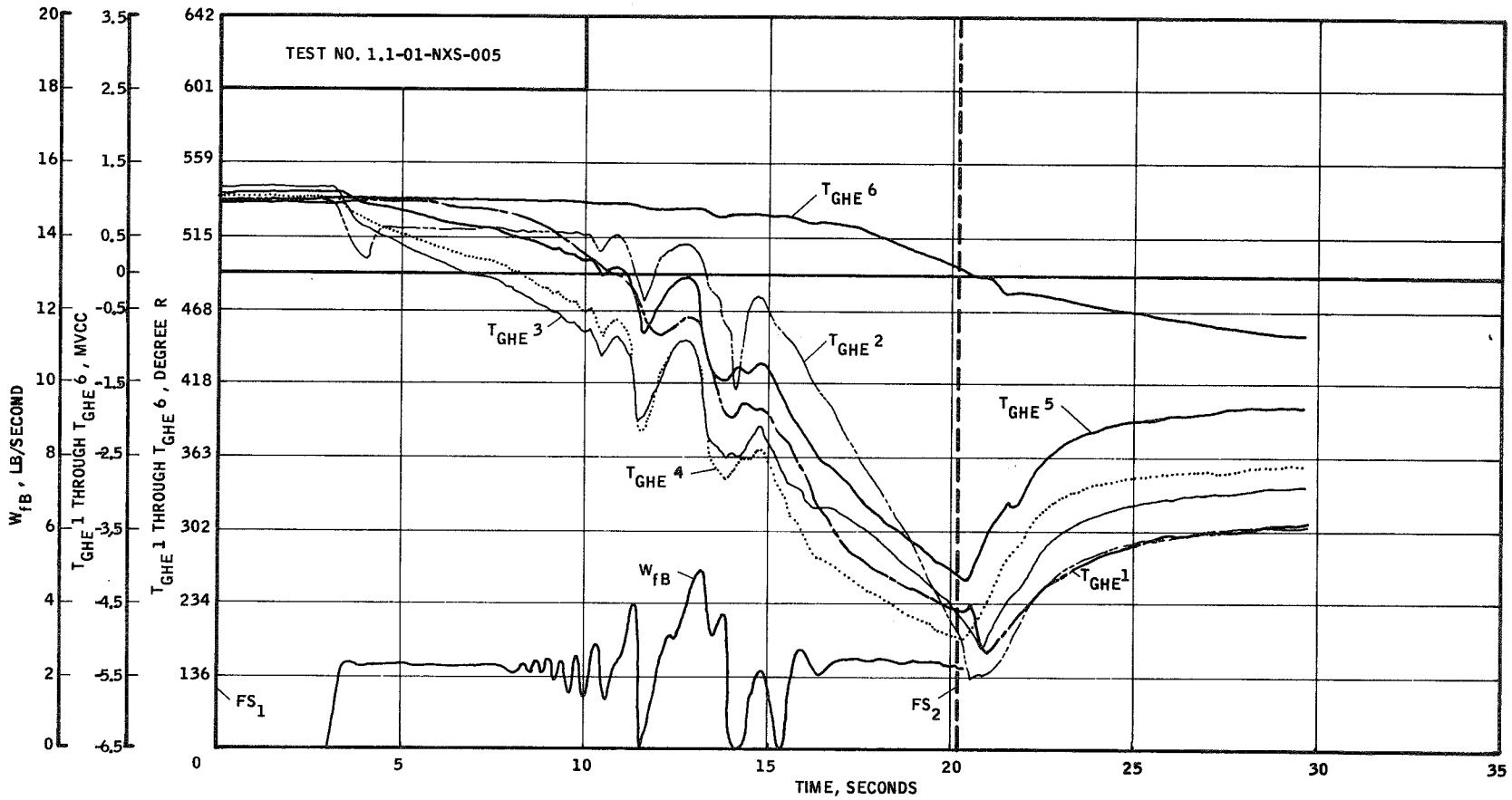

LH_2 PUMP HEAT EXCHANGER PERFORMANCE
10-05-61

Figure V-E,3

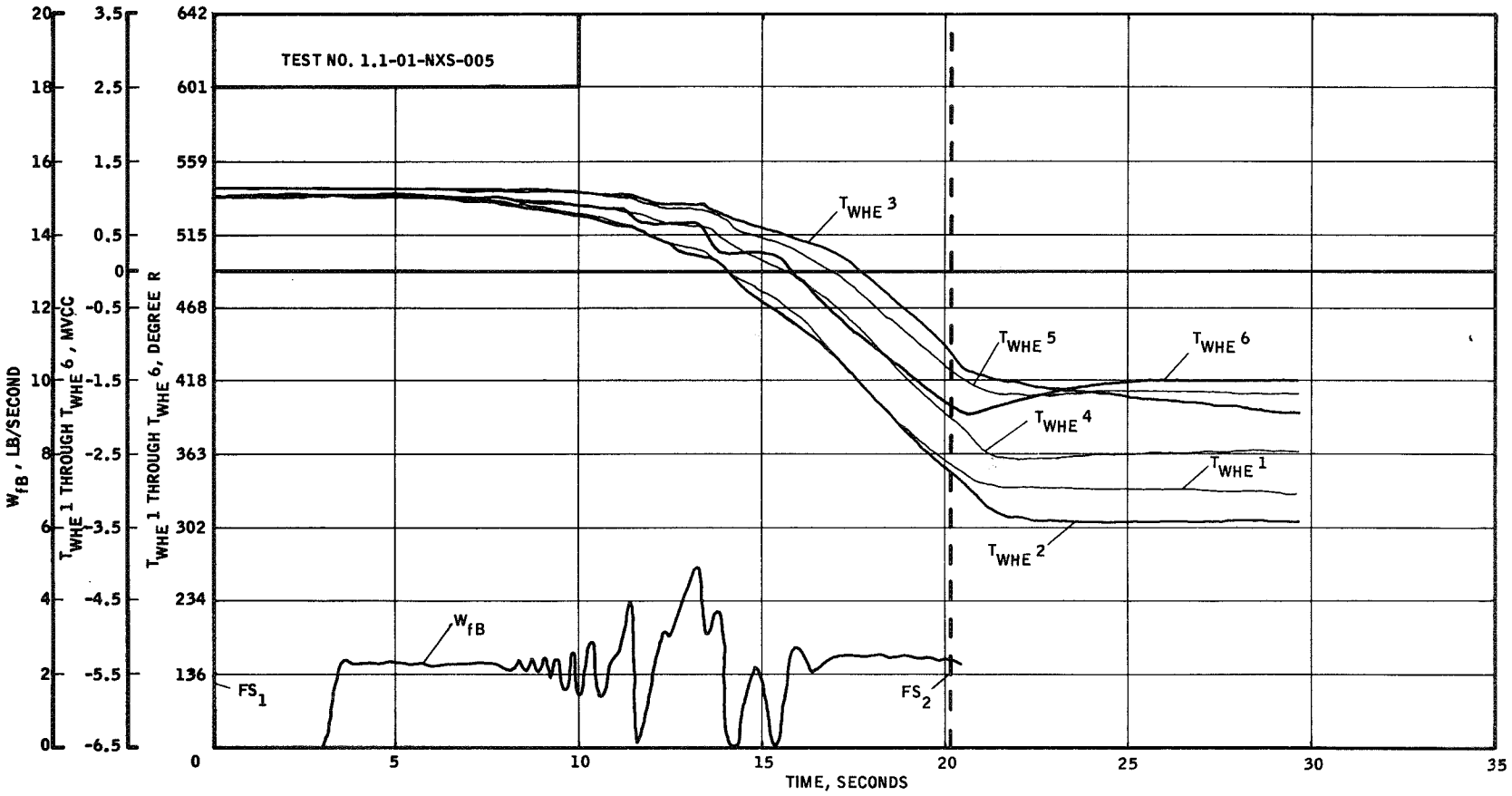

LH_2 PUMP HEAT EXCHANGER PERFORMANCE
10-05-61

Figure V-E,4

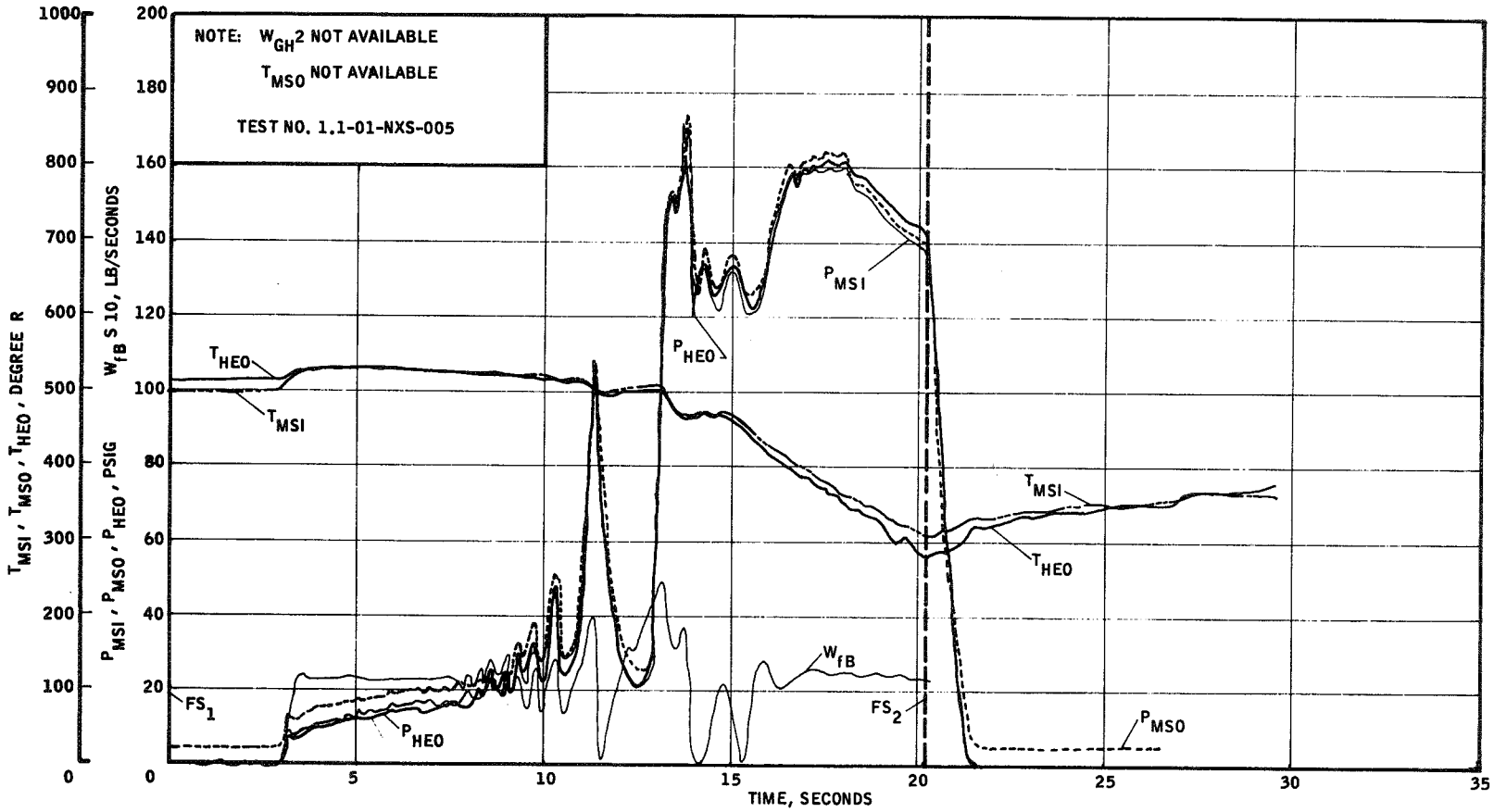

LH_2 PUMP MIX SECTION PERFORMANCE
10-05-61

Figure V-E,5

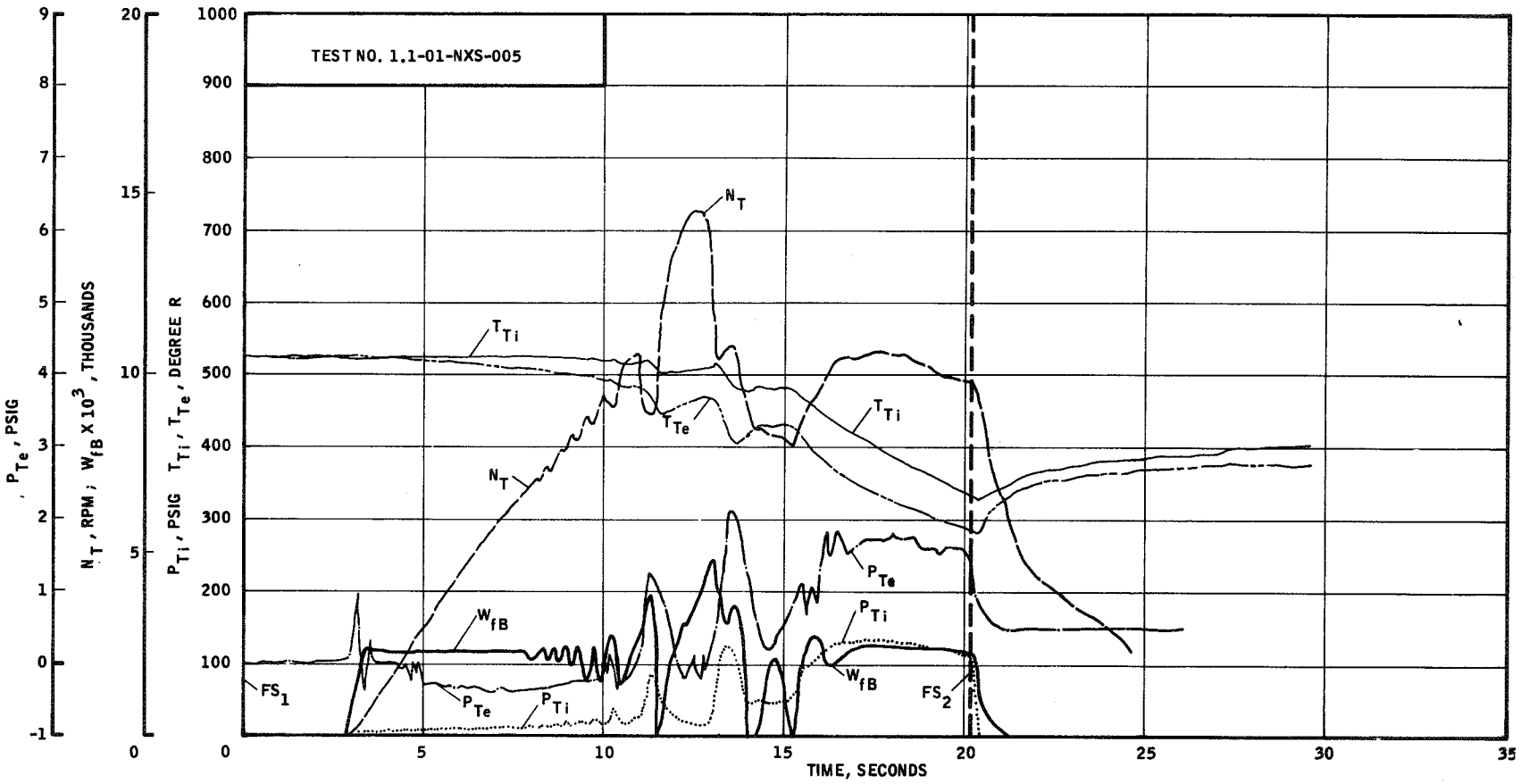

LH_2 PUMP PERFORMANCE CHARACTERISTICS
10-05-61

Figure V-E,6

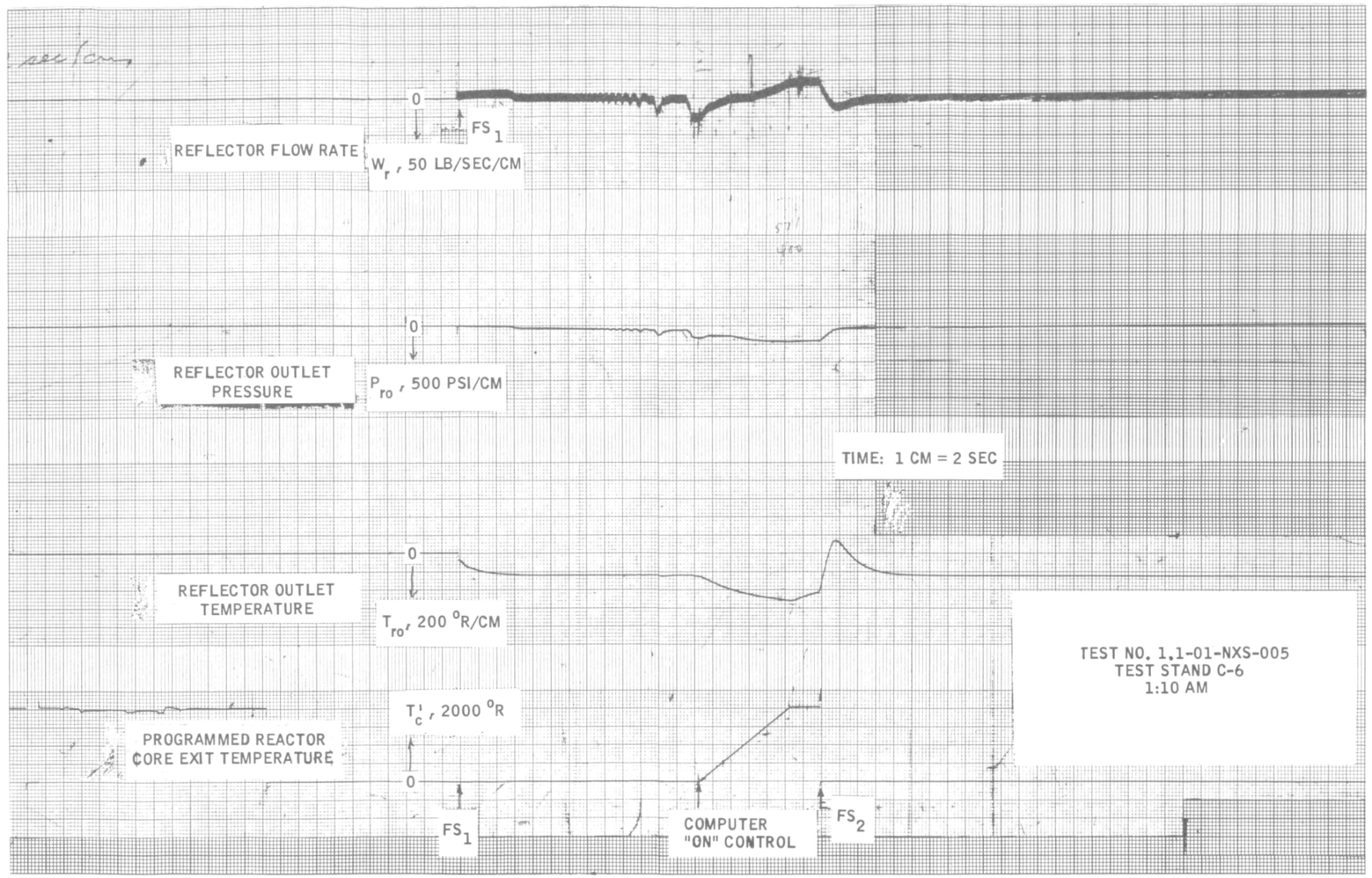

REACTOR SIMULATOR OUTPUTS GEN. I COLD-BLEED ENGINE SIMULATOR SYSTEM
10-05-61

Fig. V-E,7

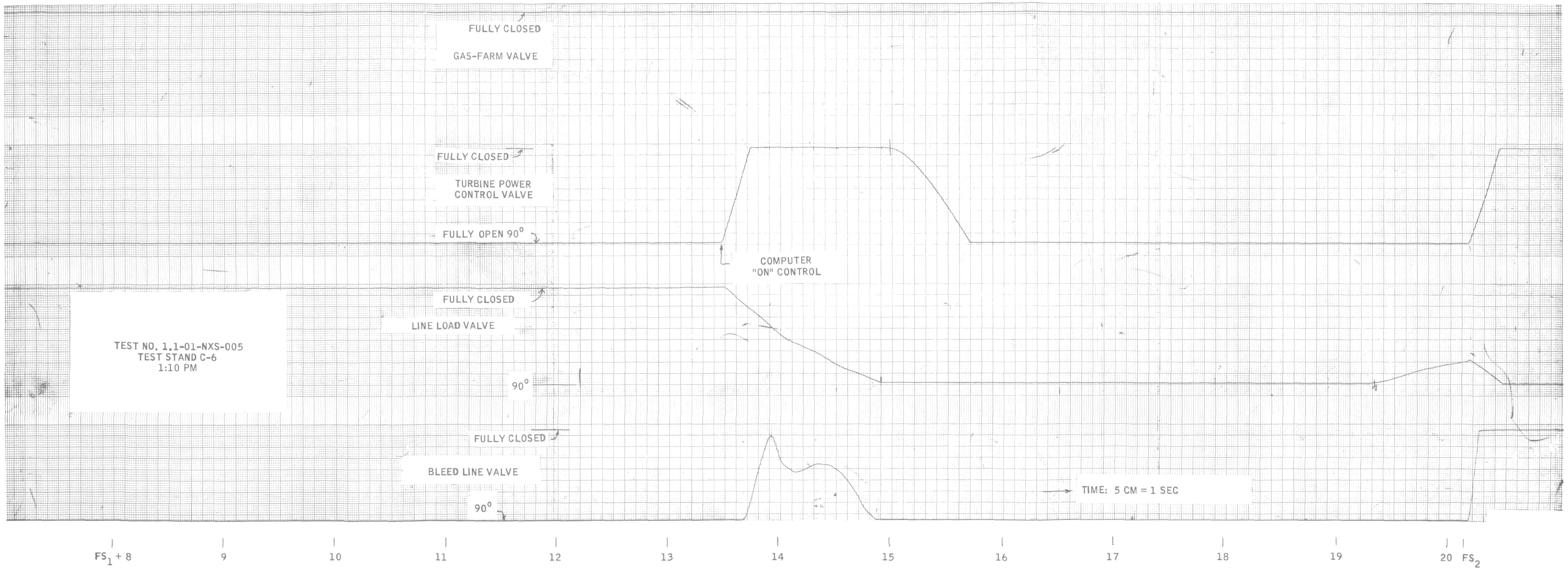

VALVE POSITIONS, GEN. I COLD-BLEED ENGINE SIMULATOR SYSTEM
10-05-61

Figure V-E,8

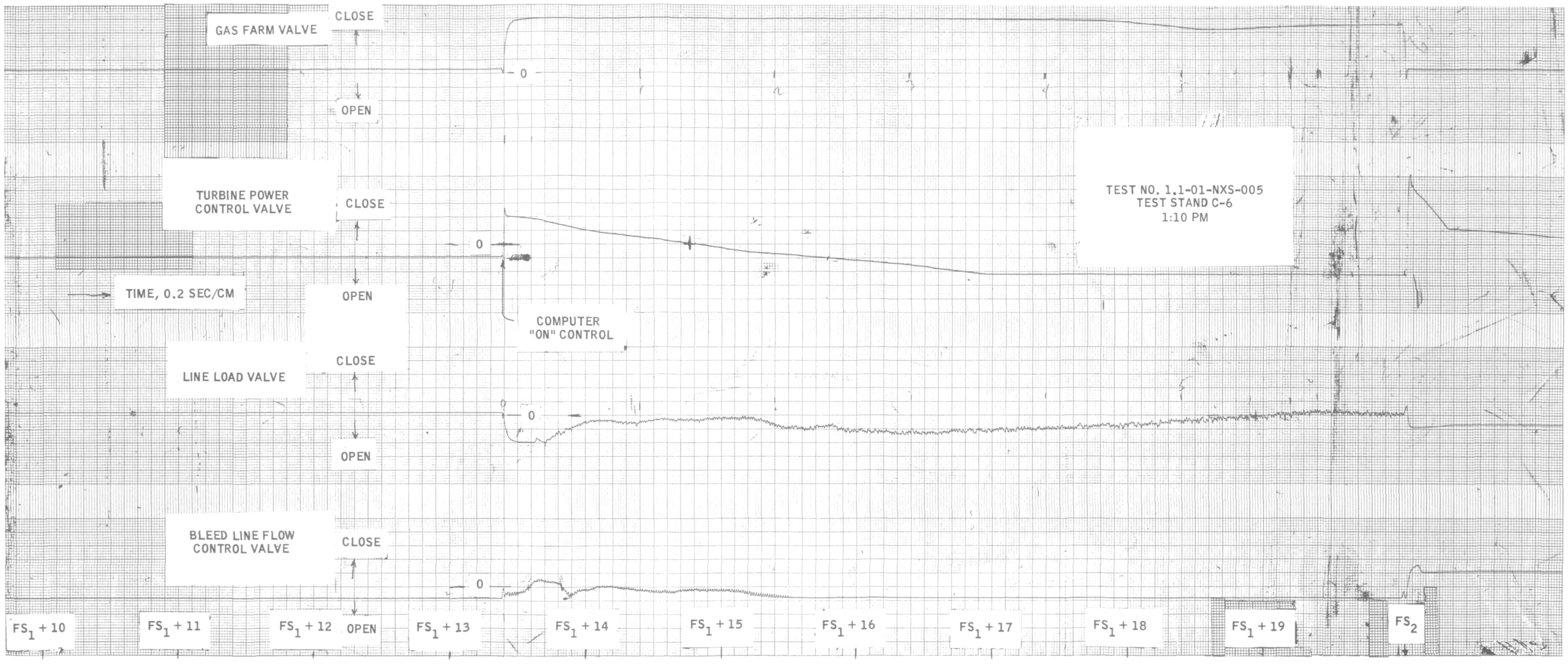

VALVE ERROR SIGNALS, GEN.I COLD-BLEED ENGINE SIMULATOR SYSTEM
10-05-61

Figure V-E,9

F. TEST RUN NO. 1.1-01-NXS-006B (Figures V-F, 1 through 9)

The previous test had shown that when the ramp input of P_c reference was started at the time of "Sin Run," pump discharge pressure was already at a high level. Correspondingly, P_c, generated in the computer, was also at a high level. The resulting error signal caused the TPCV to close.

To avoid the possibility of TPCV closure during a heat-capacity start and to allow the turbopump to reach steady-state operation, P_c reference was changed from a ramp, to a fixed set-point, which was lowered to 412 psia, corresponding to a P_{fD} of 525 psig.

Analysis of previous test data showed that a torque balance was not achieved with P_c reference at 495 psia; the demand for higher discharge pressures was incompatible with the low turbine inlet temperature for which the system had been designed. Calculations were made to determine conditions required for a torque balance, and, for P_c reference equivalent to 412, a turbine inlet temperature of -160°F was required. Therefore, the reference temperature (T_{mso}) for operating the Gas-Farm valve was raised to -160°F by biasing potentiometer No. 6, Figure II-B-6, 1. Finally, the T_c reference ramp input was lengthened to 20 seconds and started at FS-1 to avoid over-riding P_{fD}, the input to the computer from the pump.

The ΔP_{fDo} pressure transducer was relocated to its proper place. A diode limiter was placed around Amplifier 2, Figure II-B-6, 1, to keep w_r from changing sign.

Tank pressure was again set at 40 psig. The heat-capacity start was similar to those of previous runs, Figure V-F, 1. Control was transferred to the computer at FS-1 + 12.76 sec, at which time turbopump speed was 13,000 rpm and P_{fD} was 310 psig.

By contrast with the previous test, the Gas Farm Valve, only, opened this time, at 2.3 seconds after "Sim Run." The valve position traces and computer outputs are shown in Figures V-F, 7 and 8, respectively (in the latter figure, the 20 second T_c reference ramp input was limited by the recorder because the channel gain had been set too high). It is apparent that the GFV control loop was stable for almost the entire run, even though T_{mso}, the controlled temperature, was oscillatory. The oscillations apparently were caused by T_{Heo}, which was also oscillating, but with greater amplitude. About two seconds before shutdown, the Gas-Farm control loop broke into a diverging oscillation. The data indicated that sonic flow existed at the Gas-Farm valve at the time the oscillations started. This, plus the fact that P_{GH_2S} (GFV supply pressure) was also oscillating at the same frequency, leads to the conclusion that the fault lay with the pressure regulators.

According to the valve error signals (see Figure V-F, 9) the open or closed position of each of the other three valves (as shown in Figure V-F-7) was correct.

UNCLASSIFIED

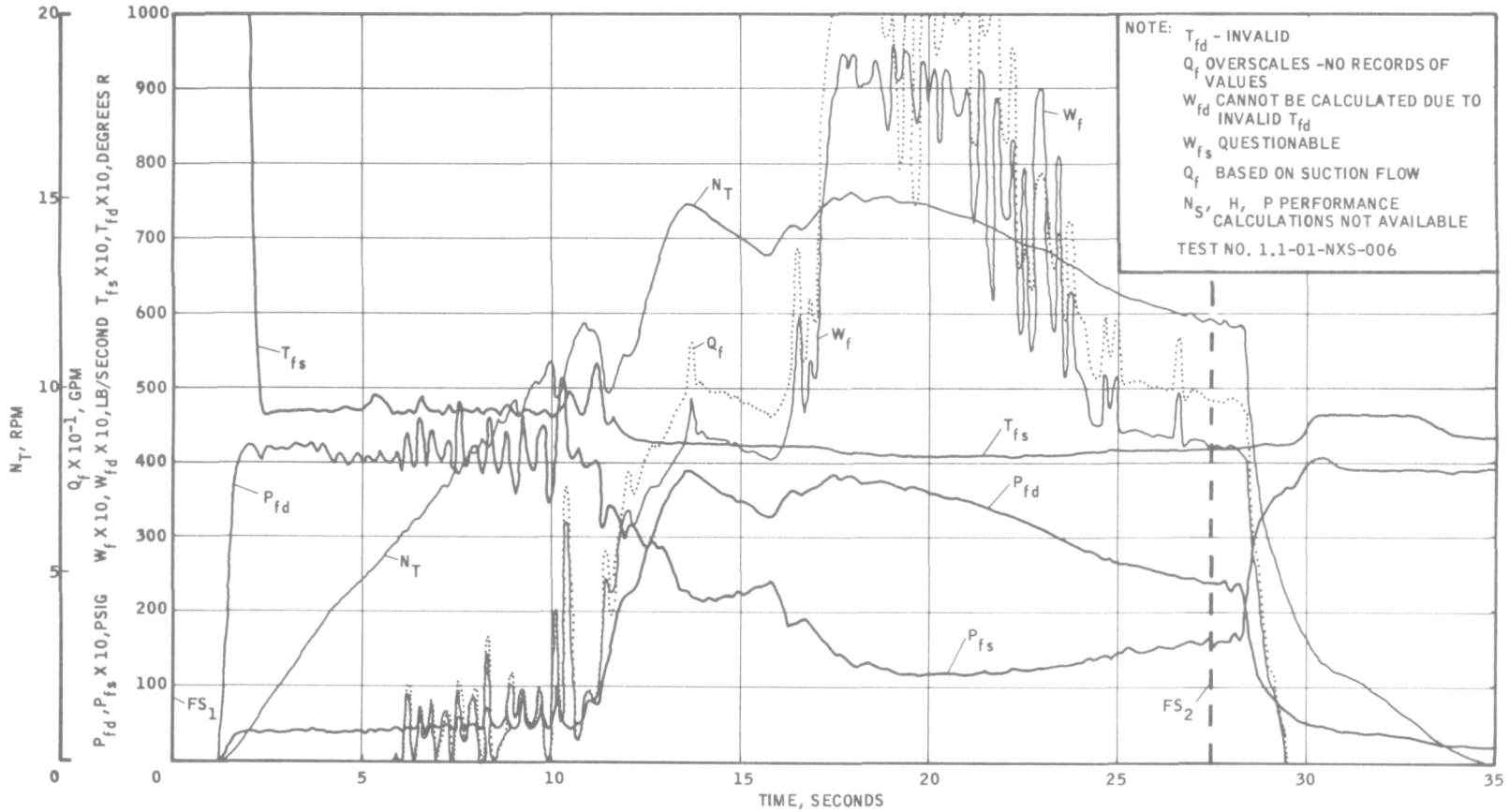

LH$_2$ PUMP PERFORMANCE CHARACTERISTICS
10-06-61

Figure V-F,1

UNCLASSIFIED

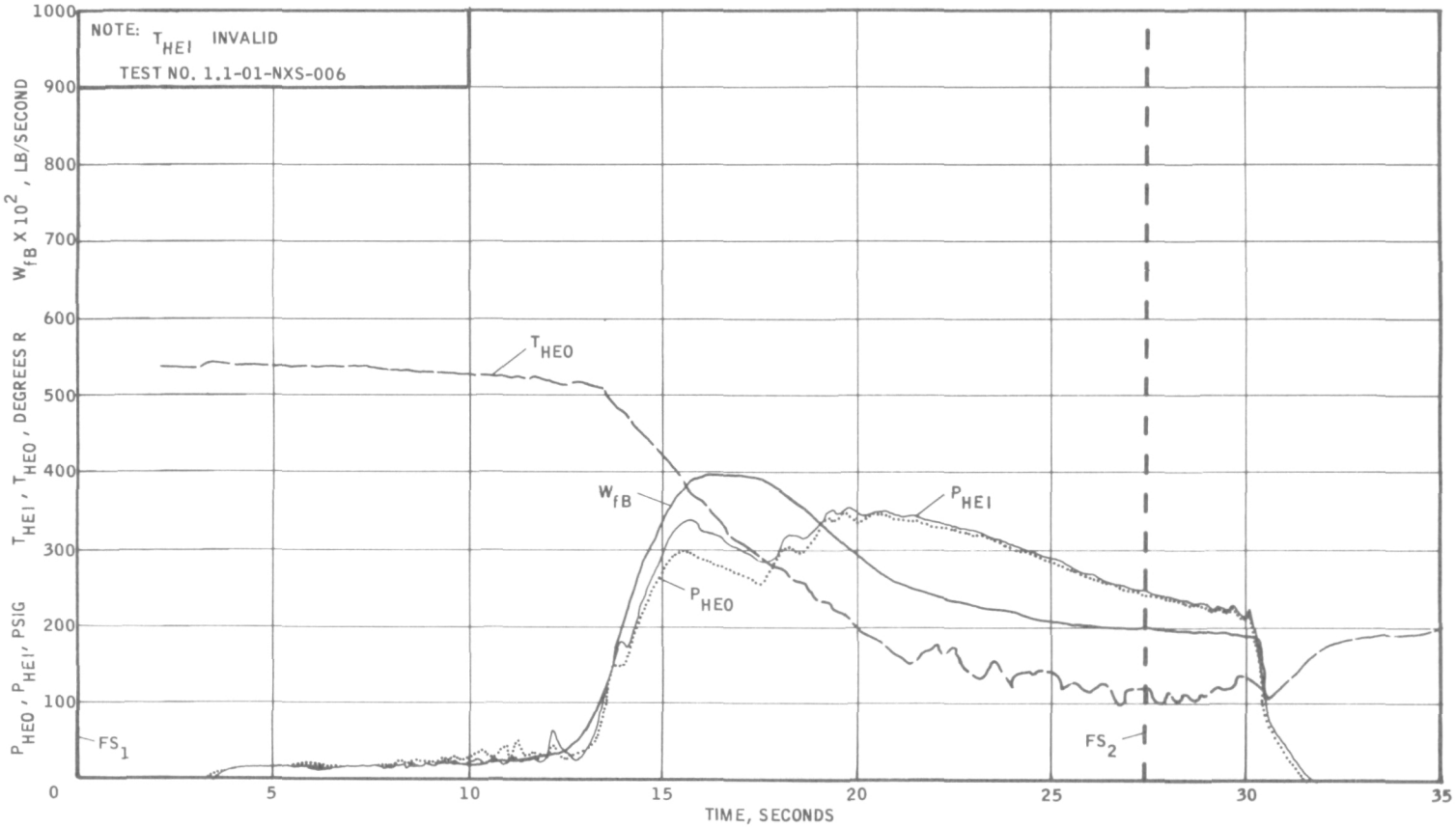

LH_2 PUMP HEAT EXCHANGER PERFORMANCE
10-06-61

Figure V-F,2

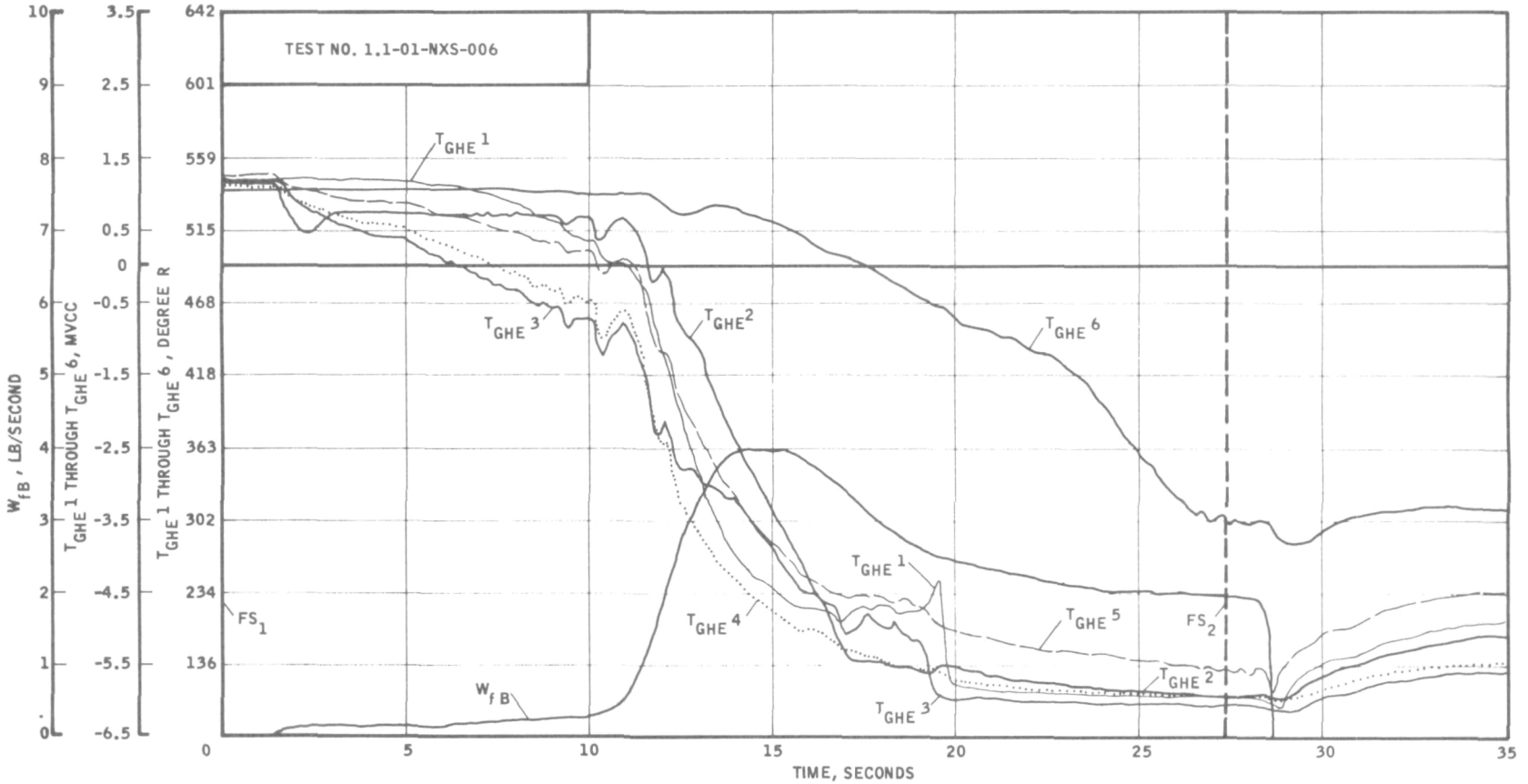

LH_2 PUMP HEAT EXCHANGER PERFORMANCE
10-06-61

Figure V-F,3

UNCLASSIFIED

Figure V-F,4

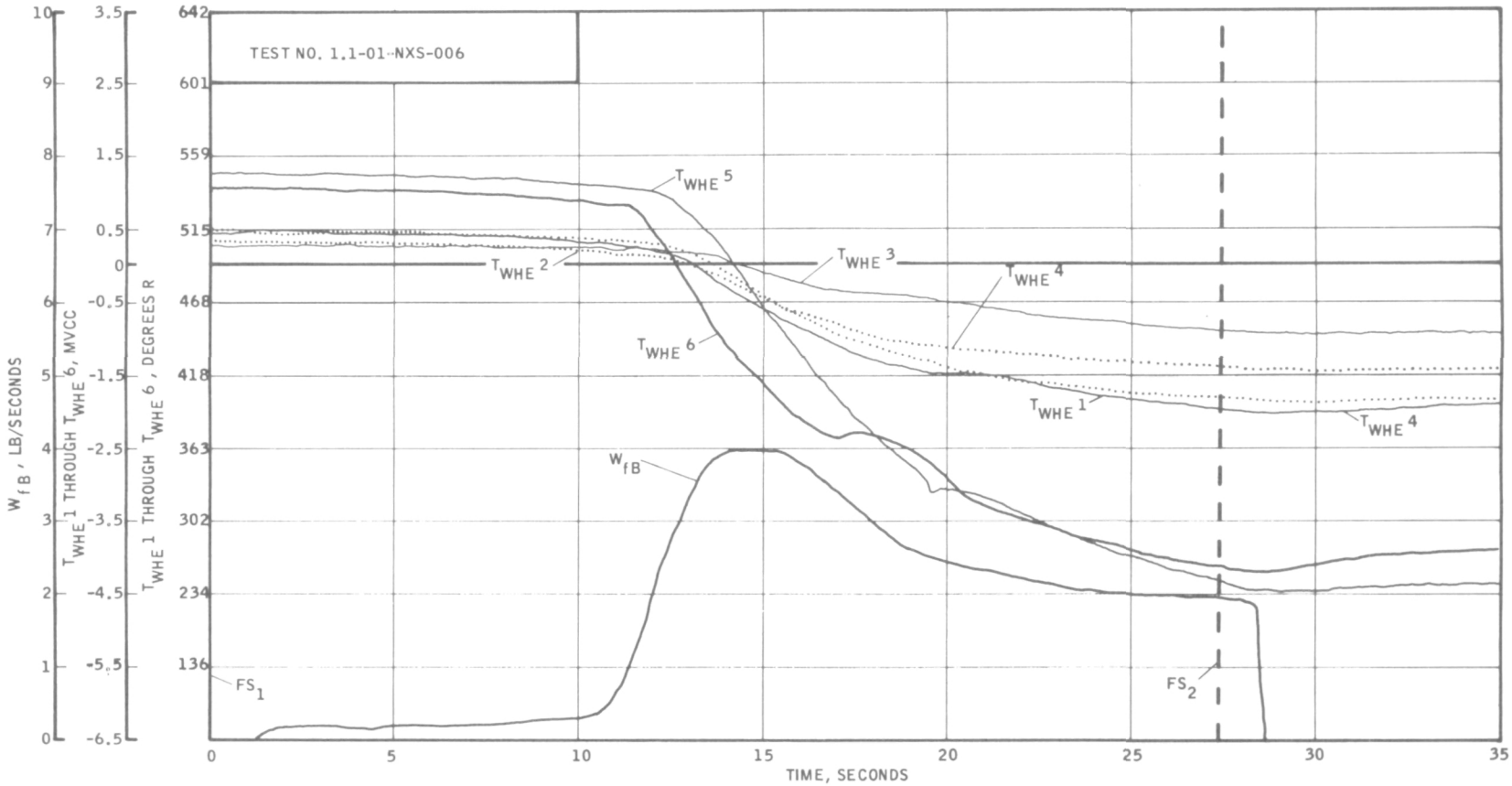

LH_2 PUMP HEAT EXCHANGER PERFORMANCE

10-06-61

UNCLASSIFIED

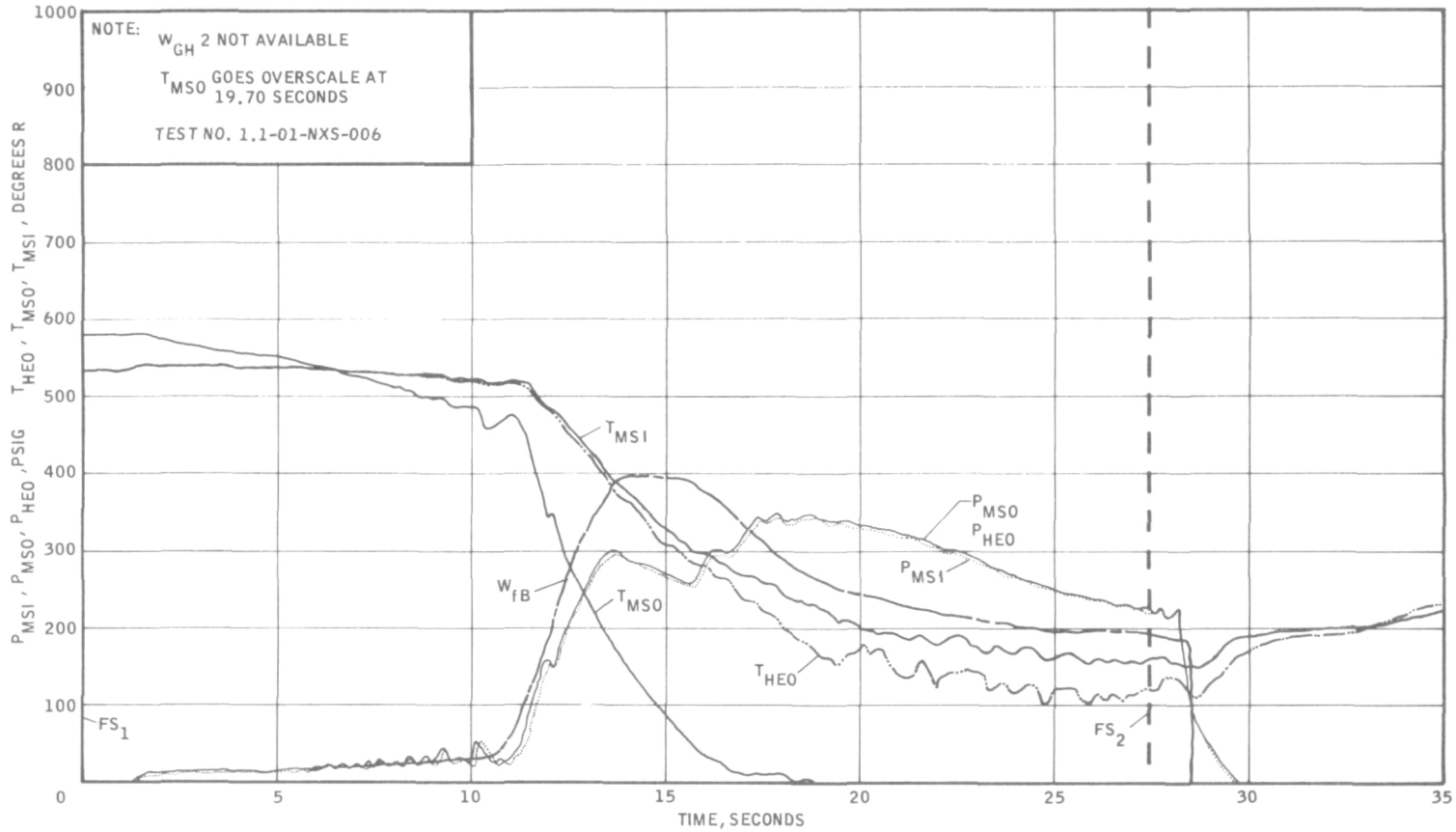

LH_2 PUMP MIX SECTION PERFORMANCE
10-06-61

Figure V-F,5

UNCLASSIFIED

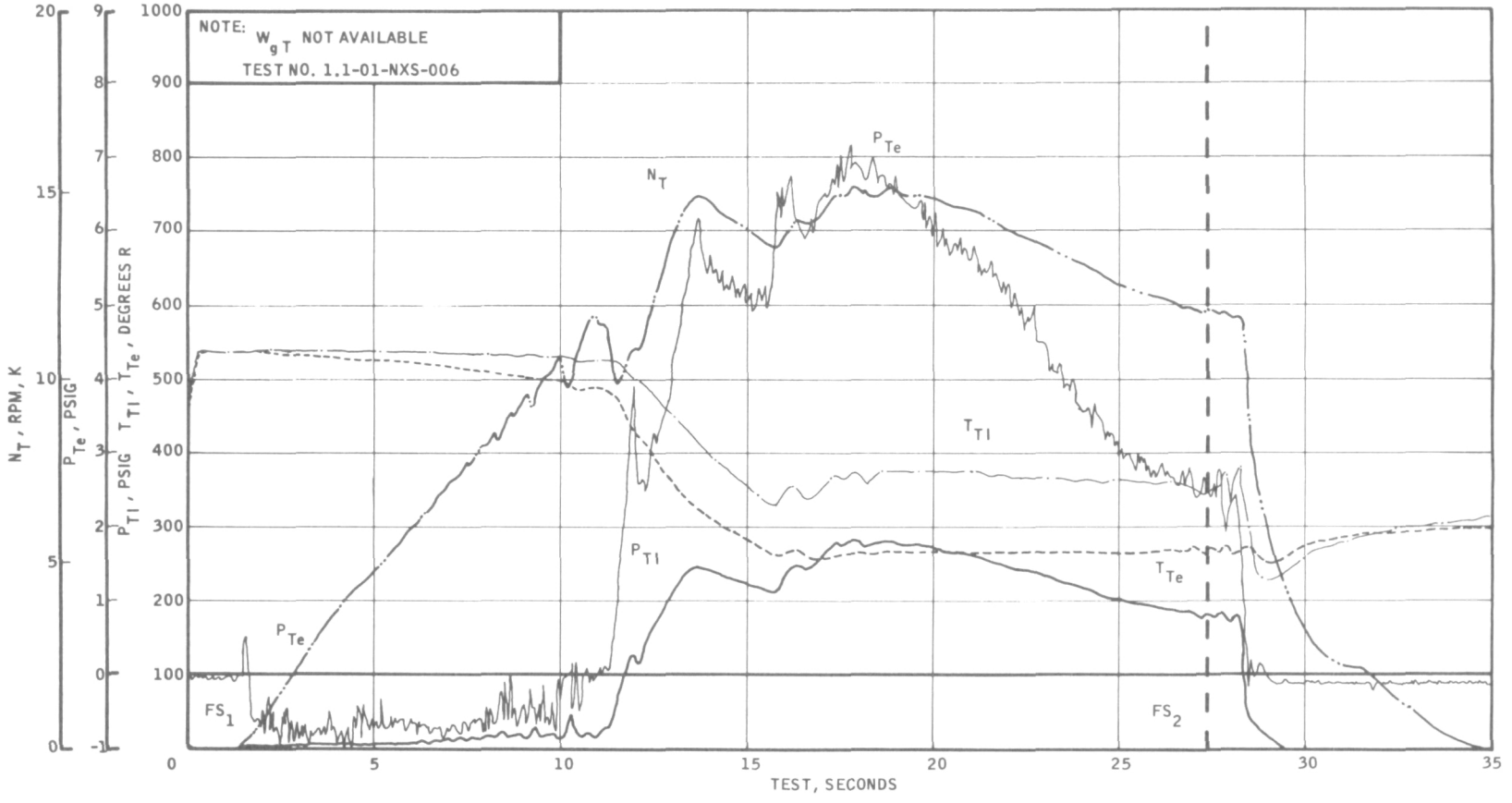

LH_2 PUMP TURBINE PERFORMANCE
10-06-61

Figure V-F,6

UNCLASSIFIED

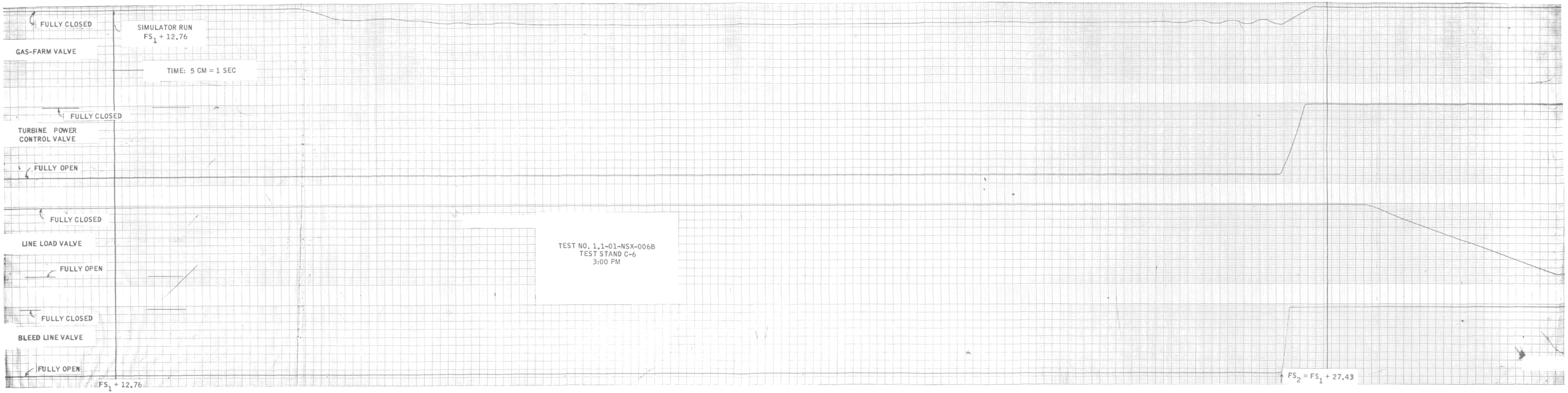

VALVE POSITIONS, GEN. I COLD-BLEED ENGINE SIMULATOR SYSTEM
10-06-61

Figure V-F,7

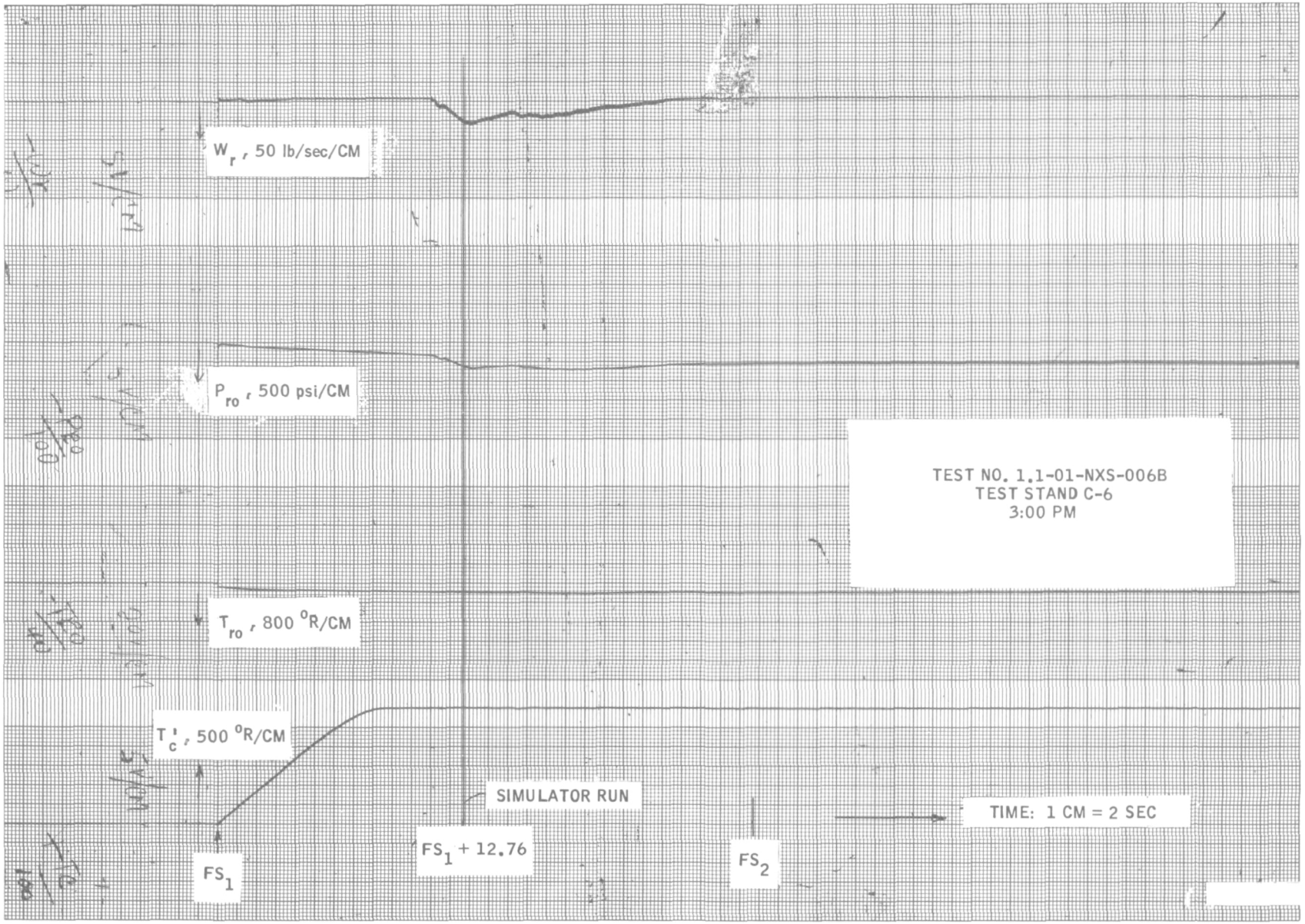

Figure V-F,8

REACTOR SIMULATOR OUTPUTS GEN. I COLD-BLEED ENGINE SIMULATOR SYSTEM
10-06-61

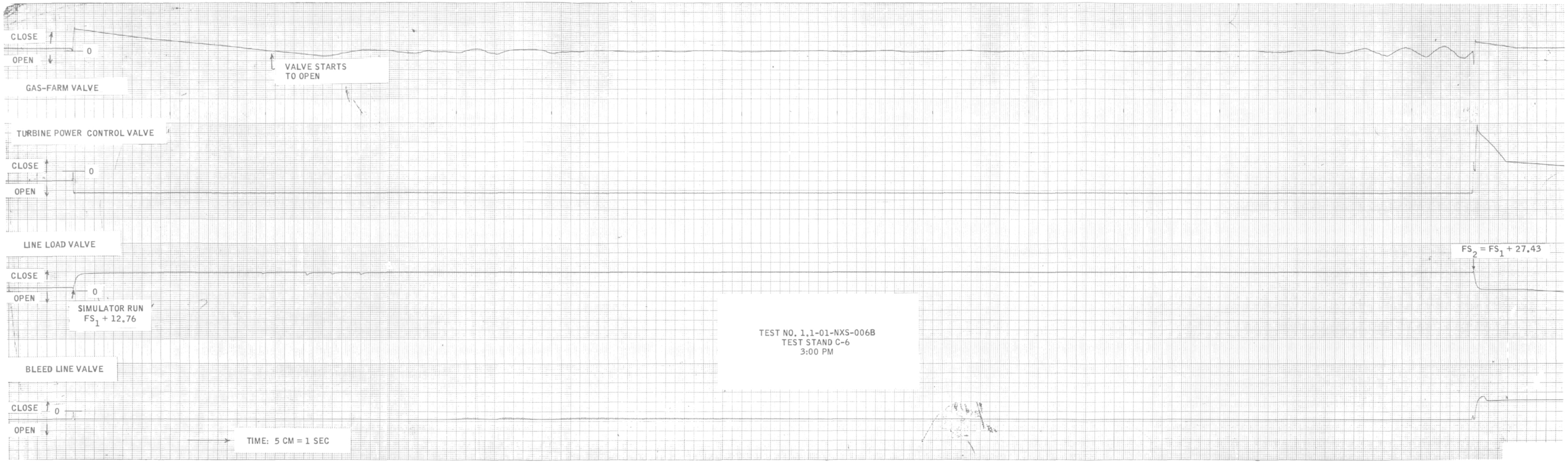

VALVE ERROR SIGNALS, GEN. I COLD-BLEED ENGINE SIMULATOR SYSTEM
10-06-61

Figure V-F,9

G. TEST RUN NO 1 1-01-NXS-007

In the previous run, the load valve had remained closed because P_{fD} had not reached a level high enough to generate a value for w_r in the computer which was greater than the actual flow. In an effort to obtain more control over pump load to achieve steady-state operation, the load valve was opened to 23° prior to the start of the test and, to maintain the same flow area as before, a 1 5-in -dia orifice replaced the 2 35-in. -dia orifice in the bypass section The starting positions of the other valves were unchanged. A torque balance based on the data of the preceding test showed that the pump load exceeded the available turbine power, therefore, $T_{mso\ reference}$ was moved up to -120°F from -160°F. The ramp input for reactor power remained as before.

When it appeared, from observation of P_{fD}, that stable liquid hydrogen existed in the pump, control of the system was given to the computer. The Load valve immediately closed, turbopump speed exceeded the overspeed trip limit, and the system promptly shut down before any damage could occur

Although, by observation of rapidly increasing P_{fD}, there was an indication of stable liquid in the pump, the temperature T_{fD} had not yet dropped below critical, consequently, the pump was carrying little load The Load valve closed because ΔP_{fDo}, higher for two-phase than for liquid flow, was greater than the demanded ΔP Load-valve closure had the combined effect of unloading the pump still more while causing more fluid to go to the turbine.

H. TEST NO. 1.1-01-NXS-008 (Figures V-H,1 through 15)

For this test, tank pressure was again set at 40 psig because pump suction pressure had dropped to 12 psig during the run of Test -006.

The $P_{c\ reference}$ was further reduced to 345 psia (3.45 volts) to achieve a steady-state operating point. The pump discharge pressure that would produce a P_c equal to 345 psia, with a T_c of 4090°R, was about 500 psia, by the computer equations. A new torque-balance calculation showed that, when T_{mso} was equal to T_{T1}, or 340°R, a pump discharge pressure of 460 psig was required. Therefore, the $T_{c\ reference}$ set-point was reduced to 3000°R (30 volts). The correspondingly lower reactor power level produced a smaller (simulated) reflector pressure drop, so the required input to the computer was 460.

The steady-state value of T_{ro} for these conditions was 180°R. However, the output of the amplifier was biased to maintain the set-point temperature for the Gas-Farm control loop at -120°F (340°R). It was feared that the GFV would open too soon if the reference temperature was raised any higher.

The $T_{c\ reference}$ ramp input was lengthened to 30 sec (100°R/sec) to slow the rate of decrease of w_r (volts), when the computer assumed control, and, in this manner, rapid closure of the Load valve would be avoided. The 1.5-in. bypass orifice was retained, but the initial Load-valve position was increased to 32° for a total flow area of 6 in.^{2}, to increase the rate of pump cooldown during the heat-capacity start.

Since an oscillation appeared in the Gas-Farm control loop (see Figure V-F, 7) near the end of the run of Test -006, the gain of the servo-amplifier was reduced by a half to provide a greater margin of stability.

The heat-capacity start was similar to previous runs, and at 15.2 sec after FS-1, the computer assumed control. Although the Load valve immediately started to close, pump speed continued to rise until a power saturation (with the GFV still closed) occurred at 15.8 sec. The LV closed because w_f was 48.6 lb/sec (see Figure V-H, 3) while computed flow (w_r) was 40 lb/sec (see Figure V-H, 13), at 15.2 sec.

Then at 16.5 sec, the Gas-Farm valve started to open when T_{mso}, (Figure V-H, 10) reached a temperature of 350°R. Since T_{ro} had already reached its steady-state level, the reference temperature was supposedly fixed at 340°R. This discrepancy is most probably due to some confusion that existed, before the run, over the exact calibration of the temperature probe. A second calibration curve was given which differed by about 10° in this region from a prior curve, and the computer was set-up according to the first calibration.

As the GFV came open, turbopump speed began to increase again, rising to 17,500 rpm, at which point the TPCV began to close, at 18 9 sec It may be seen that P_c was not recorded in Figure V-H, 13, however, the value of P_{ro}, corresponding to a P_c of 345 psia, was determined to be 395 psia on the computer, prior to the test run It is evident that the TPCV began to close just when P_c exceeded the P_c set-point. (The preceding is true even though T_c was still below its steady-state value, this is, the ramp input was still increasing The reason is that T_c had only a small effect on P_c, as can be seen from the computer circuit) Within two seconds after it started controlling, the Turbine Power control system maintained P_c at the set-point value, as inferred from the fact that P_{ro} was held to 395 psia (3.95 volts), as nearly as the oscillograph could be read (see Figure V-H-13).

The bleed-line valve had started to close at 17 7 seconds At that moment, a P_{mso} of 420 psia (or rather, 405 psig) was the value actually seen at the computer, as no attempt had been made to bias the transducer signals by 0 147 volts The corresponding value of P_{ro} was about 380 psi at 17 7 sec. During that portion of the run where P_{ro} was held to 395-400 in the computer, the controlled variable, P_{mso}, was held to about 415 psig Since the controllers were integrating types, the error signal had to be zero Hence, the difference of 15-20 psi between P_{ro} and P_{mso} was attributed to attenuation of the P_{mso} signal in the transmission lines (450 feet) and/or in the circuit between the transducer amplifier and the computer

A similar condition existed with respect to P_{fD}. In the steady-state condition, P_{ro} was 395 psia (see Figure V-H, 13), therefore, P_c had to be 345 psia (3 45 volts) to satisfy the computer equations The corresponding pump pressure input to the computer had to be 4.6 volts (460 psia). The actual pressure recorded was 495 psig, Figure V-H, 2 Thus, a loss of 0.35 volts occurred in the transmission line, and/or the circuit between transducer amplifier and computer

The ramp input of T_c reference, or of power, had a greater effect on P_{ro}, and therefore on w_r, than on P_c Thus, as the ramp input continued to increase, w_r decreased, and the load valve gradually closed From about 20 to 26 seconds, the correspondence between w_r and w_f was very good, but w_r was consistently about 2 5 lb/sec higher than w_f This discrepancy could arise from the calculation of w_f (see Par. V,A) or from the manner in which ΔP_{fDo} reference was generated in the computer

As the load valve slowly closed, w_f was decreased, lightening the load on the pump Consequently, the TPCV was gradually closed by its feedback loop, reducing turbine power to hold P_{fD}, and P_c in the computer, steady.

It is evident that the BLV control loop became unstable about 8 seconds after the computer began controlling the test The oscillations were

reflected in P_{T1}, and therefore in turbopump speed. About two seconds before shutdown, the gas-farm control loop began to oscillate at about 1.7 cps, and the bleed-line control loop began to follow the slower oscillation. A divergent instability developed throughout the system, resulting in an overspeed trip shutdown at 28.2 sec. Coincidentally, the shutdown occurred at the same time tank capacity reached minimum safe level of 15%.

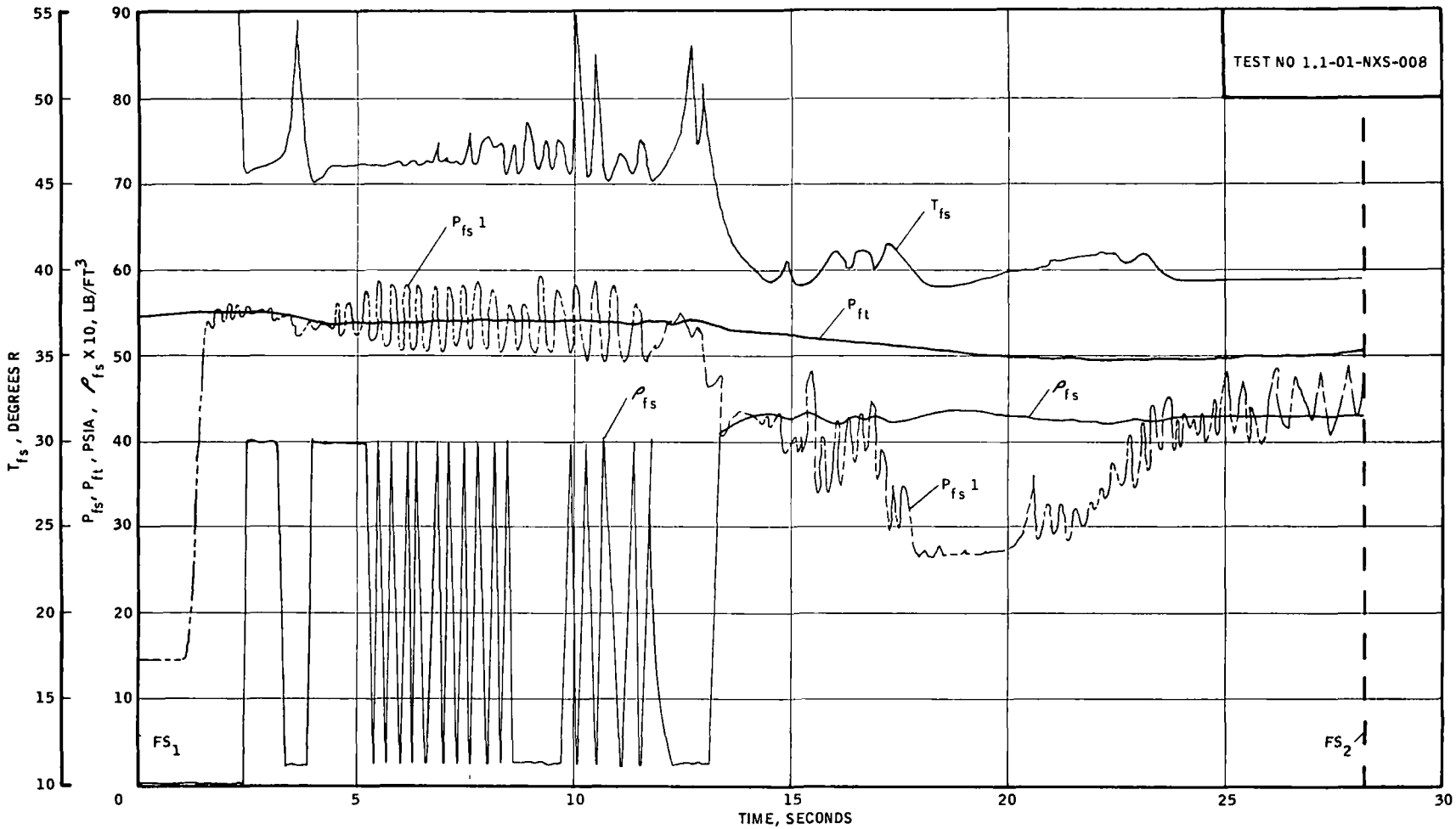

Figure V-H,1

LH_2 PUMP SUCTION CONDITIONS
10-07-61

UNCLASSIFIED

Figure V-H,2

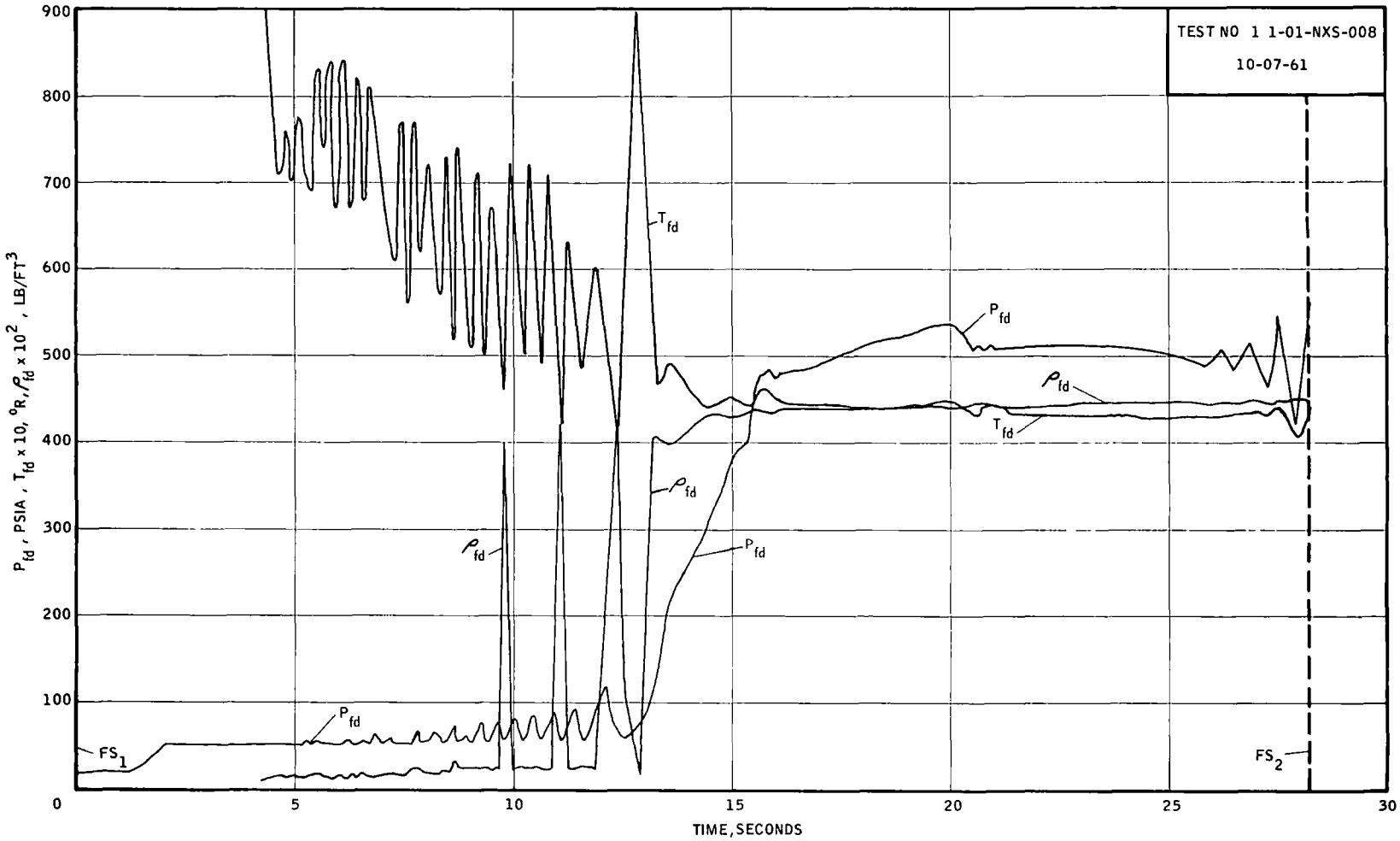

LH_2 PUMP DISCHARGE CONDITIONS

UNCLASSIFIED

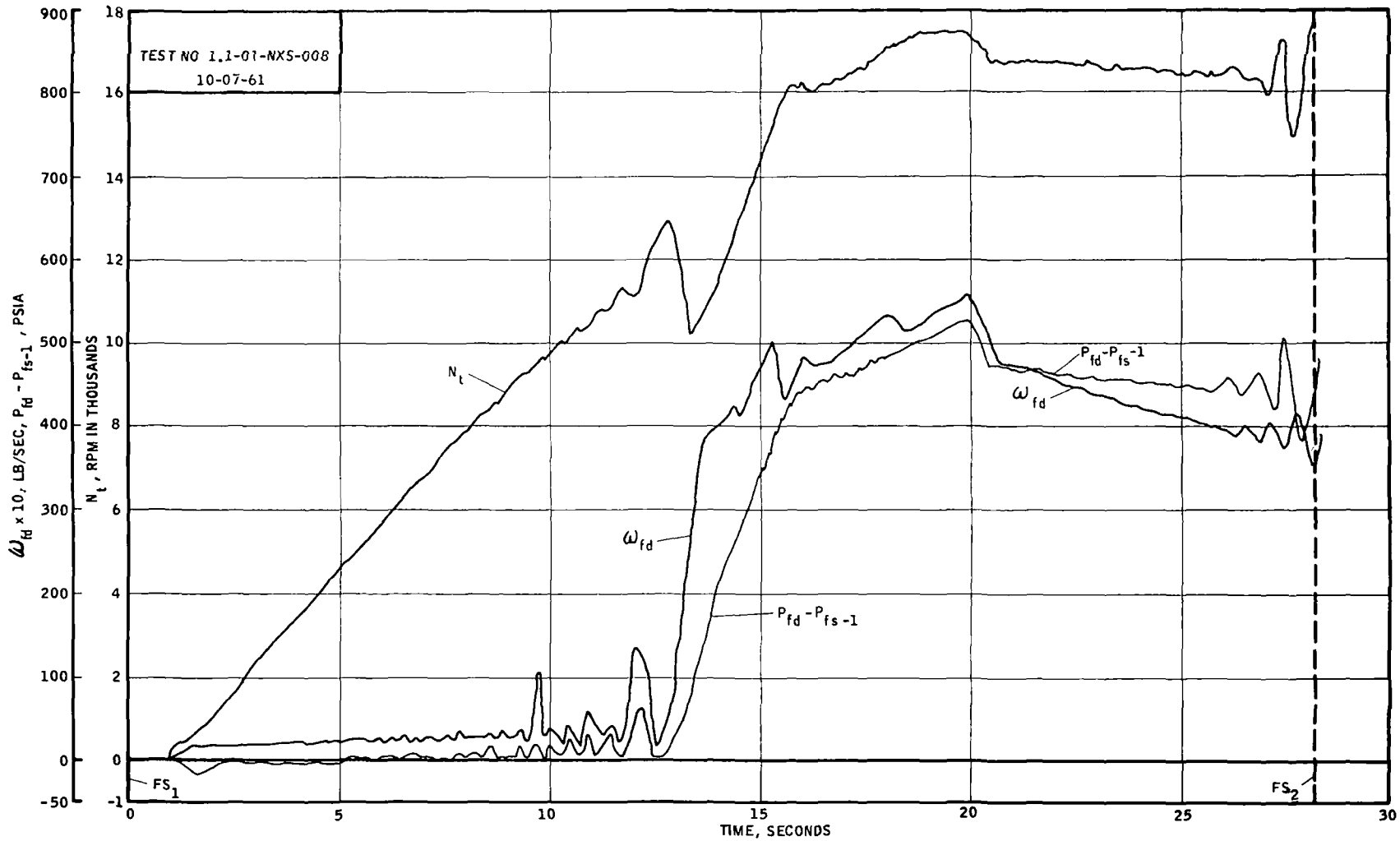

LH_2 PUMP PERFORMANCE

Figure V-H,3

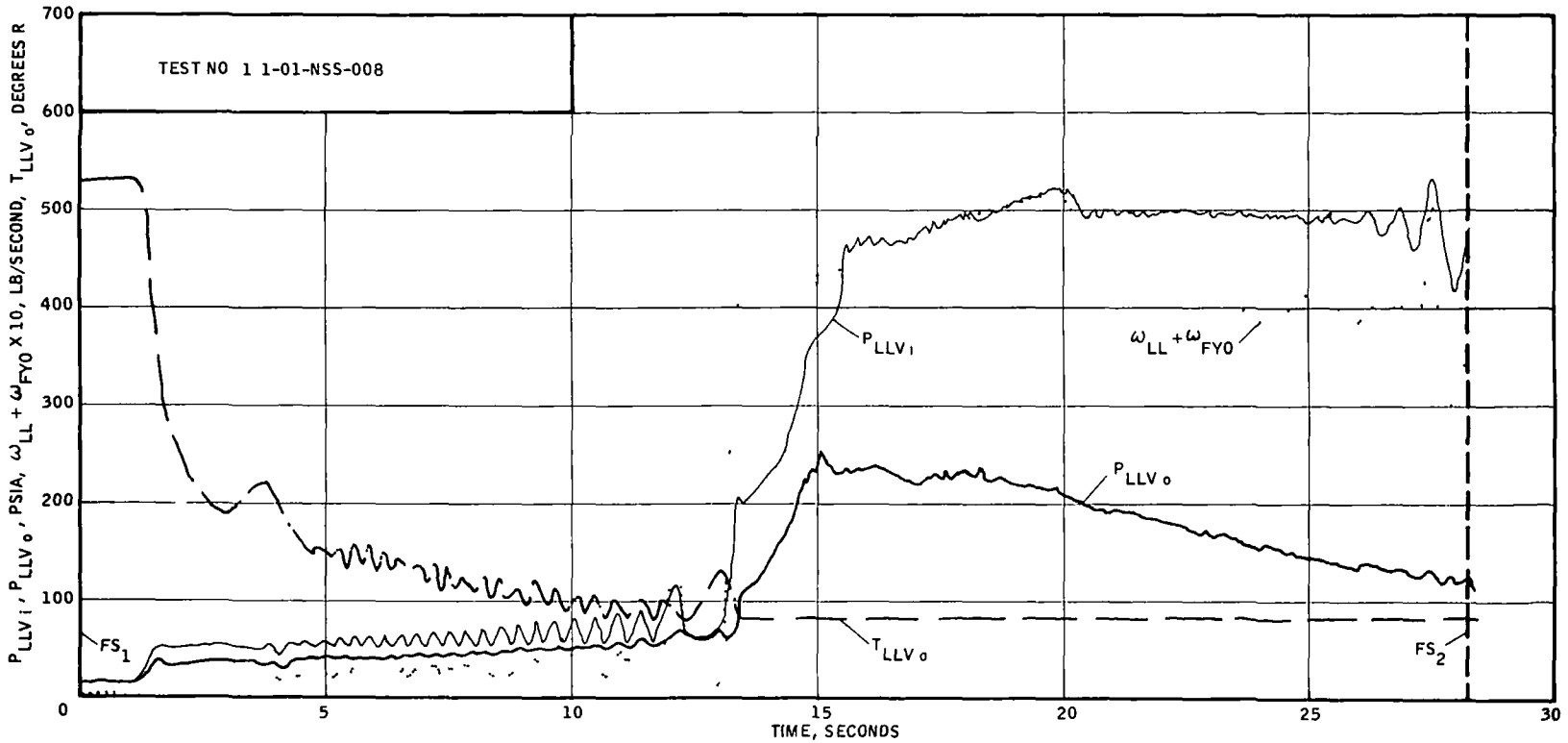

LINE LOAD VALVE PERFORMANCE
10-07-61

Figure V-H,4

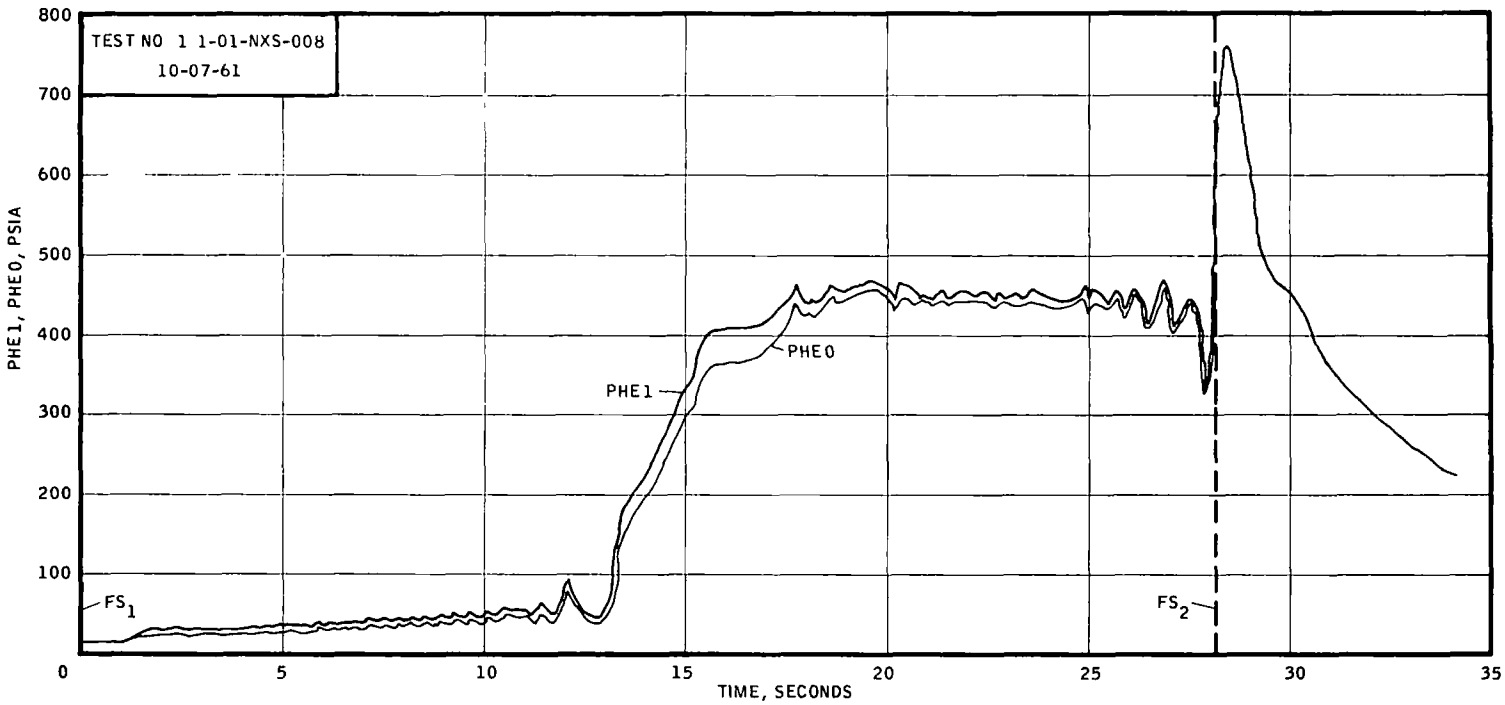

HEAT EXCHANGER INLET AND OUTLET PRESSURES

Figure V-H,5

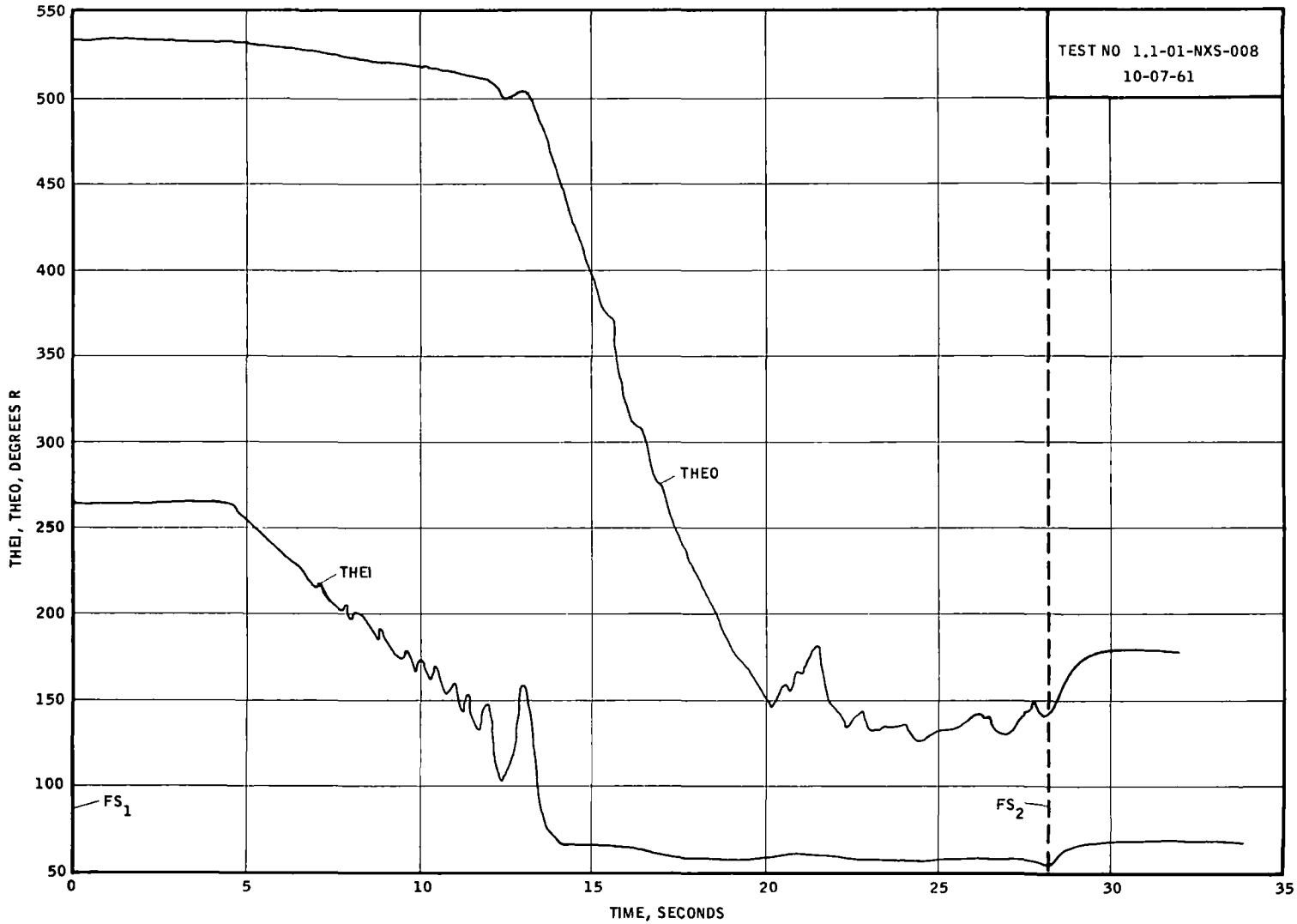

HEAT EXCHANGER INLET AND OUTLET TEMPERATURES

Figure V-H,6

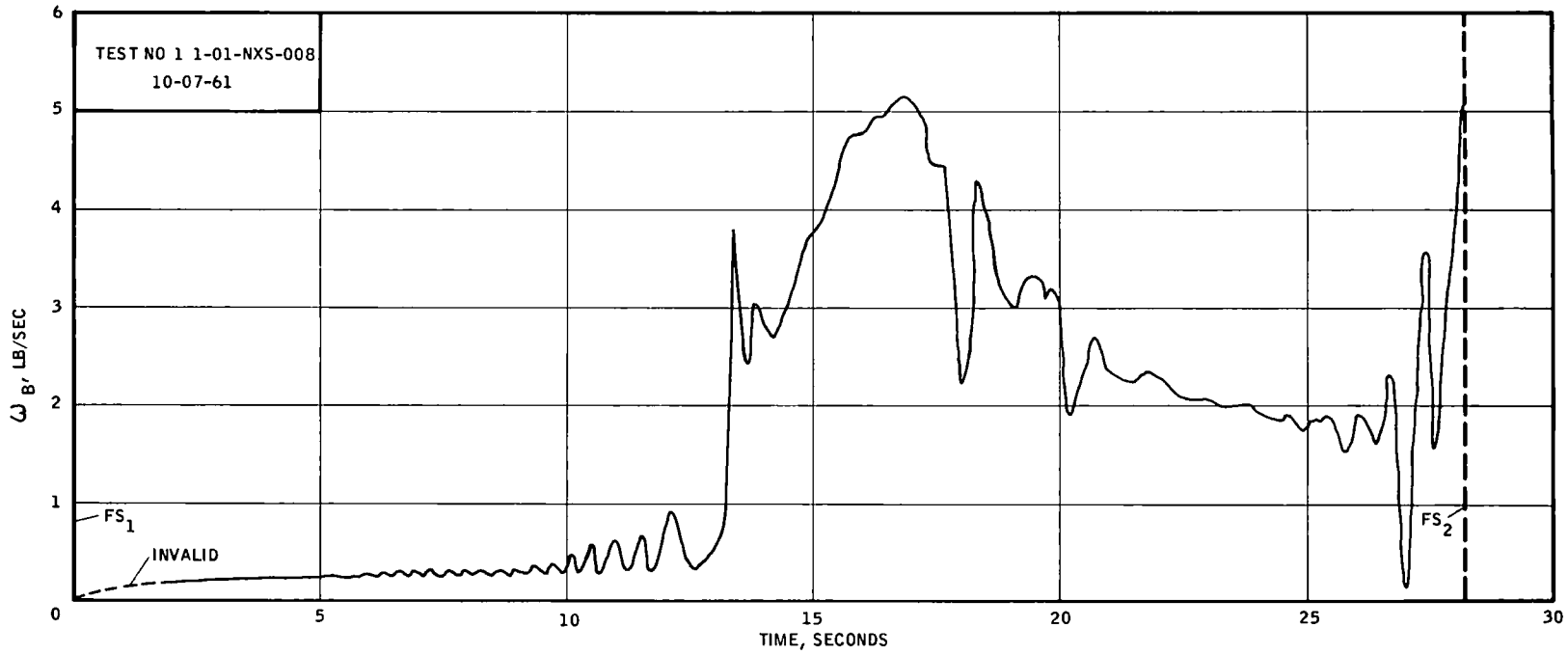

HEAT EXCHANGER FLOW RATE

Figure V-H,7

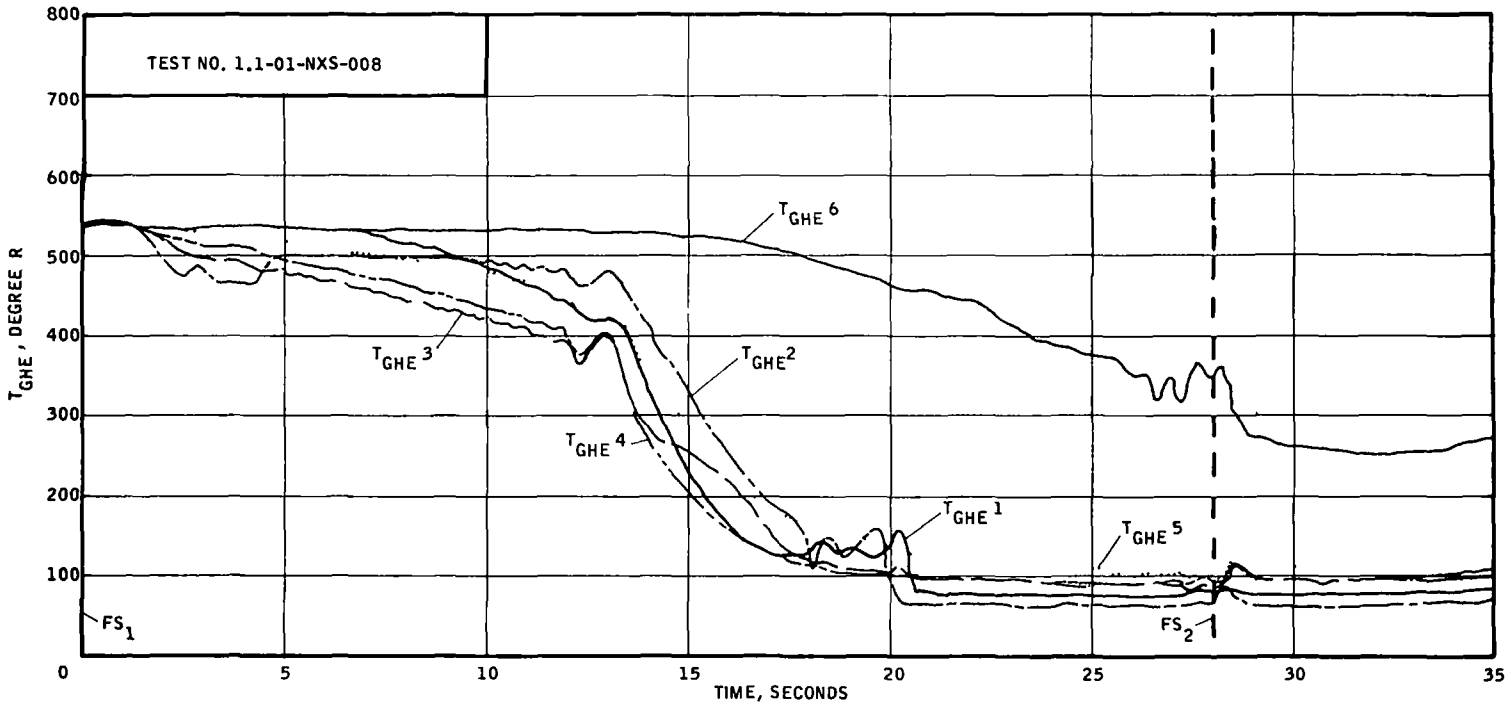

HEAT EXCHANGER FLUID BULK TEMPERATURES
10-07-61

Figure V-H,8

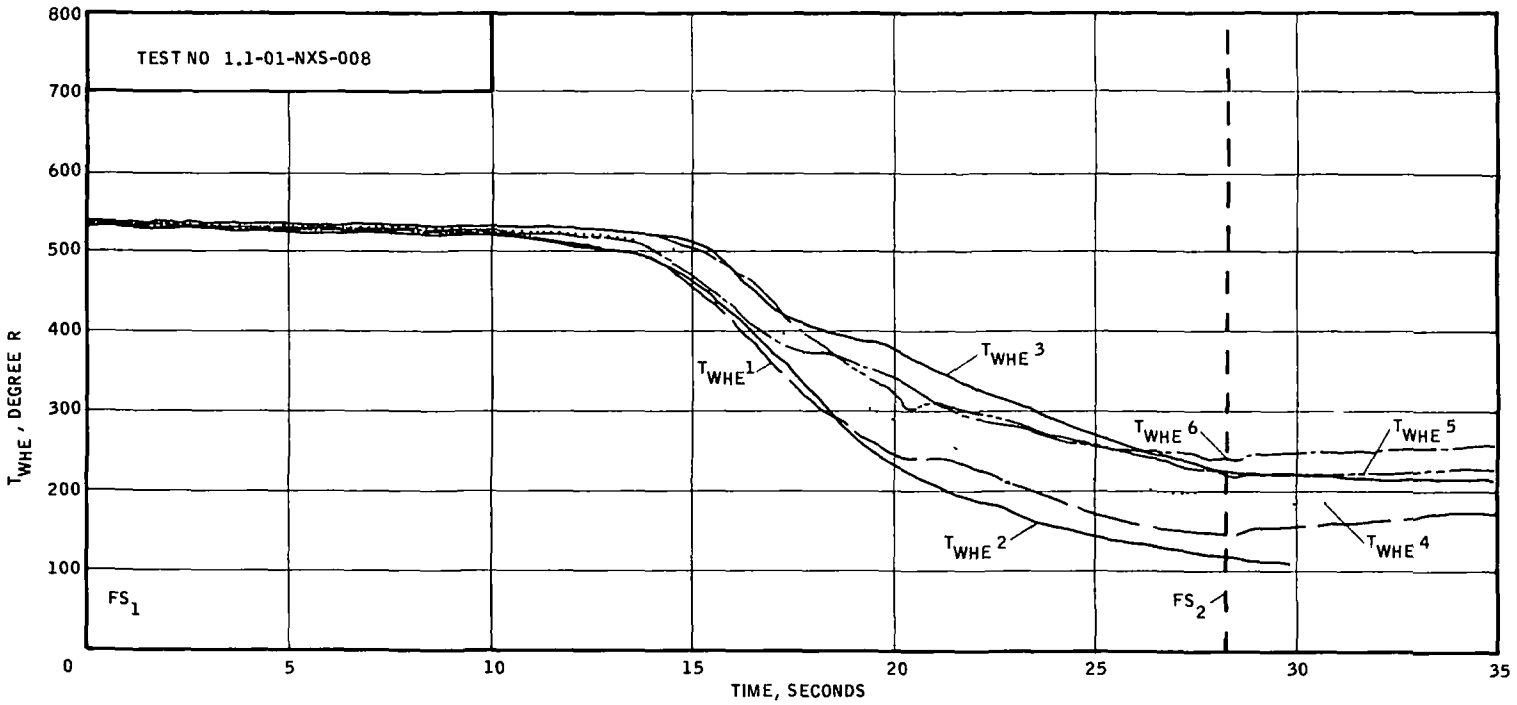

HEAT EXCHANGER WALL TEMPERATURES
10-07-61

Figure V-H,9

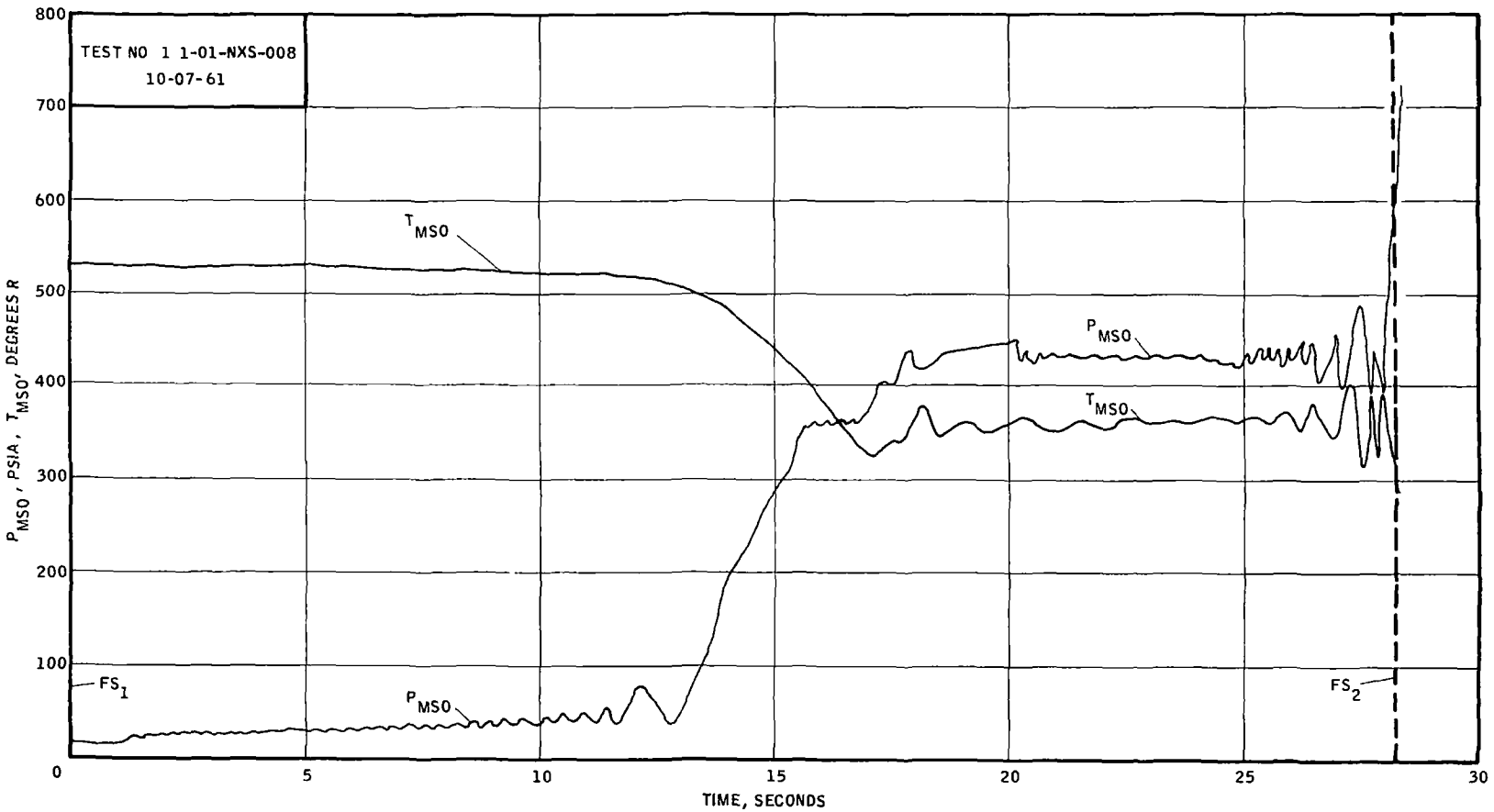

MIXING SECTION OUTLET CONDITIONS

Figure V-H,10

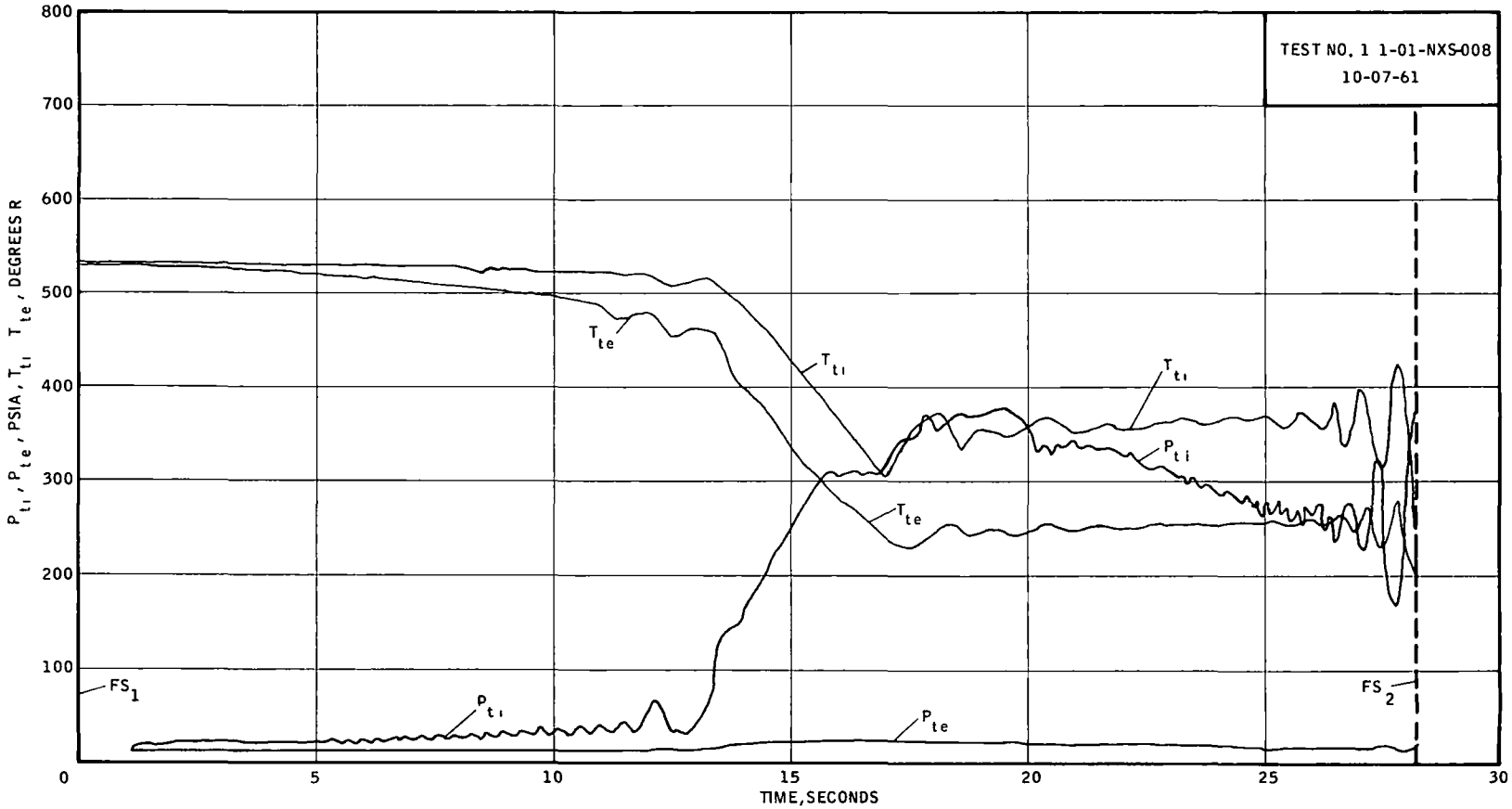

TURBINE INLET AND EXHAUST CONDITIONS

Figure V-H,11

UNCLASSIFIED

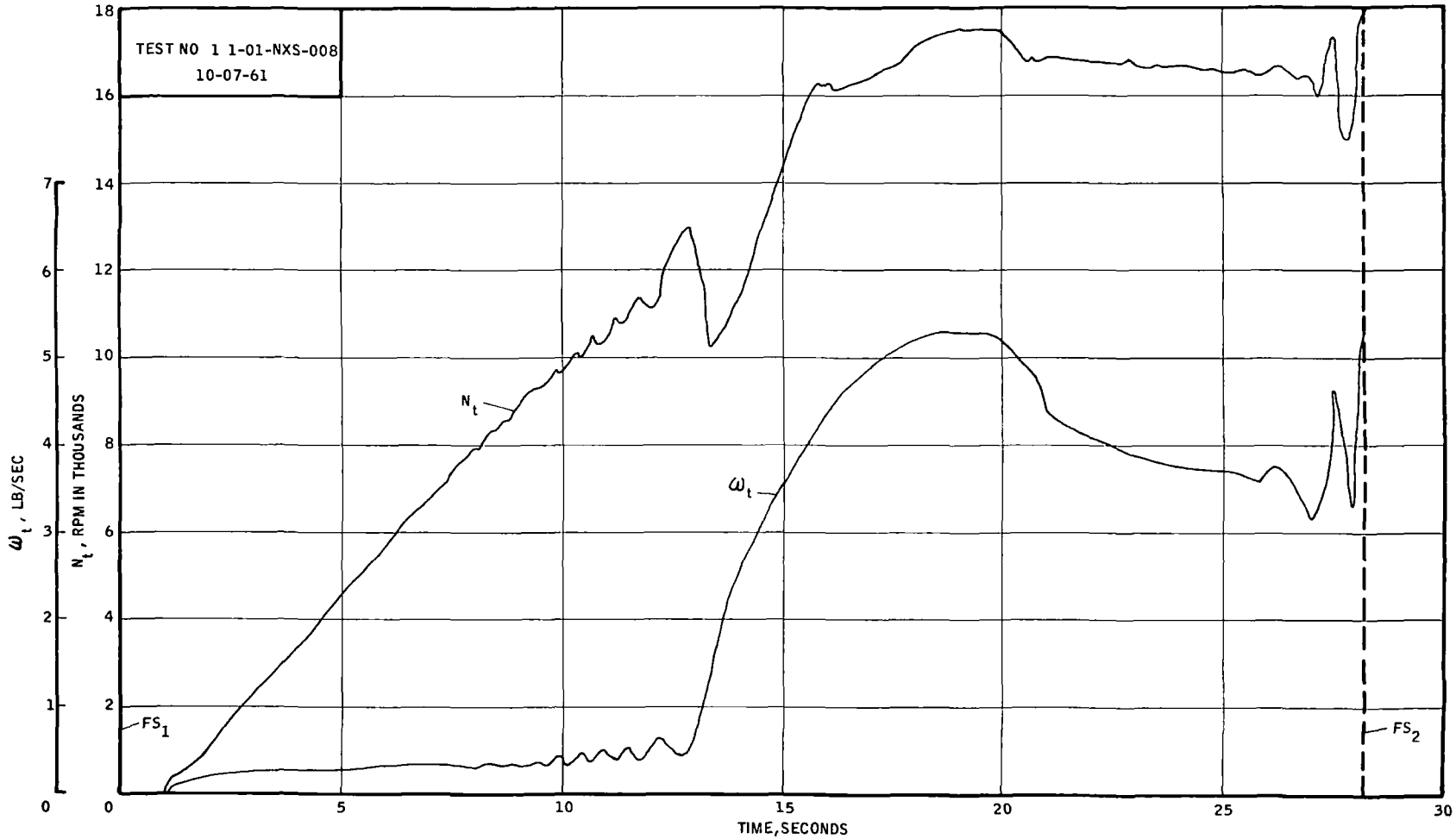

TURBINE PERFORMANCE

Figure V-H,12

UNCLASSIFIED

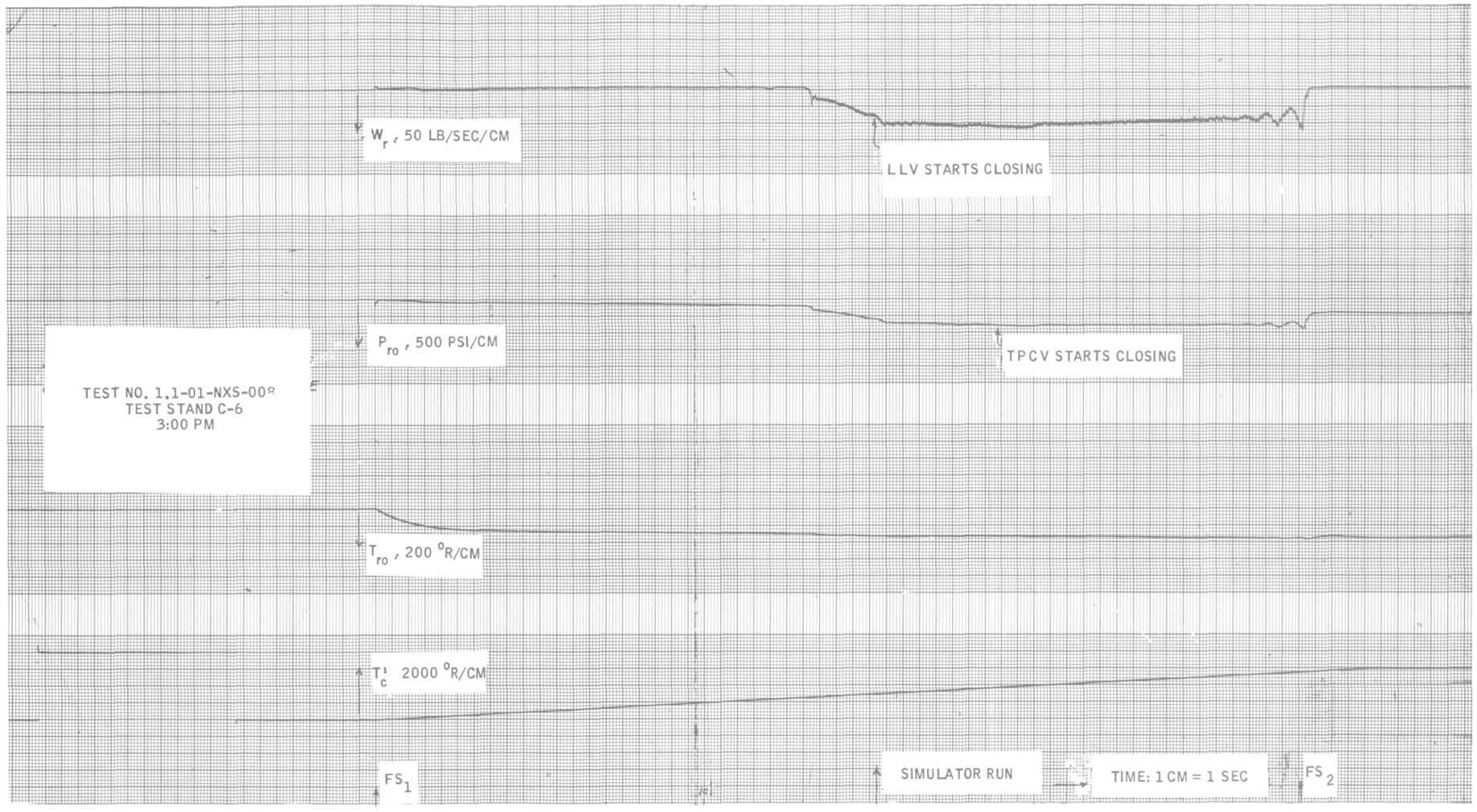

REACTOR SIMULATOR OUTPUTS, GEN. I COLD-BLEED ENGINE SIMULATOR SYSTEM
10-07-61

Figure V-H,13

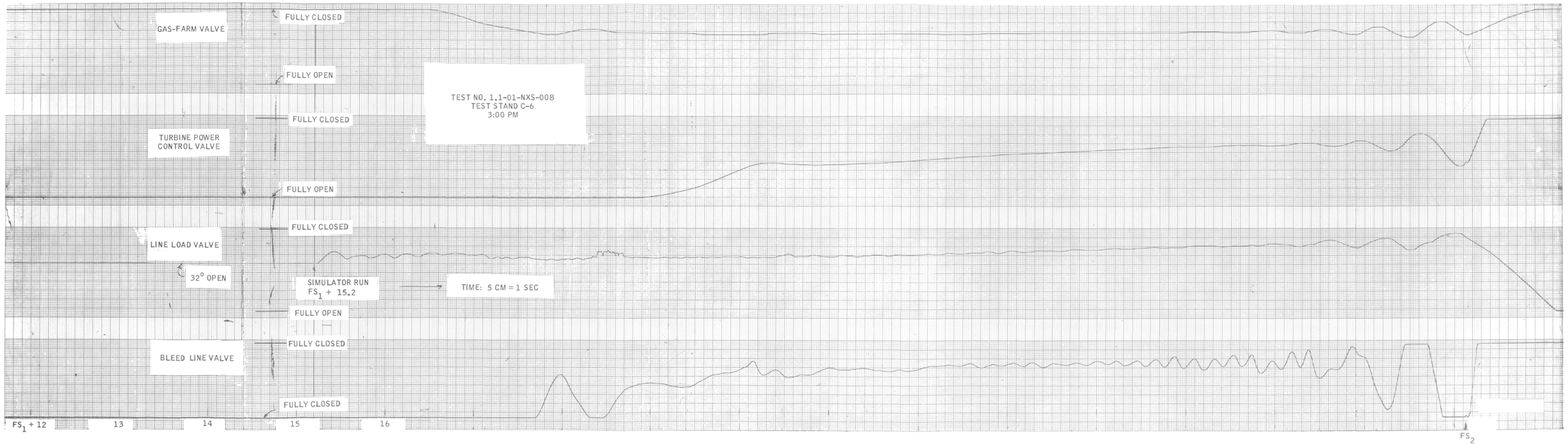

VALVE POSITIONS, GEN.I COLD-BLEED ENGINE SIMULATOR SYSTEM
10-07-61

Figure V-H,14

VALVE ERROR SIGNALS, GEN. I COLD-BLEED ENGINE SIMULATOR SYSTEM
10-07-61

Figure V-H,15

VI ANALYSIS OF TEST RESULTS

Only the data of Test No. 1 1-01-NXS-008 (see V,H) was selected for complete analysis In all previous tests, at least one temperature probe was inoperative, in addition, the erroneous location of ΔP_{fDo} differential pressure pickup was not discovered and corrected until after the run of Test -005. In the eighth test, pressures and temperatures at all flow-metering orifices, and on both sides of the pump and heat-exchanger were recorded.

A. CORRELATION OF FLOW RATES

The weight flow rates at each orifice (see Figure 1-C,2) were calculated by the hydraulic equation,

$$w = KA \sqrt{2g\rho\Delta P} \tag{17}$$

If an orifice flowed gas, the expansion factor was taken into account. Thus,

$$w = KAY \sqrt{2g\rho\Delta P} \tag{18}$$

where

$Y = f\left(\frac{P_2}{P_1}, k, \beta\right)$ as defined in Reference 5

Table VI-A,1 lists the flow equations for the orifices, the Load valve, and the turbine nozzle. In the case of the Load valve, an empirically determined flow coefficient (for water) was used to calculate the flow rates of both gas and liquid. The compressible flow relation was used for the turbine nozzle

The calculated flow rates are given in Table VI-A,2 for a number of points taken during the duration of the run. At each point in time, the recorded variables were assumed to be at steady-state. The density values were obtained from a hydrogen temperature-entropy diagram, and corresponded to the pressures and temperatures recorded at each orifice.

The empirical flow coefficient for the Load valve was plotted as a function of butterfly-blade angle, which was determined from the valve position trace, as shown in Figure V-H,13

Only representative points, sufficient for flow-rate correlation, are given in Table V-H,2 Many more points in time were taken to plot the calculated flow rates in Figures V-H,3,4,7, and 12.

In an effort to determine the degree of accuracy of the equations used to determine weight flows, the total weight flows were compared to the sum of the component flows In particular, two comparisons are made in Table VI-A,2 w_f is compared to $(w_{lv} + w_{fyo} + w_b)$, and w_t is compared to $(w_b + w_{gh_2})$. Both w_f and w_t were consistently lower than the respective sum of their components. Over the entire run, on the average, w_f and w_t were 18 5% and 18.6% lower, respectively, than the sum of their components Over the period from 13 6 to 28 seconds, where conditions were steady-state or nearly so, w_f and w_t were 8 27% and 11 7% lower, respectively, than the sum.

These errors are due to several causes

1. While data was recorded by a sampling system which recorded data at 50 millisecond intervals, still different groups of instrument readings were recorded at different time intervals. In some instances, the pressure and temperature at a point in the system were recorded at different time intervals.

2 An error was introduced in the summation of component flow rates by neglecting the transport lag between the points in the system where the component flows were measured

3. The larger difference between total flows and the component summation resulted from the rapid changes in conditions throughout the system at the beginning and end of the run.

4. The error in the flow rate calculated for each orifice is probably on the high side, so that the errors were added in the component summation

5. Since no calibration of the orifices was made with hydrogen, it was impossible to separate out errors in the calculations made for individual orifices However, it is safe to assume that the flow coefficients given by Reference 5 are fairly accurate since these coefficients were correlated on the basis of Reynolds Number for a large number of fluids. Then the errors appearing in the flow-rate correlation were most probably due to errors arising in flow rates of the Load valve and turbine nozzle There was an unknown error in determination of the blade angle of the Load valve, and another unknown error in using a flow coefficient based on water flow tests. The largest error in w_t of the turbine nozzle would be due to an error in the use of a single nozzle throat area equivalent to the three tandem nozzles that actually existed

TABLE VI-A, 1

FLOW-METERING ORIFICE EQUATIONS

NOTES

1. Flow coefficients and expansion factors, unless otherwise noted, were obtained from the ASME Fluid Meters Report, Reference 5.

2. Pressure tap locations for all orifices were at 1 D and 1/2 D, ahead and after the orifice, respectively.

3. Reynolds No. was 10^6 or greater at each orifice in all flow calculations.

4. Thin-plate, square-edged orifices were used.

A. ΔP_{fDo} ORIFICE

$$w_f = YK\left(\frac{\pi d^2}{4}\right)\sqrt{2g\ \rho_{fD}\ \Delta P_{fDo}} \qquad (1)$$

where

K 0.734 for $\beta = 0.75$

Y for liquid = 1

Y for gas = $f\left(\frac{P_2}{P_1}, k, \beta\right)$

$$\frac{P_2}{P_1} = \frac{P_{fD} - \Delta P_{fDo}}{P_{fD}}$$

d = 3.807 in.

D = 5.07 in.

k = 1.4

B. ΔP_{BPO} ORIFICE

$$w_b = YK\left(\frac{\pi d^2}{4}\right)\sqrt{2g\ \rho_{BPO}\ \Delta P_{BPO}} \qquad (2)$$

where

$k = 0.604$ for $\beta = 0.407$

Y for liquid = 1

Y for gas = $f\left(\frac{P_2}{P_1}, k, \beta\right)$

$$\frac{P_2}{P_1} = \frac{P_{BPO} - \Delta P_{BPO}}{P_{BPO}}$$

$d = 1.25$ in.

$D = 3.068$ in.

$k = 1.4$

C. ΔP_{fyo} ORIFICE

$$w_{fyo} = YK\left(\frac{\pi d^2}{4}\right)\sqrt{2g\,\rho_{fyo}\,\Delta P_{fyo}} \qquad (3)$$

where

$K = 0.6176$ for $\beta = 0.49$

Y for liquid = 1

Y for gas = $f\left(\frac{P_2}{P_1}, k, \beta\right)$

$$\frac{P_2}{P_1} = \frac{P_{fyo} - \Delta P_{fyo}}{P_{fyo}}$$

$d = 1.5$ in.

$D = 3.068$ in.

$k = 1.4$

D. LOAD VALVE

$$w_{\ell v} \quad K_w \frac{\rho_{LLV}\,\Delta P_{LLV}}{62.4} \qquad (4)$$

where

K_w = empirical flow coefficient obtained from plot of K_w versus butterfly blade angle, and where flow coefficient K_w was obtained with water

$$\Delta P_{LLV} = P_{LLV(1)} - P_{LLV(o)}$$

$$\rho_{LLV} = \rho_{fD}$$

E. TURBINE NOZZLE

$$w_t \quad \frac{C}{\sqrt{1-\beta^4}} \quad A_t \sqrt{\frac{2g}{RT_{T1}}} \quad P_{TI} \quad \psi_t \tag{5}$$

where

$$\psi_t, \text{ for sonic flow} = \left\{ \left(\frac{2}{k+1}\right)^{1/(k-1)} \sqrt{\frac{k}{k+1}} \right.$$

$$\psi_t, \text{ for subsonic flow} = \sqrt{\frac{k}{k-1}\left[\left(\frac{P_{Te}}{P_{T1}}\right)^{2/k} - \left(\frac{P_{Te}}{P_{T1}}\right)^{(k+1)/k}\right]}$$

$C = 0.98$

$A_t = 1.87 \text{ in.}^2$

$$\beta = \sqrt{\frac{A_t}{A}} = \frac{1.87}{7.4} = 0.504$$

$R = 767$

$k = 1.4$

F. ΔP_{gh_2s} ORIFICE

$$w_{gh_2} = YK\left(\frac{\pi d^2}{4}\right)\sqrt{2g\,\rho_{gh_2s}\,\Delta P_{gh_2s}} \tag{6}$$

where

$K = 0.724$ for $\beta = 0.733$

$$Y \text{ for gas} = f\left(\frac{P_2}{P_1}, k, \beta\right)$$

$$\frac{P_2}{P_1} = \frac{P_{gh_2s} - \Delta P_{gh_2s}}{P_{gh_2s}}$$

$d = 2.25$ in.

$D = 3.068$ in.

$k = 1.4$

"Page missing from available version"

TABLE VI-A,2

CORRELATION OF FLOW RATES
TEST NO 11-01-NXS-008

TIME SECONDS AFTER FS_1	PUMP DELIVERY W_f LB/SEC	LOAD VALVE FLOW W_{lv} LB/SEC	BYPASS ORIFICE FLOW W_{fyo} LB/SEC	BLEED LINE FLOW W_b LB/SEC	GAS FARM FLOW W_{gh_2} LB/SEC	TURBINE FLOW		
						W_t LB/SEC	$W_{lv}+W_{fyo}+W_b$ LB/SEC	$W_b+W_{gh_2}$ LB/SEC
1.170	INV	INV	INV	INV	0	0.05	INV	INV
2.047	INV	INV	INV	INV	0	0.20	INV	INV
5.119	2.27	1.52	0.77	0.24	0	0.26	2.53	0.24
6.582	3.01	1.61	0.89	0.32	0	0.32	2.82	0.32
7.167	2.94	2.13	0.99	0.32	0	0.33	3.44	0.32
7.606	3.21	1.39	0.91	0.33	0	0 33	2.63	0.33
7.801	3.39	2 46	0.84	0.42	0	0.30	3.72	0.42
8.044	2.25	1.29	0.79	0.28	0	0.30	2.36	0.28
8.191	3.08	2.04	1.07	0.35	0	0.37	3.46	0.35
8.776	2.01	1.45	0.82	0.31	0	0.31	2.58	0.31
8.873	3.88	2.57	0.94	0.45	0	0.36	3.96	0.45
9.068	2.80	1.23	0.90	0.35	0	0.33	2.48	0.35
9.605	3.63	2 83	0.86	0.45	0	0.35	4.14	0.45
9.897	1.74	1.07	0.93	0.28	0	0.34	2.28	0.28
10 043	4.25	3.03	0.93	0.52	0	0.38	4.48	0.52
10.677	2.09	1.33	1.01	0.43	0	0.36	2.77	0.43
10.970	5.53	2.87	1.56	0.60	0	0.51	5.03	0.60
11.214	1.44	1.19	0.95	0.28	0	0.47	2.42	0.28
11.506	18.20	9.21	1.70	0.65	0	0.54	11.56	0.65
11.701	9.19	5.29	0.93	0.31	0	0.38	6.53	0.31
12.237	16.86	7.77	2.64	0.56	0	0.69	10.97	0.56
12.725	1.11	0.73	0.50	0.32	0	0.40	1.55	0.32
13.603	34.34	23 74	14.50	3.14	0	1.68	41.38	3.14
16.089	48.30	23.95	21.83	4.96	0	4.38	50.74	4.96
17.991	52.99	29.59	23.06	3.00	2.85	5.18	55.65	5.85
19.844	55 92	21.66	25.25	2.71	3.16	5.29	49.62	5.87
20.088	55.38	27.88	25.49	2.18	3.28	5.14	55.55	5.46
20.771	47.72	25.16	25.08	2.69	2.78	4.84	52.93	5 47
22.916	44.96	24.03	26.65	2.12	3.02	4.42	52.80	5.14
25.014	40 95	14.83	28.97	1 74	2 62	3.70	45.54	4.36
25.891	39.72	9.86	29.45	1.56	2.46	3.58	40.87	4.02
26.282	38.95	12.68	29.84	1.68	2.36	3.76	44.20	4.04
27.062	38.96	7.41	29.83	1.12	2.93	3.14	38.36	4.05
27.208	40.24	0.24	29.14	1.45	1.66	3.39	30.83	3.11
27.501	37.17	21.46	31.16	3.60	2.92	4.69	56.22	6.52
27.940	38.61	0	27.49	2.45	1.52	3.29	29.94	3.97
28.233	35.21	10.98	31.53	5.47	2.27	6.16	47.98	7.74

Table VI-A,2

B TURBOPUMP PERFORMANCE

The ideal turbine power was calculated by

$$P_{T_{ideal}} = \frac{w_t C_o^2}{2g} \tag{19}$$

where

$$C_o = \sqrt{\frac{2gk\,R\,T_{T1}}{k-1}\left[1 - \left(\frac{P_{Te}}{P_{T1}}\right)^{(k-1)/k}\right]}$$

and w_t is available from Table VI-A,2.

The turbine shaft power was obtained by multiplying the ideal power by the turbine efficiency, Figure VI-B,1, and the turbine shaft torque is then given by

$$M_t = \frac{\eta_s P_{T_{ideal}}}{N\left(\frac{rad}{sec}\right)}, \text{ ft-lb} \tag{20}$$

In the steady-state, pump input torque would be equal to turbine shaft torque. However, the rotor inertia must be taken into account for the transient case. Hence,

$$M_p = M_t - J\frac{dN}{dt} \tag{21}$$

where

$J = 0.292$ ft-lb-sec^2

dN/dt is measured on the speed-time plot

Pump input power is then

$$P_{p_{shaft}} = N\,M_p \tag{22}$$

The pump efficiency is

$$\eta_p = P_{p_{out}}/P_{p_{shaft}} \tag{23}$$

where

$$P_{p_{out}} = \frac{144\,(P_{fD} - P_{fs})\,w_f}{\rho_{fD}}$$

Turbine efficiency was determined, at a given point in time, from Figure VI-B,1, for a measured value of $\nu = U/C_o$. The peripheral velocity was U = 0.456 N, ft/sec.

The results of the calculations are given in Table VI-B,1, in which each point in time was assumed to be a steady-state point, and the instantaneous acceleration was measured at that point on the transient. The negative values of pump-shaft torque indicate that the fluid helped to accelerate the turbopump at the start of the transient. During the period of two-phase flow in the pump, most of the torque developed by the turbine went into turbopump acceleration.

At the peak of the heat-capacity start, just before the Gas-Farm valve started to open, the shaft power developed by the turbine was 2105 horsepower, or almost 47% of design point.

After the extra energy was added from the gas farm, the ideal power available to the turbine was 5027 horsepower at the peak point. Nearly half of this power was contributed by the gas flowing yhrough the heat exchanger.

TABLE VI-B,1

TURBOPUMP PERFORMANCE TEST NO 11-01-NXS-008

TIME SECONDS AFTER FS_1	SPEED N_T RPM	ISENTROPIC VELOCITY Co FT/SEC	IDEAL TURBINE POWER $P_{t_{IDEAL}}$ H.P.	TURBINE EFFICIENCY η_s	TURBINE SHAFT POWER $P_{t_{SHAFT}}$ H P.	TURBINE SHAFT TORQUE M_T FT-LB	ACCEL TORQUE $J\frac{dn}{dt}$ FT-LB	PUMP SHAFT TORQUE M_P FT-LB	PUMP SHAFT POWER $P_{P_{SHAFT}}$ H P	PUMPING POWER $P_{P_{OUT}}$ H P.	PUMP EF-FICIENCY η_P
1.170	30	960.47	1.3	.077	.1	17.7	34.8	-17.1	0	0	
2.047	909	2877.27	48.2	.077	3.7	21.4	34.8	-13.4	-2	0	
5.119	4683	3455.21	90.4	.308	27.8	31.2	34.8	-3.6	-3	-.1	.04
6.582	6264	4062.27	153.6	.342	52.6	44.1	34.8	9.3	11	10.9	
7.167	6813	4166.22	166.8	.357	59.5	45.9	34.8	11.1	14	36.3	
7.606	7389	4058.11	143.9	.390	56.1	39.9	34.8	5.1	7	8.3	
7.801	7536	3816.95	127.3	.412	52.4	36.5	12.8	23.7	34	55.9	
8.044	7926	3816.95	127.3	.426	54.2	35.9	34.8	1.1	2	11.8	
8.191	7854	4162.06	186.6	.400	74.6	49 9	0	49 9	75	42 9	.58
8.776	8628	3812.79	131.2	.454	59.6	36.3	0	36.3	60	24.1	.40
8.873	8484	4157.90	181.2	.421	76.3	47.2	34.8	12.4	20	60.1	
9.068	8916	4041 48	157 0	.445	69.9	41.2	34.8	6.4	11	13.6	
9.605	9207	4153.74	175.8	.449	78.9	45.0	15.6	29.4	52	77.3	
9.897	9744	4153.74	170.8	.465	79.4	42.8	0	42.8	79	14.9	.19
10.043	9513	4361.64	210.5	.443	93.3	51.5	0	51.5	93	90.9	
10.677	10359	4245.22	188.9	.478	90.3	45.8	50 5	-4.7	-9	9.1	
10.970	10194	4848.11	349.1	.428	149.4	77.0	0	77.0	150	87 9	.59
11.214	10947	4232.72	193.0	.491	94.8	45.5	0	45 5	95	13 7	.14
11.506	10698	5022.74	396.7	.438	173.8	85.3	57.1	28.2	57	22.5	.39
11.701	11394	4112.16	187.1	.510	95.4	44.0	0	44.0	96	3.6	.04
12.237	11085	5326 27	570.0	.426	242.8	115.1	59.1	56.0	118	23.7	.20
12.725	12819	4315 90	217.0	.526	114.1	46.8	42.8	4.0	10	15.4	
13 603	10524	6178 64	1867.6	.369	689.1	344.0	48.0	296.0	594	404.0	.68
16.089	16233	5633.95	4048.5	.520	2105.2	681.3	0	681.3	2107	1270.3	.60
17.991	17094	5742.06	4973.4	.526	2616.0	803.9	27.8	776.1	2528	1512.3	.60
19.844	17514	5712.95	5027.7	.530	2664.7	799.3	0	799.3	2668	1672.2	.63
20.088	17439	5733.74	4920.7	.529	2603.1	784.1	-25.6	809.7	2691	1664.1	.62
20.771	16833	5671.38	4533.3	.526	2384.6	744.2	0	744.2	2387	1350.4	.57
22.916	16806	5791.95	4317.8	.521	2249.6	703.2	0	703.2	2252	1253.5	.56
25.014	16554	5821.06	3650.9	518	1819.2	600.1	-8.6	608 7	1920	1101.1	.57
25.891	16464	5862.64	3583.1	513	1838.1	586.5	-12.8	599.3	1880	1049.8	.56
26.282	16707	5688.01	3542.4	.523	1852.7	582.5	0	582.5	1854	1056.1	.57
27.062	16248	6033.11	3328.2	.505	1680.7	543.4	-26.0	569.4	1763	1011.6	.57
27.208	15873	5937.48	3480.1	.503	1750.5	579.3	0	579.3	1742	992.2	57
27.501	17394	5363.69	3929.1	545	2141 4	646.7	0	646.7	2144	1109.1	.52
27.940	14994	5563.27	2965.2	.505	1497 4	524.6	0	524.6	1499	842.4	56
28.233	17706	5939.37	4555.4	560	2551.0	756.9	0	756.9	2554	1076.6	.42

Table VI-B,1

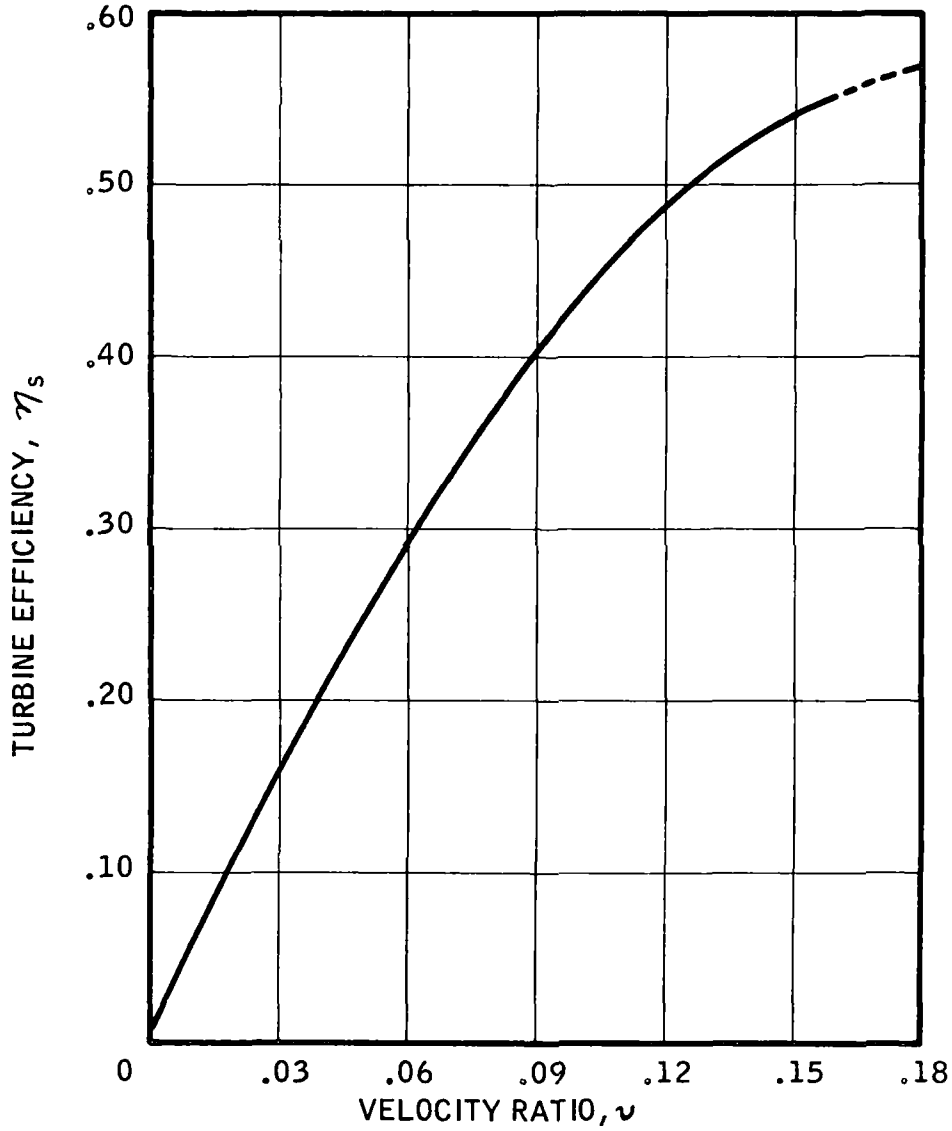

TURBINE EFFICIENCY AS A FUNCTION OF VELOCITY RATIO

Figure VI-B,1

C. HEAT CAPACITY HEAT EXCHANGER PERFORMANCE

The applicability of this analysis to NERVA is questionable on a quantitative basis because of the error in heat-capacity heat-exchanger simulation of the NERVA engine reflector. The flow geometry was not the same as is planned for the NERVA reflector, therefore (as demonstrated in Section II.B.3), the similitude of pressure drop and heat transfer for the heat exchanger and reflector cannot be established. In addition, since the heat-exchanger segment was to Cold-Bleed Engine Scale, 13/83 (or 15.7%) of the size of the actual reflector, but only 5.4% (Heated-Bleed Engine scale) of the flow was passed through it, more heat capacity was available per pound of fluid than is available in the real engine and a lower pressure drop occurred.

Test data for the internal wall and gas temperatures seemed to be invalid at the individual stations, when comparing one station against another, because calculation of film coefficients indicated contradictory heating and cooling between consecutive stations. Averages of the T_{WHE} and T_{GHE} curves, as given in Figures V-H,8 and 9, were therefore used to determine average film coefficients as a function of time. From these data, the average heat-transfer rates, heat flux, and film coefficients were calculated between FS_1 and FS_2.

The equations used for data analysis were as follows

1. <u>Average Heat Transfer Rate, $\dot{Q}$, Btu/sec</u>

$$\dot{Q}_x = \dot{W}_x (ho - hi) \tag{24}$$

where

ho = enthalpy at outlet, Btu/lb

hi = enthalpy at inlet, Btu/lb

$\dot{W}_x$ = gas flow rate at time x, lb/sec

$\dot{Q}_x$ = heat transfer rate at time x, Btu/sec

Subscript x denotes time x

2. <u>Average Heat Flux, Q_x/A_{he}, Btu/in.^{2} sec</u>

This quantity is obtained by dividing Equation (24) by the total-heat transfer area, $A_{he} = 6100$ in.^{2}

3 Average Experimental Film Coefficient, h_g, Btu/sec in.^{2}-^{o}R

$$h_{gx} = \frac{\dot{Q}_x}{A_{he}\,(T_{WHE} - T_{GHE})} \tag{25}$$

where

$\frac{\dot{Q}_x}{A_{he}}$ = average heat flux, Btu/in.^{2} sec

T_{WHE} = average wall temperature, ^{o}R

T_{GHE} = average gas temperature, ^{o}R

4. Average Theoretical Film Coefficient, h_g, Btu/sec in.^{2}-^{o}R

$$h_{gx} = \frac{.023}{D^{.2}} \left(\frac{\dot{W}_{bx}}{A} \; \frac{T_{GHE_x}}{T_{fx}} \right)^{0.8} \left(\frac{c_p^{\,0.4}\, k^{\,0.6}}{\mu^{0.4}} \right)_{fx} \tag{26}$$

where

h_{gx} = average film coefficient at time, x, Btu/sec in.^{2}-^{o}R

D = 3/16-in.-dia hole

$\dot{W}_{bx}$ = gas flow rate at time x, lb/sec

$= KA \sqrt{2g\ \Delta p_{BPO} \rho_{BPO}}$ in liquid state

$= YKA \sqrt{2g\ \Delta p_{BPO} \rho_{BPO}}$ in gaseous state

$A = \frac{\pi}{4}\,(3/16)^2 \times 200 = 5.52$ in.^{2} = flow area

T_{GHE} = average gas temperature. ^{o}R

$T_{fx} = \frac{T_{GHE} + T_{WHE}}{2}$ = film temperature, ^{o}R

C_p = specific heat

K = thermal conductivity

μ = viscosity

$$\left(\frac{C_p^{0.4} K^{0.6}}{\mu^{0.4}}\right)_{fx} = \text{transport properties evaluated for film temperature at time x}$$

Figures VI-C, 1 and 2 contain plots of the calculated results obtained for heat-transfer rates, heat fluxes, and film coefficients.

The fluid conditions at the entrance to the heat exchanger are important because of the concern regarding two-phase flow in the reflector. Figure VI-C, 3 shows the fluid conditions during Test Run -008 on a hydrogen T-S diagram. It can be seen that the fluid conditions at no time lie under the dome, therefore, two-phase flow did not exist in the heat exchanger.

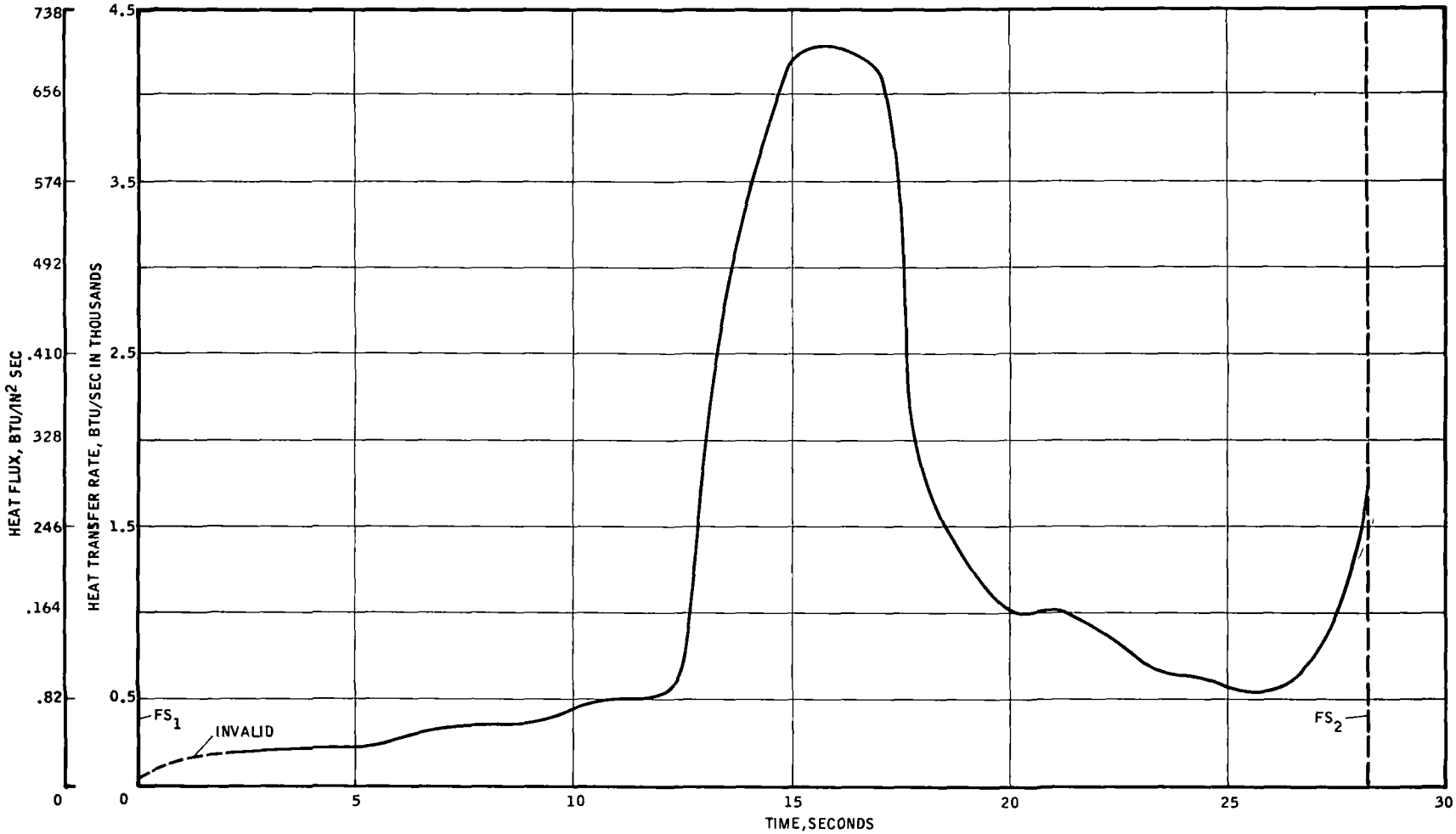

HEAT-TRANSFER RATE AND HEAT FLUX

Figure VI-C,1

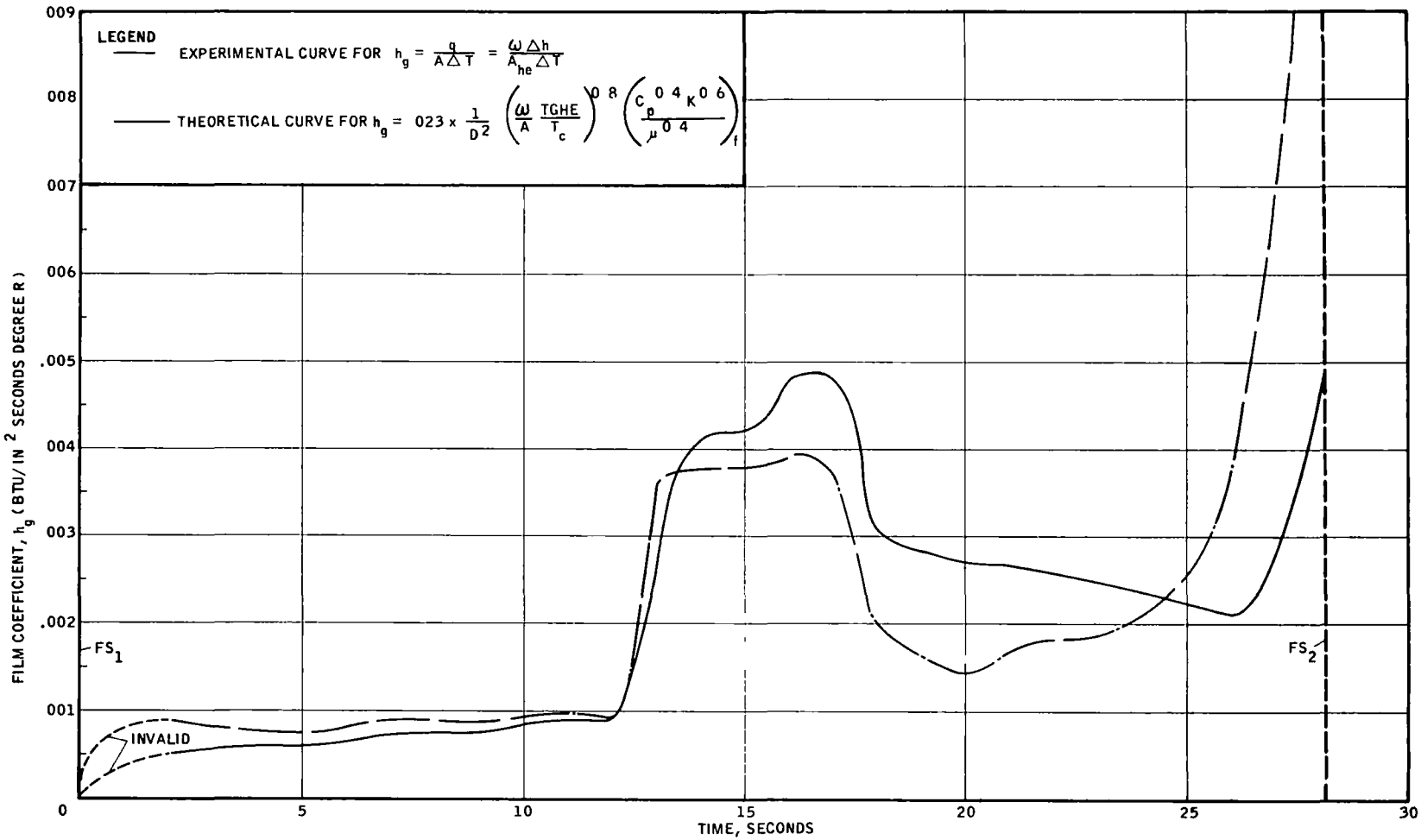

HEAT – TRANSFER COEFFICIENTS

Figure VI-C,2

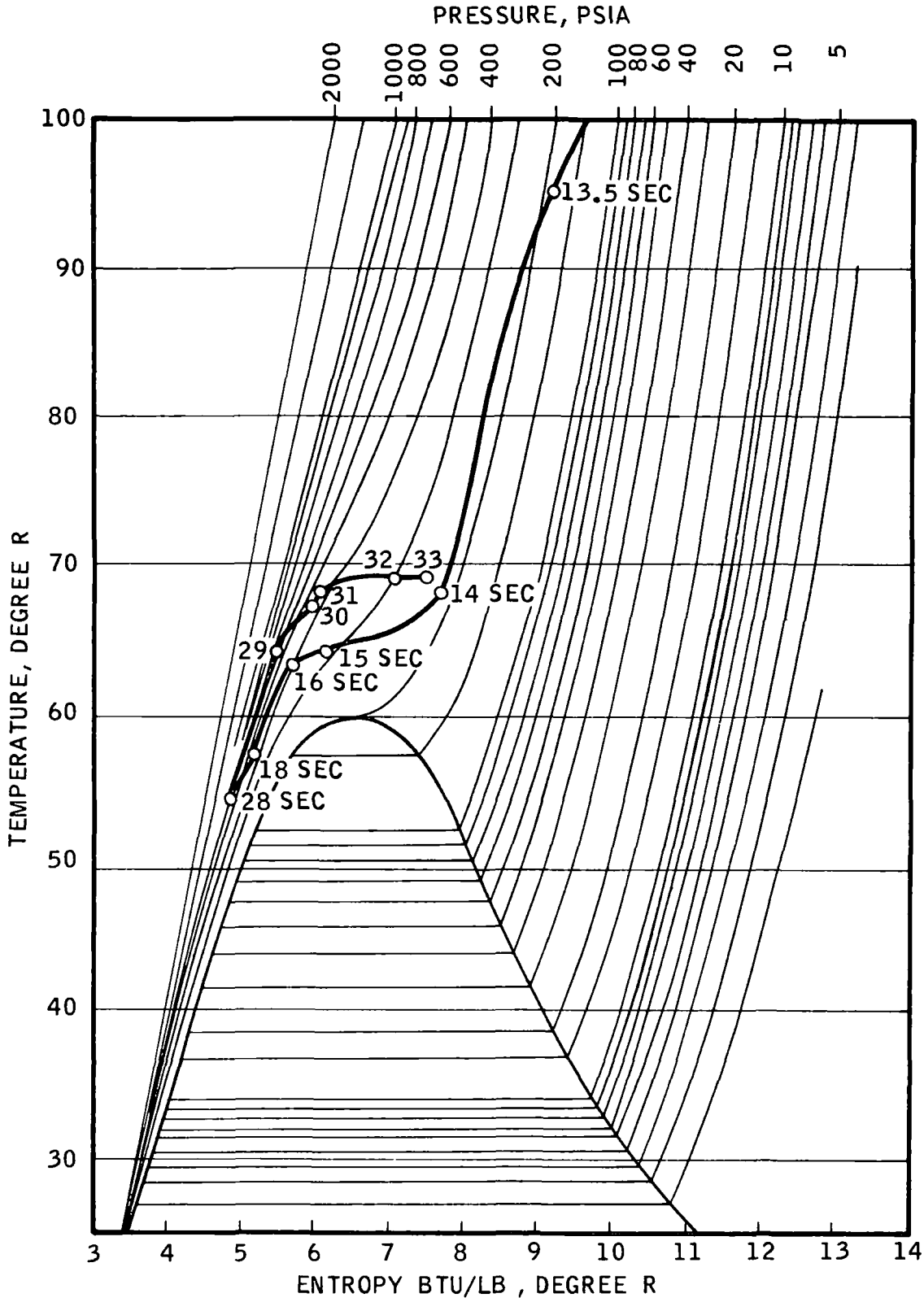

FLUID CONDITIONS AT HEAT EXCHANGER INLET
FOR TEST NO. 1.1-01-NXS-008

Figure VI-C,3

VII CONCLUSIONS AND RECOMMENDATIONS

A. HEAT-CAPACITY STARTUP

The major objective of the Generation I Engine Simulator was achieved, that is, the turbopump was successfully "bootstrapped" by utilizing the thermal energy initially stored in the metal parts of the propellant feed system to heat the turbine drive fluid. In Test No. 1.1-01-NXS-008, for example, 217 hp was available to the turbine at the point where stable liquid-phase hydrogen first appeared in the pump. The speed at that point was 12,500 rpm, so that sufficient energy was available in the rotor to boost pump pressure. As flow increased through the pump, the speed slowed because of the greater pump load. However, because of the greater flow to the turbine, the available power increased to 1867 hp (at 13.6 sec), and continued to increase as heat was extracted from the heat-capacity heat exchanger. Sufficient energy was acquired by the turbine fluid in the heat exchanger to boost the turbopump to 16,200 rpm, which corresponded to the power saturation point in the heat-capacity start portion of Test Run -008. The power available to the turbine at the power saturation point was 4048 hp, and the turbine shaft horsepower was 2105. The corresponding temperature rise of the fluid in the heat exchanger was 276°.

The other heat-capacity start tests (that is, the second and third tests in the series) showed that after the power saturation point was reached, the transient decay of turbopump speed was much slower than the bootstrap phase. The slow decay was the result of the turbine fluid continuing to extract nearly enough energy from the heat-capacity heat exchanger to balance the load on the pump. By contrast, turbopump speed decayed very rapidly in those cases where an overspeed trip caused rapid closure of the turbine shutoff valve while the pump was delivering a high flow rate.

The results of the Generation I Engine Simulator heat-capacity start tests can be extended to the NERVA engine. There the bootstrap process would be extended to the full power level as a result of reactor core heating. Before the heat-capacity of the reflector could be exhausted, reactor power would have reached such a level as to greatly heat the fluid in the core. The large change in fluid density is essentially an increase in the resistance to flow through the core, and consequently, more fluid would be forced through the turbine bleed line.

Further heat-capacity start tests are recommended, but these should be conducted with the prototype system (excluding the reactor) to provide more realistic flow paths and heat capacities. The heat-capacity startup of a prototype system is expected to be similar to that obtained with the Generation-I

Simulator. However, the rate of pump cooldown, and the amount of energy reaching the turbine will be significantly different, sufficiently different to justify further tests with a prototype system.

Provision should also be included in the prototype system to investigate turbine power control during the heat-capacity portion of engine startup. In the Generation I system, the TPCV was held wide open during the start transient. This permitted a higher pump delivery than is called for in the proposed NERVA startup schedule. In the NERVA engine, thrust-chamber pressure is the quantity directly controlled by the turbine power control loop, but P_c is a function of flow from the pump. Therefore, further tests should be conducted on the prototype system to determine whether $P_{c\ reference}$ should be initially fixed at some percentage of the design point value, or whether it should follow a program from the start of propellant flow. It appears from the Generation-I test results that scheduling $P_{c\ reference}$ from the very beginning of propellant flow would be the better approach, since pump pressure rose too rapidly with this factor fixed at the design point.

B. PROPELLANT FEED SYSTEM OPERATION

Much valuable data and operating experience with a full-scale liquid-hydrogen turbopump was gained in these tests. The information obtained will be useful in both the design of the propellant feed system, and in the analysis and design of the NERVA engine control system.

Thermal shock caused by flowing liquid hydrogen into an ambient temperature pump produced adverse effects neither on the pump nor its operation. This results allows the tank shutoff valve to be located upstream of the pump, where the location of the valve in this position is especially advantageous, because the problem of sealing the pump bearings is much less stringent than when the pump is initially immersed in propellant.

The vaporization of liquid hydrogen in the suction line and pump, during the cooldown period, was found to be an inverse function of tank pressure: the lower the tank pressure, the longer the time required for chilling the suction line and pump. Cooldown took 6 seconds for a tank pressure of 63 psig, and as long as 28 seconds with tank pressure set at 23 psig. In the three tests where tank pressure was set at 40 psig vaporization in the pump lasted for an average period of 11 seconds. The shorter cooldown periods are, of course, a result of higher initial flow rates produced by higher tank pressures.

Turbopump acceleration was also a function of tank pressure. More flow was available at the turbine for higher tank pressures. Acceleration varied directly with tank pressure, from 940 rpm/sec with tank pressure at 23 psig, to 2960 rpm/sec with tank pressure at 63 psig. The mean was 1100 rpm/sec for a tank pressure of 40 psig.

During the period of 2-phase flow in the suction line of the pump, pressure oscillations appeared on the discharge side of the pump and were reflected throughout the system. In most of the heat-capacity starts, the frequency of oscillation varied from 2 to 3 cps. There was apparently no relation of the frequency to either tank pressure or downstream flow impedances. However, the amplitude of these oscillations was related to tank pressure and to pump speed. Since the higher tank pressures produced correspondingly higher accelerations of the turbopump, the amplitudes of the pressure pulses varied directly with tank pressure and speed. This fact, plus the fact that the fluid density on the suction side of the pump alternated from liquid to vapor, indicated that slugs of liquid hydrogen were entering the pump. Apparently, these slugs were accelerated by the pump, producing the pressure pulses on the discharge side, and, because the speed was greater each time a slug entered the pump, the amplitude of each succeeding pressure pulse was greater than the preceding

pulse. The oscillations in pressure disappeared when liquid-phase hydrogen appeared in the pump. In other words, the suction line and pump were cooled down to LH_2 temperature, suggesting that the two-phase flow was largely due to heat transfer from the walls of the line and pump. After the appearance of stable liquid, pump discharge pressure rose smoothly. No oscillations existed during pump discharge pressures greater than the critical pressure, after stable liquid-phase hydrogen appeared in the pump.

The preceding observations on two-phase flow must be qualified because of the manner in which fluid density was determined. Only pressure and temperature were measured at each side of the pump. The density was obtained from a temperature-entropy diagram for normal hydrogen (NACA, 1958) for instantaneous values of pressure and temperature. The response of both the temperature probe and pressure pickup, at each location, were assumed to be much faster than the system transient. Actually, the temperature probe has a relatively slow response which varies with temperature and flow rate. Furthermore, a single measurement of pressure and of temperature, at any given station, is not sufficient to determine the quality of two-phase fluid, nor the stream conditions - stratified, homogenous, or slugging. For future tests, attention should be given to the selection of instruments, and the number required at a given location, to obtain reliable and accurate measurements of two-phase flow of hydrogen.

C. COMPUTER-CONTROL SYSTEM OPERATION

The operation and performance of the analog computer in these tests proved the feasibility of computer application to development testing of an unfueled nuclear engine. Considering the degree of simulation achieved with the small computer, the most that can be said for the Generation-I Engine Simulator is that its behavior was similar to that of a nuclear engine. However, from the point of view of computer-control system development, the test program is considered highly successful because, in only three attempts, satisfactory operation of all four control loops was achieved. Of particular significance in this respect is the fact that each of the control loops was only closed with hydrogen in the system.

The operation of the turbine power control loop demonstrated that the turbopump can be accurately controlled. During the rise of simulated reactor power (Test No. 1.1-01-NXS-008), the pump flow rate was gradually decreased, with a corresponding decrease in pump load. Consequently, the turbopump tended to speed up, generating a higher discharge pressure and chamber pressure. However, when P_c exceeded $P_{c\ reference}$ by a small amount, the TPCV operated to reduce speed and discharge pressure. The small error in P_c existed during the period that the flow rate was being reduced. This error was on the order of 10 psi, or 2.5%, and is the best measurement than can be made on the Sanborn oscillographic record of computer outputs.

The method of controlling the load flow by comparing the computed to the measured flow rate worked very satisfactorily. This method has application to future simulated engine tests because it is considered to be the simplest and most direct way of matching pipeline impedance with simulated reactor core impedance to flow.

The Gas-Farm control loop operated satisfactorily, and indicated that fairly accurate control of temperature can be achieved. However, the Bleed-line control loop tended to "hunt," because the piston in the BLV actuator turned out to be single-ended rather than balanced. The servo-actuator in this loop should have had positional feedback to compensate for the unbalanced piston.

The development of a diverging instability near the end of Test Run -008 is attributed principally to the nonlinear characteristics of the system. The large change in heat-exchanger exit temperature removed the system from the operating range for which the linear system analysis was valid. At the point where the computer first took control, the operating conditions corresponded closely to those on which the linear analysis was based, and the system was stable.

A linear system analysis is not adequate for the design of a simulated engine system, particularly if the anticipated range of operation is broad, and if more than one control loop is involved. The design of future NERVA engine simulators should be based on an extensive nonlinear system analysis, which can be conducted with the aid of an analog-computer model of the complete system. A linear analysis should be conducted concurrently as a guide and as a check on the nonlinear computer analysis.

D. HEAT-CAPACITY HEAT-EXCHANGER

In the case of the heat-capacity heat-exchanger, the quantity and usefulness of the data obtained was somewhat disappointing. The manner in which the heat-exchanger had been instrumented did not permit rigorous analysis of two-phase heat transfer nor a correlation of heat-transfer coefficients in the boiling region. However, as pointed out in the data analysis, Section VI, C, fairly good correlation of heat-transfer coefficients based on Nusselt's equation was obtained. This correlation was very good where fluid conditions in the heat exchanger were gaseous, and rather poor for the boiling region.

A result of some importance that was obtained in the heat-capacity start tests was that, when boiling did occur in the heat exchanger, the pressure was above critical and temperature below critical, but pressure oscillations did not appear. This indicates that, in the real engine, two-phase flow instability will not be a problem in the reflector, provided that reflector exit pressure is above critical. The test results indicate that pressure oscillations may only appear whenever boiling of liquid hydrogen takes place at pressures below critical.

VIII. NOMENCLATURE

Note. See Figure I-C,2 Instrumentation Diagram, for subscripts not shown here

A_c, A_r	Cross-sectional area, reactor core or reflector flow passage
A_d	Cross-sectional area, pump discharge duct
A_n, A_t	Throat area, thrust nozzle or turbine nozzle
A_{sc}, A_{sr}	Heat transfer surface area, core, reflector
c_{cw}, c_{rw}	Specific heat, core wall, reflector wall
c_{pc}, c_{pr}	Specific heat at constant pressure, core, reflector
C_i	Concentration of ith group of delayed neutron precursors
D_c, D_r	Diameter of a flow passage, core, reflector
D_d	Diameter of pump discharge duct
f	Pipe friction factor
g	Gravitational constant
$G_c, G_{cb}, G_{cg}, G_{ct}$	Gain, error detecting amplifier, as defined in text
h_c, h_r	Convective heat transfer coefficient, core, reflector
k	Ratio of specific heats
K_1, K_2	Power generated per neutron per second, reflector, core
$K_a, K_{ab}, K_{ag}, K_{at}$	Servo-amplifier gain, as defined in text
K_{cr}	Controller gain constant, simulated reactor control loop

K_T	Negative temperature coefficient of reactivity
K_V	Velocity error coefficient as defined in text
ℓ^*	Mean neutron life time
L_c, L_r	Length of a flow passage, core, reflector
L_d	Length of pump discharge duct
M_t, M_p	Torque developed, turbine, pump
n	Total neutrons in the core
N	Turbopump speed
P	Pressure, absolute
P_c	Thrust chamber pressure
P_{fD}	Pump discharge pressure
P_{ri}, P_{ro}	Reflector inlet or outlet pressure
P_{ti}, P_{te}	Turbine inlet or exhaust pressure
R	Gas constant
S	Complex Laplace operator
t	Time
T	Temperature, absolute
T_c	Thrust chamber temperature
T_{cw}, T_{wr}	Wall temperature, core, reflector
T_{ri}, T_{ro}	Reflector inlet or outlet temperature
T_{ti}, T_{te}	Turbine inlet or exhaust temperature

T_g	Temperature of gas-farm supply
T_a	Heat-capacity heat exchanger wall temperature
V_c, V_p	Volume, thrust chamber, core inlet plenum
w_c	Weight flow rate, core
w_r	Weight flow rate, reflector
w_t	Weight flow rate, turbine
w_b	Weight flow rate, bleed line
w_g	Weight flow rate, gas farm supply
w_ℓ	Weight flow rate, load valve and bypass orifice
W_{cw}, W_{rw}	Total weight, core, reflector
β_i	Fraction of neutrons that are the ith group of delayed neutron precursors
λ_i	Decay constant, ith group of delayed neutron precursors
ρ_c	Propellant density, thrust chamber
ρ_{fD}	Propellant density, pump exit
ρ_{ri}, ρ_{ro}	Propellant Density, reflector inlet or outlet
ψ_t, ψ_n	Compressible flow factor, turbine nozzle, thrust nozzle
δk	Net reactivity, reactor core
δk_c	Reactivity contribution of control drums
τ	Time constant
τ_{cr}	Controller time constant, simulated reactor control loop

APPENDIX A

LINEARIZATION OF NEUTRON KINETICS EQUATIONS

The standard neutron kinetics equations,

$$\frac{dn}{dt} = \frac{\delta k\ n}{\ell^*} - \frac{\beta\ n}{\ell^*} + \sum_{i=1}^{6} \lambda_i C_i \tag{A-1}$$

$$\frac{dC_i}{dt} = \frac{\beta_i n}{\ell^*} - \left[\lambda_i C_i\ ,\right] \tag{A-2}$$

where

$i = 1, \ldots .6$

can be linearized by developing the expressions for the total differentials of n and C_i:

$$\frac{d}{dt}(\Delta n) = \frac{\delta k_o}{\ell^*}\Delta n + \frac{n_o}{\ell^*}\Delta(\delta k) - \frac{\beta}{\ell^*}\Delta n + \sum_{i=1}^{6} \lambda_i C_i \tag{A-3}$$

$$\frac{d}{dt}(\Delta C_i) = \frac{\beta_i}{\ell^*}\Delta n - \left[\lambda_i C_i\ ,\right] \tag{A-4}$$

where

$i = 1, \ldots .6$

The parameters δk_o and n_o are the steady-state values from which the incrementals vary; that is, the variables n and δk have been replaced by $(n_o + \Delta n)$ and $(\delta k_o + \Delta\delta k)$, where the new variables are the incrementals. To achieve a steady-state in a reactor, the effective multiplication factor must equal unity; hence, $\delta k = \delta k_o = 0$. By performing a Laplace transformation of both equations, the second can be solved for ΔC_i,

$$\Delta C_1 = \frac{\beta_1/\ell^*}{S + \lambda_1} \Delta n \tag{A-5}$$

which, upon substitution in Equation (A-1), yields

$$S\ \Delta n = \frac{n_o}{\ell^*} \Delta(\delta k) - \frac{1}{\ell^*} \left[\beta - \frac{\lambda_1\ \beta_1}{S + \lambda_1} - \ldots . \frac{\lambda_6\ \beta_6}{S + \lambda_6} \right] \Delta n \tag{A-6}$$

Since $\beta = \sum_{i=1}^{6} \beta_i$, the terms in brackets can be combined. The final form of the reactor transfer function, with six groups of delayed neutrons, is

$$\frac{\Delta n}{\Delta(\delta k)} = \frac{n_o}{\ell^*} \left[\frac{1}{S \left(1 + \frac{1}{\ell^*} \sum_{i=1}^{6} \frac{\beta_i}{S + \lambda_i} \right)} \right] \tag{A-7}$$

Using the values for the β_i and λ_i and ℓ^* given in Table II-B-3,1, and expanding the summation within the parentheses, there is obtained

$$\frac{\Delta n}{\Delta(\delta k)} = \frac{n_o}{\ell^*} \frac{1}{S} \left[\frac{(S+0.0128)(S+0.0315)(S+0.125)(S+0.325)(S+4.5)(S+1.55)}{(S^6+268.2\ S^5+1616\ S^4+2132.8\ S^3+568.4\ S^2+36.41\ S+0.2708)} \right] \tag{A-8}$$

And, after factoring the denominator,

$$\frac{\Delta n}{\Delta(\delta k)} = \frac{n_o}{\ell^*} \frac{1}{S} \left[\frac{(S+0.0128)(S+0.0315)(S+0.125)(S+0.325)(S+4.5)(S+1.55)}{(S+0.0818)(S+1.41)(S+4.4)(S+0.00854)(S+0.2386)(S+262)} \right] \tag{A-9}$$

or

$$\frac{\Delta n}{\Delta(\delta k)} = (4.21\text{x}10^{-4} \frac{n_o}{\ell^*} \frac{1}{S} \left[\frac{(78.2S+1)(31.8S+1)(8S+1)(3.08S+1)(0.222S+1)(0.645S+1)}{(12.23S+1)(0.71S+1)(0.227S+1)(117S+1)(4.19S+1)(0.00382S+1)} \right] \tag{A-10}$$

A good approximation to the last transfer function is

$$\frac{\Delta n}{\Delta(\delta k)} = (4.21 \times 10^{-4}) \frac{n_o}{\ell^*} \left[\frac{10\ S+1}{S\,(0.00382\ S+1)} \right] \qquad \text{(A-11)}$$

A comparison of the two transfer functions is shown in Figure App. A-1.

APPENDIX B

ANALYTICAL AND EXPERIMENTAL DETERMINATION OF CONTROLLER TRANSFER FUNCTIONS

I. INTRODUCTION

Each of the four flow-control valves in the Generation-I Engine Simulator system is positioned by an electrohydraulic servo-actuator which may be considered as a single element in each flow-control loop. In order to conduct both linear and non-linear analyses of system stability and performance, it is necessary to determine the non-linear equations and, from these, the transfer functions that describe the dynamic behavior of each servo-actuator. The non-linear equations are required to complete the non-linear analog-computer simulation of the system while the transfer functions, derived from the linearized versions of the non-linear equations, are needed for linear analyses of each control loop. Thus, the objective of this analysis is to derive the controller equations, and to verify their validity by comparing theoretically derived frequency response characteristics with experimentally determined characteristics.

II. DESCRIPTION OF ELECTROHYDRAULIC SERVO ACTUATORS

The operation of a typical electrohydraulic servo-valve and actuator is shown in Fig. App. B-1. The amplifier output produces a differential current in the torque-motor coils, resulting in a displacement of the servo-valve spool. Output flow from the valve, at a fixed valve pressure drop, is proportional to spool displacement. Depending upon the polarity of the input signal, the output flow is applied to the appropriate end of the actuator piston, to drive the load, i.e., the flow-control valve. When used as a positional control system, load position (that is, butterfly position) is measured by a potentiometer and fed back for comparison with the position command signal. Any error signal is amplified to provide a current input to the servo-valve torque motor. Without the position feedback, the servo-actuator will operate as a velocity controller.

The essential difference between any of the actuator systems lies in the linkage used to relate actuator-piston displacement to flow-control valve motion. The various linkages used in this program are shown in Fig. App. B-2. Both the Load and Gas-Farm valves are butterfly valves rotated by a crank-arm mechanism connecting the butterfly shaft to the actuator piston. A rack-and-pinion is used to convert actuator translation to rotation of the butterfly shaft in the TPCV. In the Bleed-Line valve, a rocker arm produces a 1:1 displacement of both actuator and valve pintle. It was necessary to retain the return spring mounted in the poppet cavity in the Bleed-Line valve, since the spring is essential for proper valve operation. However, the springs normally used in the Load, Gas-Farm, and TPC valve actuators were removed to increase their speed of response. Detailed design information on each actuator system, as furnished by Dept. 8140 of LRP, is listed in Tables App. B-1, 2, 3, and 4, and servo-actuator characteristics are given in Figure App. B-3 to 11.

A hydraulic power supply system, using hydraulic fluid per MIL-H-5606, provided a regulated pressure (P_s) of 800 psig at the supply ports of the servo-valves. This system was capable of supplying the maximum flow of 12 gpm for simultaneous operation of all four actuators.

III. ANALYTICAL DETERMINATION OF FREQUENCY RESPONSE CHARACTERISTICS

The analytical development of transfer functions considers each controller a positional servomechanism as in Figure App. B-1, since the experimental frequency responses were obtained for both closed and open loop operation.

A. DERIVATION OF EQUATIONS

Except for the actuator-to-valve linkage, the general equations are identical for each controller. By considering a load force acting on the actuator, the effects of load dynamics can be readily taken into account for different linkages.

The error voltage applied to the servo amplifier is the difference between a position command signal, V_i, and a voltage proportional to the output position, θ_o, of the flow-control valve.

$$E = V_i - K_f \theta_o \tag{B-1}$$

where

K_f = gain of the position feedback potentiometer, in volts per unit displacement

A differential current, i, is generated in the coils of the servovalve torque motor when a voltage equal to $K_a E$ is applied. Because of the coil inductance, the current lags the applied voltage. Thus,

$$\tau_m \frac{di}{dt} + i = K_a E \tag{B-2}$$

where

$\tau_m = \frac{L}{R}$ = torque motor time constant, sec

R = coil resistance, ohms

L = coil inductance, henrys

K_a = gain of servo amplifier and torque motor, milliamps/volt

The no-load flow characteristics of the servo valves are shown in Figures App. B-3 and -4. Under no-load conditions, the no-load flow, Q_o, through the servo valve is given by

$$Q_o = K_{sv} \sqrt{i} \tag{B-3}$$

where

K_{sv} = static gain of the servo valve.

However, since both servo valves had internal load pressure feedback, the net flow, Q, is also a function of the load pressure, as shown in Figures App. B-5 and -6, which illustrate the load flow characteristics. If P_s is supply pressure, and P_a the pressure drop across the actuator piston, then

$$Q = K_v \sqrt{i} \sqrt{P_s - P_a} \tag{B-4}$$

If the piston is stationary and a force, F, is applied to it, a differential pressure, P_a, will develop on the piston. To establish this differential pressure, the fluid is compressed an amount, ΔX. A hydraulic spring rate may be defined by

$$K_h \Delta X = A_p P_a \tag{B-5}$$

where

A_p = piston area (assume equal areas both sides) in.^{2}

K_h = hydraulic spring rate, lb/in.

The displacement, ΔX, can be expressed in terms of the bulk modulus, β, of the fluid, since $\Delta V = A_p \Delta X$,

$$\beta \triangleq \frac{V}{2} \frac{\Delta P}{\Delta V} \tag{B-6}$$

and

$$\Delta X = \frac{(V/2)P_a}{\beta A_p} \tag{B-7}$$

since $\Delta P = P_a$. Thus,

$$K_h = \frac{2\,\beta\,A_p^2}{V} = \frac{2\,A_p\,\beta}{L} \tag{B-8}$$

where one-half the total actuator volume or stroke, is used because the fluid on one side of the actuator is compressed.

Now, if the piston is moving against an external load, F_o, part of the fluid entering the actuator must replace that lost to compression (Ref. 6). From Equation (B-6) we have

$$\frac{dV}{dt} = Q_c = \frac{V}{2\beta}\frac{dP_a}{dt} \tag{B-9}$$

The total flow into the actuator is then the sum of the incompressible and compressible parts

$$Q = A_p\frac{dX_a}{dt} + \frac{A_p^{\,2}}{K_h}\frac{dP_a}{dt} \tag{B-10}$$

where

β has been replaced from Equation (B-8)

X_a = actuator displacement

The force applied to the piston, $A_p\,P_a$, is in equilibrium (by D'Alembert's Principle) with the sum of the inertia force, the dissipative force, and the external force on the actuator piston.

$$A_p P_a = M_a \frac{d^2X_a}{dt^2} + D_a \frac{dX_a}{dt} + K_a X_a + F_o \qquad \text{(B-11)}$$

where

An actuator spring is included for generality, and

M_a = piston mass

D_a = damping factor

K_a = spring rate

The external force F_o is exerted by the load, which in this case is a flow-control valve. For expediency, F_o will be derived for each valve in the section dealing with the development of individual transfer functions.

B. TRANSFER FUNCTIONS

All of the equations developed in the preceding section, except Equation (B-4), are linear. If small displacements of the servo-valve spool are considered, it is possible to linearize the flow equation. Thus,

$$\Delta Q = \left(\frac{\partial Q}{\partial i}\right)_{P_a = C} \Delta i + \left(\frac{\partial Q}{\partial P_a}\right)_{i=C} \Delta P_a \qquad \text{(B-12)}$$

The partial derivatives are the slopes of the curves in Figures App. B-3, -4, -5, and -6, taken at appropriate points. Since the serve valve operates about a null position, the incrementals in Equation (B-12) are really total variables. Then Equation (B-12) can be written as

$$Q = K_1 \, i - K_2 \, P_a \qquad \text{(B-13)}$$

The minus sign results from the fact that $\partial Q/\partial P_a$ is negative.

The open-loop transfer function for the servo valve and actuator may now be derived by combining the Laplace transformations of Equations (B-2), (B-10), (B-11), and (B-13). Thus,

$$\left(\frac{K_1 K_a}{\tau_m S+1}\right) E = \left[\frac{A_p M_a}{K_h} S^3 + \left(\frac{K_2 M_a}{A_p} + \frac{A_p D_a}{K_h}\right) S^2 + \left(\frac{K_2 D_a}{A_p} + A_p + \frac{A_p K_a}{K_h}\right) S + \frac{K_2 K_a}{A_p}\right] X_a + \left[\frac{A_p}{K_h} S + \frac{K_2}{A_p}\right] F_o \qquad \text{(B-14)}$$

In the following sections, F_o will be related to X_a in terms of actuator-valve linkages.

1. Load Valve

Linear displacement of the actuator results in rotation of the 5-in. butterfly valve by means of a slider-crank mechanism. A vector diagram can

be drawn relating the external force, F_o, applied by the piston, to a force, F_r, acting at the end of and perpendicularly to the butterfly crank arm. The torque applied to the butterfly shaft is $F_r r$, r being the crank-arm radius. Graphical resolution of the vector diagram for each actuator position yields the relation between F_o and T_o, the butterfly torque, shown in Figure App. B-7. The relation between actuator displacement and butterfly-blade angle, also determined graphically, is given in Figure App. B-8. Comparison of the two plots shows that the ratio F_o/T_o is nearly constant over a considerable portion of the angular blade displacement. Then, we may consider that, at least for small servo-valve displacements,

$$\frac{F_o}{T_o} = \text{constant} = C_o \tag{B-15}$$

Assuming viscous friction in the butterfly shaft bearings and considering that hydrodynamic torque on the butterfly, if it exists, is nearly linear with blade angle, the equation of motion of the butterfly is

$$\left[I_b S^2 + D_b S + K_b\right] \theta_o = T_o \tag{B-16}$$

From Figure App. B-8,

$$\theta_o = K_o X_a \tag{B-17}$$

Combining Equations (B-15), (B-16), and (B-17), we obtain

$$F_o = \left[I_b C_o K_o S^2 + D_b C_o K_o S + K_b C_o K_o\right] X_a \tag{B-18}$$

Note that the factor, $C_o K_o$, has the effect of converting the coefficients of Equation (B-16) to translational units. Replacing the F_o in Equation (B-14) by the F_o in Equation (B-18) yields

$$\frac{X_a}{E} = \frac{K_1 K_a}{(\tau_m S+1)\left[\frac{A_p M_e}{K_h} S^3 + \left(\frac{K_2 M_e}{A_p} + \frac{A_p D_e}{K_h}\right) S^2 + \left(\frac{K_2 D_e}{A_p} + A_p + \frac{A_p K_e}{K_h}\right) S + \frac{K_2 K_e}{A_p}\right]} \tag{B-19}$$

Some simplications were made here by letting

$$M_e = M_a + I_b C_o K_o \tag{B-20}$$

$$D_e = D_a + D_b C_o K_o \tag{B-21}$$

$$K_e = K_a + K_b C_o K_o \tag{B-22}$$

Equation (B-19) agrees with Equation (A-12 of Reference 7, obtained for a dynamic pressure feedback servo valve, if $K_e = 0$, A_p is divided out, and K_2/A_p^2 is equal to the constant K_b of Equation (A-12).

2. Gas-Farm Valve

The open-loop transfer function for the GFV is the same as Equation (B-19), since identical actuators were used on both valves. Only the butterfly moment-of-inertia and the damping factor are different.

3. Turbine Power Control Valve

In this case, actuator motion is transferred to the butterfly shaft by means of a rack and pinion. Hence, C_o in Equation (B-15) is just the reciprocal of the pinion pitch radius, r_p. By the same token, K_o in Equation (B-17) is equal to C_o. Then Equations (B-20), (B-21), and (B-22) become

$$M_e = M_a + I_b/r_p^{\,2} \tag{B-23}$$

$$D_e = D_a + D_b/r_p^{\,2} \tag{B-24}$$

$$K_e = K_a + K_b/r_p^{\,2} \tag{B-25}$$

The transfer function of Equation (B-19) also applies to this valve.

4. Bleed-Line Valve

The external force F_o is given by

$$\left[M_p\, S^2 + D_p\, S + K_p\right] X_o = F_o \tag{B-26}$$

where

$X_o = X_a$

Then the equivalent mass, damping factor, and spring rate become

$$M_e = M_a + M_p \tag{B-27}$$

$$D_e = D_a + D_p \tag{B-28}$$

$$K_e = K_a + K_p \tag{B-29}$$

where

subscript p refers to the poppet.

The moment of inertia of the rocket arm has been neglected. In this case, K_e is not zero, but is equal to K_p.

C. THEORETICAL FREQUENCY RESPONSES

1. Load Valve Servo

No flow existed in the flow-control valves during experimental frequency response tests; therefore, K_e in Equation (B-19) is zero. Then the transfer function becomes

$$\frac{X_a}{E} = \frac{\dfrac{K_a K_1 A_p}{K_2 D_e + A_p^2}}{S(\tau_m S+1)\left(\dfrac{S^2}{\omega_n^2} + \dfrac{2\zeta}{\omega_n} S + 1\right)} \qquad \text{(B-30)}$$

where

$$\omega_n = \sqrt{\frac{K_h}{M_e}\left(1 + \frac{K_2 D_e}{A_p^2}\right)}\ , \quad \text{rad/sec} \qquad \text{(B-31)}$$

and

$$\zeta = \frac{K_2 K_h M_e + A_p^2 D_e}{2\sqrt{M_e K_h \left(K_2 D_e + A_p^2\right)}} \qquad \text{(B-32)}$$

To evaluate ω_n and ζ, a value for the equivalent damping factor, D_e, must be estimated. Generally speaking, hydraulic servos have very low damping ratios, so a value of D_e was chosen to make the damping ratio 0.10. The slope, K_2, of the load-flow characteristic is obtained from Figure App. B-6, assuming small input currents. The hydraulic spring rate, K_h, is the slope of the upper portion of the curve in Figure App. B-9, the experimentally measured bulk spring rate.

The torque motor time constant, τ_m, was difficult to determine exactly. However, these time constants generally lie between 2 and 7 milliseconds. A value for τ_m of 4 ms was chosen for a first approximation. The parameter values are:

$$K_h = 266{,}000, \text{ (lb/in.)}$$

$$M_e = 4.62 \times 10^{-2}, \text{ (lb sec}^2\text{/in.)}$$

$$K_2 = 5.9 \times 10^{-3}, \text{ (in.}^5\text{/lb sec)}$$

$$D_e = 1.47, \text{ (lb sec/in.)}$$

$$A_p = 10.3, \text{ (in.}^2\text{)}$$

$$C_o = .75$$

Then

$$\omega_n = 2400 \text{ rad/sec}$$
$$\zeta = 0.1$$

It should be noted that the natural frequency is unaffected by the very small damping factor, since K_h is so large. Now the non-dimensionalized open-loop transfer function can be written.

$$G(S) = \frac{1}{S\,(0.004\,S + 1)\left[\dfrac{S^2}{(2400)^2} + \dfrac{2\,(0.1)}{2400}\,S + 1\right]} \qquad \text{(B-33)}$$

2. Gas-Farm Valve Servo

The only difference between this valve and the Load valve is that the moment-of-inertia of the butterfly blade and shaft is much smaller in the GFV. Thus, for a damping ratio of 0.1, the natural frequency of the GFV actuator and load is 4610 rad/sec. Then the non-dimensionalized open-loop transfer function for the GFV servo is

$$G_1(S) = \frac{1}{S\,(0.004\,S + 1)\left[\frac{S^2}{(4610)^2} + \frac{2\,(0.1)}{(4610)}\,S + 1\right]} \qquad \text{(B-34)}$$

3. Turbine Power Control Valve Servo

For this valve also, $K_e = 0$, D_e is chosen to yield a damping ratio of 0.1, and τ_m is again assumed to be 0.004 seconds. The hydraulic spring rate is determined to be 99,000 lb/in. from Figure App. B-10, and the remaining parameters from Table App. B-3.

The natural frequency is 4100 rad/sec and the open-loop transfer function is, in non-dimensional form,

$$G_2(S) = \frac{1}{S\,(0.004\,S + 1)\left[\frac{S^2}{(4100)^2} + \frac{2\,(0.1)}{(4100)}\,S + 1\right]} \qquad \text{(B-35)}$$

4. Bleed-Line Valve Servo

No spring was contained in the actuator cavity, but it was necessary to retain the spring acting on the poppets for proper valve operation; therefore, $K_e = K_p = 320$ lb/in., by Equation (B-29). The actuator spring rate is determined, from Figure App. B-11, to be 119,000 lb/in. The damping coefficient, D_e, for assumed $\zeta = 0.1$, was determined to be 0.75 lb sec/in. The remaining parameters are:

$$\tau_m = 0.004, \text{ (sec)}$$

$$A_p = 2.95, \text{ (in.}^2\text{)}$$

$$M_e = 1.129 \times 10^{-3}, \text{ (lb sec}^2\text{/in.)}$$

$$K_2 = 2.4 \times 10^{-3}, \text{ (in.}^5\text{/lb sec)}$$

A comparison of the open and closed-loop transfer functions based on Equation (B-19), with K_e = 320 lb/in., and with K_e = 0, shows that the return spring on the poppet has negligible effect. Hence, the transfer function for the Bleed-Line valve is

$$G_3(S) = \frac{1}{S\,(0.004\,S + 1)\left[\dfrac{S^2}{(10{,}280)^2} + \dfrac{2\,(0.1)}{10{,}280}\,S + 1\right]} \qquad \text{(B-36)}$$

IV. COMPARISON OF THEORETICAL AND CLOSED-LOOP FREQUENCY RESPONSES

Both closed-loop and open-loop experimental frequency responses were obtained for each of the servo-actuator systems. In the open-loop tests, the input was the current in the servo-valve coils, connected in series; and the output, in one set of tests, was the velocity of the poppet (BLV), or the angular velocity of the butterfly blade (TPCV, LV). The output velocity of the poppet in the Bleed-Line valve was obtained with a linear velocity transducer attached directly to the poppet. An angular velocity transducer was specially built to measure the output blade velocity of the Load and Turbine-Power Control valves. Another set of open-loop frequency responses was obtained, but, in these, output position was recorded rather than velocity. In all the open-loop tests, the input signal was biased continuously to prevent the actuator piston from drifting off-center; the degree of biasing was made proportional to piston drift by a potentiometer bridge circuit with the arm of one potentiometer attached to the piston rod. Open-loop responses were obtained only with the Bleed-Line, Turbine-Power Control, and Load valve actuators, and it was assumed that the data obtained for the Load valve was applicable to the Gas-Farm valve.

The closed-loop frequency responses were obtained with the servo actuators set up as positional servomechanisms, as shown in Figure App. B-12. The servo valve and actuator are represented by a simplified transfer function which can be obtained from Equation (B-30) by dropping the second-order term in the denominator, and noting that K_2D_e, in the numerator, is negligible by comparison with A_p^2. The values of K_a and K_f used in the closed-loop tests were derived from Dept. 8130, LRP. The value of K_1 is the slope on the static flow characteristic taken at a differential current of 4 ma. Closed-loop frequency responses were obtained only on the Bleed-Line, Turbine-Power-Control, and Gas-Farm valve actuators. The closed-loop frequency response of the Load-Valve actuator was assumed to be the same as that of the Gas-Farm valve actuator, since the actuators, servo valves, and control circuitry were the same in both cases.

A. LOAD-VALVE AND GAS-FARM VALVE SERVO ACTUATOR

The LV and GFV actuators are considered simultaneously because open-loop responses were obtained only for the LV actuator, while closed-loop responses were obtained only for the GFV actuator. The open-loop experimental responses of the Load valve are shown in Figures App. B-13 and -14. It is evident that there is no correlation between the experimental response and the theoretical response, as given by Equation (B-33). Since the theoretical open-loop response for the Gas-Farm valve actuator, Equation (B-34), is nearly identical to that of the Load-Valve actuator up to about 1000 rad/sec, it is clear that no correlation exists between the open-loop responses of the GFV actuator.

In order to determine a reasonable closed-loop response, the data in Figure App. B-13 were fitted with the following transfer function:

$$G(S) = \frac{1}{S\,(0.0455\,S + 1)} \tag{B-37}$$

This transfer function was assumed to apply to the Gas-Farm valve servo-actuator as well. The open loop response data for blade position output were chosen for Fitting (B-37) as that data was considered more reliable than was the velocity output data.

Figure App. B-12 indicates a closed-loop response:

$$\frac{\theta_o}{V_1} = \frac{1/K_f}{\dfrac{S^2}{\omega_r^2} + \dfrac{2\zeta}{\omega_r} S + 1} \tag{B-38}$$

where

$$\omega_r = \sqrt{\frac{K_a K_1 K_o\,(57.3)\,K_f}{A_p\,\tau_h}}$$

$$\zeta = \frac{\sqrt{A_p}}{2\sqrt{\tau_h K_a K_1 K_o K_f (57.3)}}$$

Equation (B-38) applies to both the Load and Gas-Farm valve servo-actuators. Using the gain constants of Figure App. B-12, and with τ_h equivalent to 0.0455 sec., the closed-loop response becomes

$$\frac{\theta_o}{V_1} = \frac{32}{\frac{S^2}{(12.4)^2} + \frac{2\,(0.885)}{12.4}\,S + 1} \qquad \text{(B-39)}$$

The closed-loop response is plotted in Figure App. B-15, where it is compared to the experimental closed-loop response obtained with the Gas-Farm valve and actuator. Even if a value for τ_h of 0.004 sec is used instead of 0.0455 sec, the resulting closed-loop response would be virtually identical to the theoretical response shown in Figure App. B-15.

Since the LV and GFV actuators were to be used as velocity controllers in the simulated engine, the extrapolated transfer function, Equation (B-37), was used for the dynamic analysis of both the Load valve and Gas-Farm valve control loops in the Engine Simulator.

B. TURBINE-POWER-CONTROL VALVE SERVO

The theoretical open-loop frequency response is compared to experimental data in Figure App. B-16, where output (blade) position was recorded. The scattering of the data for the smaller input is due to the difficulty of measuring, on the oscillograph, amplitude, and phase of the output signal. The trend of the data indicates the existence of a quadratic factor with a break-point at about 600 rather than 4100 rad/sec. The open-loop data obtained with output (blade) angular velocity showed the existence of two quadratic factors in the same frequency range. However, it was believed that one of these factors was contributed by the network used for measuring angular velocity, so that data was discarded. In any case, the quadratic factors can be neglected so far as the closed loop response is concerned.

Experimental and corresponding theoretical closed-loop frequency responses are shown in Figure App. B-17. The theoretical closed-loop response is characterized by two first-order lags, one at 27.3, and the other at 224 rad/sec. The theoretical response plotted in Figure App. B-17 was determined for a K_1 of 1.95 in.^{3}/sec, corresponding to a small-amplitude input. Since the correlation was good to at least 32 cps, which was well beyond the bandwidth expected in the Turbine-power control loop, the simplified transfer function with a τ_h of 0.004 sec was used in the analysis of the Engine Simulator.

C. BLEED-LINE VALVE SERVO

The experimental points, for input currents of 4 and 10 ma, peak-to-peak, are superposed, in Figure App. B-18, on the open-loop response of Equation (B-36). There appears to be a quadratic factor present in the range of 70-80 cps. However, the gain and phase were difficult to determine from the oscillographs, for frequencies greater than 100 rad/sec, because of the large attenuation of the output, as well as the effects of backlash in the valve mechanism.

The closed-loop frequency response, based on Equation (B-36), and using the values for K_a and K_f (amplifier and feedback gains, respectively), as given in Figure App. B-19, is

$$\frac{X_o}{V_1} = \frac{0.1431}{\left[\frac{S^2}{(167.5)^2} + \frac{2(0.738)}{167.5} S + 1\right]\left[\frac{S^2}{(10,280)^2} + \frac{2(0.523)}{10,280} S + 1\right]} \qquad \text{(B-40)}$$

The experimental closed-loop response is also given in Figure App. B-19, where it is seen that the correlation is very good to 150 rad/sec. If the closed-loop response is obtained from the simplified transfer function, with $\tau_h = 0.004$ sec, then

$$\frac{X_o}{V_1} = \frac{0.1431}{\frac{S^2}{(192)^2} + \frac{2\ (.65)}{192} S + 1} \qquad \text{(B-41)}$$

and it is clear that, for all practical purposes, the simple open-loop transfer function, characterized by an integration with first-order lag, is adequate for synthesizing the Bleed-Line control loop in the Engine Simulator.

TABLE APP. B-1

REACTOR-LOAD SIMULATOR VALVE AND SERVO ACTUATOR

A. FLOW-CONTROL VALVE

Nomenclature	Modified 5 in. TCOV, P/N 1-230650
Type	Butterfly
Total Valve Travel	$90^{\circ} \pm 1\text{-}1/2^{\circ}$
Flow Area Vs Blade Position	See Figure III-D,2
Blade Position Vs Actuator Displacement	See Figure App . B-8
Force·Torque Ratio Vs Actuator Displacement	See Figure App. B-7
Crank Arm Length	1.5 in.
Connecting Rod Length	2.44 in.
Moment of Inertia, Blade, Shaft, and Arm	63.7×10^{-3} in.-lb-sec^2

B. ACTUATOR

Nomenclature	TCV Actuator (springs removed), P/N 1-218330-10
Piston Area	10.3 in.^{2} (opening) 10.0 in.^{2}(closing
Stroke	2.12 in.
Piston and Rod Weight	4.0 lb
Equivalent Hydraulic Spring Rate	See Fig. App. B-9

C. SERVO VALVE

Nomenclature	Moog, Servocontrols, Inc., Model M4369 (or 16-100B)
Type	Flow control with dynamic pressure feedback
Static Flow Gain	See Figure App. B-4
Load-Flow Characteristics	See Figure App. B-6
Supply Pressure	800 psig
Coil Resistance	200 Ω each coil
Rated Current	12.5 milliamperes

TABLE APP. B-2

GAS FARM VALVE AND SERVO ACTUATOR

A. FLOW-CONTROL VALVE

Nomenclature	Modified 3 in. TCFV, P/N 1-224470
Type	Butterfly
Total valve travel	$90^{\circ} \pm 1\text{-}1/2^{\circ}$
Flow Area vs Blade Position	See Figure III-D,8
Blade Position vs Actuator Displacement	See Figure App. B-8
Force·Torque Ratio vs Actuator Displacement	See Figure App. B-7
Crank Arm Length	1.5 in.
Connecting Rod Length	2.44 in.
Moment of Inertia, Blade, Shaft, and Arm	3.7×10^{-3} in.-lb-sec^2

B. ACTUATOR

Nomenclature	TCV Actuator (springs removed) P/N 1-218330-10
Piston Area	10.3 in.^{2} 10.0 in.^{2} (closing)
Stroke	2.12 in.
Piston and Rod Weight	4.0 lb
Equivalent Hydraulic Spring Rate	See Figure App. B-9

C. SERVO VALVE

Nomenclature	Moog Servocontrols, Inc., Model M4369 (or 16-100B)
Type	Flow control with dynamic pressure feedback
Static Flow Gain	See Figure App. B-4
Load-Flow Characteristics	See Figure App. B-6
Supply Pressure	800 psig
Coil Resistance	200 Ω each coil
Rated Current	12.5 milliamperes

TABLE APP. B-3

TURBINE POWER CONTROL VALVE AND SERVO ACTUATOR

A. FLOW CONTROL VALVE

Nomenclature	AGC Dwg. 251808-9
Type	Butterfly
Total Valve Travel	90°
Flow Area vs Blade Position	See Figure III-D,11
Blade Position vs Actuator Displacement	See Figure App. B-2
Pinion Pitch Diameter	1.75 in.
Moment-of-Inertia, Blade, Shaft, and Pinion	2.111×10^{-3} lb-in.-sec^2
Equivalent Mass of Blade, Shaft, and Pinion referred to Actuator	2.76×10^{-3} lb-sec^2/in.
Valve Shaft Resistance Torque	50 in.-lb (no flow)

B. ACTUATOR

Nomenclature	HGV Actuator, Dwg. 1-239790
Piston Area	4.0 in.^{2} (open and close)
Stroke	1.90 in.^{2}
Piston Weight	1.14 lb
O-Ring Friction	65 psig at 1000 psig actuator pressure
Equivalent Hydraulic Spring Rate	See Figure App. B-10

C. SERVO VALVE

Nomenclature	Moog Servocontrols Inc., Model 2106A
Type	Flow Control
Static Flow Gain	See Figure App. B-3
Load-Flow Characteristics	See Figure App. B-5
Supply Pressure	800 psig
Coil Resistance	200 Ω each coil
Rated Current	12.5 milliamperes

TABLE APP. B-4

BLEED LINE VALVE AND SERVO ACTUATOR

A. FLOW CONTROL VALVE

Nomenclature	Double Booster, GGV, P/N 1-223330
Type	Poppet
Total Valve Travel	0.6 in.
Return Spring Rate	320 lb/in. (both ports)
Effective Flow Area vs Valve Displacement (both ports)	See Figure III-D,5
Spring Load - Valve Closed	264 lb
Weight of Pintle Assembly (both pintles)	0.47 lb
Moment of Inertia, Rocker Arm	7.543×10^{-4} in.-lb-sec^2
Rocker Arm Radius (each side)	1.25 in.

B. ACTUATOR

Nomenclature	See Same Dwg. as Flow Control Valve
Piston Area	2.95 in.^{2} (open and close)
Stroke	Limited to 0.6 in.
Piston Weight	0.203 lb
Equivalent Hydraulic Spring Rate	See Figure App. B-11

C. SERVO VALVE

Nomenclature	Moog Servocontrols, Inc., Model 2106A
Type	Flow Control
Static Flow Gain	See Figure App. B-3
Load-Flow Characteristic	See Figure App. B-5
Supply Pressure	800 psig
Coil Resistance	200 Ω each coil
Rated Current	12.5 milliamperes

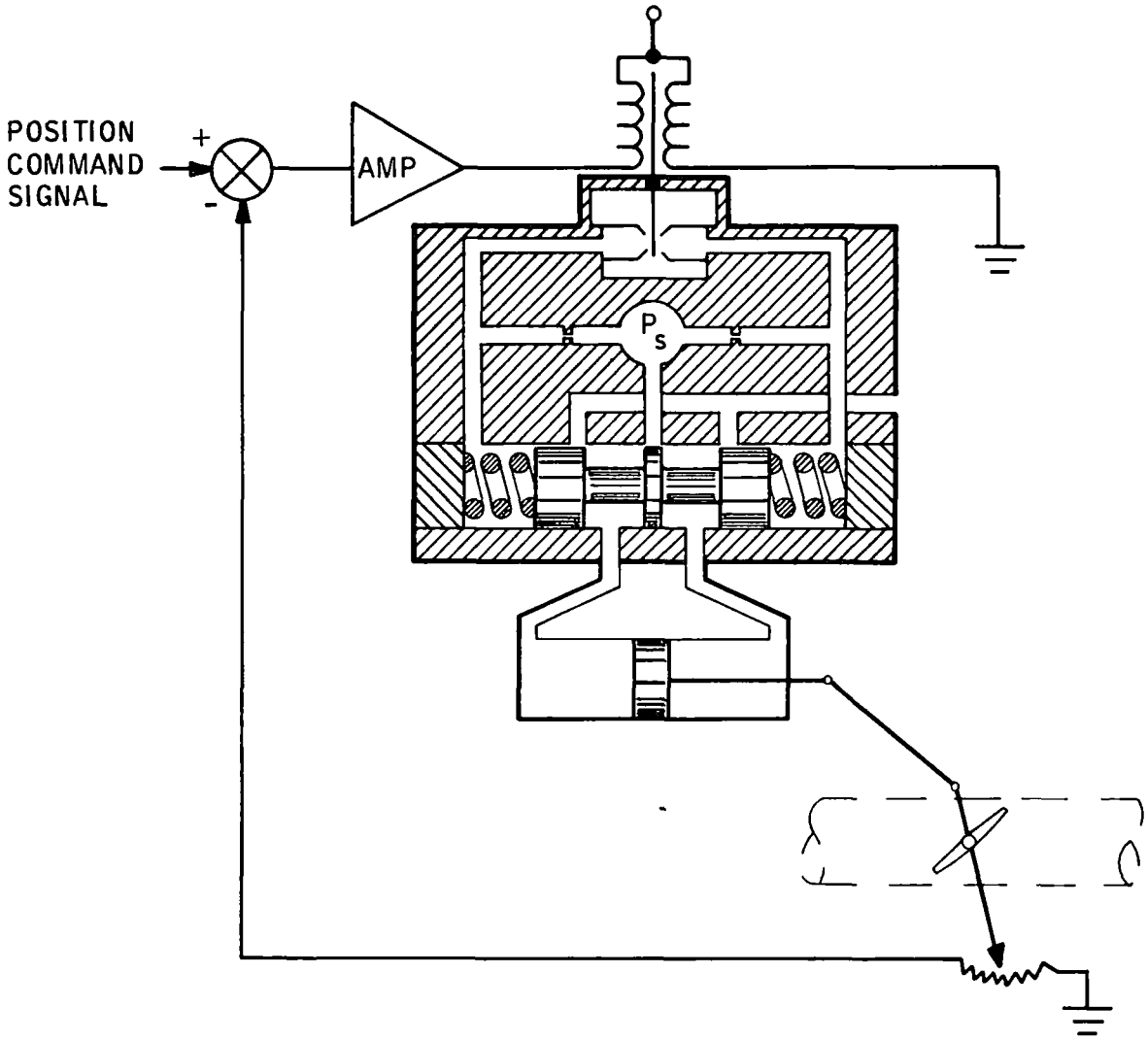

SCHEMATIC OF ELECTROHYDRAULIC POSITIONING SERVO

Fig. App. B-1

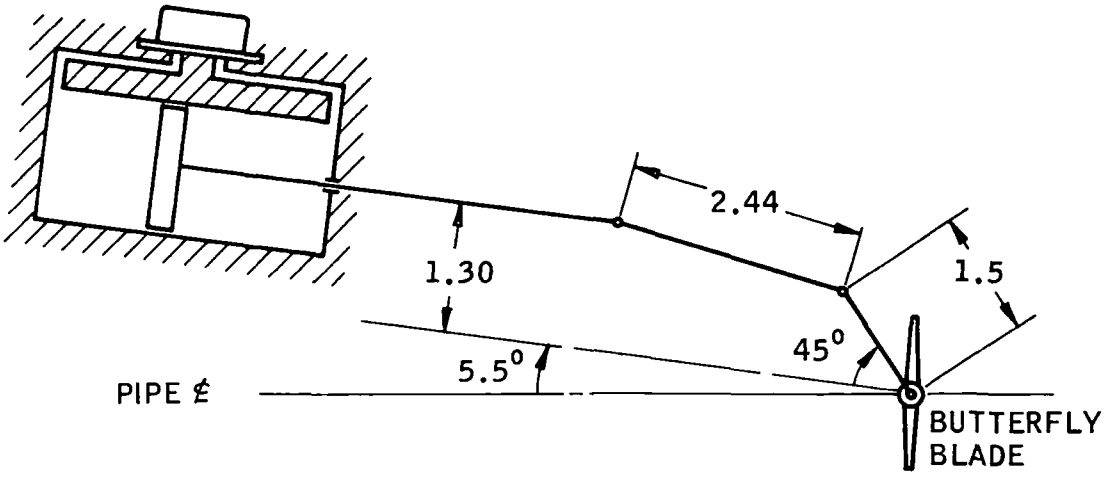

REACTOR-LOAD SIMULATOR VALVE AND
GAS-FARM VALVE

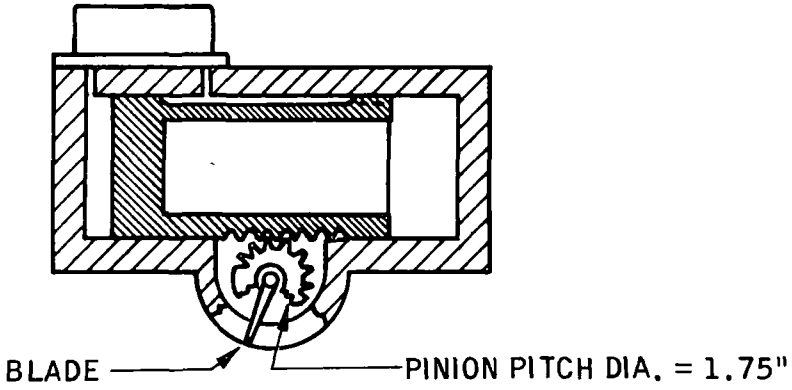

TURBINE POWER CONTROL VALVE

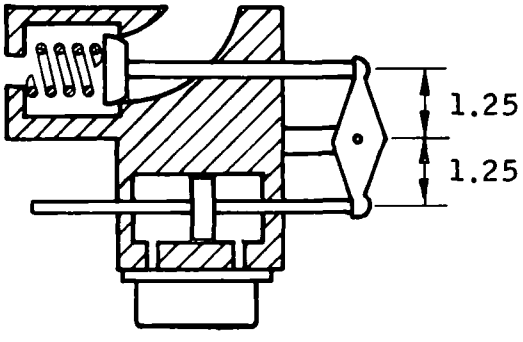

BLEED LINE VALVE

MECHANISM FOR CONNECTING ACTUATOR
DISPLACEMENT TO VALVE MOTION

Fig. App. B-2

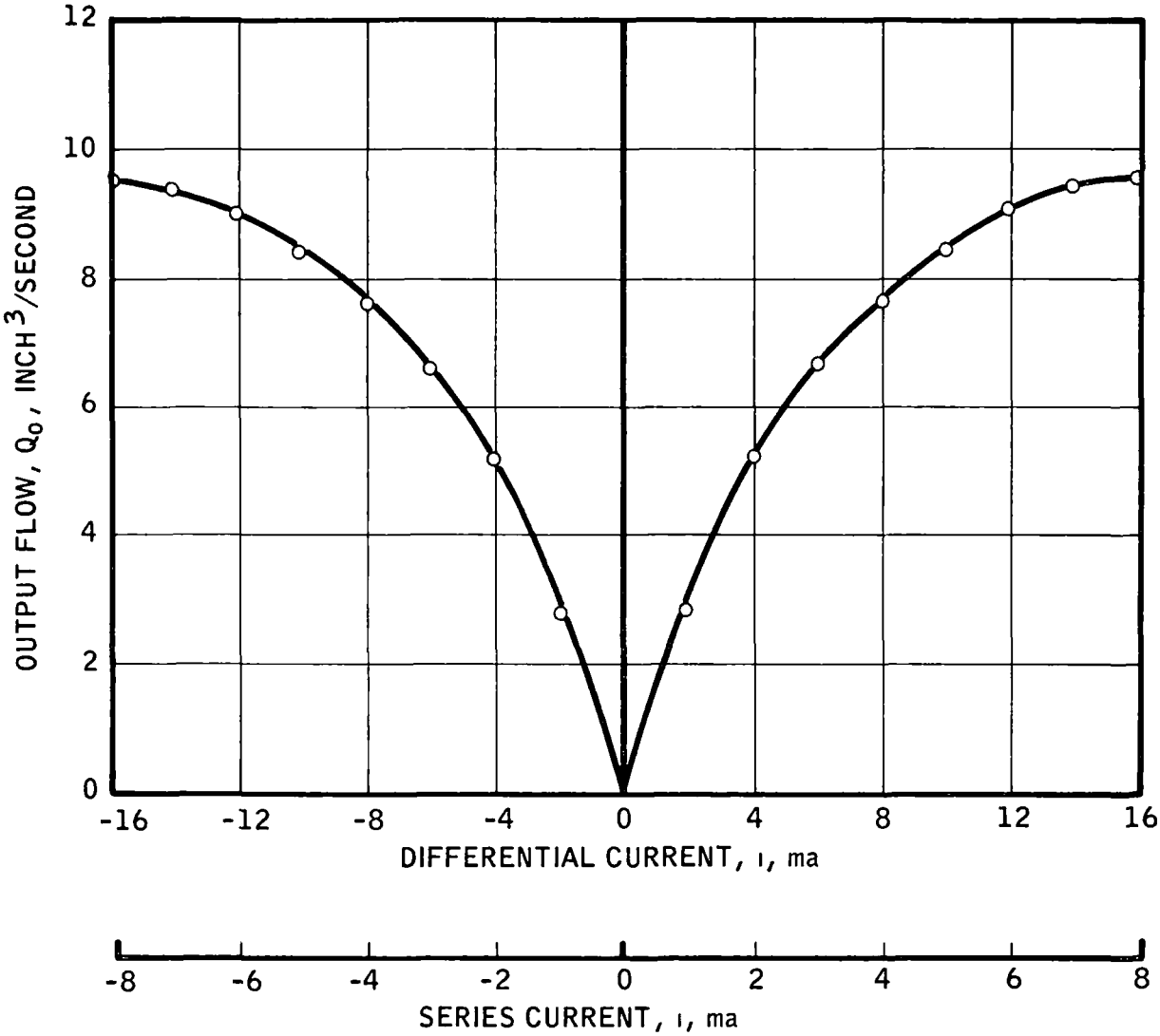

GAIN PLOT MOOG SERVOVALVE MODEL 2106 A

SUPPLY PRESS-800 PSIG NO LOAD FLOW

Fig. App. B-3

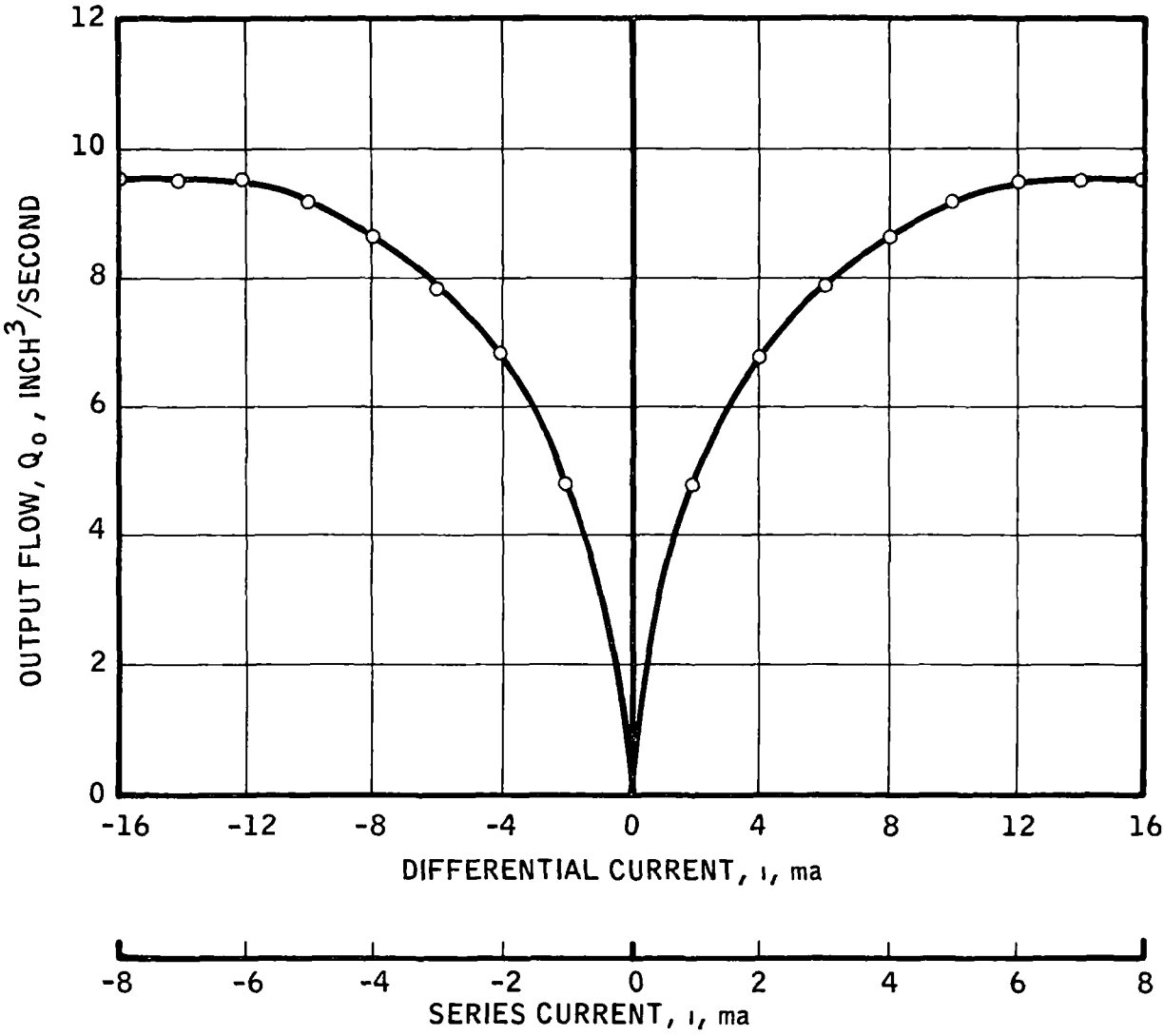

GAIN PLOT MOOG SERVOVALVE MODEL M4369

SUPPLY PRESS-800 PSIG, NO LOAD FLOW

Fig. App. B-4

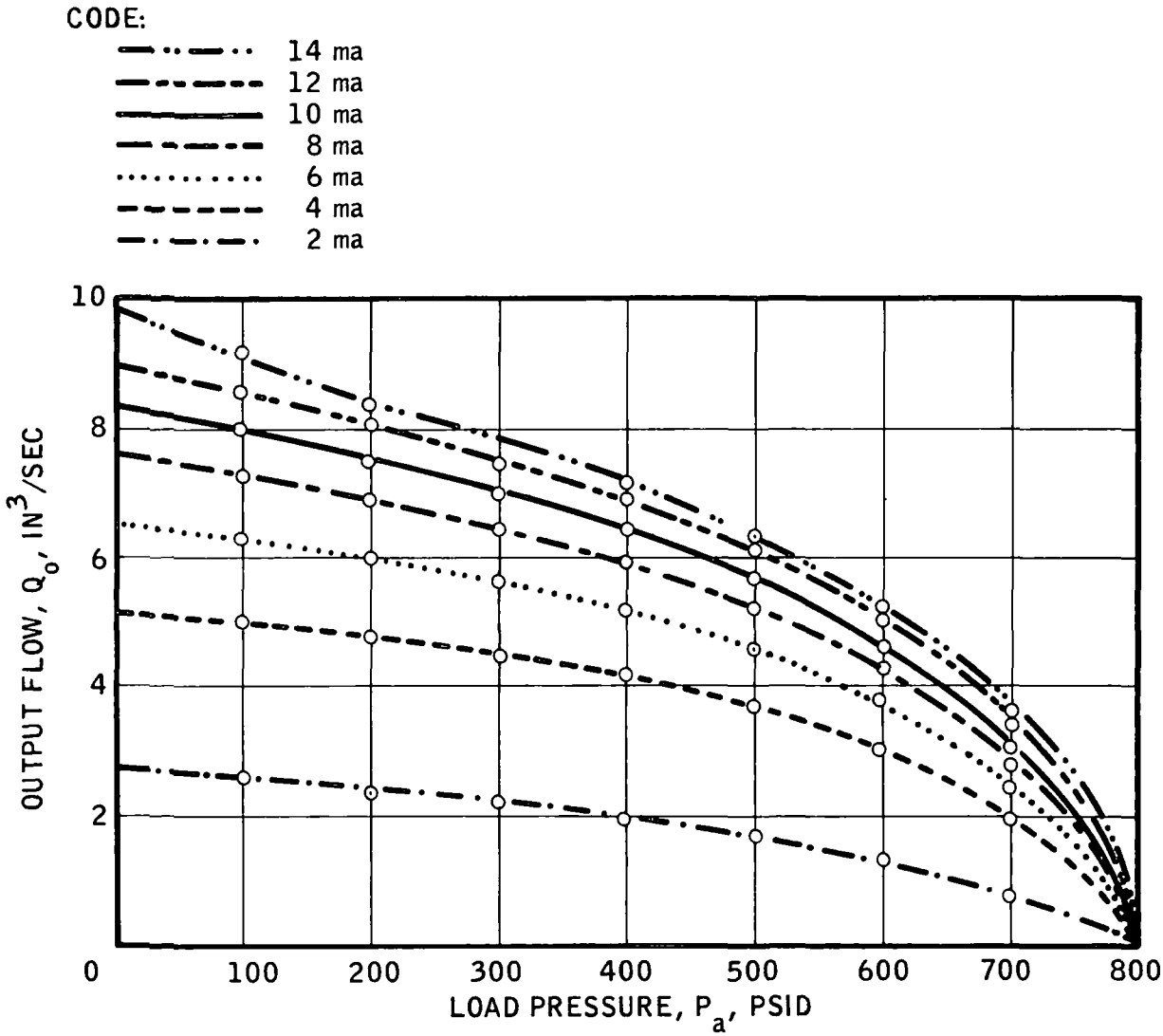

LOAD FLOW CHARACTERISTICS
MOOG SERVOVALVE MODEL 2106A
SUPPLY PRESS -800 PSIG

Fig. App. B-5

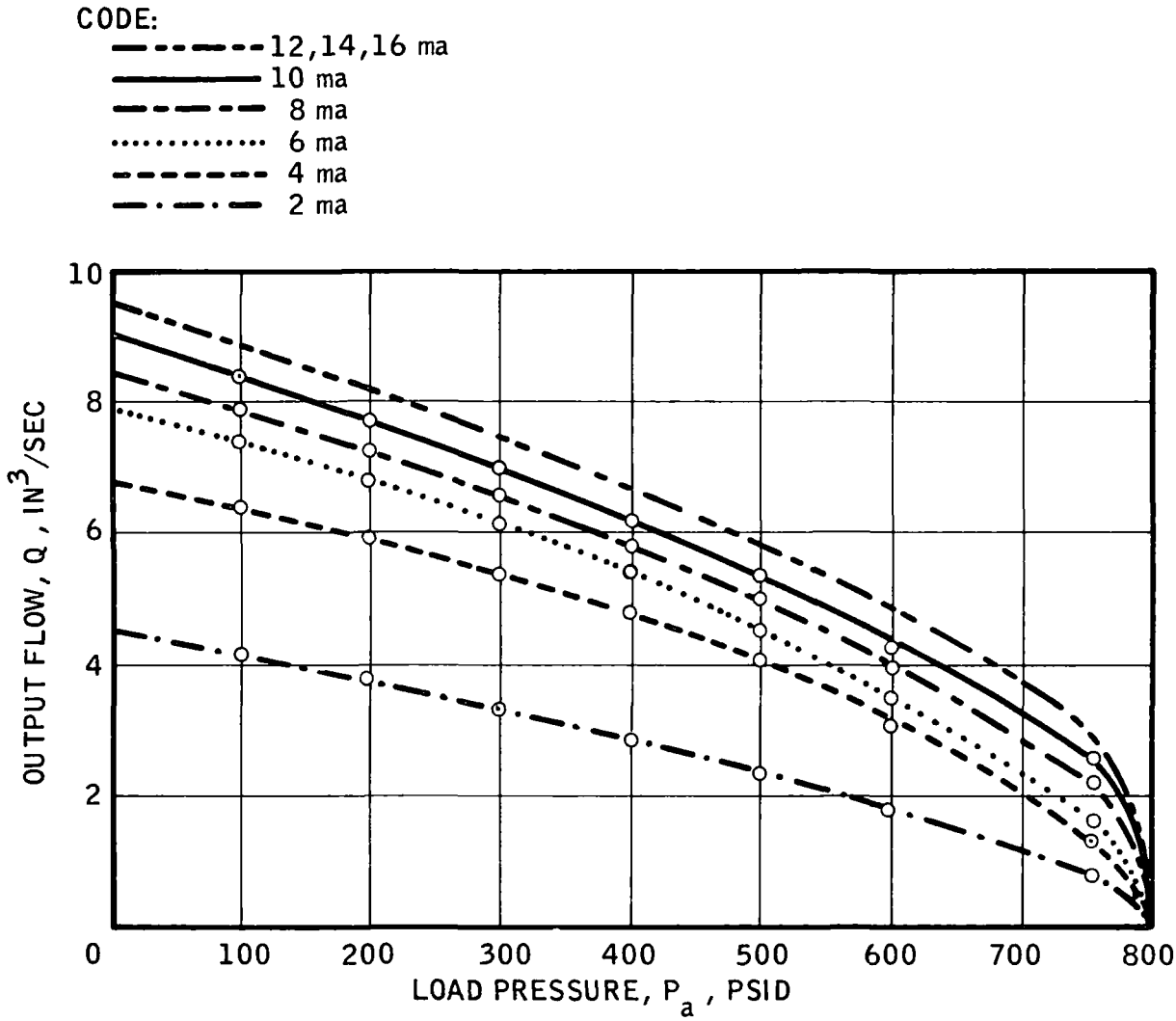

LOAD FLOW CHARACTERISTICS
MOOG SERVOVALVE MODEL M4369
SUPPLY PRESS -800 PSIG

Fig. App. B-6

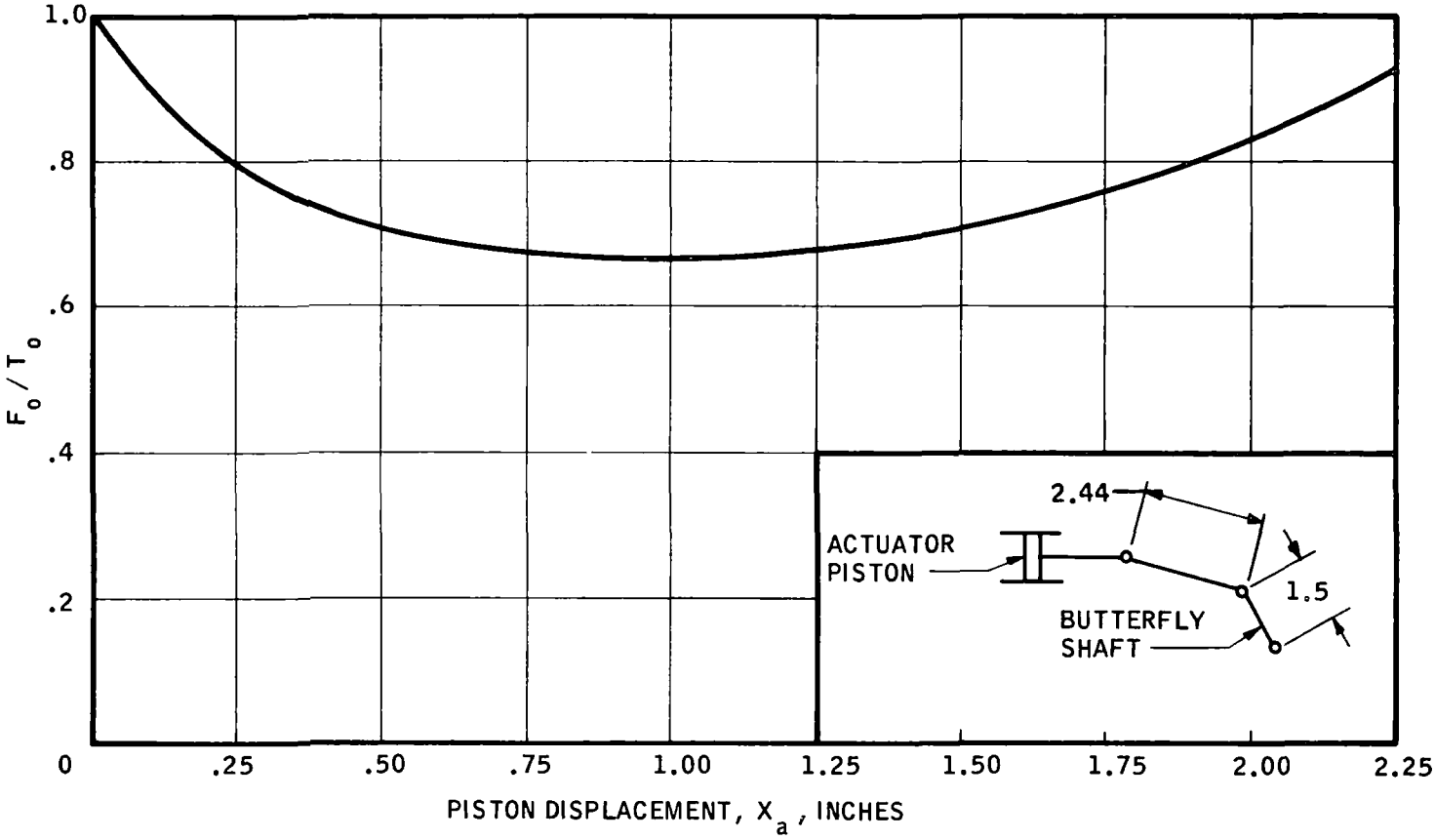

LOAD AND GAS-FARM VALVES TORQUE RATIO

Fig. App. B-7

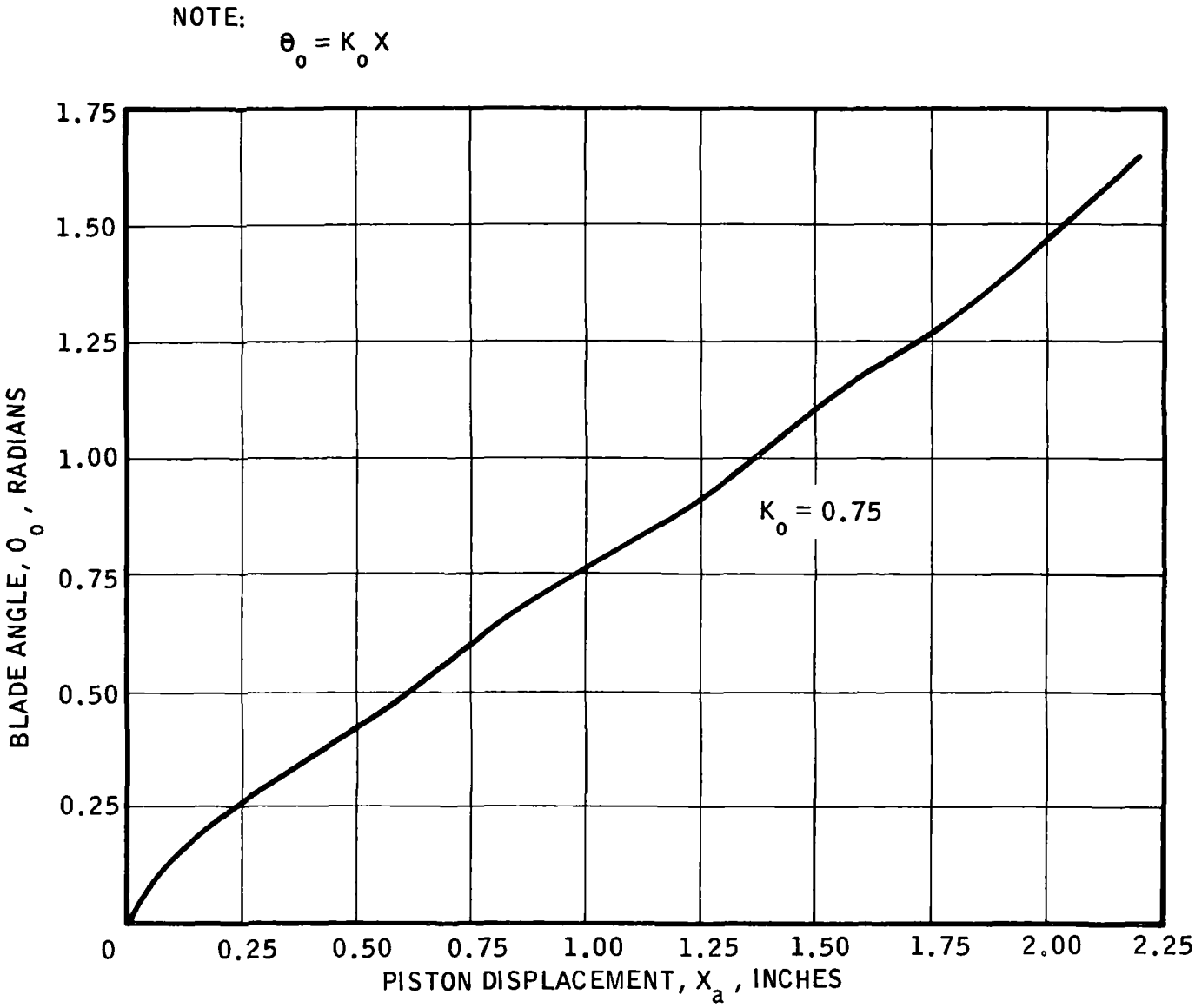

BLADE POSITION AS A FUNCTION OF ACTUATOR DISPLACEMENT FOR LOAD VALVE AND GAS FARM VALVES

Fig. App. B-8

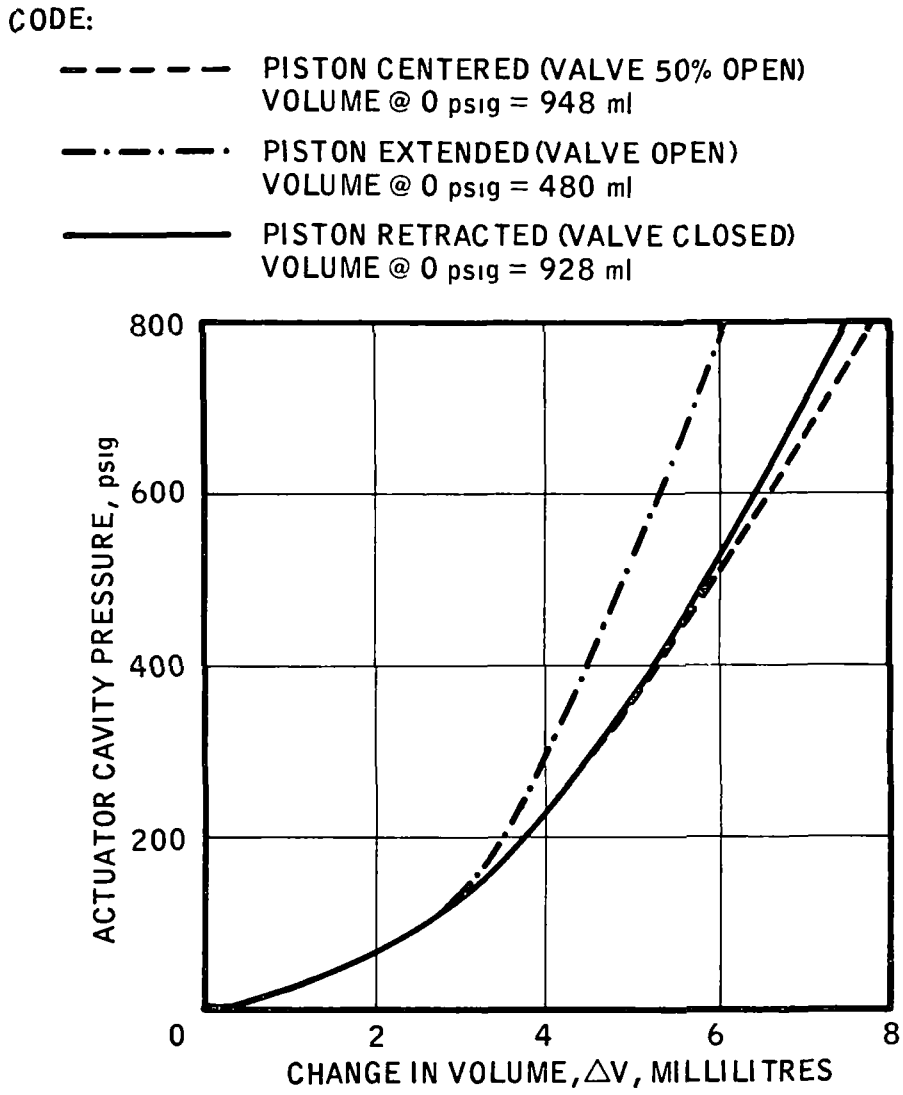

BULK SPRING RATE
GFV, RLSV AND ALT. TPCV
ACTUATORS

Fig. App. B-9

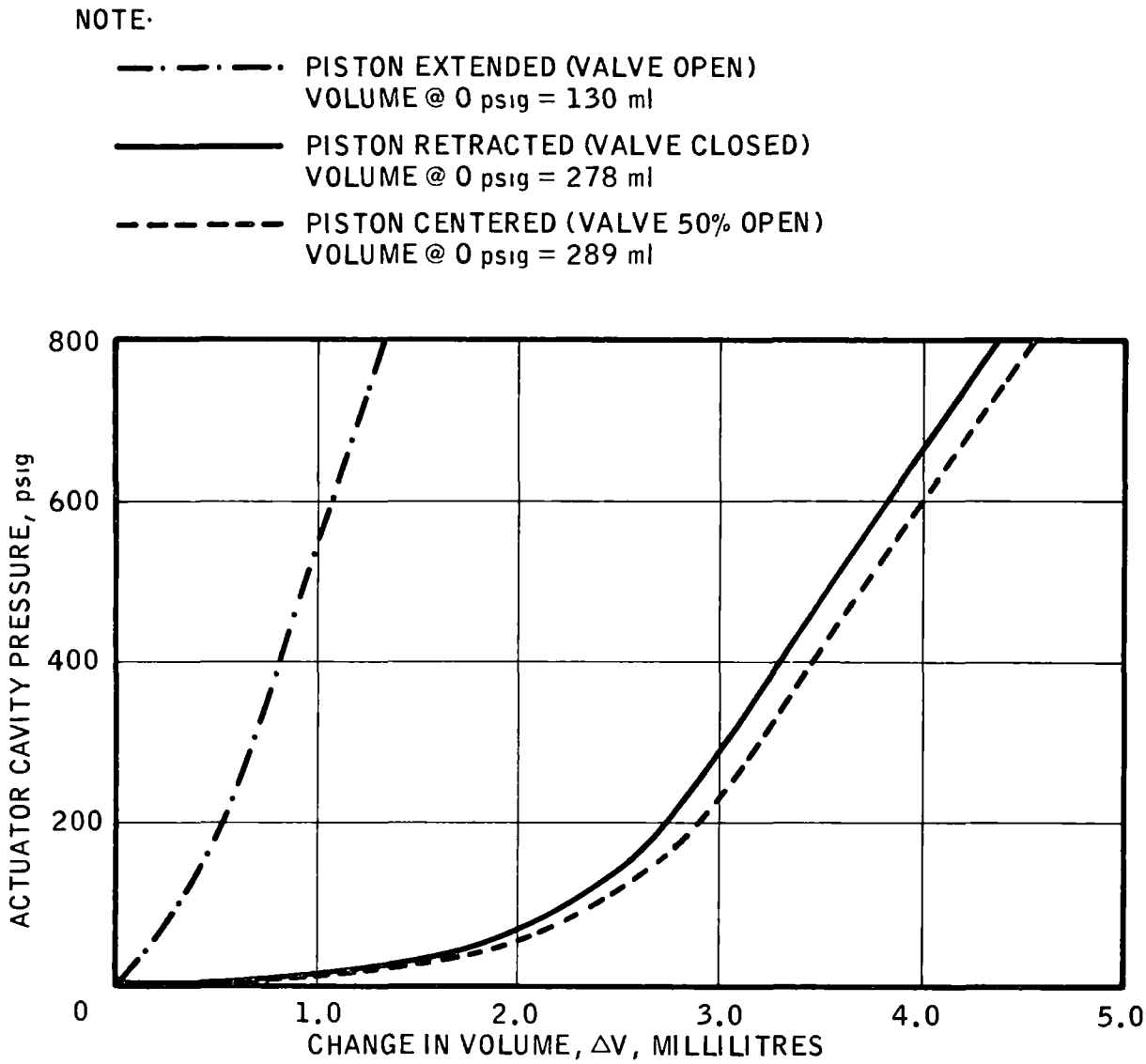

BULK SPRING RATE PROTOTYPE TPCV

Fig. App. B-10

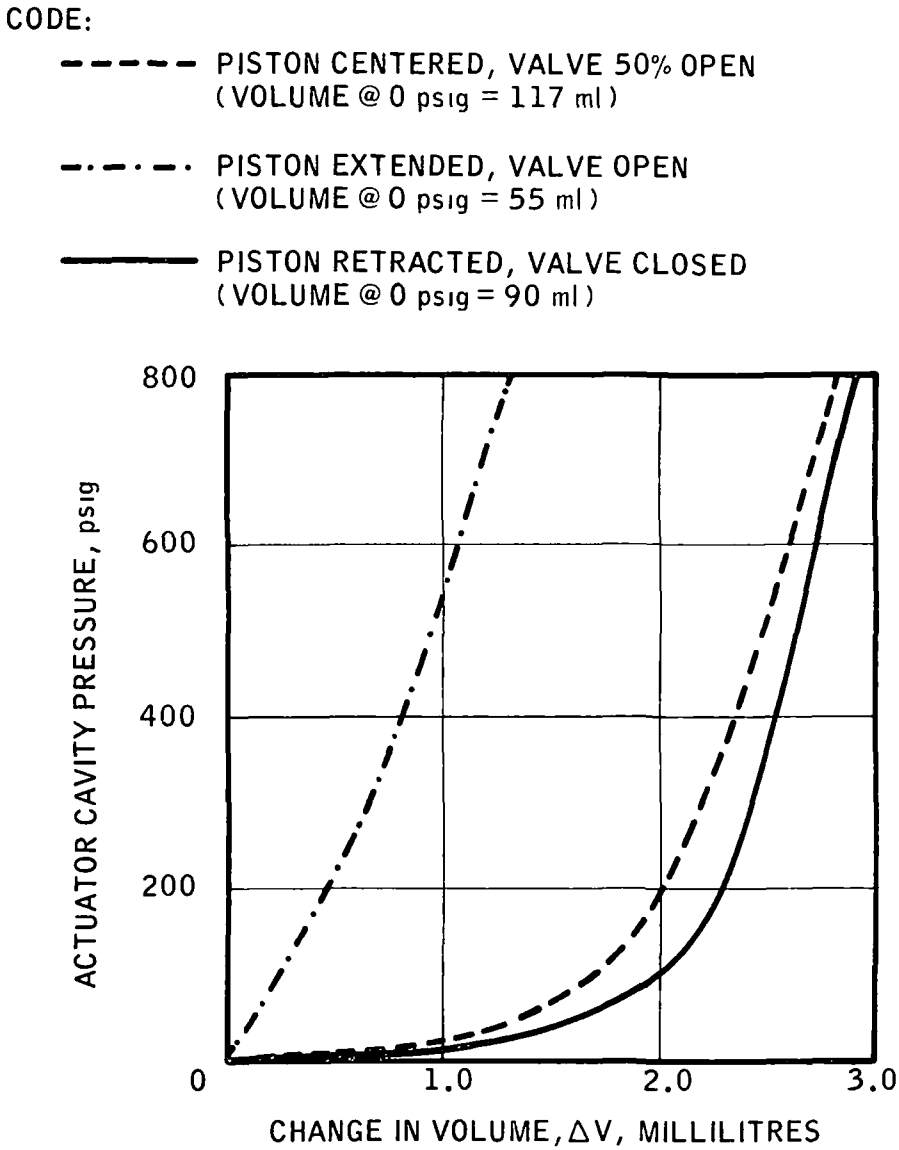

BULK SPRING RATE BLV ACTUATOR

Fig. App. B-11

LEGEND:

K_a = 25 MA/VOLT

K_1 = 2.15 IN.^{3}/SEC/MA

K_o = 0.75 RAD/IN.

K_f = 0.0312 VOLTS/DEGREE

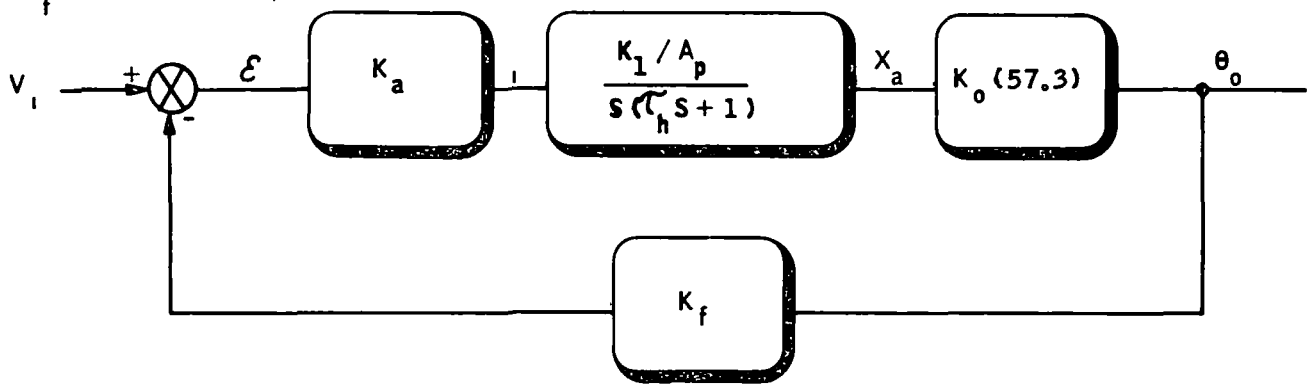

LOAD OR GAS-FARM VALVE SET-UP

FOR CLOSED-LOOP FREQUENCY RESPONSE

Fig. App. B-12

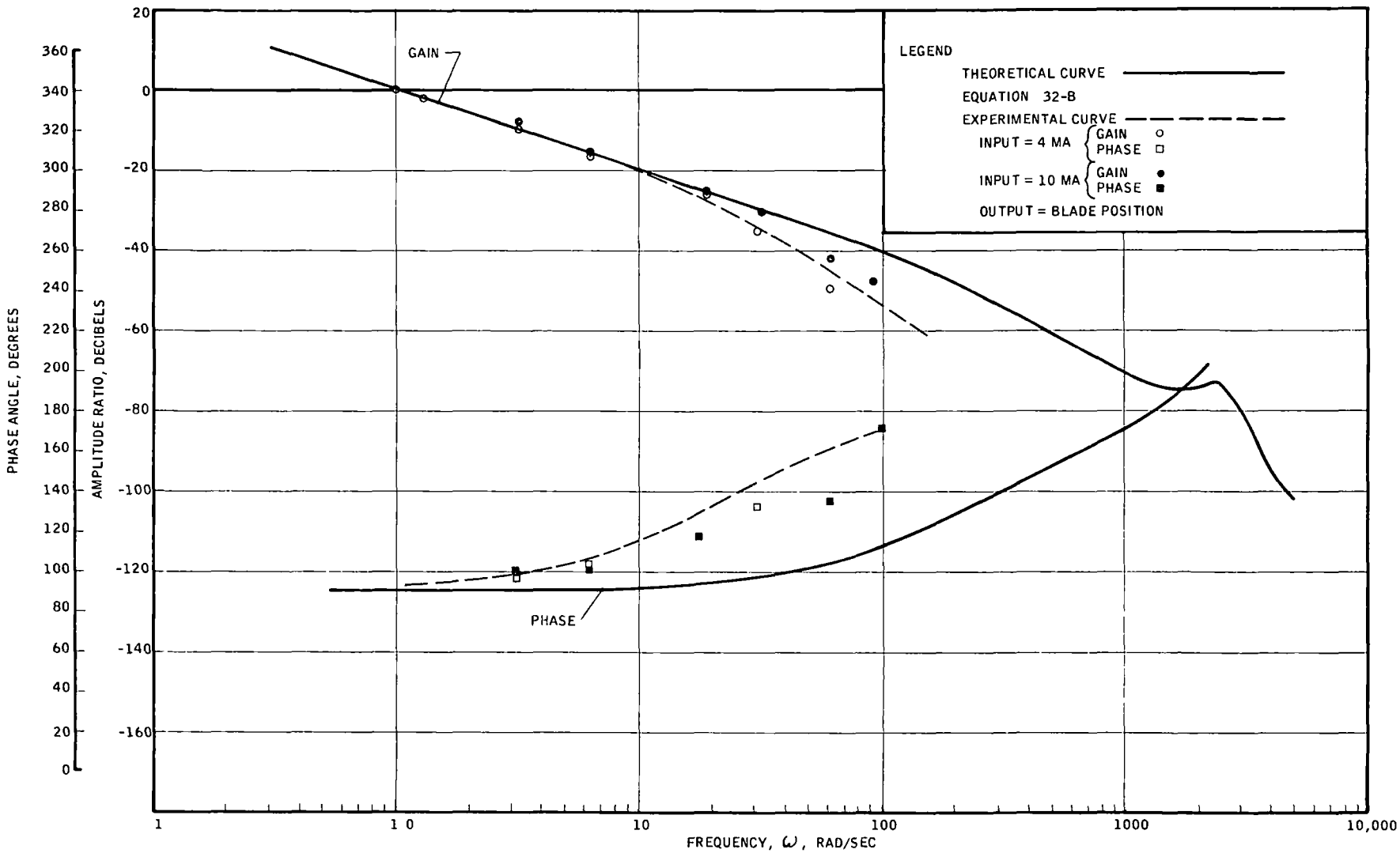

Fig. App. B-13

CORRELATION OF OPEN-LOOP FREQUENCY RESPONSES

LOAD VALVE SERVO-ACTUATOR

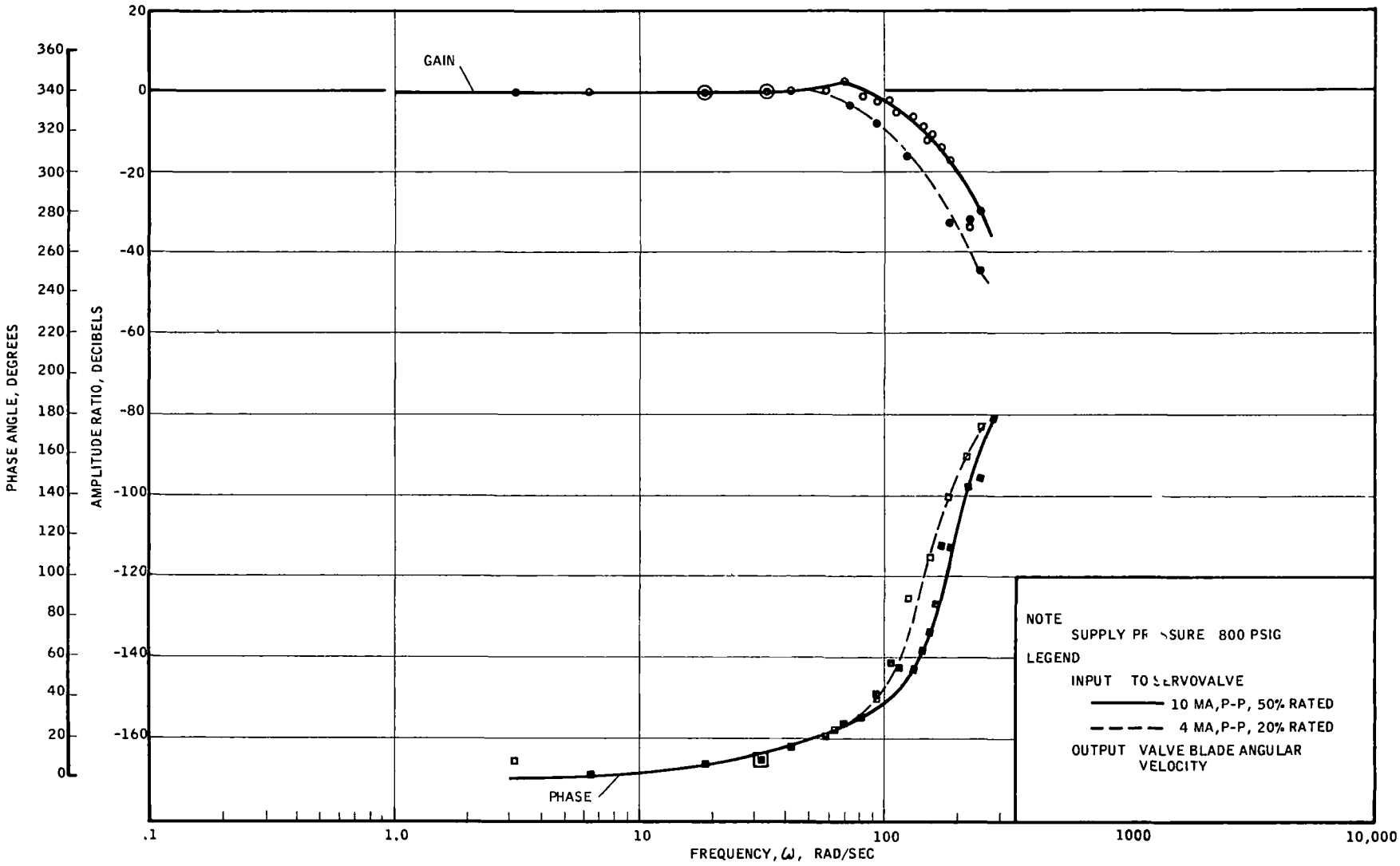

EXPERIMENTAL OPEN-LOOP FREQUENCY RESPONSE
LOAD VALVE SERVO-ACTUATOR

Fig. App. B-14

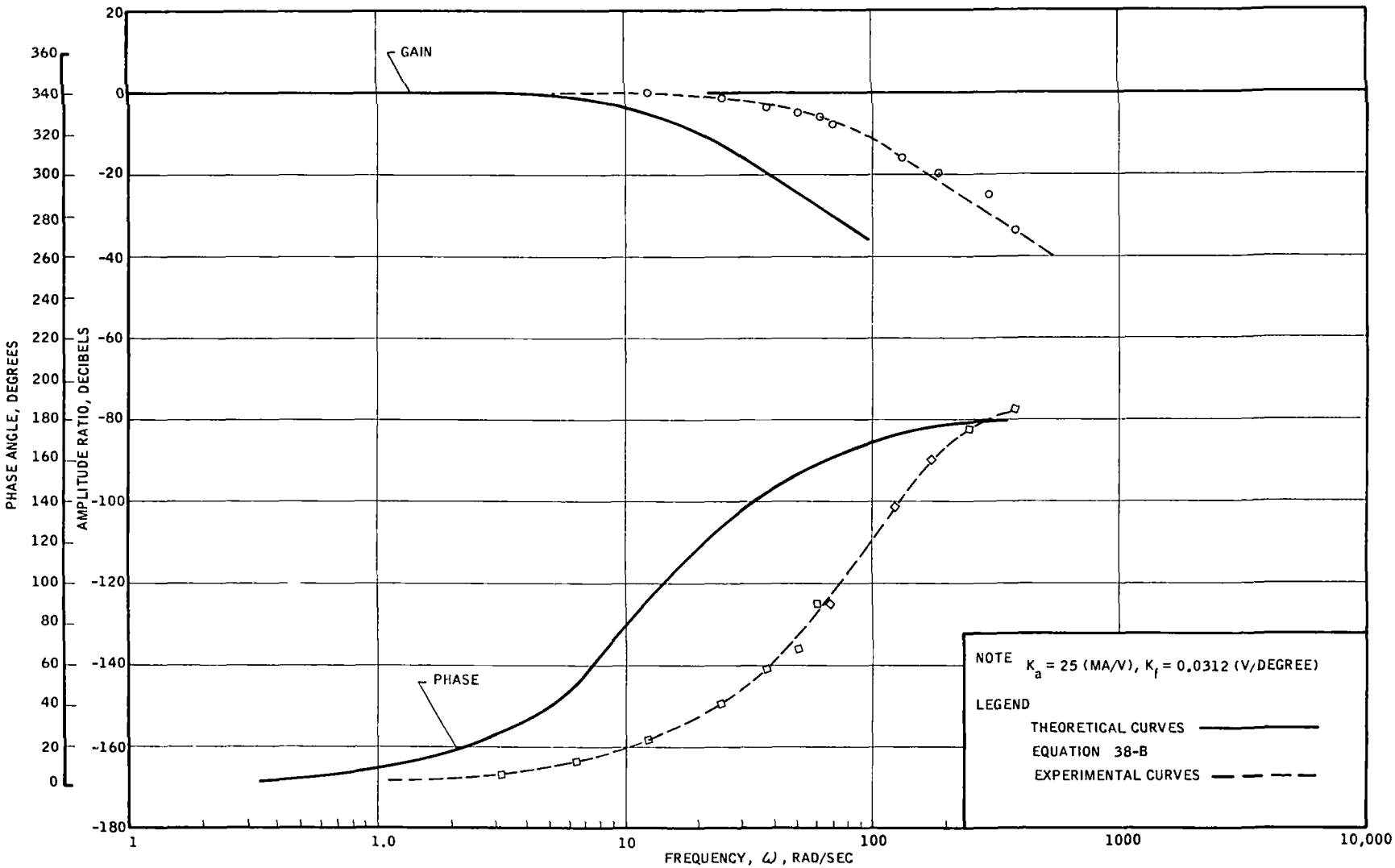

CORRELATION OF CLOSED-LOOP FREQUENCY RESPONSES
GAS-FARM VALVE AND LOAD VALVE SERVO-ACTUATORS

Fig. App. B-15

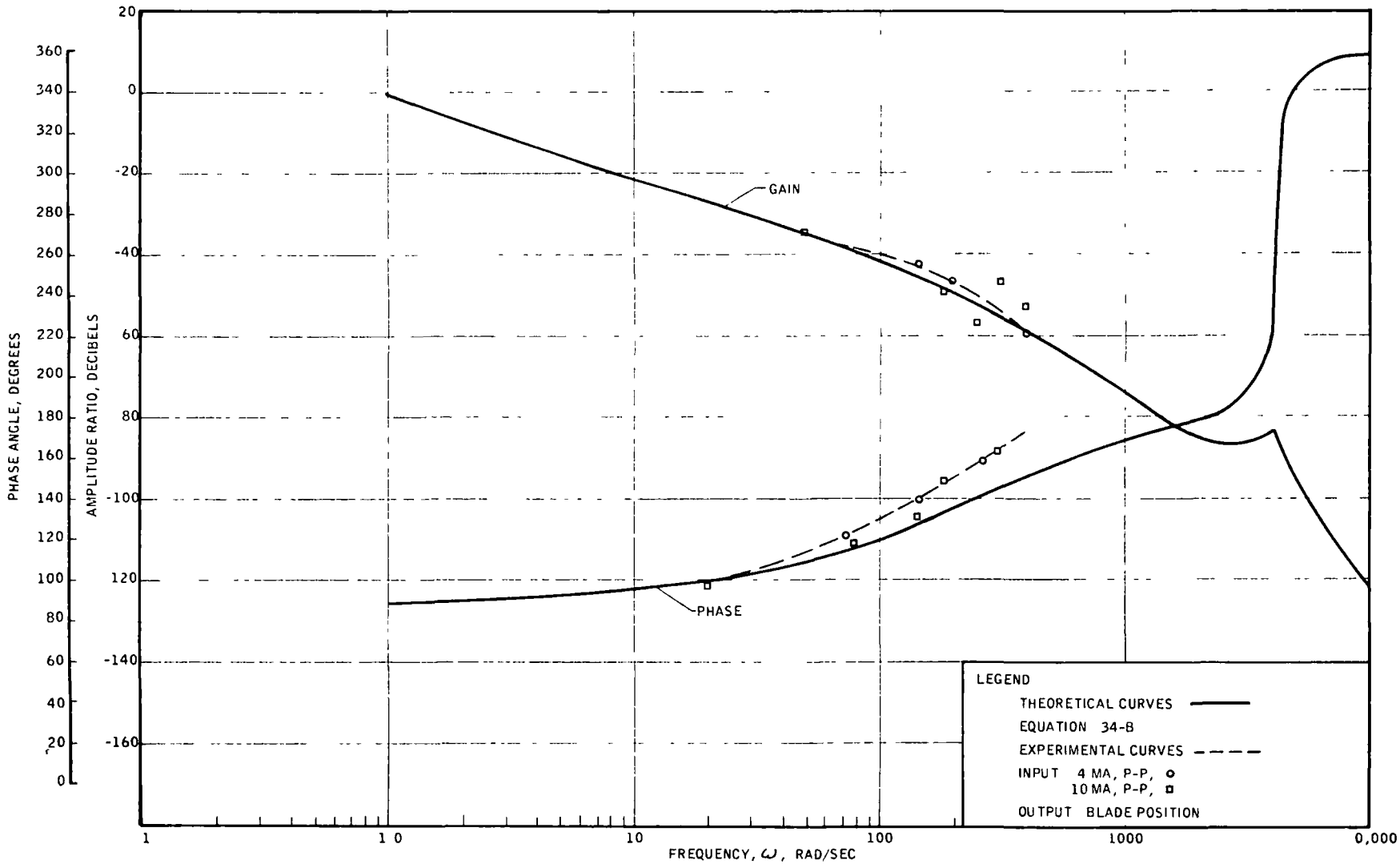

Fig. App. B-16

CORRELATION OF OPEN-LOOP FREQUENCY RESPONSES
TURBINE POWER CONTROL VALVE SERVO-ACTUATOR

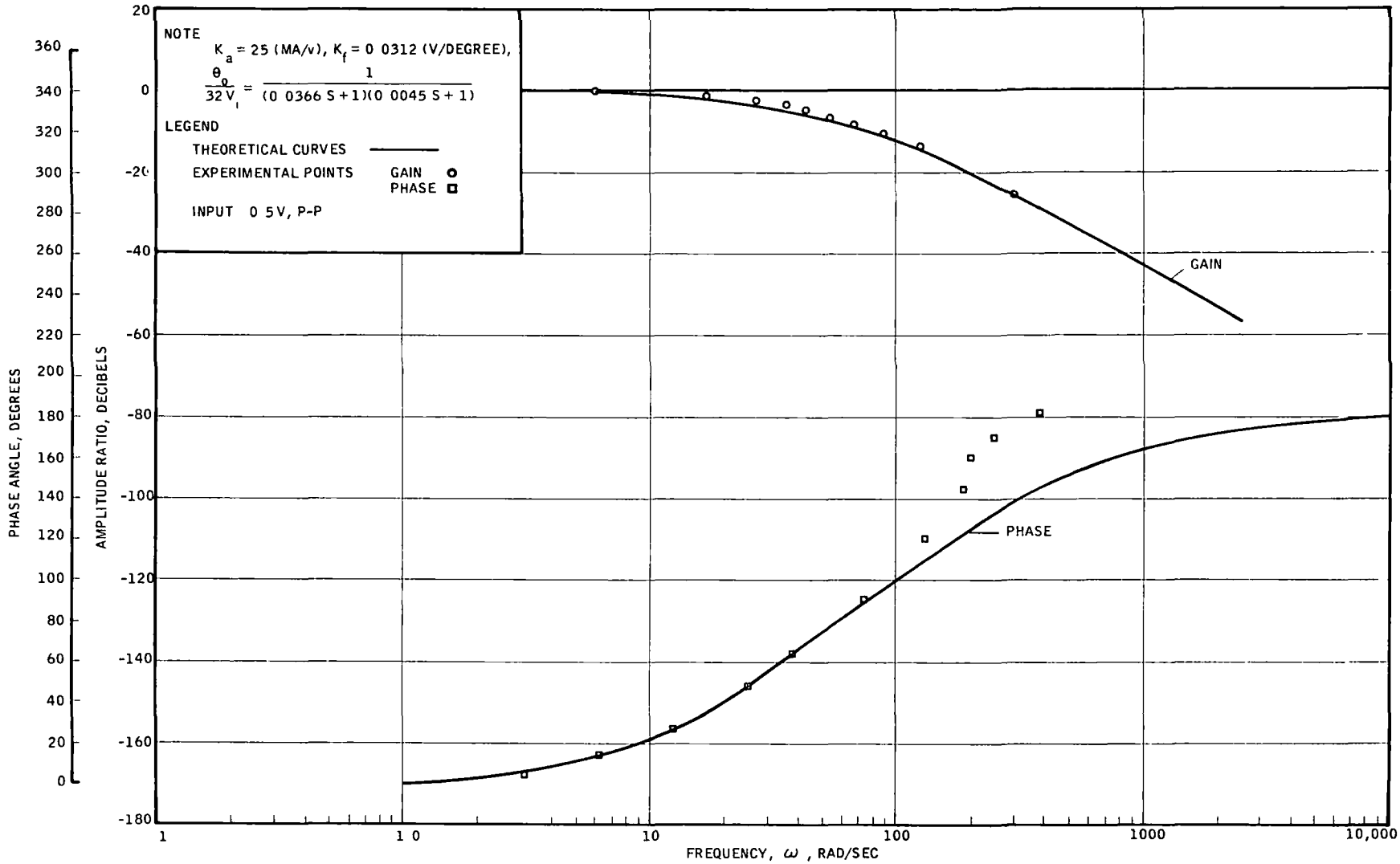

CORRELATION OF CLOSED-LOOP FREQUENCY RESPONSES
TURBINE POWER CONTROL VALVE SERVO-ACTUATOR

Fig. App. B-17

UNCLASSIFIED

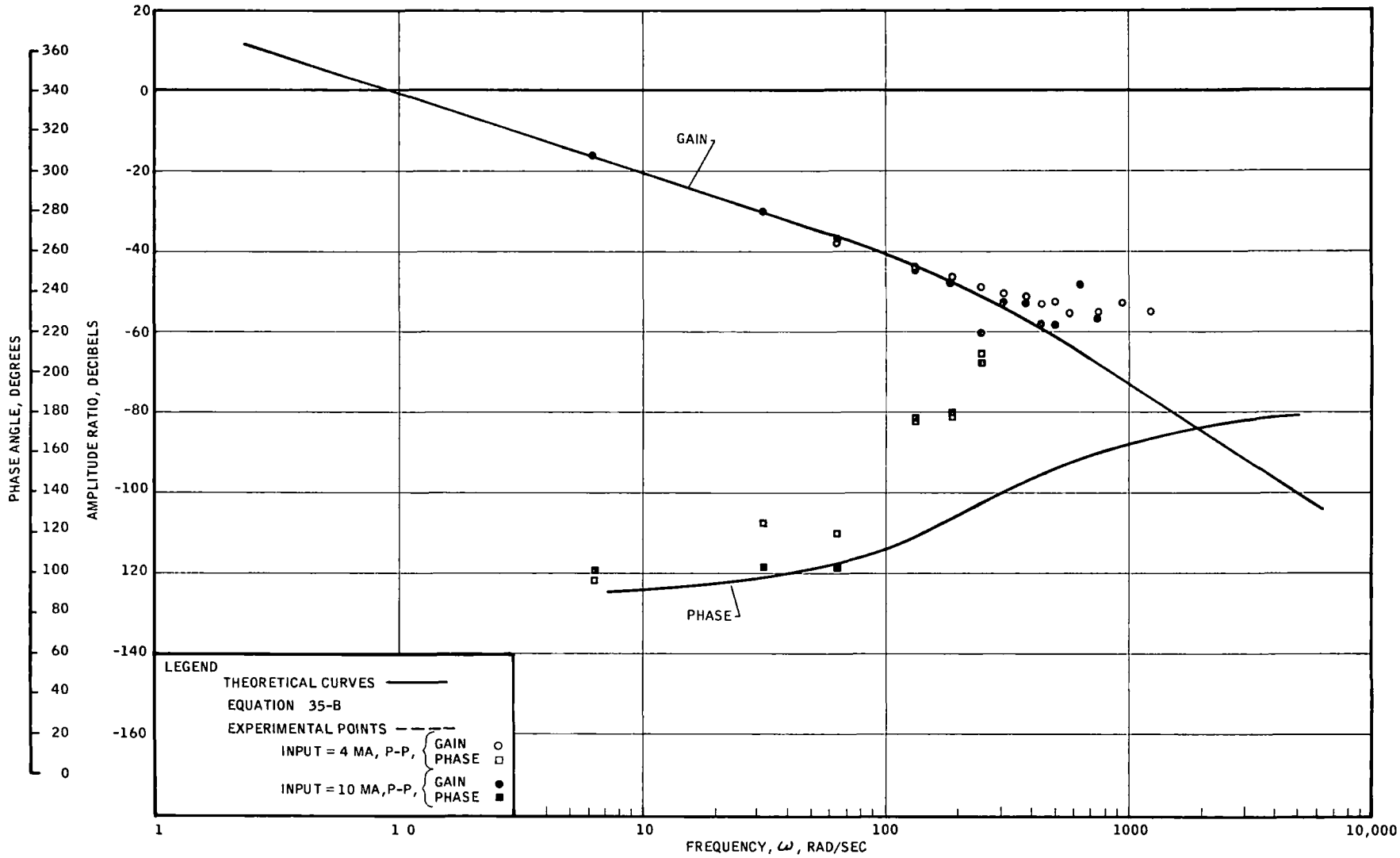

Fig. App. B-18

CORRELATION OF OPEN-LOOP FREQUENCY RESPONSES

BLEED-LINE VALVE SERVO-ACTUATOR

UNCLASSIFIED

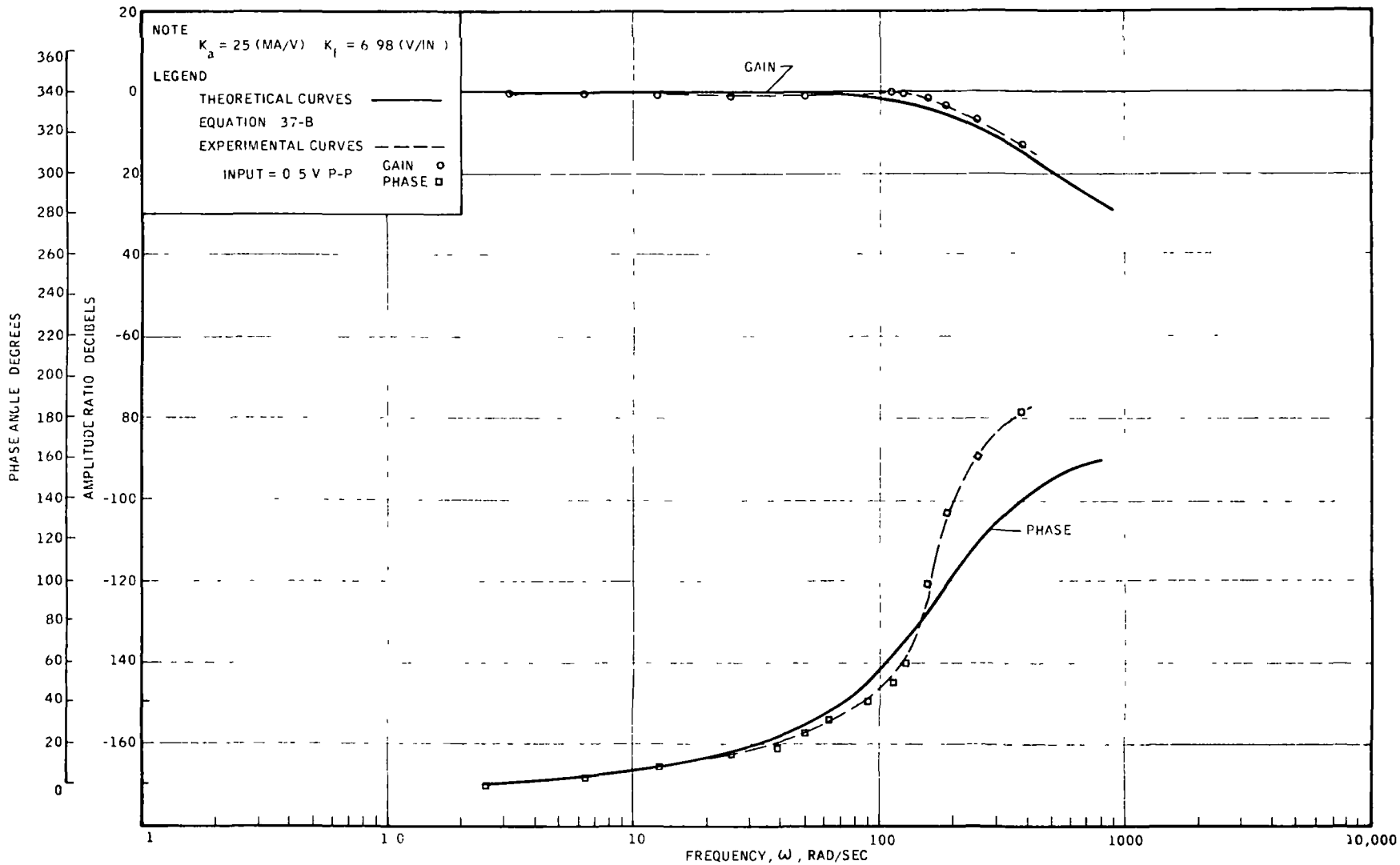

CORRELATION OF CLOSED-LOOP FREQUENCY RESPONSES
BLEED-LINE VALVE SERVO-ACTUATOR

Fig. App. B-19

~~CONFIDENTIAL RD~~

~~RESTRICTED DATA~~

~~ATOMIC ENERGY ACT OF 1954~~

~~CONFIDENTIAL RD~~